Transcriptional regulation of North American wood frog (*Rana sylvatica*) dorsal skin during development and in response to chronic exposure to a microplastics mixture

by

John Drew Thompson

A thesis

presented to the University of Waterloo

in fulfillment of the

thesis requirement for the degree of

Master of Science

in

Biology

Waterloo, Ontario, Canada, 2024

© John Drew Thompson 2024

Author's Declaration

This thesis consists of material all of which I authored or co-authored: see Statement of Contributions included in the thesis. This is a true copy of the thesis, including any required final revisions, as accepted by my examiners.

I understand that my thesis may be made electronically available to the public.

Statement of Contributions

This thesis consists of three chapters: an introductory chapter, a chapter presenting the methods used and results of this thesis, and a discussion chapter. Writing and analysis for all chapters was conducted solely by the thesis author, J. Drew Thompson. Collectively, versions of these three chapters are intended to be submitted for publication in the form of two manuscripts. The names of the authors that will be on each manuscript are listed below. This research was conducted at the University of Waterloo under the supervision of Dr. Barbara A. Katzenback, who contributed to the conceptualization and design of the research, intellectual input towards methodology, formal analysis, and review of material, and project administration, funding acquisition, and resources.

Chapter 2: Methods and Results

Manuscript #1: J. Drew Thompson, Sam M. Gene, Lauren A. Todd, Diane M. Orihel, Jennifer F. Provencher, Chelsea M. Rochman, and Barbara A. Katzenback. Transcriptional regulation of wood frog (*Rana sylvatica*) dorsal skin during development (tentative title).

Manuscript #2: J. Drew Thompson, Sam M. Gene, Diane M. Orihel, Jennifer F. Provencher, Chelsea M. Rochman, and Barbara A. Katzenback. Effects of exposure to a microplastics mixture on the dorsal skin transcriptome of North American wood frogs (*Rana sylvatica*) (tentative title).

Sam M. Gene, Dr. Diane M. Orihel, and Dr. Barbara A. Katzenback designed the mesocosm exposure experiment, with J. Drew Thompson leading the selection of sampling regimens for use in this thesis.

Sam M. Gene led the mesocosm experiment, including collection of the samples used in this thesis, under the supervision of Dr. Orihel, with technical assistance from Dalila Seckar, Chloe Robinson, Lydia Johnson, and Heather Vanderlip.

Dr. Lauren A. Todd assisted in the isolation of RNA from dorsal skin samples used for RNA sequencing.

Dr. Chelsea M. Rochman contributed the plastics used in the study and to funding acquisition.

Dr. Jennifer F. Provencher contributed to conceptualization and funding acquisition.

Alexander J. Douglas provided technical support in the form of procuring laboratory supplies and development of standard operating procedures for animal handling and sampling for this thesis prior to J. Drew Thompson joining the project.

RNA sequencing was performed by The Centre for Applied Genomics, The Hospital for Sick Children, Toronto, Canada.

Computational resources were provided by the Digital Research Alliance of Canada (alliancecan.ca).

Funding

Funding for this project was provided by an Environment and Climate Change Canada Increasing Knowledge on Plastic Pollution Grant to Dr. Diane Orihel, Dr. Barbara Katzenback, and Dr. Mark Mallory, and an NSERC Discovery Grant and Ontario Early Researcher Award to Dr. Barbara Katzenback.

J. Drew Thompson was supported by a National Sciences and Engineering Research Council of Canada Graduate Scholarship – Master's, an Ontario Graduate Scholarship, University of Waterloo President's Graduate Scholarships, Science Graduate Awards, Graduate Research Studentships, Graduate Teaching Assistantships, and a University of Waterloo Graduate Scholarship.

Abstract

Amphibian populations have been experiencing declines globally for decades due to factors such as habitat loss, invasive species, climate change, overexploitation, pollution, and disease. Skin is an important immune organ in amphibians, employing physical, chemical, microbiological, and immunological defences to prevent infection. Amphibian skin also undergoes dramatic morphological changes during metamorphosis. Therefore, it is important to gain a deeper understanding of the biological changes that amphibian skin undergoes during metamorphosis and whether these tightly regulated processes can be disrupted by environmental contaminants.

Microplastics are a persistent, ubiquitous environmental contaminant of increasing concern with a wide range of effects on exposed organisms. Previous studies have reported mortality, reduced growth, behavioural changes, and hepatotoxicity in amphibians exposed to microplastics. However, few studies have evaluated sub-organismal effects of microplastic exposure on amphibians, particularly in relation to the immune system. Furthermore, few studies have chronically exposed amphibians to an environmentally realistic microplastics mixture.

To address these gaps, an outdoor mesocosm experiment was performed where developing North American wood frogs (*Rana sylvatica*) were exposed from embryos throughout metamorphosis to a microplastics mixture consisting of an equal number of particles by count of polypropylene, polystyrene, and polyethylene terephthalate microplastics. Developing wood frogs were exposed to one of three concentrations: a 0× negative control of 0 g/L, a 1× treatment of 0.069 g/L, or a 10× treatment of 0.691 g/L of the microplastics mixture. This thesis reports on the transcriptomic analysis of dorsal skin of wood frogs from three different developmental timepoints: (1) after 50 days of exposure, average Gosner stage (GS) 34; (2) after 74 days of exposure, average GS 42; and (3) GS 45, 74 – 82 days of exposure.

The first analysis performed compared the dorsal skin transcriptome in the 0× unexposed wood frogs at different timepoints to evaluate changes in dorsal skin gene expression during development. Trends corresponding to known developmental phenomena such as keratinization of the skin and active ion transport nearing the end of metamorphosis were observed in the data. Downregulation of immune genes was also seen in the skin after the first timepoint, and is in line with the systemic immunosuppression metamorphosing amphibians undergo leading up to and during metamorphic climax. This result demonstrates that the systemic immunosuppression is paired with suppression of immune function in skin tissues.

The second analysis evaluated the effects of microplastic exposure on the dorsal skin transcriptome at each of the three selected developmental stages. Concentration- and timepoint-dependent effects were observed, with the greatest number of differentially expressed genes found in the 1× treatment at the first timepoint (GS ~34). Clusters of differentially expressed genes involved in mitochondrial function, protein synthesis, transmembrane transport, and immunity were found in at least one timepoint/treatment group. Developmental plasticity, morphological and behavioural changes during development, and a potential nonmonotonic dose response to microplastics in the wood frog are ideas proposed to account for the differences in response seen to different microplastic concentrations and at different developmental timepoints. Downregulation of immune genes was seen at the first developmental timepoint in response to the 1× microplastic treatment, suggesting that microplastics could cause developmental stage-specific immunosuppression in developing wood frogs. Because amphibian populations are already experiencing declines due to infectious diseases, it is important for future studies to continue to evaluate the potential for microplastics to act as a stressor and predispose amphibians to infection.

Acknowledgements

I would first like to thank my supervisor and mentor, Dr. Barb Katzenback. Barb, I could never have imagined all the amazing doors that would be opened when I approached you about joining your lab for an undergraduate thesis all those years ago. Your support, guidance, and mentorship has been unwavering during my time as your student. You continuously push me to be a better scientist by encouraging me to think critically and creatively. You are always able to provide both critiques and words of encouragement when I need them. I am proud to have been your student, and I hope you are proud of the scientist I have grown into under your guidance.

I would also like to thank my committee members, Dr. Laura Hug and Dr. Paul Craig for their guidance and mentorship during my thesis work. Thank you to all the Biology Department faculty and staff who I had the pleasure of working with or simply conversing with during my studies.

Thank you to all the current and past members of the Katzenback Lab that I had the pleasure of working with – Lauren, Nat, Alex, Yubing, Max, Emma, Mina. Each of you has been instrumental in me arriving at this point. Special shout out to Cailyn for taking this MSc journey with me. We did it! You have been such an amazing friend and support for me during this time. I will miss our coffee breaks and after-hours chats. There are so many other amazing friends I have made along the way, thank you to all of you.

Thank you to Sam Gene for collecting samples for me, and for always being willing to help me with details of the mesocosm study or just chatting about frogs and microplastics. Thank you to Dr. Diane Orihel, Dr. Chelsea Rochman, and Dr. Jenn Provencher for your support during our collaborations.

To all my pELAstics Pals: I am so fortunate to have been able to join this amazing project and to meet all of you. My time at ELA was one of the highlights of my time as a

grad student. Thank you to all the staff at IISD-ELA for the amazing science you conduct and your welcoming attitude towards all the students that travel to conduct research at ELA.

Thank you to my family and friends - Mom, Dad, Lorie, Kody, Jami, Morgan, Ethan, Lauren, Earvin, and many others (sorry, I couldn't possibly manage to list all of you) - for your support during my graduate studies. I know sometimes it seemed like I would be a student forever. Not anymore!

Dedication

For Grandma and Grandpa.

Table of Contents

Author's Declaration ii

Statement of Contributions iii

Abstract v

Acknowledgements vii

Dedication ix

List of Figures xiii

List of Tables xvii

List of Abbreviations xviii

Chapter 1 Introduction 1

1.1 General Information on Amphibians 1

1.1.1 Amphibian Declines and Implications 2

1.1.2 Amphibians and Stressors 4

1.2 Microplastics 5

1.2.1 Microplastics and Amphibians 7

1.3 The Immune System and the Importance of Amphibian Skin 17

1.4 Knowledge Gaps 19

1.5 Thesis Objectives and Hypotheses 20

Chapter 2 Methods and Results 22

2.1 Methods 22

2.1.1 Animal Ethics 22

2.1.2 Outdoor Mesocosm Exposure Experiment 22

2.1.2.1 Overview of Experimental Setup 22
2.1.2.2 Microplastics Mixture 26
2.1.2.3 Phase I: Collection and Rearing of Wood Frog Eggs for Microplastic Exposure Experiment 28
2.1.2.4 Phase II and III: Setup of Mesocosms for Microplastic Exposure Experiment 28
2.1.2.5 Overview of Animal Handling 29
2.1.2.6 Sampling of Tissues 30
2.1.2.7 Collection of Skin Swabs and Water Filters 31
2.1.3 Samples Used in this Thesis 34
2.1.4 RNA Extraction 34
2.1.5 RNA Sequencing 36
2.1.6 Quality Filtering of RNA-seq Reads 39
2.1.7 Reference-Guided Assembly and Abundance Estimation 39
2.1.8 Transcriptome Annotation 40
2.1.9 Differential Gene Expression Analysis 41
2.1.10 Gene Set Enrichment Analysis 42
2.1.11 Data Analysis and Figure Generation 42
2.1.12 Code and Data Availability 43
2.2 Results 45
2.2.1 Study Design and RNA Sample Quality 45
2.2.2 RNA-seq Quality Control and Reference-Guided Assembly 47
2.2.3 Transcriptome Trends 53

2.2.4 Analysis of Transcriptomic Changes in Dorsal Skin from Control (0× Microplastics) Wood Frog Larvae Across Developmental Stages 55

2.2.5 Analysis of Transcriptomic Changes in the Dorsal Skin of Wood Frog Larvae Resulting from Microplastic Exposure at Several Developmental Stages 76

Chapter 3 Discussion, Conclusions, and Future Directions 99

3.1 Discussion 99

3.1.1 Transcriptome Characteristics 100

3.1.2 Wood Frog Dorsal Skin Transcriptome Profile 102

3.1.3 Transcriptional Changes in Wood Frog Dorsal Skin During Development 105

3.1.4 Effects of Microplastics on Gene Expression in the Dorsal Skin of Developing Wood Frogs 106

3.1.5 Limitations 110

3.2 Conclusions 112

3.3 Future Directions 113

References 117

Appendix A RNA-seq Quality Control 156

Appendix B Supplemental Figures 168

Appendix C R sessionInfo() 176

List of Figures

Figure 2.1. Schematic of the experimental setup used to expose developing North American wood frogs to a microplastics mixture in outdoor mesocosms from eggs until the completion of metamorphosis. 24
Figure 2.2. Schematic of samples collected from a mesocosm experiment exposing developing North American wood frogs to a microplastics mixture. 33
Figure 2.3. Bioinformatics analysis workflow to analyze dorsal skin RNA samples from wood frogs exposed to varying concentrations of a microplastics mixture. 44
Figure 2.4. Gosner stages and days of exposure of wood frog larvae that were exposed to a microplastics mixture prior to being sampled for use in RNA sequencing of dorsal skin. 46
Figure 2.5. Length distribution of StringTie-assembled transcripts. 51
Figure 2.6. Length distribution of predicted candidate coding sequences. 52
Figure 2.7. Developmental stage is a greater driver of transcriptional change than microplastic exposure across the entire sample set. 54
Figure 2.8. Overview of Gene Ontology (GO) terms assigned to transcribed genes in the dorsal skin of Gosner stage ~34 wood frog tadpoles from the control (0× microplastics exposure) group. 56
Figure 2.9. Overview of KEGG pathways assigned to transcribed genes in the dorsal skin of Gosner stage ~34 wood frog tadpoles from the control (0× microplastics exposure) group. 58
Figure 2.10. Differentially expressed genes in the dorsal skin of control (0× microplastics exposure) wood frog larvae and pro-metamorphs across developmental stages. 61
Figure 2.11. Core differentially expressed genes in wood frog dorsal skin during development. 62
Figure 2.12. Top enriched GO terms in the dorsal skin of control (0× microplastics exposed) wood frog larvae across developmental timepoints. 66

Figure 2.13. Enrichment map of GO terms enriched in the dorsal skin of Gosner stage ~42 control (0× microplastics exposed) wood frogs compared to the dorsal skin of Gosner stage ~34 control wood frogs. 68
Figure 2.14. Enrichment map of GO terms enriched in the dorsal skin of Gosner stage 45 control (0× microplastics exposed) wood frogs compared to the dorsal skin of Gosner stage ~42 control wood frogs. 69
Figure 2.15. Enrichment map of GO terms enriched in the dorsal skin of Gosner stage 45 control (0× microplastics exposed) wood frogs compared to the dorsal skin of Gosner stage ~34 wood frogs. 70
Figure 2.16. Top enriched KEGG pathways in the dorsal skin of control (0× microplastics exposed) wood frog larvae across developmental timepoints. 71
Figure 2.17. Enrichment map of KEGG pathways enriched in the dorsal skin of Gosner stage ~42 control (0× microplastics exposed) wood frogs compared to the dorsal skin of Gosner stage ~34 control wood frogs. 73
Figure 2.18. Enrichment map of KEGG pathways enriched in the dorsal skin of Gosner stage 45 control (0× microplastics exposed) wood frogs compared to the dorsal skin of Gosner stage ~42 control wood frogs. 74
Figure 2.19. Enrichment map of KEGG pathways enriched in the dorsal skin of Gosner stage 45 control (0× microplastics exposed) wood frogs compared to the dorsal skin of Gosner stage ~34 control wood frogs. 75
Figure 2.20. Microplastic exposure causes differential expression of genes in the dorsal skin of developing wood frogs. 78
Figure 2.21. Overlap of differentially expressed genes in the dorsal skin of microplastic-exposed wood frog larvae at several developmental stages. 80
Figure 2.22. Top enriched GO terms in the dorsal skin of Gosner stage ~34 wood frog larvae exposed to a 1× or 10× microplastics mixture. 84
Figure 2.23. Enrichment map of GO terms enriched in the dorsal skin of Gosner stage ~34 wood frog larvae following exposure to a 1× microplastics mixture. 85

Figure 2.24. Enrichment map of GO terms enriched in the dorsal skin of Gosner stage ~34 wood frog larvae following exposure to a 10× microplastics mixture. 86
Figure 2.25. Top enriched KEGG pathways in the dorsal skin of Gosner stage ~34 wood frog larvae exposed to a 1× or 10× microplastics mixture. 87
Figure 2.26. Enrichment map of KEGG pathways enriched in the dorsal skin of Gosner stage ~34 wood frog larvae folloing exposure to a 1× microplastics mixture. 88
Figure 2.27. Enrichment map of KEGG pathways enriched in the dorsal skin of Gosner stage ~34 wood frog larvae following exposure to a 10× microplastics mixture. 89
Figure 2.28. Top enriched GO terms in the dorsal skin of Gosner stage ~42 wood frogs exposed to a 10× microplastics mixture. 91
Figure 2.29. Enrichment map of GO terms enriched in the dorsal skin of Gosner stage ~42 wood frogs exposed to a 10× microplastics mixture. 92
Figure 2.30. Enriched KEGG pathways in the dorsal skin of Gosner stage ~42 wood frogs exposed to a 10× microplastics mixture. 93
Figure 2.31. Enrichment map of KEGG pathways enriched in the dorsal skin of Gosner stage ~42 wood frogs exposed to a 10× microplastics mixture. 94
Figure 2.32. Top enriched GO terms in the dorsal skin of Gosner stage 45 wood frogs exposed to a microplastics mixture. 96
Figure 2.33. Enrichment map of GO terms enriched in the dorsal skin of Gosner stage 45 wood frogs following exposure to a 1× microplastics mixture. 97
Figure 2.34. Enrichment map of GO terms enriched in the dorsal skin of Gosner stage 45 wood frogs following exposure to a 10× microplastics mixture. 98

Figure A.1. Bioanalyzer reports of sequenced RNA samples from the dorsal skin of developing wood frogs exposed to varying concentrations of a microplastics mixture. 156

Figure A.2. Sequence quality of RNA-seq reads from the dorsal skin of developing wood frogs exposed to a microplastics mixture. 163
Figure A.3. GC content of RNA-seq reads from the dorsal skin of developing wood frogs exposed to a microplastics mixture. 164
Figure A.4. N content of RNA-seq reads from the dorsal skin of developing wood frogs exposed to a microplastics mixture. 164
Figure A.5. Sequence duplication levels of RNA-seq reads from the dorsal skin of developing wood frogs exposed to a microplastics mixture. 165
Figure A.6. Adaptor content in raw RNA-seq reads from the dorsal skin of developing wood frogs exposed to a microplastics mixture. 166
Figure A.7. Length of cleaned RNA-seq reads from the dorsal skin of developing wood frogs exposed to a microplastics mixture. 167

Figure B.1. Overview of Gene Ontology (GO) terms assigned to transcribed genes in the dorsal skin of Gosner stage ~42 wood frog tadpoles from the control (0× microplastics exposure) group. 168
Figure B.2. Overview of Gene Ontology (GO) terms assigned to transcribed genes in the dorsal skin of Gosner stage 45 wood frog tadpoles from the control (0× microplastics exposure) group. 170
Figure B.3. Overview of KEGG pathways assigned to transcribed genes in the dorsal skin of Gosner stage ~42 wood frog tadpoles from the control (0× microplastics exposure) group. 172
Figure B.4. Overview of KEGG pathways assigned to transcribed genes in the dorsal skin of Gosner stage 45 wood frog tadpoles from the control (0× microplastics exposure) group. 174

List of Tables

Table 1.1. Summary of studies examining the effects of microplastics on amphibians. 11
Table 2.1. Experimental microplastic treatments used in this study.....25
Table 2.2. Formulations of the plastics used in this study. 27
Table 2.3. Information on total RNA extracted from the dorsal skin of wood frogs exposed to varying concentrations of a microplastics mixture throughout development. 37
Table 2.4. RNA-seq and Transcriptome Summary Statistics. 49
Table 2.5. Transcriptome Annotation Rates. 50
Table 2.6. Number of differentially expressed genes between developmental stages in the dorsal skin of developing wood frogs in the control (0× microplastics exposure) group.....60
Table 2.7. Number of enriched Gene Ontology (GO) terms in the dorsal skin of control (0× microplastics exposure) wood frog larvae between developmental stages. 65
Table 2.8. Number of enriched KEGG pathways in the dorsal skin of control (0× microplastics exposure) wood frog larvae between developmental stages.....65
Table 2.9. Number of differentially expressed genes in the dorsal skin of microplastics-exposed wood frog larvae at several developmental stages. 77
Table 2.10. Number of enriched GO terms in the dorsal skin of microplastic-exposed wood frog larvae at several developmental stages. 82
Table 2.11. Number of enriched KEGG pathways in the dorsal skin of microplastic-exposed wood frog larvae at several developmental stages. 82

List of Abbreviations

AChE	acetylcholinesterase
AMP	antimicrobial peptide
BChE	butyrylcholinesterase
CAT	catalase
CbE	carboxylesterase
DEG	differentially expressed gene
DNA	deoxyribonucleic acid
FV3	*Frog Virus 3*
GAA1	First Global Amphibian Assessment
GAA2	Second Global Amphibian Assessment
GO	Gene Ontology
GS	Gosner stage
GSEA	gene set enrichment analysis
GST	glutathione-S-transferase
IUCN	International Union for Conservation of Nature
KEGG	Kyoto Encyclopedia of Genes and Genomes
MS-222	tricaine methanesulfonate
NES	normalized enrichment score
PAMP	pathogen associated molecular pattern
PCA	principal component analysis

PET	polyethylene terephthalate
PP	polypropylene
PRR	pattern recognition receptor
PS	polystyrene
RLR	RIG-I-like receptor
RNA	ribonucleic acid
ROS	reactive oxygen species
SOD	superoxide dismutase
QUBS	Queen's University Biological Station

Chapter 1
Introduction

1.1 General Information on Amphibians

Amphibians are a vertebrate taxon encompassing the orders Anura (frogs), Urodela (salamanders), and Gymnophiona (caecilians). As of December 4, 2023, there are 8,698 described amphibian species (7,662 frogs, 815 salamanders, and 221 caecilians) with over 100 new species discovered each year (*AmphibiaWeb*, n.d.). Amphibians are dispersed globally, with species found on every continent except Antarctica (*AmphibiaWeb*, n.d.). They act as both a predator and prey species and can move between aquatic and terrestrial environments, contributing numerous ecosystem services (reviewed by Hocking & Babbitt, 2014).

Many amphibians have a biphasic lifecycle, beginning life with an aquatic larval stage and transitioning to a terrestrial adult stage through a process termed metamorphosis. However, there is diversity in their lifecycle, with some species remaining fully aquatic, or having evolved direct development or vivipary (reviewed by Liedtke et al., 2022). For those species of amphibian that undergo metamorphosis, they undergo a process of dramatic morphological rearrangements to prepare aquatic larvae for terrestrial adulthood. In anurans (frogs), the process of metamorphosis is divided into three phases: premetamorphosis, prometamorphosis, and metamorphic climax. Premetamorphosis is the life stage from hatching to the onset of growth of the hindlegs, prometamorphosis follows until the breakthrough of the forelegs, which marks the onset of metamorphic climax, a rapid period of changes to the digestive tract and resorption of the gills and tail (Etkin, 1932). Metamorphosis is under control of the endocrine system, with thyroid hormone being the ultimate driver of metamorphosis (Duellman & Trueb, 1994). Numerous functional and morphological rearrangements take place during metamorphosis, including calcification of the skeleton, growth of limbs and muscle, growth of brain structures such as the cerebellum, resorption of the pronephros, restructuring of the pancreas and gastrointestinal tract

(Duellman & Trueb, 1994), and reorganization of the immune system (reviewed in Rollins-Smith, 1998). In addition, the skin undergoes dramatic morphological changes during metamorphosis to prepare for life on land. This includes the loss of ciliated epidermal cells and neuromasts, sensory cells of the lateral line system which detect water movement, in most species (Nishikawa et al., 1992; Nokhbatolfoghahai et al., 2005, 2006; Quinzio & Fabrezi, 2014; Quinzio & Goldberg, 2019). Furthermore, the epidermis of larvae is typically two cell layers thick and is covered by a mucus layer secreted by unicellular glands called Leydig cells (Duellman & Trueb, 1994; Kelly, 1966). During metamorphosis the epidermis expands to five to seven cell layers and becomes covered by a keratinized stratum corneum (Brunelli et al., 2015; Duellman & Trueb, 1994). Multicellular granular and mucous glands also develop during metamorphosis (Regueira et al., 2016). Considering these dramatic morphological rearrangements, larval amphibian skin is quite a different organ than the skin of adults.

1.1.1 Amphibian Declines and Implications

At the First World Congress of Herpetology in 1989, shared stories of difficulty finding known amphibian populations lead concerned scientists to initiate the first International Union for Conservation of Nature (IUCN) Global Amphibian Assessment (GAA1), the results of which were published in 2004 by Stuart et al. The findings were concerning: of the 5,743 amphibian species described at the time, 32.5% were classified as globally threatened (either vulnerable, endangered, or critically endangered) (Stuart et al., 2004). What was perhaps even more concerning at the time was that the scientists conducting the GAA1 could not definitively identify the main driving forces behind many of these declines. Habitat loss and overexploitation were major contributors; however, these did not account for the full scale of the declines (Stuart et al., 2004). The second Global Amphibian Assessment (GAA2), completed in 2022, revealed that the previously classified enigmatic declines were largely due to the emerging disease chytridiomycosis, caused by the fungus *Batrachochytrium dentrobatidis* (Luedtke et al., 2023), though infectious diseases caused by *Frog Virus 3* and protists of the phylum Perkinsea have also been linked to amphibian

declines (Isidoro-Ayza et al., 2017; Robert, 2010). The GAA2 increased the number of assessed species to 8,011 (Luedtke et al., 2023), therefore covering over 90% of known amphibian species, and found that over 40% are now globally threatened, making amphibians the most threatened vertebrate class (Luedtke et al., 2023). The total number of confirmed amphibian extinctions is 37 species, but could be as high as 222 extinctions over the last 150 years (Luedtke et al., 2023).

The decline of amphibian populations can have consequences for the ecosystems they inhabit, including on humans. A review by Whiles et al. (2006) found that amphibian population declines in Neotropical stream ecosystems can result in changes to primary production, insect populations, and reduced energy transfer to the riparian zone. Because of the biphasic lifestyle of amphibians, Whiles et al. (2006) posit that when considering ecosystem structure and function, the loss of one amphibian species is like losing two species. Furthermore, a review of the literature demonstrates that amphibian population declines can result in the loss of other taxonomic groups and biotic homogenization (Zipkin & DiRenzo, 2022). Since amphibians are a key predator species of disease-carrying vector species such as mosquitoes, it is possible to see an increase in insect-transmitted communicable diseases in areas which have experienced a decline in amphibian populations. Springborn et al. (2022) demonstrated the occurrence of this phenomenon in Central America, where disease-driven amphibian population declines resulted in an increase of between 0.76 to 1.1 additional malaria cases per 1000 people per year, nearly a doubling in some areas, within regions of Costa Rica and Panama following the introduction of *B. dendrobatidis* to the region in the 1990s.

The study of amphibians has the potential to lead to the development of next-generation therapeutics. Amphibians are a rich source of antimicrobial peptides (AMPs), small proteins which have anti-pathogen activity (Xu & Lai, 2015) and are being investigated as next-generation treatments for diseases of both humans and other animals, particularly agricultural livestock (Xuan et al., 2023). As we are currently seeing the emergence of antibacterial resistant bacteria (Murray et al., 2022), AMP-derived antimicrobials could be

essential in coming years to prevent easily antibiotic-treatable pathogens from becoming untreatable once again. However, the extinction of an amphibian species means that we lose the opportunity to study any AMPs or other molecules produced by that species (barring studies on any DNA sequences collected prior to extinction). An example of this is the extinction of the gastric brooding frog. This species would put the digestive function of their stomach on hold to allow its young to develop inside of the stomach (Corben et al., 1974). As Joseph Mendelson points out, the hormone which controls this halt of digestive function might have led to treatments for stomach ulcers (Resnick, 2016). What other unique amphibians has the world lost, along with our chance to study them?

1.1.2 Amphibians and Stressors

Acute stress responses are important for dealing with stressors an organism is exposed to over the course of its lifecycle. However, chronic stress can have deleterious effects. The response to stress in amphibians is controlled by the hypothalamic-pituitary-interrenal axis with the glucocorticoid steroid corticosterone being the primary hormone controlling the stress response (Narayan et al., 2013a). Although elevated corticosterone alone cannot be used as a diagnostic marker of stress (Narayan et al., 2019), chronic stress does lead to chronically elevated levels of corticosterone (Romero et al., 2009). The stress response can influence many different physiological pathways, particularly during development and metamorphosis. For example, tadpoles exposed to predators before the onset of metamorphosis may develop larger tails to allow them to escape predators more easily (Fraker et al., 2021; Middlemis Maher et al., 2013). Stress from environmental factors such as pond drying and lack of food can cause tadpoles to speed up the onset of metamorphosis, resulting in smaller body size post-metamorphosis (Audo et al., 1995; Székely et al., 2017). However, chronic sources of stress can result in deleterious effects such as decreased body weight (Bliley & Woodley, 2012) and teratogenic effects (Lorenz et al., 2009).

Many of the stressors that amphibians are exposed to can cause immunotoxicity, defined as any deleterious effect of a foreign substance on the functioning of the immune system (Trizio et al., 1988). Consequences such as immunosuppression or increased susceptibility to infection have been observed in amphibians exposed to stressors (Brannelly et al., 2019; Brown et al., 2021; Davis et al., 2020; Hall et al., 2020; May et al., 2019; Reeve et al., 2013; Robert et al., 2018). Stressors encountered by amphibians include contaminants in water such as elevated salinity, altered pH, pesticides, perfluoroalkyl substances, and oil-extraction by-products (Albecker & McCoy, 2017; Brown et al., 2021; Burraco & Gomez-Mestre, 2016; Davis et al., 2020; Hall et al., 2020; Robert et al., 2018), as well as elevated temperature (Narayan & Hero, 2014), predation (Fraker et al., 2021; Narayan et al., 2013b), low food levels (Crespi & Denver, 2005), pond drying (Brannelly et al., 2019), and anthropogenic noise and light (May et al., 2019; Tennessen et al., 2014). Examples of immunological consequences of stress in amphibians include decreased numbers of circulating eosinophils (Kaiser et al., 2015), decreased bacterial killing ability and antibody titres in animals developing under dry conditions (Brannelly et al., 2019), elevated susceptibility to trematode infection in tadpoles exposed to perfluoroalkyl substances (Brown et al., 2021), increased ranavirus transmission and more lethal infections in populations experiencing salinity stress (Hall et al., 2020), increased susceptibility to parasite infection in tadpoles experiencing light pollution (May et al., 2019), and increased FV3 viral loads in tadpoles exposed to oil extraction-related contaminants (Robert et al., 2018). As amphibian populations experience declines due to emerging pathogens, it is important to evaluate potential stressors for immunotoxicity.

1.2 Microplastics

Microplastics, plastic particles less than 5 mm in size (Hartmann et al., 2019), have garnered increasing attention from the scientific community in recent years as a ubiquitous contaminant of concern (Cole et al., 2011; de Souza Machado et al., 2018; Lusher et al., 2015; Wong et al., 2020). Microplastics can be directly manufactured in the form of microspheres or formed from environmental weathering of larger plastics (Hale et al., 2020).

This can result in the formation of extremely small particles, which have been further subdivided into nanoplastics, though the definition of the upper size bound for nanoplastics has not been widely agreed upon, ranging from 100 nm to 335 μm (Hartmann et al., 2019). A wide range of microplastic concentrations have been reported in the literature, with concentrations in freshwater reaching as high as 10^8 particles/m^3. Since the rate of plastic pollution input is expected to remain above the rate of mitigation efforts (Borrelle et al., 2020), and because microplastics persist in the environment for decades to thousands of years (Chamas et al., 2020), microplastic concentrations are expected to continue to increase.

The issue of microplastic pollution is compounded by the fact that microplastics are not a single contaminant, but rather a suite of contaminants formed from a variety of plastic polymers with a range of sizes, shapes, and chemical additives (Rochman et al., 2019). This complicates studies investigating the effects of microplastic pollution, as laboratory studies conducted with microplastics of a single polymer, shape, and/or size are not necessarily reflective of the actual complex exposure landscape organisms face in the environment. Conversely, studies exposing organisms to a complex microplastics mixture may not be able to determine if the mixture as a whole or distinct components of the mixture are causing any observed effects. Furthermore, plastics often contain chemical additives which serve a wide variety of purposes such as to decrease flammability, increase light and heat stability, lubricate, reduce static, and to scavenge acid and oxidants (reviewed in Hahladakis et al., 2018). Plastic additives can accumulate in exposed organisms through ingestion of plastic or through leaching of additives into water (Jang et al., 2021) and can themselves have toxic effects (Malafaia et al., 2022; Ockenden et al., 2022). Furthermore, microplastics can influence the bioaccumulation (Álvarez-Ruiz et al., 2021) and toxicity (Oliveira et al., 2013) of chemical contaminants, adding additional complexity to the study of microplastics.

Efforts to examine the potential effects of exposure to microplastics on aquatic vertebrates have largely focused on fishes and, despite the challenges of studying microplastics as a contaminant, have provided information on the routes and effects of exposure (reviewed in Amoatey & Baawain, 2019; Anbumani & Kakkar, 2018; Burns &

Boxall, 2018; de Sá et al., 2018; Hirt & Body-Malapel, 2020; Issac & Kandasubramanian, 2021; Puskic et al., 2020; Susanti et al., 2020; Tursi et al., 2022). The primary routes of exposure are through the digestive and respiratory systems, where microplastics can accumulate (Choi et al., 2018; Ding et al., 2018; Espinosa et al., 2019; Jabeen et al., 2018; Lei et al., 2018; Limonta et al., 2019). Ingestion of microplastics may cause a false sense of satiation (Cole et al., 2015; de Sá et al., 2015; Ramos et al., 2012) and damage to the intestinal epithelia including distention, hyperplasia, increased villus thickness, an increase in goblet cells, separation of the mucosal epithelium from the lamina propria, mucous hypersecretion, and increased neutrophil infiltration (Choi et al., 2018; Espinosa et al., 2019; Limonta et al., 2019). Limonta et al. (2019) also observed increased mucous secretion and neutrophil infiltration in the gills of zebrafish, as well as gross alterations of the gill epithelium. Microplastics can also cross epithelial barriers and have been found in internal organs, such as the livers of exposed fish (Ding et al., 2018; Espinosa et al., 2019; Jabeen et al., 2018). Microgranulomas, congestion of blood vessels, morphological changes, vacuolation, and hypertrophy have all been observed in the livers of fish exposed to microplastics (Espinosa et al., 2019; Jabeen et al., 2018). Various other physiological effects have also been observed including increased protease activity (Romano et al., 2018), upregulation of genes of the complement system (Veneman et al., 2017), and alterations to the gut microbiome (reviewed in Li et al., 2022). Behavioural effects including reduced swimming activity, decreased predatory performance and efficiency, and increased nocturnal activity have also been observed (Choi et al., 2018; de Sá et al., 2015; Limonta et al., 2019).

1.2.1 Microplastics and Amphibians

Due to their biphasic lifestyle with an aquatic larval stage, the potential risk of exposure to microplastics is high for amphibians. Despite this, relatively few studies have investigated the prevalence of microplastics in amphibian habitats or their effects on amphibians (Table 1.1). Many amphibian species utilize temporary, hydrologically disconnected ponds (known as vernal pools or ephemeral wetlands) for breeding and larval development (Compton et al., 2007). Notably, there is no information in the literature on the

prevalence of microplastics in vernal pools, but several studies have investigated microplastics in other small waterbodies amphibians can be found in. Iannella et al. (2020) reported the first instance of microplastics in the stomach of a European amphibian in Italian crested newts from mountain karst ponds, suggesting microplastics are present in these important breeding ponds. Microplastics are common in stormwater retention ponds, with reported concentrations as high as 22,894 microplastics/m^3, where they accumulate in vertebrates including amphibians (Liu, Olesen, et al., 2019; Liu, Vianello, et al., 2019; Olesen et al., 2019). Hu et al. (2018, 2022) investigated the microplastic content of small waterbodies in China and the tadpoles that inhabit them and found concentrations as high as 21.52 items/L in water and 168.48 items/g in tadpole whole bodies. Further study is needed to determine the exposure landscape of microplastics in the diverse environments that amphibians inhabit.

There is a growing body of literature on the effects of microplastics on amphibians (Table 1.1), though many studies conflict with each other, with some researchers finding effects from exposure and others seeing no effects with similar experimental setups but with different species. Behavioural effects including declines in activity (Bacchetta et al., 2021; Balestrieri et al., 2022), feeding rate (Boyero et al., 2020), and anti-predator response (da Costa Araújo & Malafaia, 2020) have all been reported in tadpoles following exposure to microplastics. Most effects reported in the literature involve the growth and development of amphibian larvae. Decreased growth has been observed in tadpoles of the Italian agile frog (*Rana latastei*) (Balestrieri et al., 2022), the common midwife toad (*Alytes obstetricans*) (Boyero et al., 2020), *Physalaemus cuvieri* (Malafaia et al., 2021), and the African clawed frog (*Xenopus laevis*) (Mouchet et al., 2022; Ruthsatz et al., 2023; Tussellino et al., 2015; Venâncio et al., 2022) when exposed to microplastics. Developmental defects associated with microplastic exposure have included reduced body condition, malformations, or defects and have been observed in tadpoles of the common midwife toad (Boyero et al., 2020), *P. cuvieri* (da Costa Araújo, De Melo, et al., 2020; da Costa Araújo et al., 2022), and the African clawed frog (Bacchetta et al., 2021; Pekmezekmek et al., 2022; Ruthsatz et al., 2023;

Tussellino et al., 2015; Venâncio et al., 2022). Conversely, studies have also reported no effects on tadpoles of the Balearic green toad (*Bufo balearicus*) (Balestrieri et al., 2022), the African clawed frog (De Felice et al., 2018), and the Italian agile frog (Scribano et al., 2022). These conflicting results may be explained by the use of different microplastic polymers, sizes, shapes, concentrations, exposure durations, or developmental stage of exposed tadpoles. Additionally, different species may respond differently to the same microplastic exposure (Balestrieri et al., 2022). Further studies must be performed to determine how these different factors might influence the effects of exposure to microplastics in different species.

Although organismal endpoints like mortality and developmental defects demonstrate the acute toxicity of microplastics, it is also essential to evaluate sub-organismal responses to microplastic exposure as sub-organismal effects could lead to mortality through increasing susceptibility of amphibians to disease or by reducing fitness. Various sublethal effects have been reported in *P. cuvieri* tadpoles following exposure to microplastics including hepatotoxicity, erythrocyte cytotoxicity, reductions in lipid reserves, and increased levels of reactive oxygen species (ROS) and nitrite levels (da Costa Araújo, De Melo, et al., 2020; da Costa Araújo, Gomes, et al., 2020; Malafaia et al., 2021). Changes in the activities of enzymes such as superoxide dismutase, catalase, acetylcholinesterase, butyrylcholinesterase, carboxylesterase, alkaline phosphatase, and glutathione-S-transferase have been reported in *P. cuvieri* and *Scinax squalirostris* tadpoles exposed to microplastics (Attademo et al., 2022; Lajmanovich et al., 2022; Malafaia et al., 2021). Furthermore, studies have reported changes in gene expression associated with microplastic exposure in the African clawed frog (Tussellino et al., 2015) and the Asiatic toad (*Bufo gargarizans*) (Zhang et al., 2023). Additionally, expression of the *hsp70* and *pax6* genes were found to be decreased in the offspring of *X. laevis* exposed to microplastics (Pekmezekmek et al., 2022). Finally, elevated *B. dendrobatidis* pathogen loads have been observed in tadpoles exposed to microplastics (Bosch et al., 2021), suggesting that exposure to microplastics could lead to increased disease susceptibility. Additional studies are required to test this hypothesis and to

demonstrate under what conditions exposure to microplastics might predispose amphibians to disease.

Table 1.1. Summary of studies examining the effects of microplastics on amphibians.

Reference	Microplastic	Concentration	Exposure Duration	Species	Notable Effects
(Attademo et al., 2022)	Polyethylene, 40 – 48 µm	60 mg/L	10 days	*Scinax squalirostris*	Altered carboxylesterase activity depending on substrate, decreased alkaline phosphatase activity.
(Bacchetta et al., 2021)	Polyester fibers, mean size 660 µm length, 12 µm width, 2 µm height	1, 10, or 50 µg/mL	NF stage 8/9 – 46	*Xenopus laevis*	Gut deformities, pierced gut epithelia, occlusion, reduced mobility.
(Balestrieri et al., 2022)	Expanded polystyrene, high-density polyethylene, polyester fibers, and polyvinyl chloride	1, 7, or 50 mg/L	7 days	*Rana latastei* and *Bufo balearicus*	*R. latastei*: Mortality and decreased growth and activity. *B. balearicus*: negligible.
(Bonfanti et al., 2021)	Waste microplastics (includes polyethylene and polypropylene)	0.1, 1, or 10 mg/L	NF stage 8 - 46	*Xenopus laevis*	Mechanical stress and mucus overproduction in intestines.
(Bosch et al., 2021)	Polystyrene microspheres, 10 µm, green fluorescence	18, 180, or 1,800 particles/mL	229 days	*Alytes obstetricans*	Microplastic ingestion increases *B. dendrobatidis* burden of infection, non-*B. dendrobatidis*-exposed tadpoles ingested more microplastics.
(Boyero et al., 2020)	Polystyrene microspheres, 10 µm, yellow-green fluorescence	18, 180, or 1,800 particles/mL	14 days	*Alytes obstetricans*	Mortality and decreased feeding rate at highest concentration, linear decrease with dose for growth and body condition.

Reference	Microplastic	Concentration	Exposure Duration	Species	Notable Effects
(Buss et al., 2022)	Polyester fibers, 0.19 – 0.97 mm length	2.5, 5, 10, or 20 mg/L	24 h	*Rana sylvatica*	Reduced infection success when tadpoles and parasites exposed together.
(da Costa Araújo, De Melo, et al., 2020)	Polyethylene, diameter 35.45 ± 18.17 µm (mean ± standard deviation)	60 mg/L	7 days	*Physalaemus cuvieri*	Erythrocyte cytotoxicity (changes in nuclei area, perimeter, width, length, and radius; lower nucleus:cytoplasm ratio), reduced ratio between total length and mouth-cloaca distance, caudal length, ocular area, and mouth area, increased number of melanophores in the skin.
(da Costa Araújo, Gomes, et al., 2020)	Polyethylene, diameter 35.45 ± 18.17 µm (mean ± standard deviation)	60 mg/L	7 days	*Physalaemus cuvieri*	Hepatotoxicity (blood vessel dilation, infiltration, congestion, hydropic degeneration, hypertrophy, hyperplasia, altered hepatocyte nuclei size, volume, and shape).
(da Costa Araújo et al., 2023)	Polyethylene, diameter 35.45 ± 18.17 µm (mean ± standard deviation) ± 14 xenobiotics	2.7×10^8 particles/m^3	30 days	*Physalaemus cuvieri*	Cytotoxicity compared to control. Increased swimming activity, higher total body length, tail length, and tail width, and stress response when exposed with pollutants.

Reference	Microplastic	Concentration	Exposure Duration	Species	Notable Effects
(da Costa Araújo et al., 2022)	Polyvinyl chloride acetate	2×10^5 or 4×10^6 particles/m^3	30 days	*Physalaemus cuvieri*	Lowered body condition index, deformities in the keratinized structures of the jaw sheath, changes to the position of the intestine in the body cavity, bowel tube winding condition, pseudomelanosis of the intestine, reduction of superoxide dismutase and catalase activities, changes in nitrite production.
(da Costa Araújo & Malafaia, 2020)	Polyethylene, diameter 35.45 ± 18.17 μm (mean ± standard deviation)	60 mg/L	7 days	*Physalaemus cuvieri*	Locomotor issues, anxiogenic effect syndrome, reduced anti-predator response.
(De Felice et al., 2018)	Polystyrene, diameter 2.75 ± 0.09 μm (mean ± standard deviation)	0.125, 1.25, or 12.5 μg/mL	NF stage 36-46	*Xenopus laevis*	No changes to body growth or swimming activity.
(Lajmanovich et al., 2022)	Polyethylene ± glyphosate or glufosinate ammonium	60 mg/L	48 h	*Scinax squalirostris*	Microplastics alone increased glutathione-S-transferase (GST), decreased carboxylesterase (CbE) activities. Microplastics plus herbicides increased GST, decreased acetylcholinesterase (AChE), CbE activities.

Reference	Microplastic	Concentration	Exposure Duration	Species	Notable Effects
(Malafaia et al., 2022)	Polyethylene, diameter 35.45 ± 18.17 μm (mean ± standard deviation) ± Nile red dye fluorescence	60 mg/L	96 h	*Physalaemus cuvieri*	Fluorescent microplastic leachate caused altered superoxide dismutase (SOD), catalase (CAT), and AChE activities.
(Malafaia et al., 2021)	Polylactic acid biomicroplastic	760 or 15,020 μg/L	14 days	*Physalaemus cuvieri*	Increased tail size, reduced lipid reserves, increased reactive oxygen and nitric oxide species production, increased SOD, CAT, AChE and butyrylcholinesterase (BChE) activities.
(Mouchet et al., 2022)	Carboxylated polystyrene microspheres, 50 and 350 nm; heteroaggregated 50 nm polystyrene microspheres, 350 nm	0.1, 1, 10, or 100 μg/L	12 days	*Xenopus laevis*	Altered growth rate and decreased growth, genotoxicity.
(Pekmezekmek et al., 2022)	High molecular weight polyvinyl chloride, provided by oral gavage to parental generation	1% of body weight, twice per week	6 weeks	*Xenopus laevis*	In offspring: malformations and decreased viability, decreased expression of *hsp70* and *pax6* genes.

Reference	Microplastic	Concentration	Exposure Duration	Species	Notable Effects
(Ruthsatz et al., 2022)	Polyethylene, 34 – 50 µm	60 mg/L	NF stage 45 – 57	*Xenopus laevis*	Gut length and mass increased in response to microplastics and cellulose.
(Ruthsatz et al., 2023)	Polyethylene, 34 – 50 µm	60 mg/L	NF stage 45 – 57 or 66 + 10 days	*Xenopus laevis*	Larvae: Reduced snout – vent length, increased growth rate, reduced body mass. Increased body condition, corticosterone levels, and metabolic rate. Juveniles: wider bodies, longer limbs. Results were dependant on rearing temperature.
(Scribano et al., 2022)	3 polyvinyl chloride : 3 high-density polyethylene : 3 polyester fibres : 1 expanded polystyrene	1, 7, or 10 mg/L	14 days	*Rana latastei*	No effects on behaviour, growth, or mortality.
(Tussellino et al., 2015)	Polystyrene, 50 nm, red fluorescence	4.5, 9, or 18 mg/L	NF stage 2 – 46	*Xenopus laevis*	Mortality, decreased growth rate, malformations of the head, gut and tail, altered pigment distribution, edema in the anterior ventral region, and a shorter body length. Altered expression of *bra*, *myod1*, and *sox9* genes.

Reference	Microplastic	Concentration	Exposure Duration	Species	Notable Effects
(Venâncio et al., 2022)	Polymethylmethacrylate, 40 ± 5.6 nm (mean ± standard deviation)	1, 100, or 1000 µg/L	NF stage 8-11 (embryos): 96 h NF stage 45 (tadpoles): 48 h	*Xenopus laevis*	Embryos: lower body length in embryos exposed to highest dose. Tadpoles: growth rate and body length altered, externalization of gut when exposed to highest dose.
(Zhang et al., 2023)	Polystyrene, 1 or 10 µm	1 or 4,550 particles/mL	21 days (microbial and transcriptomic analysis), subset allowed to complete metamorphosis	*Bufo gargarizans*	Developmental delays observed but mitigated by metamorphic climax, 10 µm altered gut microbiome, 1 µm resulted in upregulation of genes related to protein synthesis and mitochondrial function and downregulation of genes involved in neural functions and cellular responses.

NF stage: developmental staging system for *Xenopus laevis* (Nieuwkoop & Faber, 1994)

1.3 The Immune System and the Importance of Amphibian Skin

The vertebrate immune system uses many different types of defences to protect against pathogens. The first line of defence is the physical epithelial barriers of the skin, gastrointestinal tract, and respiratory tract (Owen et al., 2013). These barriers act to physically block pathogens from entering the body and establishing an infection. Tears, sweat, mucus, and saliva all contain chemical defences in the form of enzymes and antimicrobial peptides (AMPs), which can target a variety of pathogens, in addition to immunoglobulins, which target specific antigens (Owen et al., 2013). If a pathogen is able to circumvent these physical and chemical barriers, the cells of the body can detect it and initiate an immune response. The immune system is divided into two interconnected arms: the innate immune system, which is the first to respond to infection and activates the second arm, the adaptive immune system, which produces receptors targeted to specific antigens (Owen et al., 2013). The innate immune system includes immune cells such as neutrophils, basophils, eosinophils, dendritic cells, and macrophages which express germline-encoded pattern recognition receptors (PRRs) on the cell surface, in the cytosol, and in endosomes which detect pathogen associated molecular patterns (PAMPs), conserved molecules from pathogens such as proteins, lipids, sugars, and non-self-DNA and RNA (Owen et al., 2013). Once detected, innate cells such as neutrophils, eosinophils, basophils, and macrophages can phagocytose extracellular pathogens (Owen et al., 2013). Other innate cells such as natural killer cells can initiate apoptosis of infected self-cells by releasing perforins and granzymes (Owen et al., 2013). The innate immune system also includes the complement system, a family of proteins which circulate in blood and bind to and inactivate pathogens or assist in their recognition by immune cells (Owen et al., 2013). Non-immune cells, such as epithelial cells, also function in innate immunity, as they also express germline-encoded PRRs which allow them to detect pathogens and signal to the innate and adaptive immune systems with signalling proteins called cytokines (Owen et al., 2013). Once antigen-presenting innate immune cells have internalized and inactivated a pathogen, they present antigens on major histocompatibility complex (MHC) proteins to T and B cells of the adaptive immune system (Owen et al., 2013). These cells express rearranged receptor proteins which undergo

selection in secondary lymphoid organs to recognize antigens with high specificity (Owen et al., 2013). Once T and B cells are activated, they undergo clonal expansion, producing many daughter cells (Owen et al., 2013). Cytotoxic T cells will then survey cells of the body, scanning MHC class I molecules for the antigen they recognize and if detected, will kill the infected cell (Owen et al., 2013). Helper T cells will activate other adaptive immune cells and produce cytokines which tailor an immune response to the pathogen in question (Owen et al., 2013). B cells begin secreting soluble immunoglobulin molecules, also known as antibodies (Owen et al., 2013). The immune system is highly interconnected, with immune cells residing within tissues able to rapidly detect and respond to an infection by recruiting additional innate and adaptive immune cells to the site of infection (Owen et al., 2013).

The skin is an important immune organ in amphibians as one of the primary barriers to infection (reviewed in Varga et al., 2019), and also plays additional physiological roles in amphibians such as osmotic regulation (reviewed in Katz, 1986) and respiration (reviewed in Tattersall, 2007). Because amphibian skin functions in osmotic regulation and respiration it must be thin and permeable. This makes the skin, and amphibians, particularly sensitive to chemical contaminants (Quaranta et al., 2009), often leading to their use as a sentinel species in environmental monitoring. Despite remaining as a thin membrane to allow these functions, the skin of amphibians must still perform its function as a barrier to infection. To do this, the skin employs tight junctions between epithelial cells to form a barrier to pathogens. This is important, as the two main emerging pathogens of concern for amphibians are either infections of the skin (i.e. *B. dendrobatidis*) (pathogenesis reviewed in Baitchman & Pessier, 2013) or must pass through the physical barriers of the skin, gastrointestinal tract, or respiratory system to establish a systemic infection (i.e. FV3). Amphibian skin cells also express PRRs (Bui-Marinos et al., 2020, 2021; Ishii et al., 2007) which, as discussed above, recognize and respond to pathogens by producing cytokines which serve as a signal to activate and recruit immune cells (reviewed in Constant et al., 2021; Nguyen & Soulika, 2019). The skin of some amphibian species are also rich in AMPs, which are contained in granular glands, and exhibit activity against a variety of pathogens (reviewed in Patocka et

al., 2019). AMPs may also contribute to the regulation of the commensal microbiome (Salzman et al., 2010), though this has not been demonstrated in amphibians. The commensal skin microbiome is another defence amphibians employ against infection, as metabolites produced by some commensal bacterial species can have anti-*B. dendrobatidis* activity, and it is believed that their presence on the skin can have protective action against chytridiomycosis (Bates et al., 2022; Harris et al., 2009; Woodhams et al., 2007). In summary, the skin of amphibians plays crucial roles in immunity by acting as a barrier, producing protective compounds, hosting the commensal microbiome, and detecting and signalling the presence of pathogens to the immune system.

1.4 Knowledge Gaps

Although some progress has been made on determining how exposure to microplastics could affect amphibian species, much work remains. While providing important information which is essential for informing future studies, the existing body of literature on the effects of microplastics on amphibians has some common limitations. The plastics used in previous studies are often of a single polymer, size, and/or shape. Additionally, animals were often exposed for a short duration. Furthermore, little is known about the types and prevalence of microplastics in many amphibian habitats. Despite this, based on what is known about the types of microplastics present in other aquatic ecosystems (reviewed in Anderson et al., 2016; Andrady, 2011; Barnes et al., 2009; Koelmans et al., 2019; van Sebille et al., 2015), the exposures conducted in existing studies are not likely representative of real-life amphibian microplastics exposures, which likely involve many different shapes, sizes and polymers. Furthermore, amphibians are likely chronically exposed for the duration of the aquatic stage of their lifecycle. Additionally, few studies have investigated sublethal effects on the immune system. Finally, to my knowledge, there is only one published study investigating the effect of microplastics on a North American amphibian species. This is important as amphibians are a diverse taxon, and the literature shows highly variable effects of microplastics to different species (Table 1.1).

The knowledge gap I seek to address in this thesis is the lack of data on the sublethal effects of environmentally realistic microplastic exposure on the immune functions of amphibian skin. Given the importance of amphibian skin to immune function, and because the skin is an organ which comes into direct contact with microplastics, it was selected as the organ of interest for this thesis. The North American wood frog (*Rana sylvatica*) was selected as our study species. The North American wood frog has a widespread distribution that includes most of Canada, extending from the southern border to as far north as the boreal forest, and is often used as an indicator species (Berven & Gill, 1983). *R. sylvatica* was selected as a model Canadian species for this study because of this and their rapid development, with tadpoles completing metamorphosis within 3 months of hatching. This allows a study encompassing all developmental stages to take place within a single field season. *R. sylvatica* is susceptible to both FV3 and *B. dendrobatidis* (Forzán et al., 2017; Gahl et al., 2012), which is important for future studies to evaluate changes in disease susceptibility.

1.5 Thesis Objectives and Hypotheses

With these knowledge gaps in mind, a collaborative project was begun to study the effects of chronic exposure to a microplastics mixture of a combination of polymers and sizes on a North American amphibian species. The collaborative study aimed to investigate the effects of microplastic exposure on developing North American wood frogs by assessing whole animal endpoints including growth, development, survival, and behaviour (conducted by collaborators Dr. Diane Orihel and Sam Gene), and sub-organismal endpoints including effects on the dorsal skin transcriptome at multiple developmental stages (discussed in this thesis) and on the commensal skin microbiome (not included in this thesis). This thesis had two objectives. First, to first profile the dorsal skin transcriptome of unexposed wood frogs at several developmental stages to determine normal changes in gene expression in the dorsal skin of developing wood frogs over time. The second objective was to evaluate the potential for microplastic exposure to cause immunotoxicity by evaluating transcriptional responses of the dorsal skin of developing wood frogs at multiple developmental stages. For the analysis

of the dorsal skin transcriptome over time, I hypothesized that the expression of genes related to known developmental changes would be altered across time, such as those related to keratinization and immunity. I hypothesized that in response to microplastics exposure, genes involved in recognizing pathogens and signalling to initiate an immune response would be downregulated in the dorsal skin of developing wood frogs.

Chapter 2
Methods and Results

2.1 Methods

2.1.1 Animal Ethics

All procedures involving animals were performed in accordance with ethical standards set by the Canadian Council on Animal Care and were approved by the Queen's University Animal Care Committee (Animal Care Protocol #2021-2123). Egg masses were collected under an Ontario Ministry of Natural Resources Wildlife Scientific Collector's Authorization Permit (#1097498 issued to Dr. Diane Orihel). The transfer of wood frog tissues and skin swabs, as well as water filters to Dr. Barbara Katzenback at the University of Waterloo was approved by the University of Waterloo Animal Care Committee (Animal Tissue Utilization Protocol #43235).

2.1.2 Outdoor Mesocosm Exposure Experiment

To replicate "real-life" conditions, a mesocosm experiment was performed in 2021 at the Queen's Experimental Ecology and Ecotoxicology Living Laboratory (44º 31' 43" N, 76º 22' 54" W), located at the Queen's University Biological Station (QUBS). The experiment was led by S. Gene and Dr. D. Orihel of the QE3 research group. Due to the COVID-19 pandemic, I, J. Drew Thompson was unable to travel to QUBS to participate in the mesocosm experiment. Therefore, all procedures at QUBS were performed by S. Gene or other members of the QE3 group.

2.1.2.1 Overview of Experimental Setup

The exposure study took place in three phases. Phase I ran from April 9 to April 17 and involved rearing eggs in microcosms through hatching to Gosner stage (GS) 24 (Gosner, 1960), at which point the tadpoles were transferred to mesocosms. GS 24 tadpoles are

identified by the atrophy of external gills and development of the operculum. Phase II ran from April 18 to June 12, when tadpoles reached GS 40, during which weekly sampling was performed. GS 40 tadpoles are identified by the appearance of metatarsal and subarticular tubercles on the hindlimbs. Phase III ran from June 13 until the completion of the experiment on July 14, when all animals had reached GS 45, when just a tail stub remains, or GS 46, when metamorphosis has completed.

Three treatments were utilized in the experiment, a negative control or 0× treatment of 0 g/L of microplastics and two microplastic treatments, a 1× treatment of 0.069 g/L and a 10× treatment of 0.691 g/L (Table 2.1). Micro- and mesocosms were divided into two sets, A and B. Set A initially had quintuplicate mesocosms for each experimental condition, however, following a cold weather event on April 27, 2021, mortalities were noted in three mesocosms along the edge of the water bath they were contained in. As each of these mesocosms was from a different treatment group, the decision was made to drop these mesocosms from the experiment and reduce to quadruplicate mesocosms for each treatment. Set A mesocosms were intended for sampling larvae throughout their development. Therefore, animals were removed from the mesocosms as the experiment progressed. Set B mesocosms were mainly intended for assessing the potential for developing amphibians to act as bio-vectors transporting microplastics from the aquatic to terrestrial environment. Therefore, animals in the Set B mesocosms were not sampled throughout development, and were only removed from the experiment upon reaching metamorphic climax at GS 46. Set B was also used to collect post-metamorphic samples for other non-bio-vector analyses. Set B contained a single mesocosm for the 0× treatment and a single mesocosm for the 10× treatment and did not contain any 1× treatment mesocosms. See Figure 2.1 for a schematic of the mesocosm experimental setup. The experiment was conducted in a gated facility, and wire mesh frames and exclusion netting were utilized throughout the experiment to prevent predation.

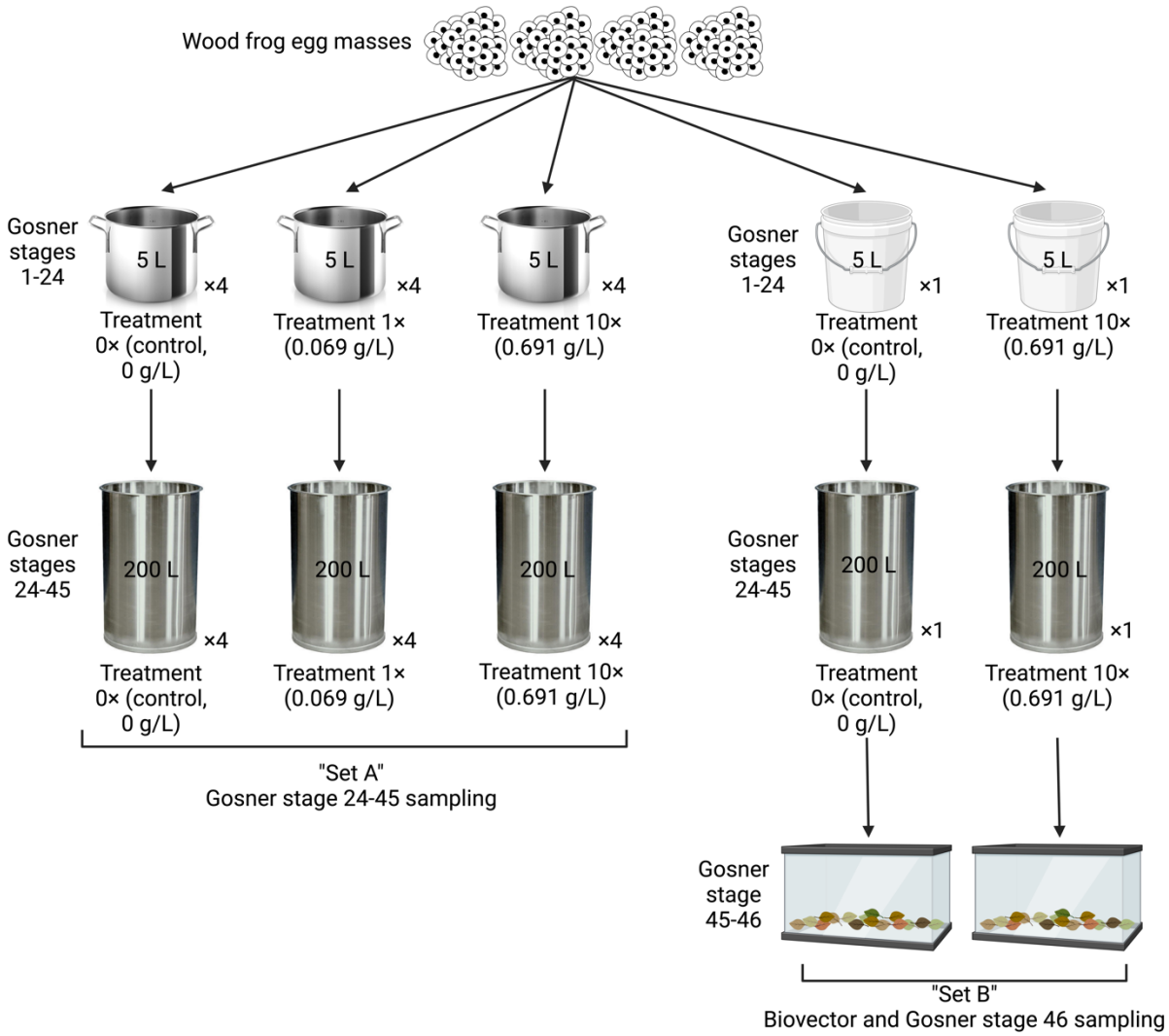


Figure 2.1. Schematic of the experimental setup used to expose developing North American wood frogs to a microplastics mixture in outdoor mesocosms from eggs until the completion of metamorphosis.

Fertilized North American wood frog eggs were collected and divided equally into steel (Set A), or polyethylene (Set B) buckets (microcosms) filled with 5 L of filtered lake water containing either 0, 0.069, or 0.691 g/L of a microplastics mixture consisting of equal parts polypropylene, polystyrene, and polyethylene terephthalate microplastics. Eggs were reared to hatching and tadpoles allowed to develop to Gosner stage 24, at which point they were moved into large steel mesocosms containing 200 L of filtered lake water and a corresponding concentration of microplastics. When metamorphs approached Gosner stage 42, a floating platform constructed from a stainless steel dog bowl, copper wire, sieved soil, and leaf litter was added to mesocosms to allow metamorphs to emerge from the water. Set A was intended for sampling during development, and therefore animals were removed from the mesocosms as the experiment progressed, until all were removed when they reached Gosner stage 45. Set

B was intended for assessing developing amphibians as a bio-vector for transporting microplastics from the aquatic to terrestrial environment. Therefore, Set B animals remained in the mesocosms for the duration of the experiment until they reached Gosner stage 45, when they were transferred to terrestrial enclosures containing soil, leaf litter, and a water dish. Set A consisted of quadruplicate mesocosms, while Set B consisted of one mesocosm for the 0× condition and one mesocosm for the 10× condition. Figure created with BioRender.com.

Table 2.1. Experimental microplastic treatments used in this study.

Treatment	Mass concentration (g/L)	Measured particle concentration (particles/L, mean ± standard error)
0×, control	0	0 ± 0
1×	0.069	$1.94 \times 10^4 \pm 2.16 \times 10^3$
10×	0.691	$1.53 \times 10^5 \pm 2.34 \times 10^4$

Particle concentrations reported in (Gene et al., n.d.) from filtered water samples collected from each mesocosm after the addition of microplastics.

2.1.2.2 Microplastics Mixture

The microplastics mixture included an equal number of polypropylene (PP), polystyrene (PS), and polyethylene terephthalate (PET) particles by count. These polymers were selected due to their prevalence in the environment and their different buoyancy properties. The plastics were additive-containing and colour-coded. PP was yellow and is positively buoyant, PS was pink and neutrally buoyant, and PET was blue and negatively buoyant. Plastics were manufactured by Techmer PM (Batvia, Illinois, USA) according to the specifications in Table 2.2 and ground into fragments with a toll grinder under liquid nitrogen by Custom Processing Service (Reading, Pennsylvania, USA). The plastics had a size range of 40 – 1450 μm (longest dimension) as assessed by Custom Processing Service.

Table 2.2. Formulations of the plastics used in this study.

Percentage	Compound	CAS Number
	Polypropylene	
	Yellow, positively buoyant	
99.55	Polypropylene resin	9003-07-0
0.25	Bismuth Vanadate pigment	14059-33-7
0.05	Chimassorb 944 HALS UV	70624-18-9
0.05	Tinuvin 622 HALS UV	65447-77-0
0.05	Benzotriazole – Acetostab 236	3896-11-5
0.025	Irganox B215 Antioxidant	6683-19-8
0.025	Irganox 168 Antioxidant	31570-04-4
	Polystyrene	
	Pink, neutrally buoyant	
99.6	Polystyrene resin	9003-53-6
0.15	Titanium Dioxide	13463-67-7
0.1	Irgafos 126 Antioxidant	27676-62-6
0.1	N,N Ethylene Bis-stearamide	110-30-5
0.05	Perylene Red	3089-17-6
	Polyethylene terephthalate	
	Blue, negatively buoyant	
99.4	Polyethylene terephthalate resin	25038-59-9
0.35	25u Rutile White	13463-67-7
0.25	Ultramarine Blue Red Shade	57455-37-5

2.1.2.3 Phase I: Collection and Rearing of Wood Frog Eggs for Microplastic Exposure Experiment

The experiment began in small microcosms where eggs were hatched, and tadpoles were allowed to develop to GS 24. There were seventeen microcosms total, fifteen constructed from stainless steel (15 L, 26 cm in diameter, 28.5 cm in height) designated to Set A, and two constructed from polyethylene buckets (19L, 31 cm in diameter) designated to Set B. Microcosms were filled with five litres of lake water filtered through a 52 μm sieve. Quintuplicate Set A microcosms were dosed with either the 0×, 1×, or 10× treatment (Figure 2.1) and single Set B microcosms were dosed with either the 0× or 10× treatment (Figure 2.1). Microcosms were aerated and placed in an outdoor water bath to regulate temperature. On April 9, 2021, four fertilized *R. sylvatica* egg masses were collected from Skycroft Ponds (44º 33' 0.31" N, 76º 21' 41.34" W), located near QUBS. The egg masses were transported to the experimental facility in an insulated cooler, then divided with sterile scissors and evenly distributed into microcosms to ensure genetic diversity in each microcosm. Microcosms were monitored daily for hatchlings and dead eggs. Feeding and monitoring of environmental properties did not occur during this phase.

2.1.2.4 Phase II and III: Setup of Mesocosms for Microplastic Exposure Experiment

While Phase I was underway, larger mesocosms were set up. These were 300 L steel tanks (67 cm in diameter, 94 cm in height) filled with 200 L of lake water filtered through a 52 μm sieve. Once tadpoles reached GS 24, they were transferred into larger mesocosms. Fifteen mesocosms were designated as "Set A" and quintuplicate mesocosms dosed with each treatment (Table 2.1), for an initial total of five replicate mesocosms per treatment, though mortalities in 0× treatment mesocosm 3, 1× treatment mesocosm 2, and 10× treatment mesocosm 2 following a cold weather event on April 27, 2021 resulted in these mesocosms being removed from the study, resulting in quadruplicate Set A mesocosms per treatment. Two mesocosms were designated at "Set B" and dosed with either the 0× or 10× treatment. Mesocosms were held in a water bath to regulate temperature, aerated, and covered with steel mesh. As Set B frogs reached GS 44 – 45, they were transferred from the mesocosms into

shaded terrestrial enclosures constructed from clear Rubbermaid containers containing soil, leaf litter, and a bowl of water with a rock platform, where they remained until GS 46, when skin swabs and tissues were collected for microbiome, transcriptome, and microplastic accumulation analysis. No analyses of Set B samples are reported in this thesis.

On April 17, 2021, when tadpoles had reached the free-feeding stage (GS 24), they were transferred from microcosms to a mesocosm with a corresponding concentration of microplastics. Twenty-four tadpoles were transferred into each Set A mesocosm, while thirty were transferred into each Set B mesocosm. Tadpoles fed on a diet of biofilm and tank debris, supplemented by *ad libitum* addition of crushed commercial tadpole food (Thrive Frog, Newt & Tadpole Diet). Daily monitoring for mortalities and signs of disease occurred throughout the mesocosm experiment. Daily monitoring of dissolved oxygen, percent oxygen saturation, water temperature, conductivity, pH, and salinity occurred throughout the experiment, while ammonia was measured every other day. These measurements were taken with a Hach dissolved oxygen probe (model HQ40d) and a Hanna pH meter (model H198129). Surface water temperature and light intensity were measured throughout the day using twenty-four-hour HOBO© Pendant monitors (model MX2202). When metamorphs began to reach GS 42, a platform constructed from a stainless-steel dog bowl, copper wire, sieved soil, and leaf litter was added to each mesocosm. Sticks were attached to the side of platforms to act as a ramp to allow metamorphs to emerge from the water.

2.1.2.5 Overview of Animal Handling

As multiple research groups were receiving data from the mesocosm experiment, additional handling of animals was performed in addition to the sampling described in Sections 2.1.2.6 – 2.1.2.7. A summary of all handling is described here, while the sampling for this thesis is described in detail in the proceeding sections. Tadpoles were not handled during Phase I until they were transferred to mesocosms. During Phase II, all Set A tadpoles were removed from the mesocosms once weekly to be photographed for assessment of growth and development. Two tadpoles per Set A mesocosm were removed from the experiment and euthanized each week. On May 28, three tadpoles were temporarily removed

from each Set A mesocosm to undergo behavioural testing. On June 6, three tadpoles (GS 36 – 41) were removed from each Set A mesocosm and swabbed before being returned to the mesocosms. Once the experiment progressed to Phase III, all Set A metamorphs were removed from the mesocosms daily for the collection of photographs to assess growth and development. Lethal sampling of one metamorph from each Set A mesocosm occurred on June 22 (GS 40 – 45). As Set A metamorphs reached Gosner stage 45, they were swabbed (Section 2.1.2.7) for microbiome analysis (not reported in this thesis), and tissues collected for transcriptomic (Sections 2.1.2.6, 2.1.3 – 2.1.10) or microplastic accumulation (reported in Gene et al., n.d.) analyses. After Set B metamorphs were transferred to terrestrial enclosures, they were not handled until completion of the experiment on July 14 (GS 46), when they were swabbed (Section 2.1.2.7) for microbiome analysis (not reported), and tissues collected (Section 2.1.2.6) for transcriptomic (not reported) and microplastic accumulation (not reported) analyses.

2.1.2.6 Sampling of Tissues

Once a week during Phase II, one tadpole was removed from each Set A mesocosm, anesthetized in a bath of 0.01% m/v tricaine methanesulphonate (MS-222), buffered with sodium bicarbonate in water for 10 min, then euthanized in a bath of 0.2% buffered MS-222 for 15 min. Tadpole abdomens were opened with flame-sterilized scissors and the whole tadpole submerged in 5 mL of RNAlater (Sigma, cat. no. R0901) in a nuclease-free 15 mL conical tube (FroggaBio, cat. no. TB15-500). Abdomens were opened to allow the RNAlater to fully saturate all tissues. The first occurrence of this weekly sampling was on April 24 and the last was on June 5, for a total of seven weekly samplings.

During Phase III, on June 22 when metamorphs were at an approximate average GS of 42, an additional whole-body sampling of one metamorph from each Set A mesocosm occurred according to the above procedure. As Set A metamorphs reached Gosner stage 45 (June 24 – July 9), they were removed from their mesocosm tank, anesthetized and euthanized as above, and the dorsal and ventral skin, gastrointestinal tract, liver, and spleen dissected in the field using sterile tools and preserved in 0.5 mL of RNAlater contained in a

nuclease-free 1.5 mL microcentrifuge tube (VWR, cat. no. 89000-028). Tissues from three metamorphs per Set A tank were collected in this manner. These GS 45 metamorphs were swabbed (Section 2.1.2.7) prior to collection of tissues, except for the following individuals: (1) 0× treatment, mesocosm 2, replicate c; (2) 10× treatment, mesocosm 1, replicate c; and (3) 10× treatment, mesocosm 4, replicate a.

In Phase III, on July 14, once all Set B animals had reached Gosner stage 46, four froglets from each treatment were euthanized as above, the dorsal and ventral sides of the skin swabbed (Section 2.1.2.7) prior to tissue collection, and the dorsal skin, ventral skin, gastrointestinal tract, liver, and spleen dissected and preserved in 0.5 mL of RNAlater contained in a nuclease-free 1.5 mL microcentrifuge tube.

All tissue samples were stored at -20 ℃ at QUBS. Samples were transported to the University of Waterloo on dry ice and upon receipt on August 24, 2021, stored at -80 ℃.

2.1.2.7 Collection of Skin Swabs and Water Filters

Although the methodology for collection of skin swabs and water samples is reported here for completeness, their analysis is not reported in this thesis. Sampling for commensal skin microbiota from Set A mesocosms occurred in Phases II and III. In Phase II, on June 6 (Gosner stages 36 – 41), three animals from each Set A mesocosm were swabbed. In phase III, Set A metamorphs were swabbed when they reached Gosner stage 45 (June 24 – July 2, 2021) until swabs had been collected from three animals per mesocosm. To collect the resident skin associated microbiota, an individual was captured and rinsed with sterile deionized water to remove transient microbes. Next the dorsal surface, both sides of the individual, and the area surrounding the mouthparts was swabbed twelve times with a sterile rayon-tipped applicator (Puritan, cat. no. 25-806). The tip of the applicator was cut into a nuclease-free 1.5 mL microcentrifuge tube (VWR, cat. no. 89000-028) using flame-sterilized scissors. To control for microbes present in the air at the time of swabbing, two field air blanks were collected by moistening a sterile rayon tip applicator with sterile deionized water and mimicking the swabbing motion in the air. For the first Set A timepoint, one field blank

was collected at the start of swabbing, and one at the end of swabbing. For the second Set A timepoint, one field blank was collected on the first swabbing day (June 24, 2021) and a second on the final swabbing day (July 2, 2021). In addition to the collection of swabs, a water sample was collected from each Set A mesocosm tank during the Phase II swabbing event. A sterile 60 mL syringe (VWR, cat. no. 76124-656) was used to collect 50 mL of water from a mesocosm tank which was then filtered through a 0.22 μm Sterivex GP filter (MilliporeSigma, cat. no SVGP01050, lot no. 1818/08234). The same syringe was then used to pass 50 mL of air through the filter to remove residual water. Each filter was placed into a sterile, nuclease-free 50 mL conical tube (FroggaBio, cat. no. TB50-500).

Set B animals were swabbed on July 14, when all were at Gosner stage 46. Six froglets from the Set B 0× treatment and eight from the Set B 10× treatment were swabbed according to the above procedure. Field blanks were not collected for the Set B samples. Water samples were not collected during swabbing of GS 45 and 46 froglets because they had moved to a terrestrial environment.

Skin swabs and water filters were stored at -20 ℃ at QUBS. Samples were transported to the University of Waterloo on dry ice and upon receipt on August 24, 2021, stored at -80 ℃.

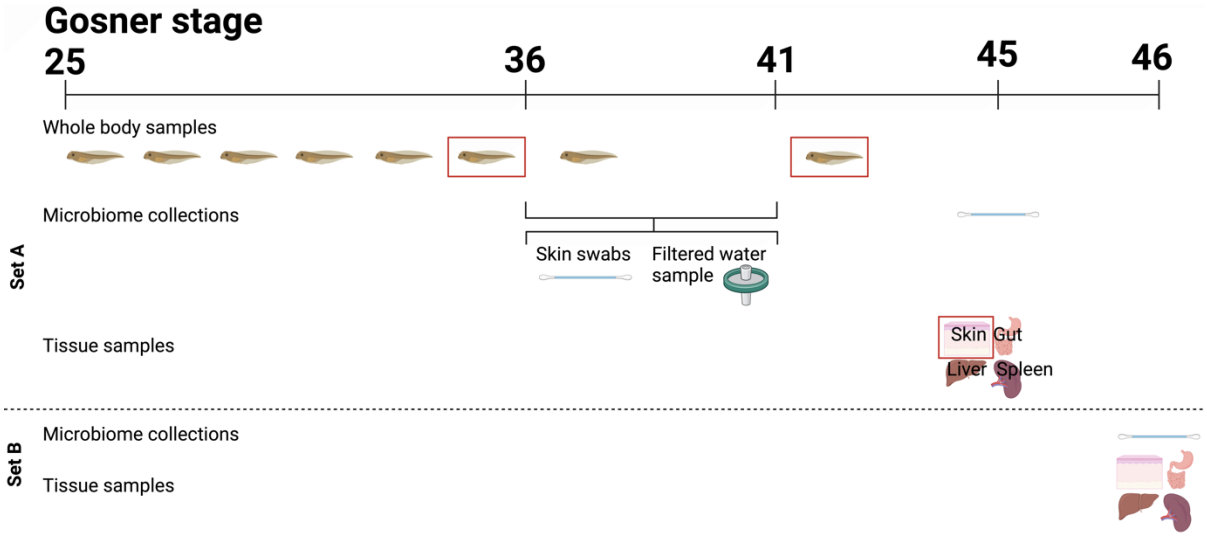


Figure 2.2. Schematic of samples collected from a mesocosm experiment exposing developing North American wood frogs to a microplastics mixture.
Once a week for seven weeks after tadpoles were introduced to the large mesocosms at Gosner stage 24, one tadpole was removed from each Set A mesocosm, euthanized, and preserved in RNAlater. When metamorphs were all at approximately Gosner stage 42, one metamorph was removed from each Set A mesocosm, euthanized, and preserved in RNAlater. As Set A animals reached Gosner stage 45, they were euthanized and the dorsal skin, ventral skin, gut, liver, and spleen collected and preserved in RNAlater. Skin swabs were collected from three animals per Set A mesocosm at two timepoints: when tadpoles were between Gosner stages 36-41, and when froglets had reached Gosner stage 45. Field blanks were also collected at this time. During the first swabbing timepoint, a 50 mL water sample was also collected from each mesocosm and filtered to capture the microbial community of the mesocosm water. Samples were only collected from Set B animals once they had reached Gosner stage 46. At this point, their skin was swabbed, and they were euthanized before collection of the dorsal skin, ventral skin, gut, liver, and spleen and preservation of tissues in RNAlater. Placement of tadpoles in the figure depict when whole-body samples were collected. Placement of swabs and water filters depict when these samples were collected. Placement of tissue images depict timepoints when these tissues were dissected in the field. Samples outlined in red boxes were analyzed in this thesis. Figure created with BioRender.com.

2.1.3 Samples Used in this Thesis

Three timepoints were selected for RNA extraction and sequencing of the dorsal skin transcriptome. These were tissues collected on May 29 (six weeks after transfer to mesocosm tanks, average GS 34, hereby referred to as GS ~34), June 22 (nine weeks and three days after transfer to mesocosm tanks, GS ~42), and at Gosner stage 45 (June 24 – July 9, nine weeks and five days – eleven weeks and six days after transfer to mesocosm tanks, GS 45) (Table 2.3). Because GS ~34 and GS ~42 collections only contained a single animal from each mesocosm, RNA was isolated from all samples from these timepoints. Because three samples were collected from each mesocosm at GS 45, a random number generator (random.org) was used to select a GS 45 replicate dorsal skin sample to isolate RNA from. The selected GS 45 samples were collected between June 24 – June 30, 2021 (nine weeks and five days to ten weeks and four days after transfer to mesocosm tanks). Therefore, RNA was extracted from four biological replicates per treatment at each timepoint.

2.1.4 RNA Extraction

Whole body samples stored in RNAlater were thawed on ice and dissected under an Optika SZN-2 stereoscope using sterile dissection tools. To prevent RNA degradation, tissues were kept submerged in RNAlater in a petri dish throughout dissection. As tissues were removed, excess RNAlater was removed by blotting on a clean Kimwipe (Kimberly-Clark Professional, cat. no 34155, vendor: Fisher Scientific, cat. no. 06-666-2), placed in a new 1.5 mL microcentrifuge tube, flash frozen in liquid nitrogen, and stored at -80 ℃. Tissues from GS 45 animals which were dissected in the field and stored in RNAlater were thawed on ice, blotted dry on a clean Kimwipe, moved to a fresh microcentrifuge tube, flash frozen in liquid nitrogen, and stored at -80 ℃.

RNA was extracted using TRI Reagent (Sigma, cat. no. T9424) following a modified version of the manufacturer's protocol. Briefly, samples were removed from the freezer and 500 µL of TRI Reagent was added to each tube. Tissues were homogenized by repeated passage through 18-, 21-, and 25-gauge needles (Air-Tite, cat nos. N18112,

N21112, N25112) attached to a 1 mL syringe (Air-Tite, cat. no. MS1), and allowed to incubate on ice for 5 min. Next, 100 µL of chloroform (Fisher Scientific, cat. no. C298-4, lot no. 164411) was added and tubes were mixed by vigorous shaking for 15 s. Following a 15 min incubation on ice, samples were centrifuged at 2 ℃ for 15 min at 12,000 × *g*. The resulting upper aqueous phase was transferred to a new 1.5 mL microcentrifuge tube and 250 µL of isopropanol was added. This was mixed by inversion and kept on ice for 15 min to allow RNA to precipitate. Samples were centrifuged at 2 ℃ for 10 min at 12,000 × *g* to pellet RNA. Pellets were washed five times by removing the supernatant, adding 750 µL of 75% ethanol, vortexing for 5 s, and centrifuging at 2 ℃ for 5 min at 7,500 × *g*. Following the final wash, the supernatant was removed, and the pellet was air-dried for 15 min under a Bunsen burner. Pellets were resuspended in 30 µL of nuclease-free water by heating at 55 ℃ for 10 min. Nucleic acid concentration, and A260/280 and A260/230 ratios were measured using a Cytation5 Multimode Reader (BioTek) with the Take3 Trio accessory (BioTek). Highly concentrated GS 45 extractions were diluted with nuclease-free water and re-quantified to obtain reliable measurements.

To improve the purity of select samples that did not meet A260/280 and A260/230 thresholds, GS ~34 samples from 0× treatment mesocosm 5, 1× treatment mesocosm 4, and 1× treatment mesocosm 5 underwent ethanol precipitation. First, 0.1 volumes of 3 M sodium acetate, pH 5.2 was added to the sample and mixed via inversion. Next, 3 volumes of 100% ethanol were added and mixed by gently vortexing. Samples were incubated at -20 ℃ overnight to facilitate RNA precipitation. RNA was pelleted by centrifugation at 2 ℃ for 30 min at 12,000 × *g*. The supernatant was removed, and the pellet washed twice by adding 1 mL of 75% ethanol, vortexing briefly, then centrifuging at 2 ℃ for 10 min at 12,000 × *g*. After the final wash, the supernatant was removed, and the pellet was air-dried for 10 min followed by the addition of 25 µL of nuclease-free water and incubation on ice for 60 min to ensure complete resuspension prior to reanalysis of A260/280 and A260/230 ratios. Rather than molecular-grade 75% ethanol, non-molecular grade 75% ethanol that had previously been used to sterilize dissection tools was mistakenly used in the wash steps. After assessing

RNA quality, integrity, and RNA-seq read quality metrics and transcriptional profiles, it was decided to include these ethanol-precipitated samples in the analysis (see Section 3.1.5 for discussion of this point). However, the GS ~34 sample from 1× treatment mesocosm 5 was excluded due to low RNA yield.

All total RNA samples were stored at -80 °C. To prepare for sequencing, 27 µL aliquots were prepared at 28 ng/µL, with two microlitres being used to quantify the aliquots and the remaining 25 µL used for sequencing.

2.1.5 RNA Sequencing

Samples from three developmental timepoints, GS ~34, GS ~42, and GS 45 were selected for RNA sequencing (Table 2.3). Four RNA samples were isolated per microplastic treatment (0×, 1×, 10×), however, GS ~34 samples from 1× treatment mesocosm 5 and 10× treatment mesocosm 1 were excluded from sequencing due to insufficient RNA yield. As a result, 34 samples were sent to The Centre for Applied Genomics, part of the Hospital for Sick Children (Toronto, Ontario, Canada) where RNA integrity was assessed with a Bioanalyzer (Aligent) (Figure A.1) and mRNA enrichment and library preparation was performed with a NEBNext Ultra II Directional RNA Library Prep Kit for Illumina (NEB). Paired-end 150 base pair sequencing was performed on one lane of a NovaSeq 6000 S4 flowcell.

Table 2.3. Information on total RNA extracted from the dorsal skin of wood frogs exposed to varying concentrations of a microplastics mixture throughout development.

Timepoint	Treatment	Mesocosm	Replicate	Gosner stage	A260/280	A260/230	Concentration (ng/µL)	RIN	DV200	Sequenced?
GS ~34	0×	1	-	34	1.93	1.8	19.3	10	85	Y
GS ~34	0×	2	-	34	1.905	2.127	22.7	8.3	81	Y
GS ~34	0×	4	-	31	2.029	2.022	15	10	90	Y
†GS ~34	0×	5	-	35	2.033	1.903	31	9.9	83	Y
GS ~34	1×	1	-	33	1.832	2.257	18.7	8.5	85	Y
GS ~34	1×	3	-	33	1.874	2.32	12.7	10	89	Y
†GS ~34	1×	4	-	35	2.028	2.131	20.7	8.2	89	Y
†GS ~34	1×	5	-	33	2.067	1.572	20.4	-	-	N
GS ~34	10×	1	-	33	2.204	0.121	4.3	-	-	N
GS ~34	10×	3	-	34	1.921	2.131	14	10	88	Y
GS ~34	10×	4	-	33	1.926	2.089	21.3	9.7	84	Y
GS ~34	10×	5	-	34	1.921	1.973	22	10	83	Y
GS ~42	0×	1	-	41	1.914	2.205	14	10	90	Y
GS ~42	0×	2	-	43	1.929	2.216	22	10	85	Y
*GS ~42	0×	4	-	45	1.945	1.787	20.7	7.7	54	Y
GS ~42	0×	5	-	40	1.963	2.031	19.3	9.1	86	Y
GS ~42	1×	1	-	42	1.956	1.97	11.3	10	86	Y
GS ~42	1×	3	-	44	1.937	2.227	13.3	2.4	46	Y
GS ~42	1×	4	-	41	1.919	2.266	8	10	89	Y
GS ~42	1×	5	-	42	1.96	1.836	14.7	10	90	Y
GS ~42	10×	1	-	43	1.959	2.221	20	9.6	85	Y
GS ~42	10×	3	-	44	1.981	2.097	13.3	9.9	82	Y
GS ~42	10×	4	-	41	1.845	2.432	16.7	9.6	85	Y

Timepoint	Treatment	Mesocosm	Replicate	Gosner stage	A260/280	A260/230	Concentration (ng/µL)	RIN	DV200	Sequenced?
GS ~42	10×	5	-	40	1.887	2.184	17.3	9.9	84	Y
GS 45	0×	1	B	45	1.975	2.147	14.7	9.8	81	Y
GS 45	0×	2	C	45	1.919	2.41	16.7	9.4	80	Y
GS 45	0×	4	B	45	2.059	2.01	18	9.5	86	Y
GS 45	0×	5	B	45	1.894	2.399	17.3	9.7	86	Y
GS 45	1×	1	B	45	1.959	2.286	12	8.1	79	Y
GS 45	1×	3	A	45	2.026	2.224	14	10	84	Y
GS 45	1×	4	B	45	1.922	2.429	12	10	84	Y
GS 45	1×	5	A	45	1.921	2.277	14	9.8	84	Y
GS 45	10×	1	C	45	2.017	1.604	17.3	9.8	82	Y
GS 45	10×	3	B	45	1.916	2.326	15.3	9.2	84	Y
GS 45	10×	4	A	45	1.952	2.396	20.7	9	82	Y
GS 45	10×	5	B	45	1.903	2.467	19.3	9.4	80	Y

RNA was extracted from thirty-six dorsal skin samples from developing wood frogs exposed to a 0× (0 g/L), 1× (0.069 g/L), or 10× (0.691 g/L) microplastic treatment. This table provides information on these samples including the sampling timepoint, treatment, Gosner stage (GS), A260/280 and A260/230 absorbance ratios of these samples, as well as RNA concentration, RNA integrity number (RIN), and DV200 (the percentage of fragments > 200 bp) as reported by the sequencing centre Bioanalyzer (Aligent) (Figure A.1). The sample denoted by the asterisk (*) was collected with GS ~42 samples, but was at GS 45, and was therefore analyzed with the other GS 45 samples. The samples denoted by a dagger (†) underwent ethanol-precipitation to improve quality for sequencing. For samples which were not sequenced, the reported concentration was measured with the Cytation5 (BioTek).

2.1.6 Quality Filtering of RNA-seq Reads

FastQC v0.12.0 (Andrews, 2010) and MultiQC v1.13 (Ewels et al., 2016) were used to monitor quality metrics including sequence quality, sequence content, N content, length distributions, duplication levels, overrepresented sequences, and adapter content throughout quality control. FastQC was provided the NEBNext adaptor sequences: AGATCGGAAGAGCACACGTCTGAACTCCAGTCA and AGATCGGAAGAGCGTCGTGTAGGGAAAGAGTGT. Rcorrector v1.0.6 (Song & Florea, 2015) was used for k-mer based error correction with default settings. To remove reads which Rcorrector deemed erroneous through its *k*-mer analysis algorithm, but was unable to correct, the FilterUncorrectabledPEfastq.py script provided by the Harvard Informatics Group (https://github.com/harvardinformatics/TranscriptomeAssemblyTools) was used. Next, fastp v0.23.4 (Chen, 2023) was used to trim the above adaptor sequences, remove leading and trailing bases with a quality score less than 20, move a sliding window of 4 bases from left to right and drop any bases before any window with an average quality less than 20, trim poly-G and -X sequences, remove any N-containing reads or reads with 10% of bases having quality scores less than 20, and drop any remaining reads with length less than 36 bases. Finally, RiboDetector v0.2.7 (Deng et al., 2022) with Python v3.9.6 was used to filter out residual reads classified as rRNA. Paired reads which passed these quality control steps were used for downstream analysis. These steps were conducted on the Digital Research Alliance of Canada (alliancecan.ca) Graham compute cluster (sharcnet.ca). See Figure 2.3 for a summary schematic of the bioinformatics workflow.

2.1.7 Reference-Guided Assembly and Abundance Estimation

Filtered paired reads from Section 2.1.6 were aligned to the *R. sylvatica* genome (GenBank accession GCA_028564925.1) using HISAT2 v2.2.1 (Kim et al., 2019) with the following optional parameters: [--rna-strandedness RF --dta]. RF represents the type of stranded RNA-seq library preparation protocol utilized, while --dta is used when the alignment will be input to an assembler. HISAT2 output was piped through SAMtools v1.17

(Danecek et al., 2021) to produce sorted BAM files. Per-sample BAM files were assembled independently using StringTie v2.2.1 (Kovaka et al., 2019) with the following optional parameter: [--rf]. To generate a set of non-redundant transcripts, StringTie was used in merge mode [--merge] again with the parameter [--rf]. The GffRead program (v0.12.7) (Pertea & Pertea, 2020) was used to obtain the sequences of the resulting transcripts in FASTA format. To estimate transcript abundances and generate read coverage tables, StringTie was run once more for each sample with the options [-B -e] (these indicate to StringTie to estimate the transcript abundances) as well as the [--rf] parameter, providing the assembled transcripts with the [-G] parameter. The prepDE.py3 script bundled with StringTie was used with Python v3.10.2 and provided the optional parameter [-l 148] (average read length) to generate a count matrix for use with DESeq2. TransRate v1.0.3 (Smith-Unna et al., 2016) was used to calculate the transcriptome N50 value. These steps were conducted on the Digital Research Alliance of Canada (alliancecan.ca) Graham compute cluster (sharcnet.ca).

2.1.8 Transcriptome Annotation

TransDecoder v5.7.1 (Haas, 2023) was used to predict coding regions in assembled transcripts. First, TransDecoder.LongOrfs was run with the [-S] parameter for stranded RNA-seq data, and [-m 50] to set the minimum CDS length to 50. Next, homology searches were run on the initial FASTA file of all potential coding regions. A BLASTP search was run using the BLAST+ software suite v2.14.0 (Camacho et al., 2009) against the UniRef90 database (retrieved July 20, 2023) (The UniProt Consortium et al., 2023) with an E-value threshold of 1×10^{-5} and [-max_target_seqs 1]. A search against the Pfam database (retrieved September 16, 2023) (Mistry et al., 2021) was performed with HMMER v3.3.2 (Eddy, 2020) with an E-value threshold of 1×10^{-5}. The results of these searches were provided to TransDecoder.Predict with the optional parameter [--single_best_only] to obtain a final set of coding sequences, retaining only the single best predicted candidate coding sequence for each transcript. These steps were conducted on the Digital Research Alliance of Canada (alliancecan.ca) Graham compute cluster (sharcnet.ca).

Trinotate v4.0.1 (Bryant et al., 2017) was used to perform functional annotation of assembled transcripts. It uses multiple softwares to perform annotation: Perl v5.30.2, sqlite v3.38.5, Python 3.10.2, BLAST+ v2.14.0 (Camacho et al., 2009), HMMER v3.3.2 (Eddy, 2020) and the Pfam database (Paysan-Lafosse et al., 2023), Infernal v1.1.4 (Nawrocki & Eddy, 2013) and the Rfam database (Kalvari et al., 2021), TMHMM v2.0c (Krogh et al., 2001), SignalP 6.0 (Teufel et al., 2022), and eggNog-mapper v2.1.12 (Cantalapiedra et al., 2021). Databases, including Swiss-Prot (The UniProt Consortium et al., 2023), were automatically retrieved by Trinotate on August 22, 2023. Trinotate was run on the Digital Research Alliance of Canada (alliancecan.ca) Cedar compute cluster (training.westdri.ca). Additional BLASTP and BLASTX searches of the UniRef90 database (retrieved July 20, 2023) with an E-value threshold of 1×10^{-5} and [-max_target_seqs 1] were performed on the Digital Research Alliance of Canada (alliancecan.ca) Graham compute cluster (sharcnet.ca).

2.1.9 Differential Gene Expression Analysis

All remaining steps were performed on an Intel MacBook Pro running macOS 14.2.1 and using R v4.3.2 (R Core Team, 2023). DESeq2 v1.42.0 (Love et al., 2014) was used to perform differential expression analysis at the gene level using gene expression counts returned by prepDE.py3 (Section 2.1.7). To find genes which had altered expression across development (objective one), pairwise comparisons of 0× (control) tissues across the three sequenced timepoints were performed. To find genes which had altered expression from microplastic exposure (objective two), each microplastic treatment timepoint was analyzed independently against that timepoint's 0× microplastic treatment samples (i.e. 1× versus 0× and 10× versus 0× at each timepoint). GS ~42 sample 0× treatment mesocosm 4 was at Gosner stage 45, and clustered with other GS 45 samples in a PCA (Figure 2.7A) and was therefore analysed with the GS 45 samples. Prior to analysis, counts from each timepoint were filtered to retain only genes with a count of 10 in at least the number of samples in the smallest group at that timepoint (e.g. if n = 3, then retain only genes with a count of 10 in at least 3 samples). Results for each comparison were extracted using default values ($\log_2$ fold change threshold of zero) and an alpha value of 0.05. To filter for biological significance, in

this case a fold change of at least two, only genes with a |$\log_2$ fold change| greater than or equal to one were considered differentially expressed.

2.1.10 Gene Set Enrichment Analysis

Gene set enrichment analysis (GSEA) of GO terms and KEGG pathways was performed with clusterProfiler v4.10.0 (Wu et al., 2021) with a seed value of 629974668 (generated at random.org) set to enable reproducibility of GSEA results. Trinotate was used for GO term assignment from Swiss-Prot BLAST results and KEGG pathway assignment from EggNOG-mapper. These mappings were provided to the GSEA function along with a ranked list of shrunken $\log_2$ fold changes for all genes detected in the experiment as calculated by DESeq2. Shrunken $\log_2$ fold changes were calculated with the apeglm v1.24.0 R package (Zhu et al., 2019), available through convenience functions in the DESeq2 package. These analyses were again performed for each differential expression comparison performed in Section 2.1.9 to determine the effects of development and microplastic treatment on the wood frog dorsal skin transcriptome. The GO.db v3.18.0 (Carlson, 2023) and KEGGREST v1.42.0 (Tenenbaum, 2023) R packages were used to obtain information on the enriched terms and pathways.

2.1.11 Data Analysis and Figure Generation

All data analysis and figure generation was performed with R v3.4.2 (R Core Team, 2023). Histograms and bar charts were plotted with ggplot2 v3.4.4 (Wickham, 2016). Principal components analysis (PCA) and heatmap clustering was performed with gene-level expression count values normalized with the varianceStabilizingTransformation function provided in the DESeq2 v1.42.0 package (Love et al., 2014). PCA was conducted with the plotPCA function in the DESeq2 package and plotted with ggplot2. For heatmap clustering, normalized counts were scaled with the built-in scale function, and plotted with pheatmap v1.0.12 (Kolde, 2019). Venn diagrams were produced with the VennDiagram v1.7.3 R package (Chen, 2022). UpSet plots were produced with the UpSetR v1.4.0 R package (Gehlenborg, 2019). Dotplots were produced with the dotplot function in the enrichplot

v1.22.0 R package (Yu, 2023). Enrichment maps were produced by calculating the Jaccard similarity coefficient between enriched terms with the pairwise_termsin function and plotting with the emapplot function in the enrichplot package. Volcano plots were produced with the EnhancedVolcano v1.20.0 R package (Blighe et al., 2023).

2.1.12 Code and Data Availability

The code used for all analyses in this thesis is available at https://github.com/dthom7/MScThesisCode.git. The output of the R sessionInfo() function from the computer used to generate the data in this thesis is provided in Appendix C. The data presented in this thesis is available upon request.

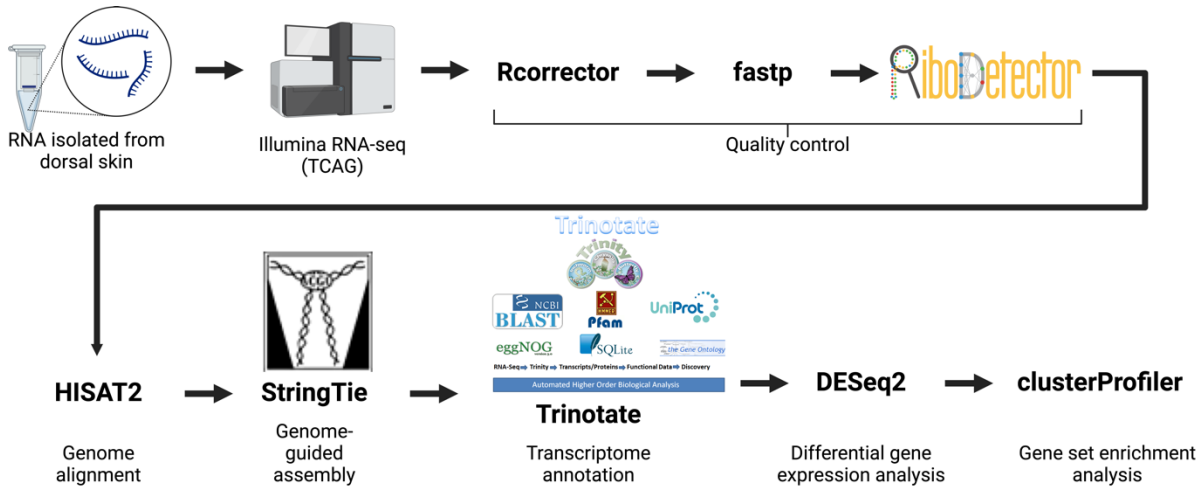


Figure 2.3. Bioinformatics analysis workflow to analyze dorsal skin RNA samples from wood frogs exposed to varying concentrations of a microplastics mixture.
RNA was isolated from dorsal skin of wood frogs exposed to varying concentrations of a microplastics mixture and sent to The Centre for Applied Genomics (Toronto, Ontario, Canada) for library preparation and RNA sequencing. Raw reads were quality filtered with a combination of Rcorrector (Song & Florea, 2015), fastp (Chen, 2023), and RiboDetector (Deng et al., 2022). Filtered paired reads were aligned to the *R. sylvatica* genome (GenBank accession GCA_028564925.1) using HISAT2 (Kim et al., 2019) and assembled with StringTie (Kovaka et al., 2019). StringTie was also used for abundance estimation. Transcripts were annotated with Trinotate (Bryant et al., 2017). DESeq2 (Love et al., 2014) was used to perform differential expression analysis at the gene level, followed by gene set enrichment analysis with clusterProfiler (Wu et al., 2021). Figure created with BioRender.com.

2.2 Results

2.2.1 Study Design and RNA Sample Quality

To emulate a real-world scenario of how exposure to microplastics might affect the transcriptomic regulation of anuran skin function, we conducted a mesocosm experiment consisting of three treatment groups (0×, 1×, 10×) in quadruplicate tanks in which wood frog (*Rana sylvatica*) larvae were continuously exposed to a microplastics mixture from eggs to the penultimate stage of metamorphic climax (Gosner stage 45). To evaluate organism-level effects, our collaborators conducted water quality measurements, evaluated growth and development, and conducted microplastic accumulation analysis. These results are reported in (Gene et al., n.d.). The focus of this thesis chapter is to report the results of a transcriptomic analysis. The first objective was to evaluate changes in the wood frog dorsal skin transcriptome across several developmental timepoints. The second objective was to evaluate the sub-organismal effects of microplastic exposure on developing wood frogs by evaluating how microplastic exposure alters transcription in the dorsal skin.

Sequencing of three developmental stages was targeted: late premetamorphosis (average Gosner stage 34; GS ~34), early metamorphic climax (average Gosner stage 42; GS ~42), and late metamorphic climax (Gosner stage 45; GS 45) (Etkin, 1932) (Figure 2.4A). These targeted Gosner stages corresponded to 50 days, 74 days, or between 74 – 82 days of exposure, respectively, to a microplastics mixture (Figure 2.4B). Initially, RNA was extracted from one individual from each replicate tank per treatment and timepoint (n = 4). However, after quality analysis and control of isolated RNA samples (Table 2.3), two samples were excluded because of insufficient quantity (GS ~34 wood frog in the 0× microplastics mixture exposure group, mesocosm 1 and GS ~34 wood frog in the 1× microplastics mixture exposure group, mesocosm 5). In total, 34 samples met the criteria for RNA sequencing and were sequenced, resulting in a sample size of n = 3 – 5 larvae from different mesocosms per treatment/developmental stage combination.

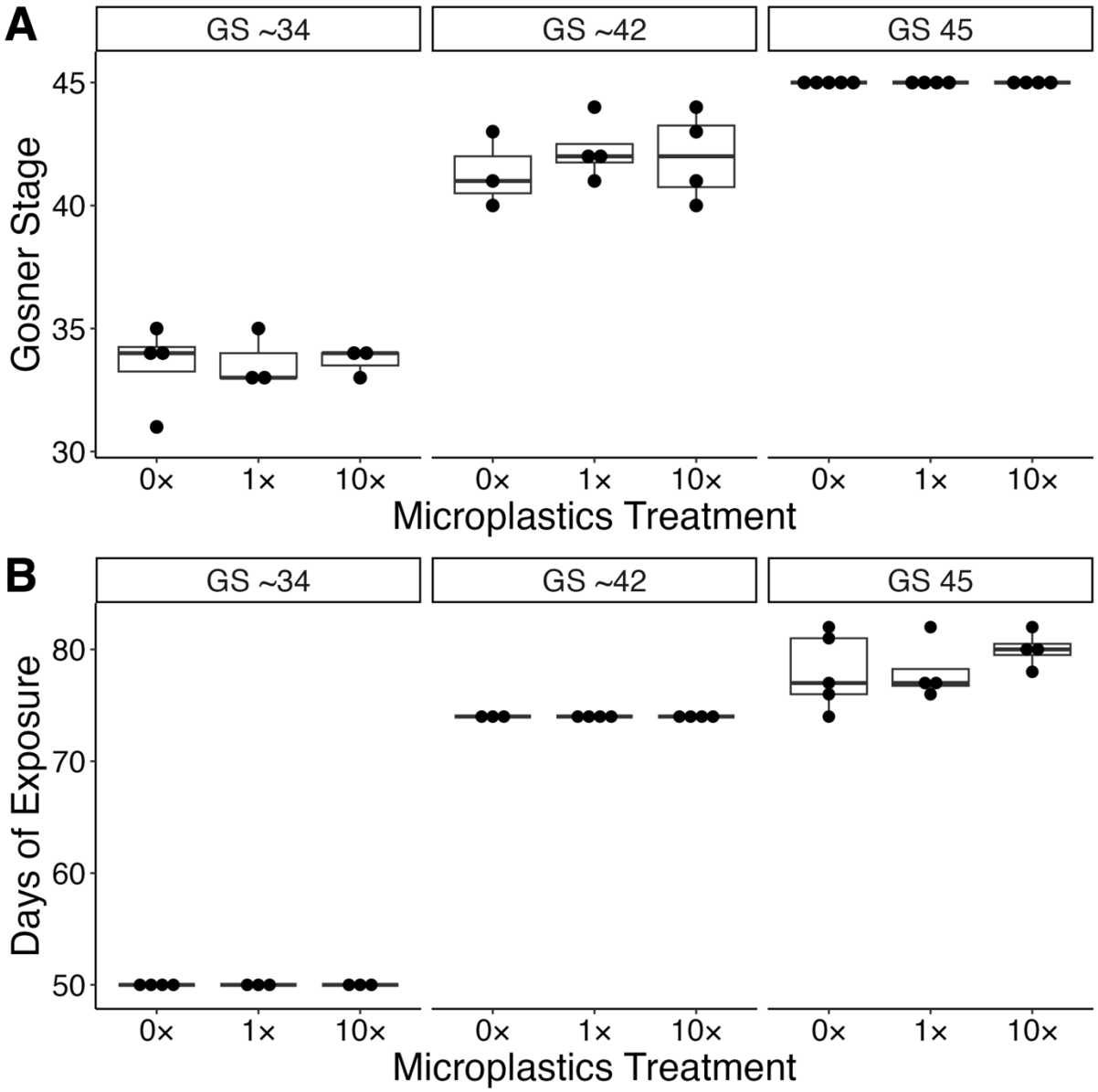


Figure 2.4. Gosner stages and days of exposure of wood frog larvae that were exposed to a microplastics mixture prior to being sampled for use in RNA sequencing of dorsal skin. Wood frog larvae were raised from eggs while exposed to a 0× (control), 1×, or 10× microplastics treatment. Three timepoints were selected to sample dorsal skin for RNA sequencing and the **A)** Gosner stage (GS) and **B)** days of exposure to microplastics of wood frog larvae (n = 3 – 5) at each sampling time point are shown. The first was after 50 days of exposure to microplastics. These larvae had an average Gosner stage of 34 (GS ~34). The second was after 74 days of exposure and had an average Gosner stage of 42 (GS ~42). The final timepoint was at Gosner stage 45 (GS 45) and these samples were collected between 74 and 82 days of exposure.

2.2.2 RNA-seq Quality Control and Reference-Guided Assembly

Because a wood frog reference genome was not available at the time of RNA sequencing, samples were sequenced deeply and a total of over 3 billion paired raw reads were obtained from the sequencing run of 34 dorsal skin samples. The number of paired reads per sample ranged from 70,532,786 to 118,753,411 (Table 2.4). After quality control steps including error correction and removal of uncorrectable reads, low-quality and adaptor sequence removal, and removal of rRNA sequences, a total of over 2.6 billion paired reads remained, with between 61,927,776 and 104,826,643 paired reads per sample (Table 2.4, Figure A.2 – Figure A.7). These reads were aligned to the wood frog genome (GenBank accession GCA_028564925.1) with an overall average alignment rate of 83.24%. Aligned reads were assembled into 96,645 transcripts by StringTie, with the transcripts belonging to 45,926 genes as assigned by StringTie (Table 2.4). The length of assembled transcripts ranged from 200 to 91,419 bases, with a mean length of 2,717 bases (Table 2.4) resulting in a positively skewed distribution of transcript lengths (Figure 2.5).

To functionally annotate assembled transcripts, the single best candidate coding sequence for each transcript was predicted with TransDecoder and the results queried in multiple databases using a combination of Trinotate and custom BLAST (Camacho et al., 2009) searches. A total of 77,223 transcripts contained a predicted candidate coding sequence. These transcripts belonged to 30,524 StringTie-predicted genes (Table 2.4). The shortest predicted candidate coding sequence was 120 bases, and the longest was 89,553 bases, with a mean of 1,374 bases (Table 2.4), resulting in a positively skewed distribution (Figure 2.6) similar to the distribution of transcript lengths. Input to Trinotate included both the assembled transcripts and predicted candidate coding sequences, which were queried against Trinotate's primary database for annotation, the Swiss-Prot database (The UniProt Consortium et al., 2023), a manually curated reference set of proteins. Homology was transferred to assembled transcripts using the BLASTP and BLASTX algorithms. Out of the 77,223 total predicted candidate peptides, 70.3% had a BLASTP hit in the Swiss-Prot database (Table 2.5). Utilizing BLASTX, 56.2% of transcripts had homology to a sequence

in the Swiss-Prot database (Table 2.5). To increase the number of functionally annotated assembled transcripts, queries of additional databases and tools were performed, including UniRef90 (The UniProt Consortium et al., 2023) for additional homology annotations, Rfam (Kalvari et al., 2021) to annotate RNA families, Pfam (Paysan-Lafosse et al., 2023) to annotate protein families, SignalP (Teufel et al., 2022) to detect signal peptides, TmHMM (Krogh et al., 2001) to detect transmembrane domains, and EggNOG (Cantalapiedra et al., 2021), which provides additional functional annotation (Table 2.5). While the successful functional annotation of assembled transcripts varied with the database queried or program/tool used, a total of 77,166 of 96,645, or 79.8% of transcripts received an annotation from at least one database or program (Table 2.5).

Table 2.4. RNA-seq and Transcriptome Summary Statistics.

Minimum raw reads per sample	70,532,786
Mean raw reads per sample	89,648,337
Maximum raw reads per sample	118,753,411
Total raw reads	3,048,043,472
Minimum clean reads per sample	61,927,776
Mean clean reads per sample	78,642,746
Maximum clean reads per sample	104,826,643
Total clean reads	2,673,853,359
Genome overall alignment rate (mean ± s.d.)	83.24% ± 1.90%
StringTie genes	45,926
StringTie transcripts	96,645
Minimum transcript length	200
Mean transcript length	2,717
Maximum transcript length	91,419
N50	4,622
Total number of predicted candidate coding sequences (CDS)	77,223
Transcripts with predicted candidate CDS	77,223
Genes with predicted candidate CDS	30,524
Minimum predicted candidate CDS length	120
Mean predicted candidate CDS length	1,374
Maximum predicted candidate CDS length	89,553

N50: the length of the shortest contig, such that this contig and all contigs larger than it covers 50% of the total transcriptome length. s.d.: standard deviation.

Table 2.5. Transcriptome Annotation Rates.

Database or Program	Polypeptide Candidates	Transcripts	Genes
Swiss-Prot (BLASTP)	54,320 (70.3%)	54,320 (56.2%)	18,631 (40.6%)
Swiss-Prot (BLASTX)	N/A	56,486 (58.4%)	20,264 (44.1%)
UniRef90 (BLASTP)	65,258 (84.5%)	65,258 (67.5%)	24,592 (53.5%)
UniRef90 (BLASTX)	N/A	75,365 (78.0%)	31,049 (67.6%)
Rfam (Infernal)	N/A	450 (0.47%)	226 (0.49%)
Pfam (HMMER)	49,499 (64.1%)	49,499 (51.2%)	16,737 (36.4%)
SignalP	6,059 (7.85%)	6,059 (6.27%)	2,316 (5.04%)
TmHMM	13,763 (17.8%)	13,763 (14.2%)	5,493 (12.0%)
EggNOG	55,323 (71.6%)	55,323 (57.2%)	19,896 (43.3%)
≥ 1 database/tool	70,756 (91.6%)	77,166 (79.8%)	31,854 (69.4%)

The total number of polypeptide candidates, transcript sequences, and genes which received annotations from the listed tools are shown, as well as the percentage of total polypeptide candidates (77,223), transcripts (96,645), or genes (45,926).

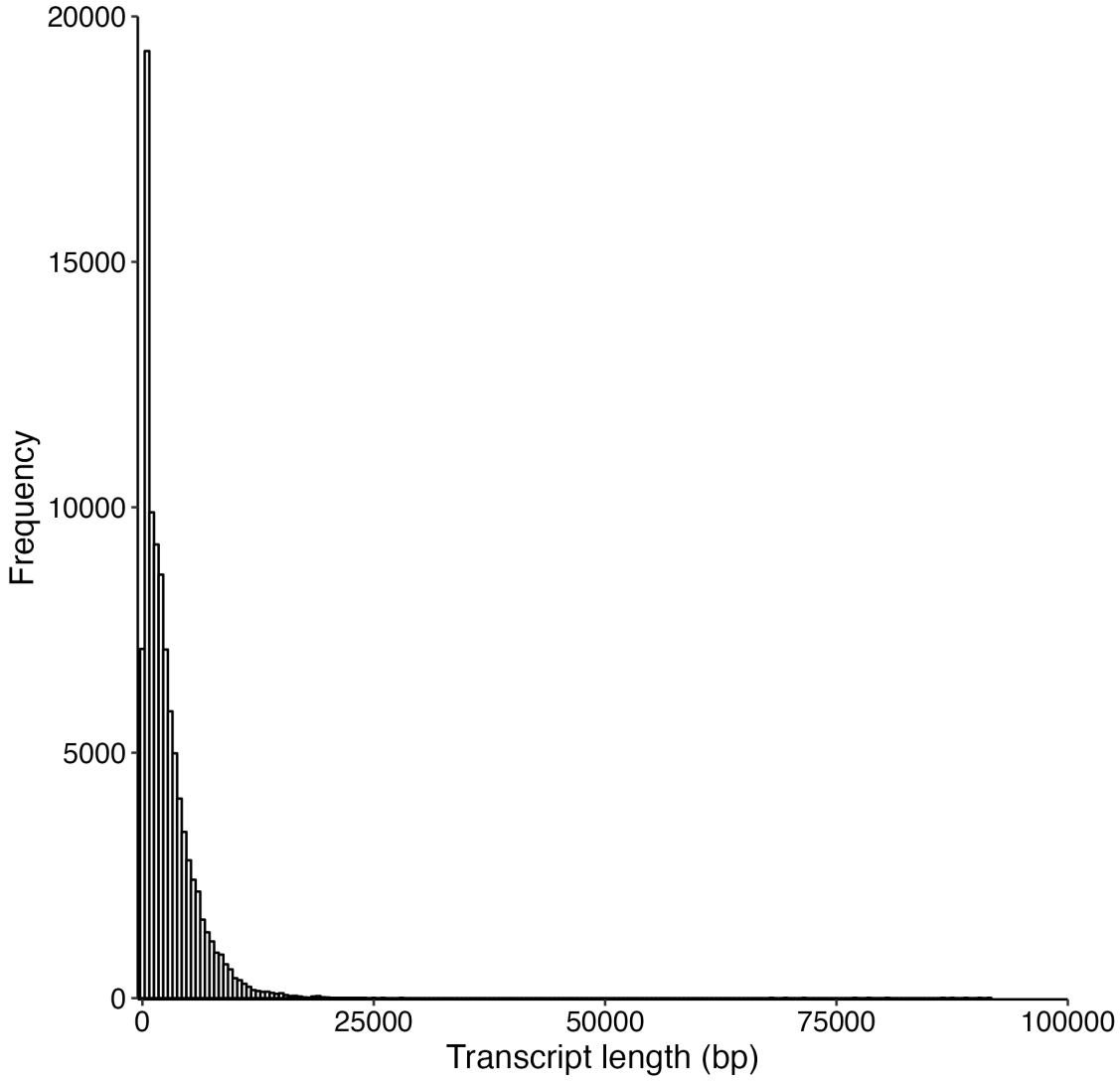


Figure 2.5. Length distribution of StringTie-assembled transcripts.
Quality-controlled RNA-seq reads obtained from the dorsal skin of developing wood frogs were aligned to the *Rana sylvatica* reference genome (GCA_028564925.1) with HISAT2 and assembled into transcripts with StringTie. The lengths of the 96,645 assembled transcripts were plotted with a bin width of 500 bp. The length distribution of StringTie-assembled transcripts demonstrates a positively skewed distribution of transcript lengths.

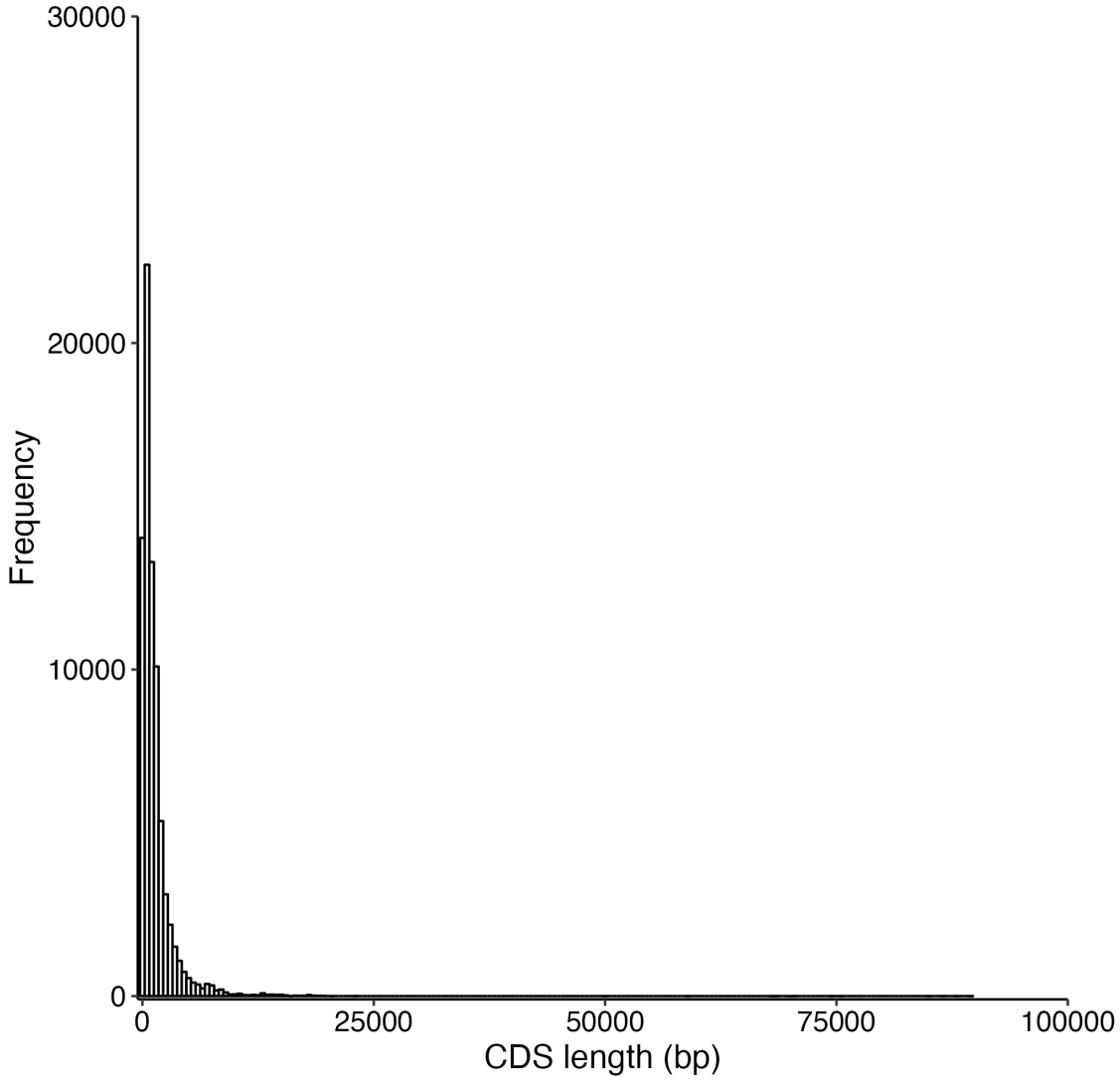


Figure 2.6. Length distribution of predicted candidate coding sequences.
Quality-controlled RNA-seq reads obtained from the dorsal skin of developing wood frogs were aligned to the *Rana sylvatica* reference genome (GCA_028564925.1) with HISAT2 and assembled into transcripts with StringTie. TransDecoder was used to predict the single best candidate coding sequences in each assembled transcript. The lengths of the 77,223 predicted candidate coding sequences were plotted with a bin width of 500 bp. The length distribution of predicted candidate coding sequences demonstrates a positively skewed distribution.

2.2.3 Transcriptome Trends

Normalized gene counts for all 34 samples provided by StringTie underwent principal components analysis (PCA) and heatmap clustering. Across the entire sample set, developmental timepoint was a stronger driver of gene expression than microplastic exposure when visualized in a PCA plot (Figure 2.7A) and a heatmap (Figure 2.7B). As a result, developmental changes in gene expression were analyzed first, followed by an analysis of the effects of microplastics on gene expression, conducted independently for each timepoint.

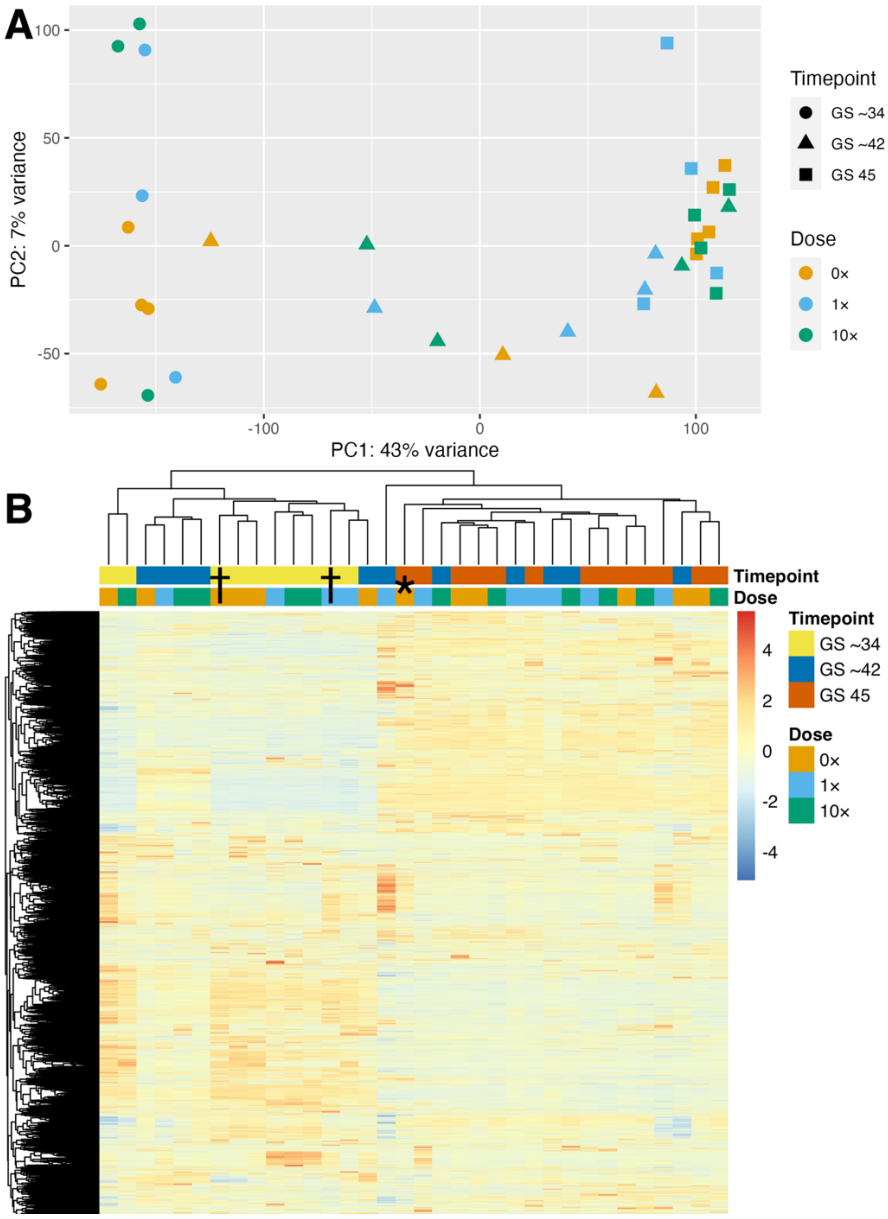


Figure 2.7. Developmental stage is a greater driver of transcriptional change than microplastic exposure across the entire sample set.
Quality-controlled RNA-seq reads obtained from the dorsal skin of developing wood frogs were aligned to the *Rana sylvatica* reference genome (GCA_028564925.1) with HISAT2 and assembled into transcripts with StringTie. The 25,000 genes with the greatest variance of normalized counts across samples were used for **A)** principal components analysis (PCA) plot generation and **B)** scaling and heatmap clustering. Asterisk (*) indicates the Gosner stage (GS) 45 wood frog dorsal skin sample collected with samples from GS ~42 wood frogs but analysed with GS 45 samples. Dagger (†) indicates the GS ~34 samples which underwent ethanol-precipitation to improve quality for sequencing.

2.2.4 Analysis of Transcriptomic Changes in Dorsal Skin from Control (0× Microplastics) Wood Frog Larvae Across Developmental Stages

Throughout amphibian development, the skin supports critical physiological processes and undergoes extensive remodelling in preparation for terrestrial life post metamorphosis (Duellman & Trueb, 1994). To understand the physiological processes supported by anuran skin during development and the changing functions of skin during remodeling, an analysis was performed of the dorsal skin transcriptomes generated from wood frog larvae in the control (0×) microplastics exposure group across the three developmental sampling timepoints: premetamorphosis (GS ~34), early metamorphic climax (GS ~42), and late metamorphic climax (GS 45). First, to understand what physiological processes are supported by the dorsal skin in developing wood frogs, the number of expressed genes assigned to Gene Ontology (GO) terms and to Kyoto Encyclopedia of Genes and Genomes (KEGG) pathways was profiled at each developmental timepoint, summarized at the second level of classification. At the earliest developmental stage examined (GS ~34), the most prominent level 2 GO terms were cellular process, biological regulation, metabolic process, and regulation of biological process under the biological process ontology, protein-containing complex under the cellular component ontology, and binding and catalytic activity under the molecular function ontology (Figure 2.8). The most prominent KEGG pathway class was signal transduction under the environmental information processing category (Figure 2.9). The immune and endocrine system classes under the organismal systems category were also prominent, as well as several classes under the human diseases category (Figure 2.9). Similar trends were seen across timepoints for both GO terms (Figure 2.8, Figure B.1, & Figure B.2) and KEGG pathways (Figure 2.9, Figure B.3, & Figure B.4). These results highlight that the skin of wood frogs appears to be a metabolically active tissue with support for roles in immunity, membrane transport, and response to the external environment, in addition to facilitating the energetic demands of skin remodelling.



Figure 2.8. Overview of Gene Ontology (GO) terms assigned to transcribed genes in the dorsal skin of Gosner stage ~34 wood frog tadpoles from the control (0× microplastics exposure) group.

Quality-controlled RNA-seq reads obtained from the dorsal skin of developing wood frogs were aligned to the *Rana sylvatica* reference genome (GCA_028564925.1) with HISAT2 and

assembled into transcripts with StringTie. TransDecoder was used to predict candidate coding sequences in the assembled transcripts and Trinotate was used to assign GO terms by homology transfer from BLASTP and BLASTX searches of the Swiss-Prot database. GO term assignments were filtered to retain level 2 GO terms, and the number of genes expressed in the 0× (control) dorsal skin samples from Gosner stage ~34 wood frogs for each level 2 GO term were plotted. Dorsal skin samples from Gosner stage ~42 and 45 wood frogs showed similar trends (Figure B.1 & Figure B.2).

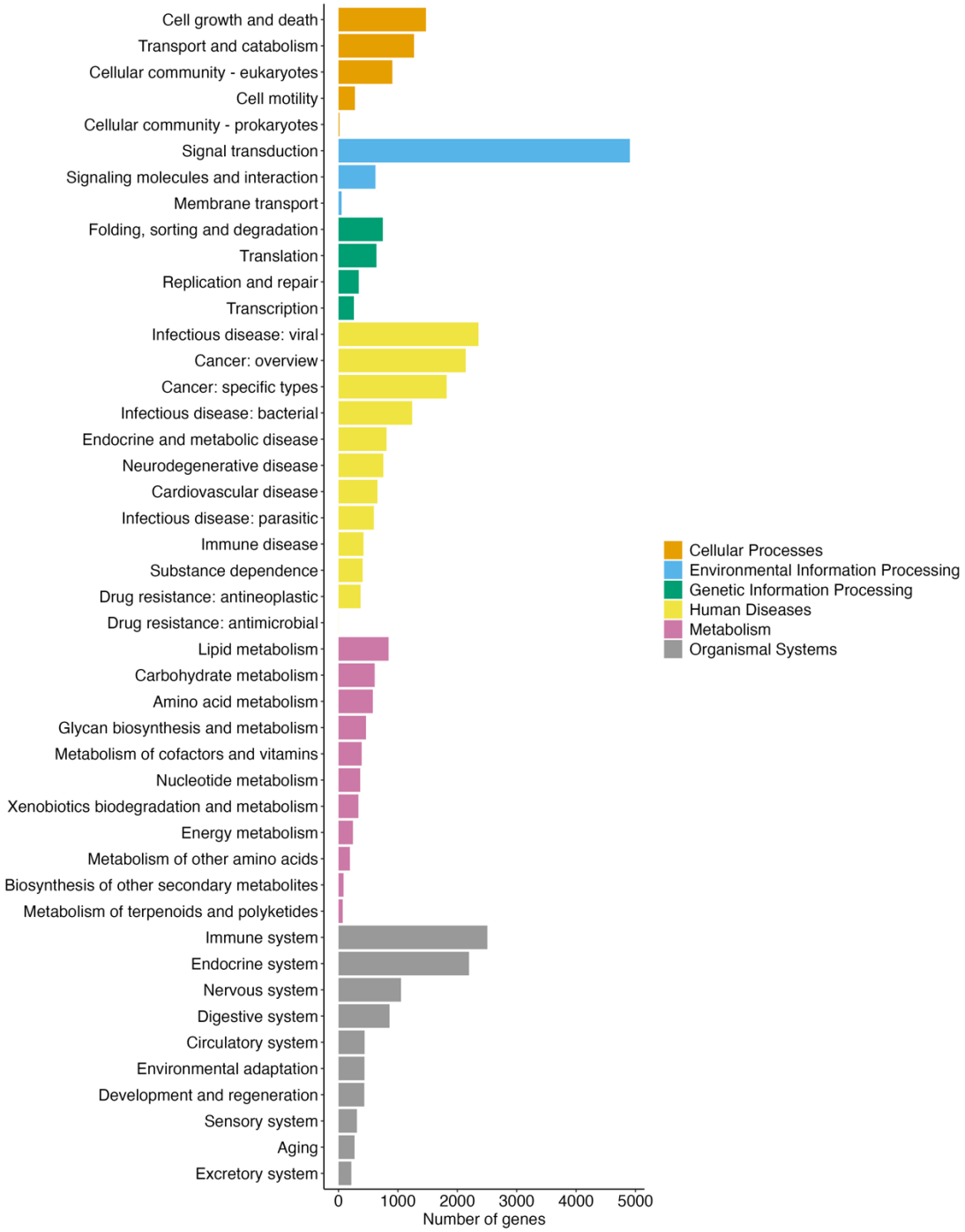


Figure 2.9. Overview of KEGG pathways assigned to transcribed genes in the dorsal skin of Gosner stage ~34 wood frog tadpoles from the control (0× microplastics exposure) group.

Quality-controlled RNA-seq reads obtained from the dorsal skin of developing wood frogs were aligned to the *Rana sylvatica* reference genome (GCA_028564925.1) with HISAT2 and

assembled into transcripts with StringTie. TransDecoder was used to predict candidate coding sequences in the assembled transcripts. Trinotate and EggNOG-mapper were used to assign KEGG pathways to assembled transcripts. The number of genes expressed in the 0× (control) dorsal skin samples from Gosner stage ~34 wood frogs for each level 2 KEGG pathway classification were plotted. Dorsal skin samples from Gosner stage ~42 and 45 wood frogs showed similar trends (Figure B.3 & Figure B.4).

To determine the skin-associated physiological processes being regulated during metamorphosis, the differentially expressed genes in dorsal skin tissues from control (0× microplastics group) wood frog larvae between the developmental timepoints were examined. A total of 5,733 differentially expressed genes (DEGs) were detected in dorsal skin tissue from wood frogs at GS ~42 compared to GS ~34, 2,011 DEGs were detected in dorsal skin tissue from wood frogs at GS 45 compared to GS ~42, and 10,351 DEGs were detected in dorsal skin tissue from wood frogs at GS 45 compared to GS ~34 (Table 2.6, Figure 2.10). There were 251 genes which were differentially expressed in all comparisons (Figure 2.10A & Figure 2.11). Volcano plots show a fairly symmetrical spread of up- and down-regulated genes for each comparison (Figure 2.10B). Heatmaps of differentially expressed genes demonstrate clustering of the timepoints by normalized expression values, with a high degree of similarity in normalized expression values between biological replicates within each timepoint (Figure 2.10C).

Table 2.6. Number of differentially expressed genes between developmental stages in the dorsal skin of developing wood frogs in the control (0× microplastics exposure) group.

Comparison	Down-regulated	Up-regulated	Total
GS ~42 vs. GS ~34	2,409	3,324	5,733
GS 45 vs. GS ~42	930	1,081	2,011
GS 45 vs. GS ~34	4,879	5,472	10,351

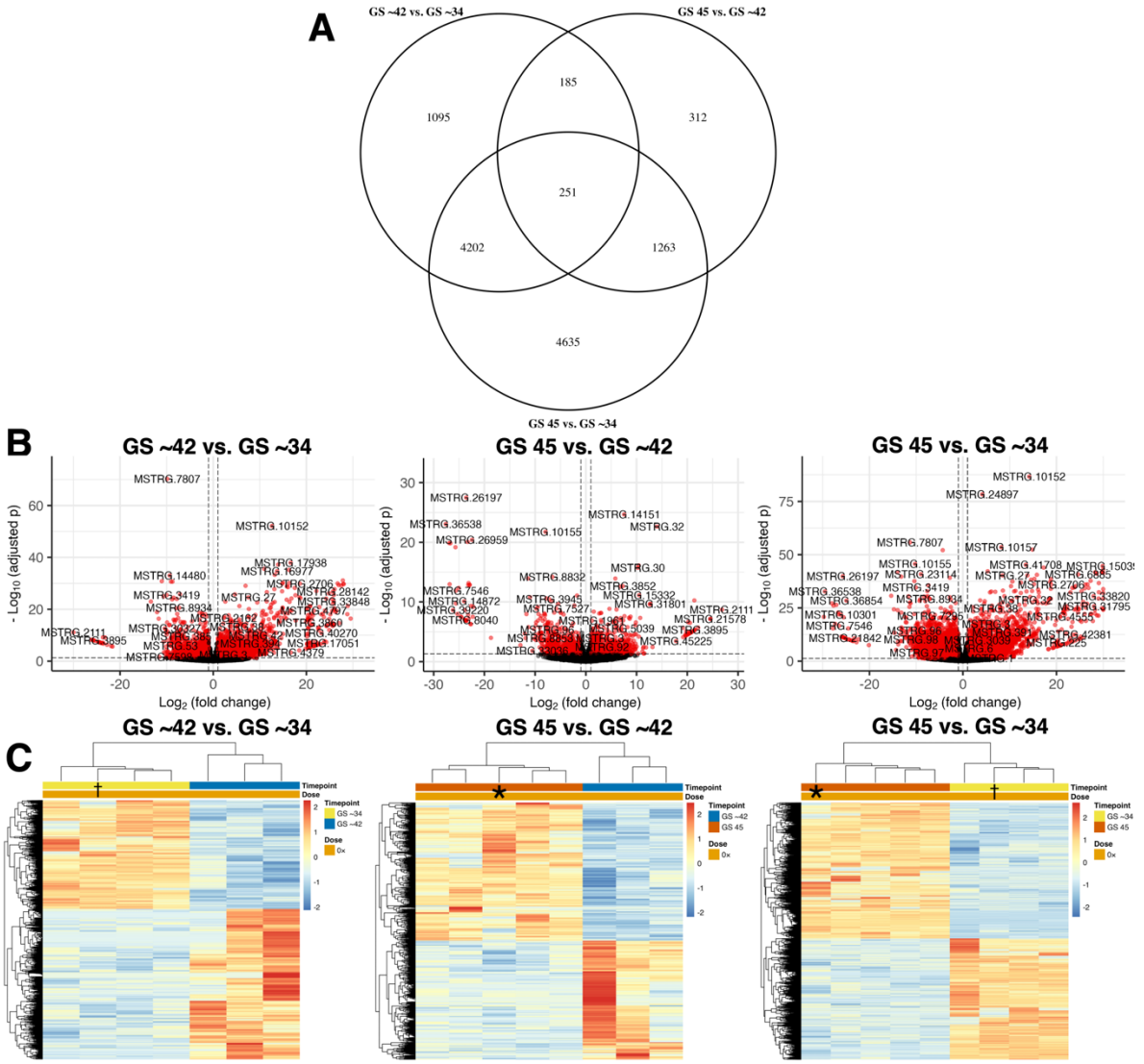


Figure 2.10. Differentially expressed genes in the dorsal skin of control (0× microplastics exposure) wood frog larvae and pro-metamorphs across developmental stages.
Quality-controlled RNA-seq reads obtained from the dorsal skin of developing wood frogs were aligned to the *Rana sylvatica* reference genome (GCA_028564925.1) with HISAT2 and assembled into transcripts with StringTie. DESeq2 was used to detect differentially expressed genes in dorsal skin samples from 0× (control) microplastics exposed wood frog larvae between developmental stages. **A)** Venn diagram showing overlap of differentially expressed genes between comparisons. **B)** Volcano plots of differentially expressed genes. **C)** Heatmaps of scaled, normalized counts for differentially expressed genes detected in the three comparisons performed. Asterisk (*) indicates the Gosner stage (GS) 45 wood frog dorsal skin sample collected with samples from GS ~42 wood frogs but analysed with GS 45 samples. Dagger (†) indicates the GS ~34 samples which underwent ethanol precipitation to improve quality prior to sequencing.

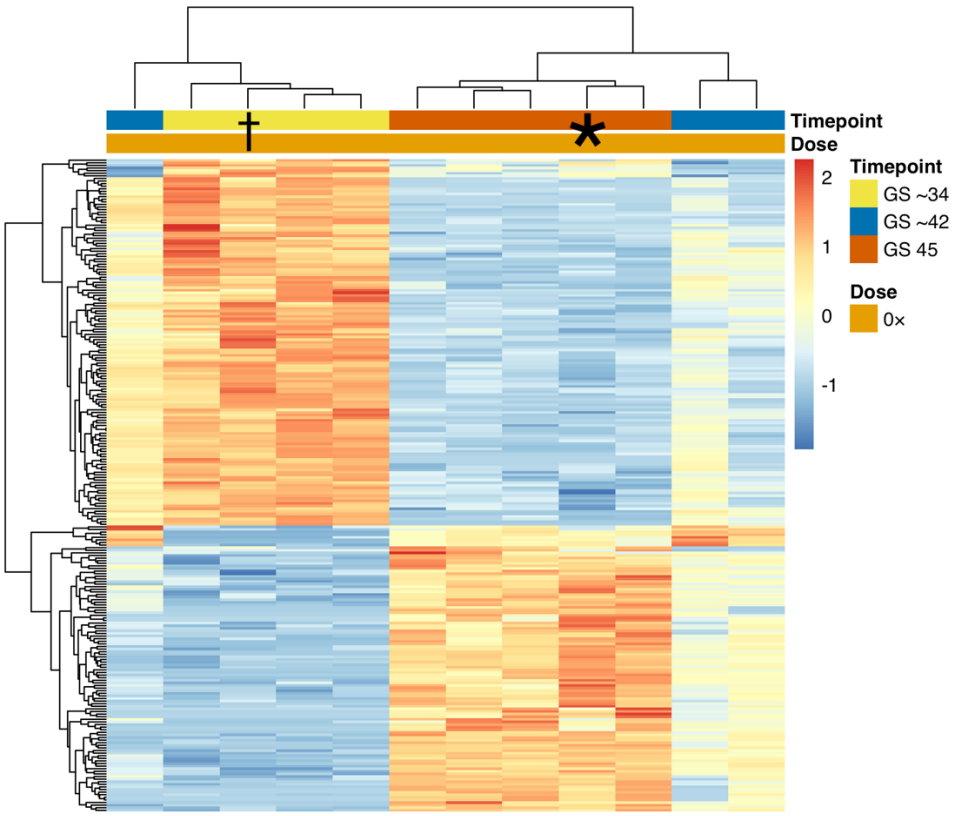


Figure 2.11. Core differentially expressed genes in wood frog dorsal skin during development.

Quality-controlled RNA-seq reads obtained from the dorsal skin of developing wood frogs were aligned to the *Rana sylvatica* reference genome (GCA_028564925.1) with HISAT2 and assembled into transcripts with StringTie. DESeq2 was used to detect differentially expressed genes in dorsal skin samples from 0× (control) microplastics exposed wood frog larvae between developmental stages. This heatmap depicts the expression levels of the 251 genes which were differentially expressed in all three pairwise comparisons between developmental stages. Asterisk (*) indicates the Gosner stage (GS) 45 wood frog dorsal skin sample collected with samples from GS ~42 wood frogs but analysed with GS 45 samples. Dagger (†) indicates the GS ~34 samples which underwent ethanol precipitation to improve quality prior to sequencing.

Gene set enrichment analysis of GO terms and KEGG pathways were performed to determine processes which were activated (normalized enrichment score > 0) or suppressed (normalized enrichment score < 0) in the dorsal skin of unexposed 0× control wood frog larvae between the developmental timepoints sequenced. Activated and suppressed GO terms (Table 2.7) and KEGG pathways (Table 2.8) were found in the dorsal skin of GS ~42 wood frogs versus GS ~34, in the dorsal skin of GS 45 wood frogs versus GS ~42, and in the dorsal skin of GS 45 wood frogs versus GS ~34. In the dorsal skin of GS ~42 wood frogs versus GS ~34, the top twenty enriched GO terms included suppressed immune-related terms (e.g. activation of innate immune response, pattern recognition receptor signaling pathway, positive regulation of innate immune response, and regulation of canonical NF-κB signal transduction), and enriched terms involved in skin structure (keratinization) and cellular functions (ncRNA processing, ncRNA metabolic process, etc.) (Figure 2.12A). In the dorsal skin of GS 45 wood frogs versus GS ~42, the top twenty enriched GO terms included suppressed terms related to translation, RNA processing and metabolic processes, and activated terms related to protein-DNA complexes and the nucleosome (Figure 2.12B). In the dorsal skin of GS 45 wood frogs versus GS ~34, the top twenty enriched GO terms included suppressed terms such as ubiquitin protein ligase activity, and enriched terms involving peptidase and ligase regulator activity and protein-DNA complexes (Figure 2.12C). An enrichment map of all enriched GO terms shows us a large cluster of suppressed immune-related terms in the dorsal skin of GS ~42 versus GS ~34 wood frogs, with some suppression of cellular signalling terms (Figure 2.13). There are also clusters of activated terms related to sensory processing, transmembrane transport, epithelia, and antigen presentation and T cell function in the dorsal skin of GS ~42 versus GS ~34 wood frogs (Figure 2.13). A GO term enrichment map of enriched terms in the dorsal skin of GS 45 versus GS ~42 wood frogs shows three main suppressed clusters related to translation, RNA processing, and mitochondria/metabolic processes (Figure 2.14), in addition to many small clusters of activated terms, with the largest involving responses to various stimuli and GTPase (Figure 2.14). A map of GO terms enriched in the dorsal skin of GS 45 versus GS ~34 wood frogs shows a core suppressed cluster of immune terms, and activation of a variety of processes

(Figure 2.15). Next, evaluating enriched KEGG pathways, the suppression of immune-related pathways is seen again, including influenza A, RIG-I-like receptor signalling pathway, and NF-κB signalling pathway in the dorsal skin of GS ~42 wood frogs versus GS ~34 (Figure 2.16A). Activated pathways in the dorsal skin of GS ~42 wood frogs versus GS ~34 include various metabolic and signalling pathways, and the complement and coagulation cascades (Figure 2.16A). In the dorsal skin of GS 45 wood frogs versus GS ~42, the suppression of pathways like ribosome and DNA replication, and activation of pathways including various signalling pathways, including IL-17 signalling, is seen (Figure 2.16B). Suppressed pathways in the dorsal skin of GS 45 wood frogs versus GS ~34 again includes the immune signalling pathways RIG-I-like receptor signalling pathway and NF-κB signalling (Figure 2.16C). Activated pathways include various metabolic and signalling pathways, in addition to the complement and coagulation cascades (Figure 2.16C). In a map of enriched pathways in the dorsal skin of GS ~42 versus GS ~34 wood frogs, two main clusters of pathways are observed: one of various activated metabolic pathways, and another of suppressed immune pathways (Figure 2.17). The map of enriched terms in the dorsal skin of GS 45 versus GS ~42 wood frogs shows a single large disperse cluster of activated pathways including various signalling pathways, such as the immune-related signalling pathways TNF signalling and T cell receptor signalling (Figure 2.18). A KEGG pathway enrichment map of enriched pathways in the dorsal skin of GS 45 versus GS ~34 wood frogs shows one suppressed cluster of immune pathways, with the remaining pathways being activated (Figure 2.19).

Table 2.7. Number of enriched Gene Ontology (GO) terms in the dorsal skin of control (0× microplastics exposure) wood frog larvae between developmental stages.

Comparison	Activated			Suppressed			Total
	BP	CC	MF	BP	CC	MF	
GS ~42 vs. GS ~34	176	15	86	145	5	26	453
GS 45 vs. GS ~42	41	12	15	26	24	7	125
GS 45 vs. GS ~34	169	19	85	84	11	17	385

The total number of enriched GO terms is shown for each differential expression analysis as well as the number with normalized enrichment score > 0 (activated) or < 0 (suppressed), separated by the GO ontologies Biological Process (BP), Cellular Component (CC), and Molecular Function (MF).

Table 2.8. Number of enriched KEGG pathways in the dorsal skin of control (0× microplastics exposure) wood frog larvae between developmental stages.

Comparison	Activated	Suppressed	Total
GS ~42 vs. GS ~34	30	10	40
GS 45 vs. GS~ 42	52	8	60
GS 45 vs. GS ~34	46	4	50

The total number of enriched KEGG pathways is shown as well as the number which were activated (normalized enrichment score > 0) or suppressed (normalized enrichment score < 0).

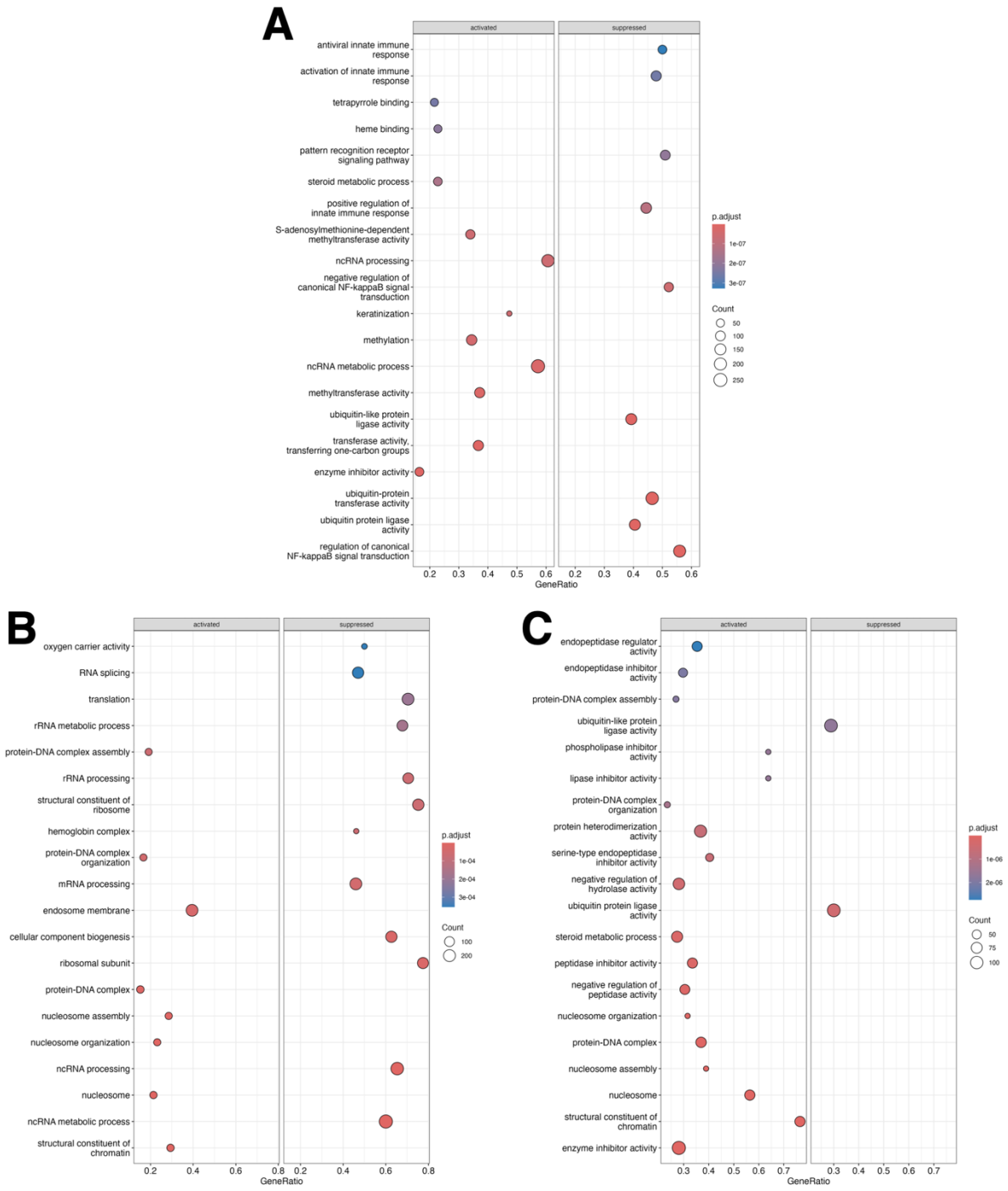


Figure 2.12. Top enriched GO terms in the dorsal skin of control (0× microplastics exposed) wood frog larvae across developmental timepoints.

Quality-controlled RNA-seq reads obtained from the dorsal skin of developing wood frogs were aligned to the *Rana sylvatica* reference genome (GCA_028564925.1) with HISAT2 and assembled into transcripts with StringTie. TransDecoder was used to predict candidate coding

sequences in the assembled transcripts and Trinotate was used to assign GO terms by homology transfer from BLASTP and BLASTX searches of the Swiss-Prot database. DESeq2 was used to detect differentially expressed genes in the dorsal skin of control (0×) animals between sampling timepoints, then clusterProfiler was used to perform gene set enrichment analysis with GO term assignments and shrunken $\log_2$ fold change values from DESeq2. The top twenty most significantly enriched GO terms by adjusted p-value in dorsal skin samples from wood frogs are plotted for **A)** Gosner stage (GS) ~42 vs. GS ~34, **B**) GS 45 vs. GS ~42, and **C)** GS 45 vs. GS ~34. "Activated" terms indicate those with a positive normalized enrichment score (NES) and "suppressed" terms are those with a negative NES. Count is the number of genes in the supplied gene list contained in the GO term. GeneRatio represents the ratio of Count over the total number of genes in the GO term.

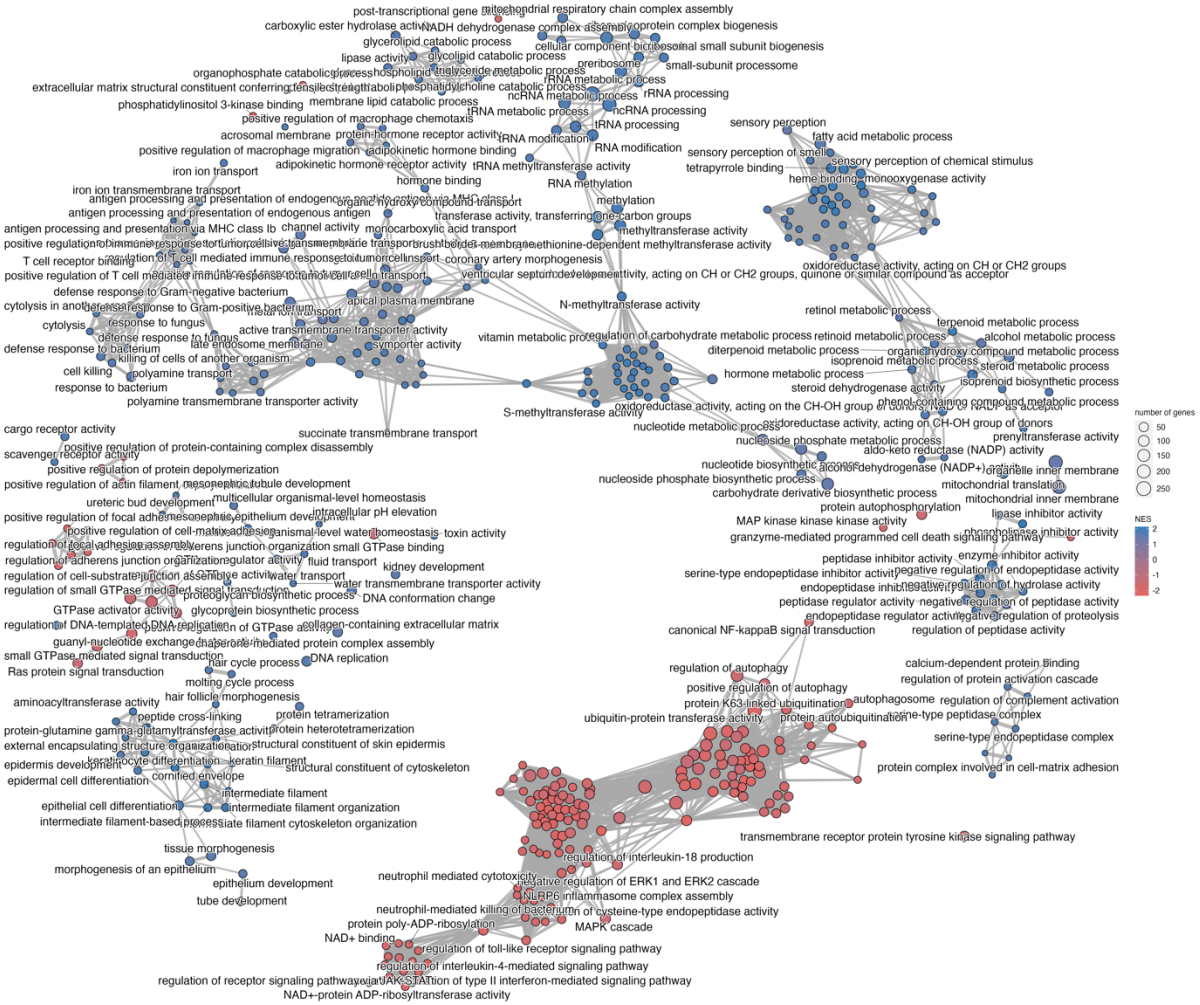


Figure 2.13. Enrichment map of GO terms enriched in the dorsal skin of Gosner stage ~42 control (0× microplastics exposed) wood frogs compared to the dorsal skin of Gosner stage ~34 control wood frogs.

Quality-controlled RNA-seq reads obtained from the dorsal skin of developing wood frogs were aligned to the *Rana sylvatica* reference genome (GCA_028564925.1) with HISAT2 and assembled into transcripts with StringTie. TransDecoder was used to predict candidate coding sequences in the assembled transcripts and Trinotate was used to assign GO terms by homology transfer from BLASTP and BLASTX searches of the Swiss-Prot database. DESeq2 was used to calculate shrunken $\log_2$ fold change values of genes in the dorsal skin of control (0×) animals at Gosner stage (GS) ~42 versus GS ~34. These were input to clusterProfiler to perform gene set enrichment analysis. Edges connect nodes with Jaccard similarity coefficient > 0.2. Nodes are coloured by the normalized enrichment score (NES).

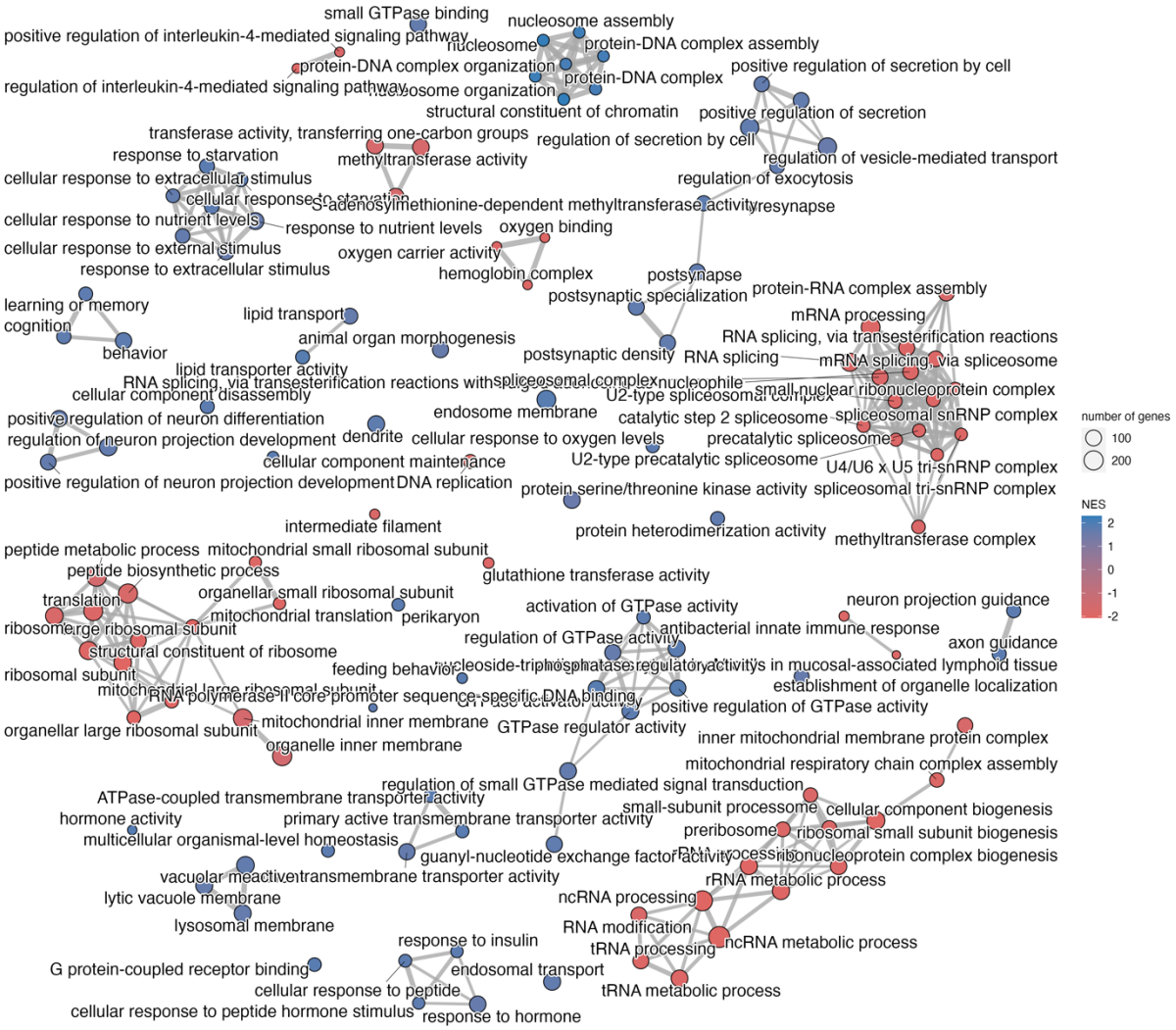


Figure 2.14. Enrichment map of GO terms enriched in the dorsal skin of Gosner stage 45 control (0× microplastics exposed) wood frogs compared to the dorsal skin of Gosner stage ~42 control wood frogs.

Quality-controlled RNA-seq reads obtained from the dorsal skin of developing wood frogs were aligned to the *Rana sylvatica* reference genome (GCA_028564925.1) with HISAT2 and assembled into transcripts with StringTie. TransDecoder was used to predict candidate coding sequences in the assembled transcripts and Trinotate was used to assign GO terms by homology transfer from BLASTP and BLASTX searches of the Swiss-Prot database. DESeq2 was used to calculate shrunken $\log_2$ fold change values of genes in the dorsal skin of control (0×) animals at Gosner stage (GS) 45 versus GS ~42. These were input to clusterProfiler to perform gene set enrichment analysis. Edges connect nodes with Jaccard similarity coefficient > 0.2. Nodes are coloured by the normalized enrichment score (NES).

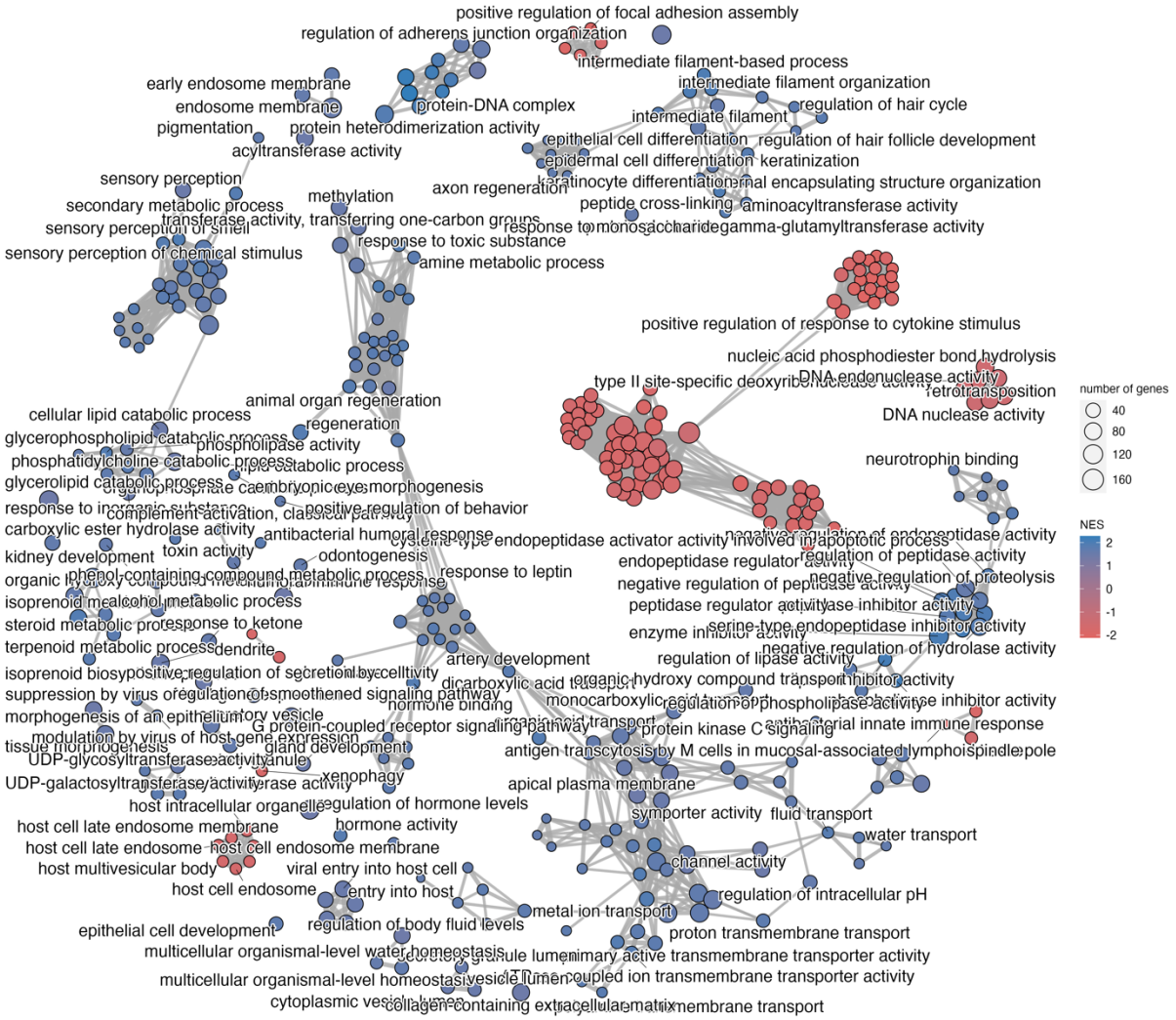


Figure 2.15. Enrichment map of GO terms enriched in the dorsal skin of Gosner stage 45 control (0× microplastics exposed) wood frogs compared to the dorsal skin of Gosner stage ~34 wood frogs.

Quality-controlled RNA-seq reads obtained from the dorsal skin of developing wood frogs were aligned to the *Rana sylvatica* reference genome (GCA_028564925.1) with HISAT2 and assembled into transcripts with StringTie. TransDecoder was used to predict candidate coding sequences in the assembled transcripts and Trinotate was used to assign GO terms by homology transfer from BLASTP and BLASTX searches of the Swiss-Prot database. DESeq2 was used to calculate shrunken $\log_2$ fold change values of genes in the dorsal skin of control (0×) animals at Gosner stage (GS) 45 versus GS ~34. These were input to clusterProfiler to perform gene set enrichment analysis. Edges connect nodes with Jaccard similarity coefficient > 0.2. Nodes are coloured by the normalized enrichment score (NES).

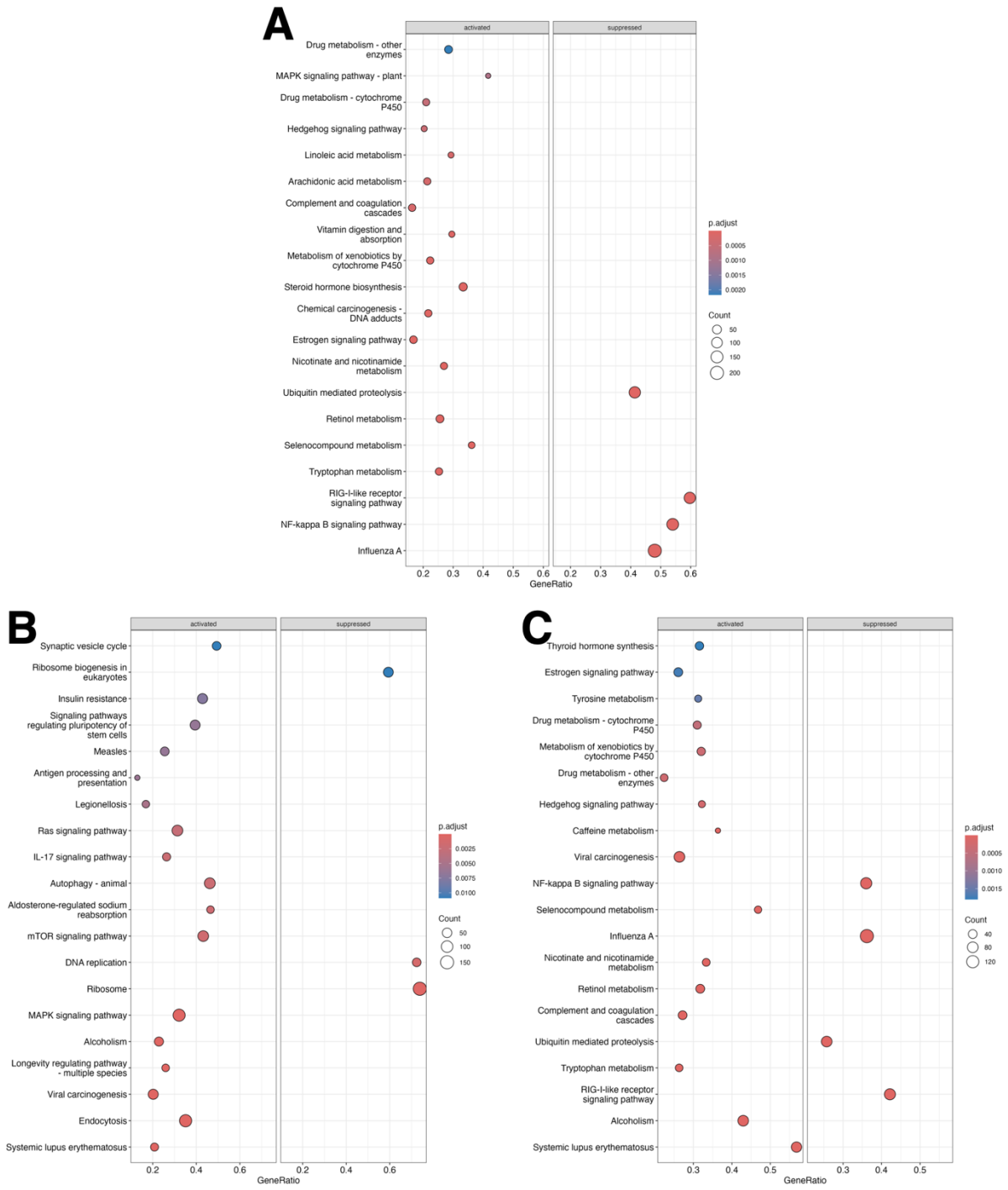


Figure 2.16. Top enriched KEGG pathways in the dorsal skin of control (0× microplastics exposed) wood frog larvae across developmental timepoints.

Quality-controlled RNA-seq reads obtained from the dorsal skin of developing wood frogs were aligned to the *Rana sylvatica* reference genome (GCA_028564925.1) with HISAT2 and

assembled into transcripts with StringTie. TransDecoder was used to predict candidate coding sequences in the assembled transcripts and Trinotate and EggNOG-mapper were used to assign KEGG pathways to assembled transcripts. DESeq2 was used to detect differentially expressed genes in the dorsal skin of control (0×) animals between sampling timepoints, then clusterProfiler was used to perform gene set enrichment analysis with KEGG pathway assignments and shrunken $\log_2$ fold change values from DESeq2. The top twenty most significantly enriched KEGG pathways by adjusted p-value in dorsal skin samples from wood frogs are plotted for **A)** Gosner stage (GS) ~42 vs. GS ~34, **B**) GS 45 vs. GS ~42, and **C)** GS 45 vs. GS ~34. "Activated" terms indicate those with a positive normalized enrichment score (NES) and "suppressed" terms are those with a negative NES. Count is the number of genes in the supplied gene list contained in the GO term. GeneRatio represents the ratio of Count over the total number of genes in the GO term.

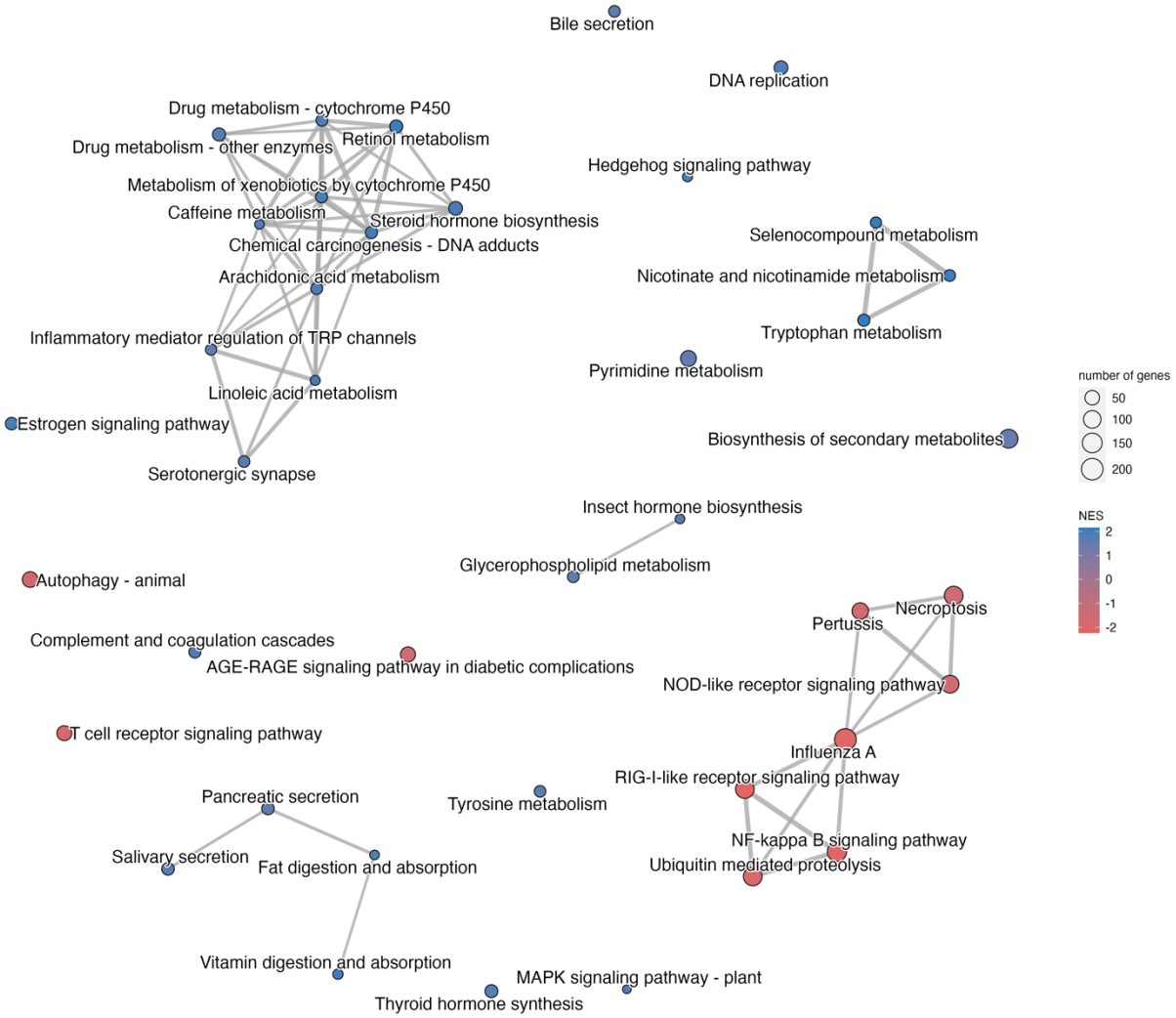


Figure 2.17. Enrichment map of KEGG pathways enriched in the dorsal skin of Gosner stage ~42 control (0× microplastics exposed) wood frogs compared to the dorsal skin of Gosner stage ~34 control wood frogs.

Quality-controlled RNA-seq reads obtained from the dorsal skin of developing wood frogs were aligned to the *Rana sylvatica* reference genome (GCA_028564925.1) with HISAT2 and assembled into transcripts with StringTie. TransDecoder was used to predict candidate coding sequences in the assembled transcripts. Trinotate and EggNOG-mapper were used to assign KEGG pathways to assembled transcripts. DESeq2 was used to calculate shrunken $\log_2$ fold change values of genes in the dorsal skin of control (0×) animals at Gosner stage (GS) ~42 versus GS ~34. These were input to clusterProfiler to perform gene set enrichment analysis. Edges connect nodes with Jaccard similarity coefficient > 0.2. Nodes are coloured by the normalized enrichment score (NES).

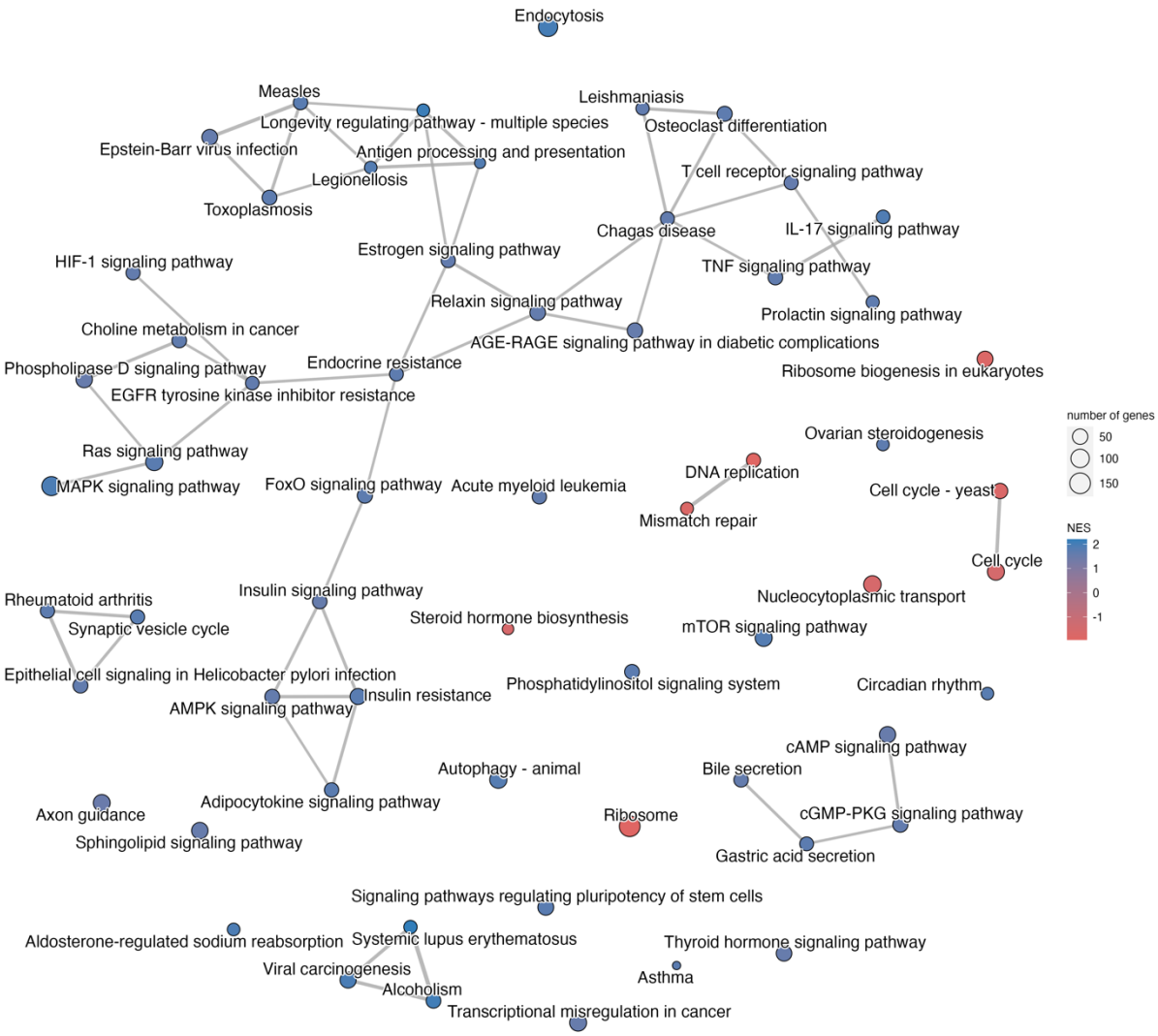


Figure 2.18. Enrichment map of KEGG pathways enriched in the dorsal skin of Gosner stage 45 control (0× microplastics exposed) wood frogs compared to the dorsal skin of Gosner stage ~42 control wood frogs.

Quality-controlled RNA-seq reads obtained from the dorsal skin of developing wood frogs were aligned to the *Rana sylvatica* reference genome (GCA_028564925.1) with HISAT2 and assembled into transcripts with StringTie. TransDecoder was used to predict candidate coding sequences in the assembled transcripts. Trinotate and EggNOG-mapper were used to assign KEGG pathways to assembled transcripts. DESeq2 was used to calculate shrunken $\log_2$ fold change values of genes in the dorsal skin of control (0×) animals at Gosner stage (GS) 45 versus GS ~42. These were input to clusterProfiler to perform gene set enrichment analysis. Edges connect nodes with Jaccard similarity coefficient > 0.2. Nodes are coloured by the normalized enrichment score (NES).

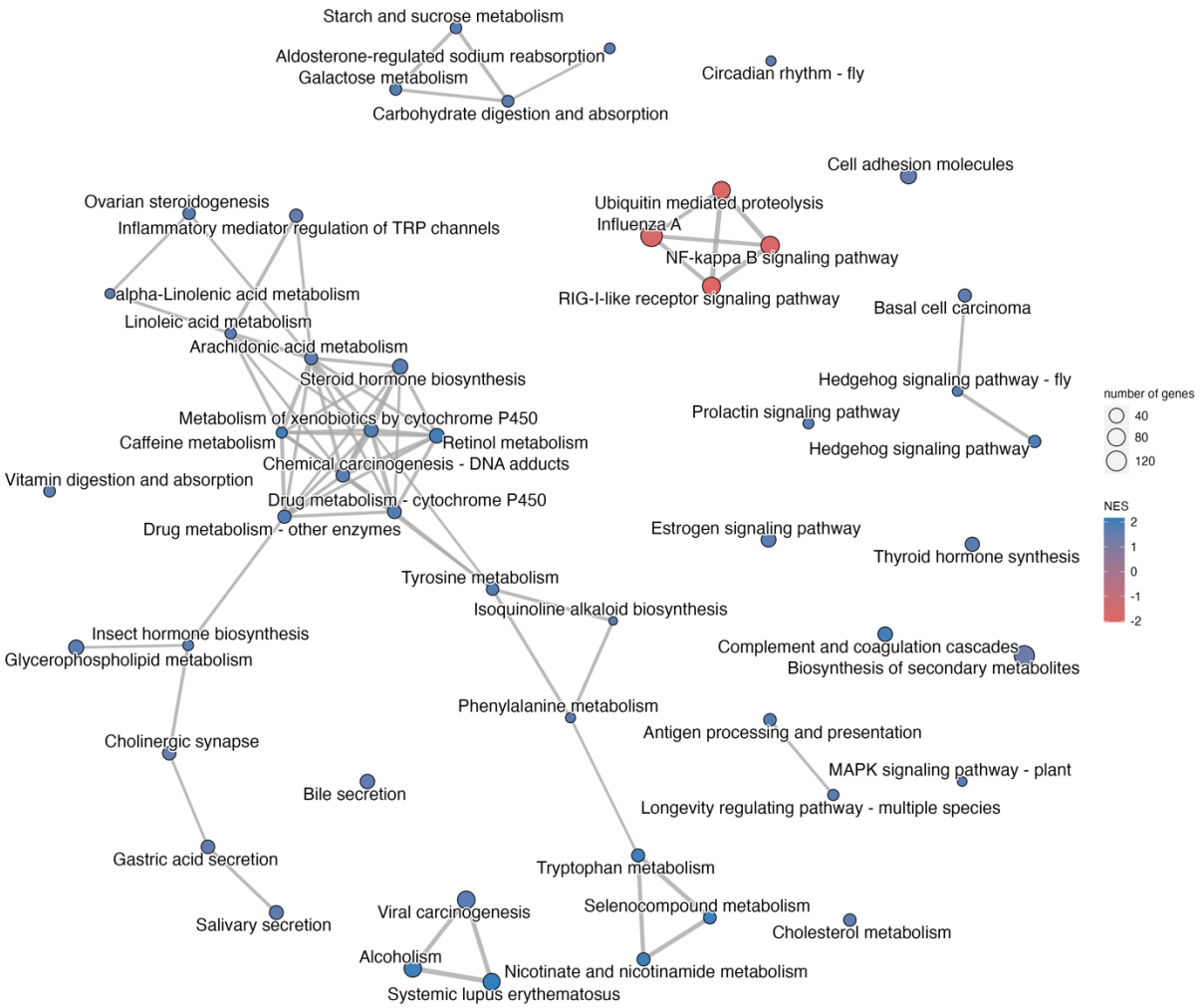


Figure 2.19. Enrichment map of KEGG pathways enriched in the dorsal skin of Gosner stage 45 control (0× microplastics exposed) wood frogs compared to the dorsal skin of Gosner stage ~34 control wood frogs.

Quality-controlled RNA-seq reads obtained from the dorsal skin of developing wood frogs were aligned to the *Rana sylvatica* reference genome (GCA_028564925.1) with HISAT2 and assembled into transcripts with StringTie. TransDecoder was used to predict candidate coding sequences in the assembled transcripts. Trinotate and EggNOG-mapper were used to assign KEGG pathways to assembled transcripts. DESeq2 was used to calculate shrunken $\log_2$ fold change values of genes in the dorsal skin of control (0×) animals at Gosner stage (GS) 45 versus GS ~34. These were input to clusterProfiler to perform gene set enrichment analysis. Edges connect nodes with Jaccard similarity coefficient > 0.2. Nodes are coloured by the normalized enrichment score (NES).

2.2.5 Analysis of Transcriptomic Changes in the Dorsal Skin of Wood Frog Larvae Resulting from Microplastic Exposure at Several Developmental Stages

Next, an analysis of how gene expression in the dorsal skin of wood frog larvae at several developmental stages responded to chronic exposure to a microplastics mixture was performed. Because developmental stage was a greater driver of the transcriptional profile of a sample than microplastic treatment, with samples displaying a greater degree of clustering on developmental stage than microplastic treatment in a PCA plot (Figure 2.7A), each developmental timepoint was analyzed independently. Upregulated and downregulated genes were found at all three developmental stages in both the 1× and 10× treatments, compared to the 0× control treatment (Table 2.9, Figure 2.20). The most DEGs were found in dorsal skin from wood frogs at GS ~34, with 829 DEGs found in the 1× treatment, and 226 DEGs found in the 10× treatment (Table 2.9). The least DEGs were found at GS 45 in the 10× treatment, where 31 DEGs were found (Table 2.9). A total of 1,176 genes were differentially expressed in at least one timepoint and treatment. There was a trend of more DEGs found in the 1× treatment than the 10×, except for at GS ~42 (Table 2.9). Expression values of DEGs at GS ~34 and GS 45 resulted in distinct clustering of samples in heatmaps, with clear patterns emerging, while at GS ~42 the clustering was less distinct, with samples displaying higher levels of biological variation (Figure 2.20). There was some overlap of DEGs between the various comparisons, with most of the overlap occurring within timepoints between the 1× and 10× treatments, as compared to the 0× control (Figure 2.21).

Table 2.9. Number of differentially expressed genes in the dorsal skin of microplastics-exposed wood frog larvae at several developmental stages.

Timepoint	1× vs 0×			10× vs 0×		
	Down-regulated	Up-regulated	Total	Down-regulated	Up-regulated	Total
GS ~34	488	341	829	71	155	226
GS ~42	12	57	69	19	86	105
GS 45	29	47	76	20	11	31

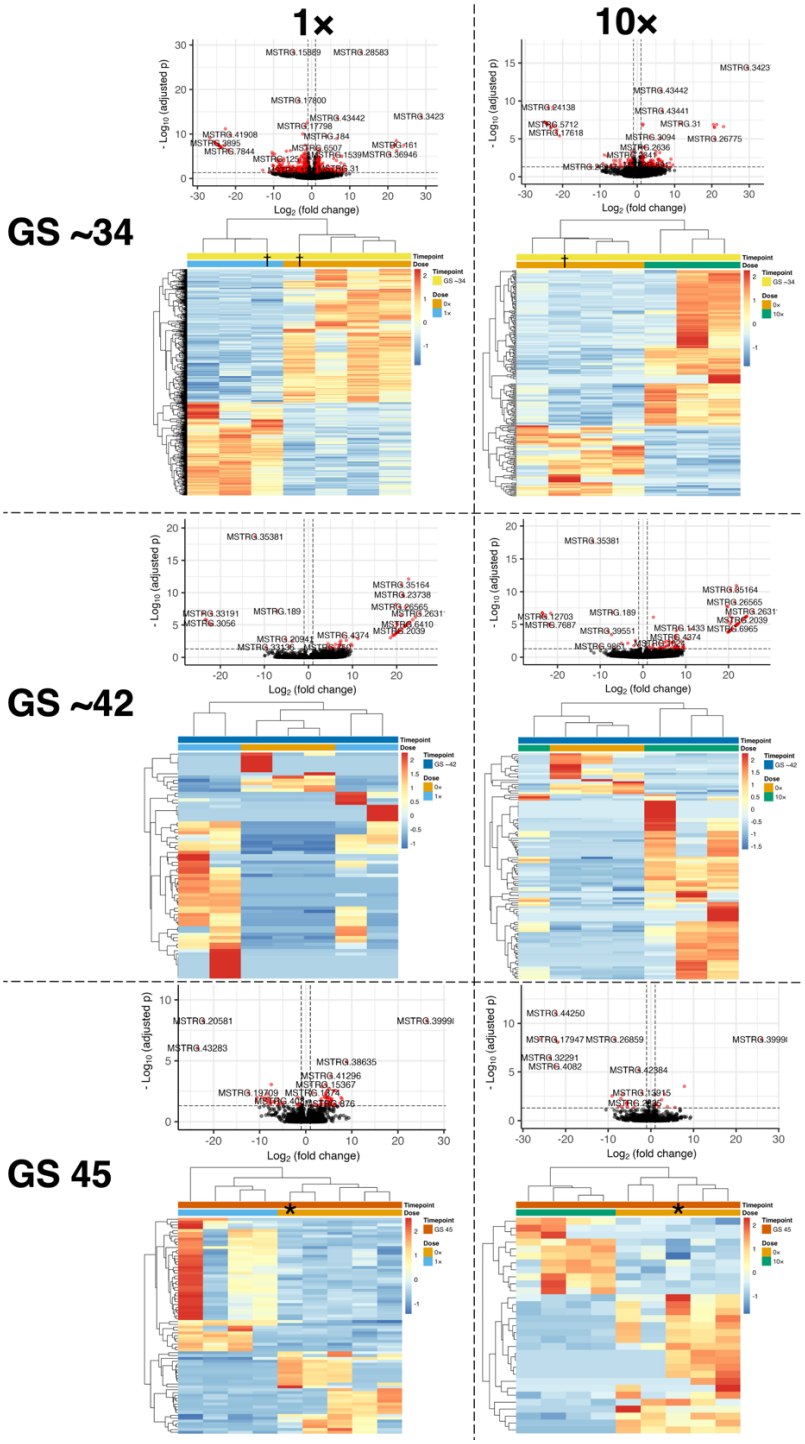


Figure 2.20. Microplastic exposure causes differential expression of genes in the dorsal skin of developing wood frogs.

Differential expression analysis was performed on RNA-seq reads from the dorsal skin of developing wood frogs exposed to varying concentrations (0×, 1×, 10×) of a microplastics

mixture. Developing wood frogs were sampled at Gosner stage (GS) ~34, ~42, and 45. Differential expression analysis was performed independently at each time point with respect to the 0× microplastics exposed control group. Asterisk (*) indicates the Gosner stage (GS) 45 wood frog dorsal skin sample collected with samples from GS ~42 wood frogs but analysed with GS 45 samples. Dagger (†) indicates the GS ~34 samples which underwent ethanol-precipitation to improve quality prior to sequencing.

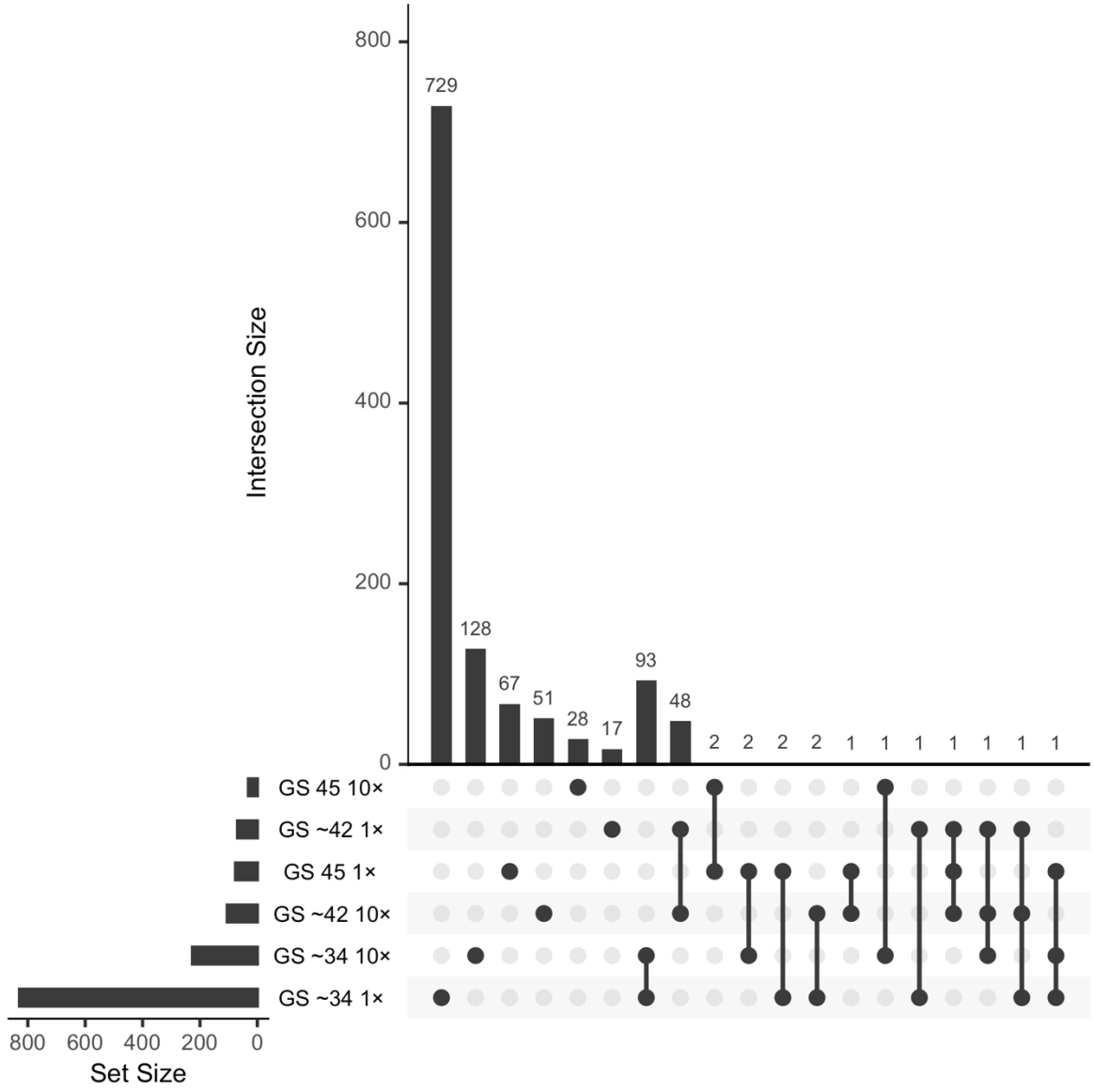


Figure 2.21. Overlap of differentially expressed genes in the dorsal skin of microplastic-exposed wood frog larvae at several developmental stages.
Differentially expressed genes were detected in the dorsal skin of wood frogs exposed to a 1× or 10× microplastics mixture, compared to the 0× control at several developmental timepoints (Gosner stage (GS) ~34, GS ~42, and GS 45). Vertical bars represent intersection sizes, with the intersection sets represented by the highlighted dots beneath the bar. Horizontal bars represent the total number of differentially expressed genes detected in each group (set size).

Next, to detect cellular processes which were activated or suppressed by either 1× or 10× microplastics exposure in the dorsal skin of wood frogs, gene set enrichment analysis of GO terms and KEGG pathways was performed. At least one GO term was enriched for all differential expression comparisons performed, except for wood frogs at GS ~42 exposed to the 1× microplastics treatment versus the 0× treatment (Table 2.10). Similarly, at least one KEGG pathway was enriched for all differential expression comparisons performed, except for wood frogs at GS ~42 and GS 45 exposed to the 1× microplastics treatment versus the 0× treatment (Table 2.11). The greatest number of enriched GO terms and KEGG pathways were both found at GS ~34 in the 1× microplastics treatment (Table 2.10 & Table 2.11). The second most enriched GO terms were seen at GS ~42 in the 10× treatment (Table 2.10), while the second most enriched KEGG pathways were seen at GS ~34 in the 10× treatment (Table 2.11).

Table 2.10. Number of enriched GO terms in the dorsal skin of microplastic-exposed wood frog larvae at several developmental stages.

Timepoint	Treatment	Activated			Suppressed			Total
		BP	CC	MF	BP	CC	MF	
GS ~34	1×	78	37	20	344	35	55	569
	10×	34	13	9	6	3	2	67
GS ~42	1×	0	0	0	0	0	0	0
	10×	7	9	9	57	34	13	129
GS 45	1×	19	0	3	4	2	4	32
	10×	0	7	5	0	1	0	13

The total number of enriched Gene Ontology (GO) terms is shown for each differential expression analysis as well as the number with normalized enrichment score > 0 (activated) or < 0 (suppressed), separated by the GO ontologies Biological Process (BP), Cellular Component (CC), and Molecular Function (MF). In every case, the comparator group is the 0× treatment at the corresponding timepoint.

Table 2.11. Number of enriched KEGG pathways in the dorsal skin of microplastic-exposed wood frog larvae at several developmental stages.

Timepoint	Treatment	Activated	Suppressed	Total
GS ~34	1×	17	32	49
	10×	19	0	19
GS ~42	1×	0	0	0
	10×	0	10	10
GS 45	1×	0	0	0
	10×	0	1	1

The total number of enriched KEGG pathways is shown as well as the number which were activated (normalized enrichment score > 0) or suppressed (normalized enrichment score < 0). In every case, the comparator group is the 0× treatment at the corresponding timepoint.

At GS ~34, in the dorsal skin of wood frogs exposed to the 1× treatment, in comparison to the 0× control, suppression of immune and proteolytic terms and activation of metabolic and cellular processing terms are observed in the top twenty enriched GO terms (Figure 2.22A), while the top twenty enriched terms in the dorsal skin of wood frogs exposed to the 10× treatment include suppression of GTPase terms and activation of terms including transmembrane transport, metabolism, and RNA processing (Figure 2.22B). When all enriched terms are clustered, three large, linked clusters of suppressed immune-related terms in the dorsal skin of GS ~34 wood frogs exposed to the 1× treatment are seen, as well as clusters of activated terms involving translation, RNA processing, and mitochondria, in addition to many disperse terms which are both activated and suppressed (Figure 2.23). In the dorsal skin of GS ~34 wood frogs exposed to the 10× treatment, three large clusters of activated GO terms are seen, which involve RNA processes, metabolic processes, and transmembrane transport (Figure 2.24). There are also two small, suppressed clusters of GTPase activity and cellular signalling cascades (Figure 2.24). The top twenty enriched KEGG pathways in the dorsal skin of GS ~34 wood frogs exposed to the 1× treatment include suppression of immune signalling pathways, cAMP signalling, and others (Figure 2.25A). Activated pathways in the dorsal skin of GS ~34 wood frogs exposed to the 1× treatment include cell cycle, DNA replication, nucleocytoplasmic transport, and nucleotide excision repair (Figure 2.25A). Suppressed pathways in the dorsal skin of GS ~34 wood frogs exposed to the 1× treatment formed two clusters: the first included RIG-I-like receptor signalling pathway and NF-kappa B signalling pathway, while the second included pathways related to the adaptive immune system and various cellular signalling pathways (Figure 2.26). In the dorsal skin of GS ~34 wood frogs exposed to the 10× treatment, no supressed pathways were found, while the 19 activated pathways included clusters of metabolic pathways and, interestingly, pathways related to cardiac muscle, though the enrichment map was sparse overall (Figure 2.25B & Figure 2.27).

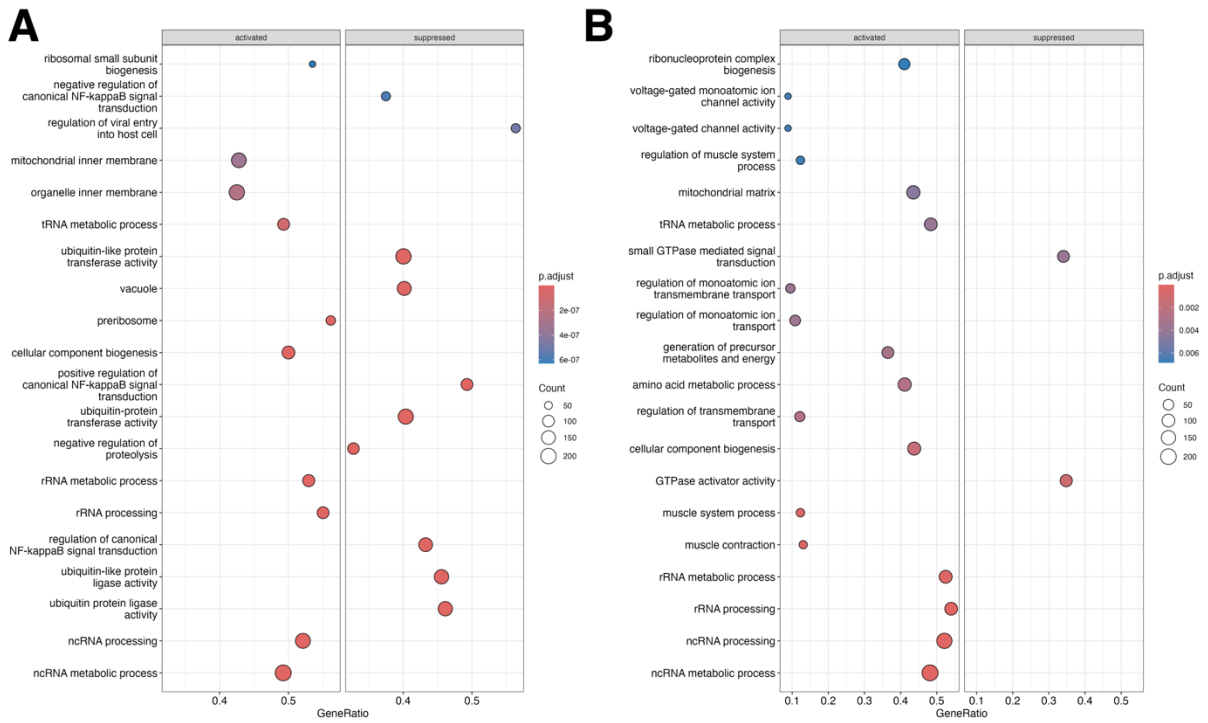


Figure 2.22. Top enriched GO terms in the dorsal skin of Gosner stage ~34 wood frog larvae exposed to a 1× or 10× microplastics mixture.

Gene set enrichment analysis was performed with clusterProfiler using shrunken $\log_2$ fold change values from DESeq2 comparisons of the dorsal skin obtained from Gosner stage ~34 wood frog larvae following exposure to a **A)** 1× microplastics treatment or **B)** 10× microplastics treatment versus the developmental stage-matched 0× control group. GO terms were assigned by homology transfer from BLASTP and BLASTX searches of the Swiss-Prot database. The top twenty most statistically significantly enriched GO terms by adjusted p-value are plotted. "Activated" terms indicate those with a positive normalized enrichment score (NES) and "suppressed" terms are those with a negative NES. Count is the number of genes in the supplied gene list contained in the GO term. GeneRatio represents the ratio of Count over the total number of genes in the GO term.

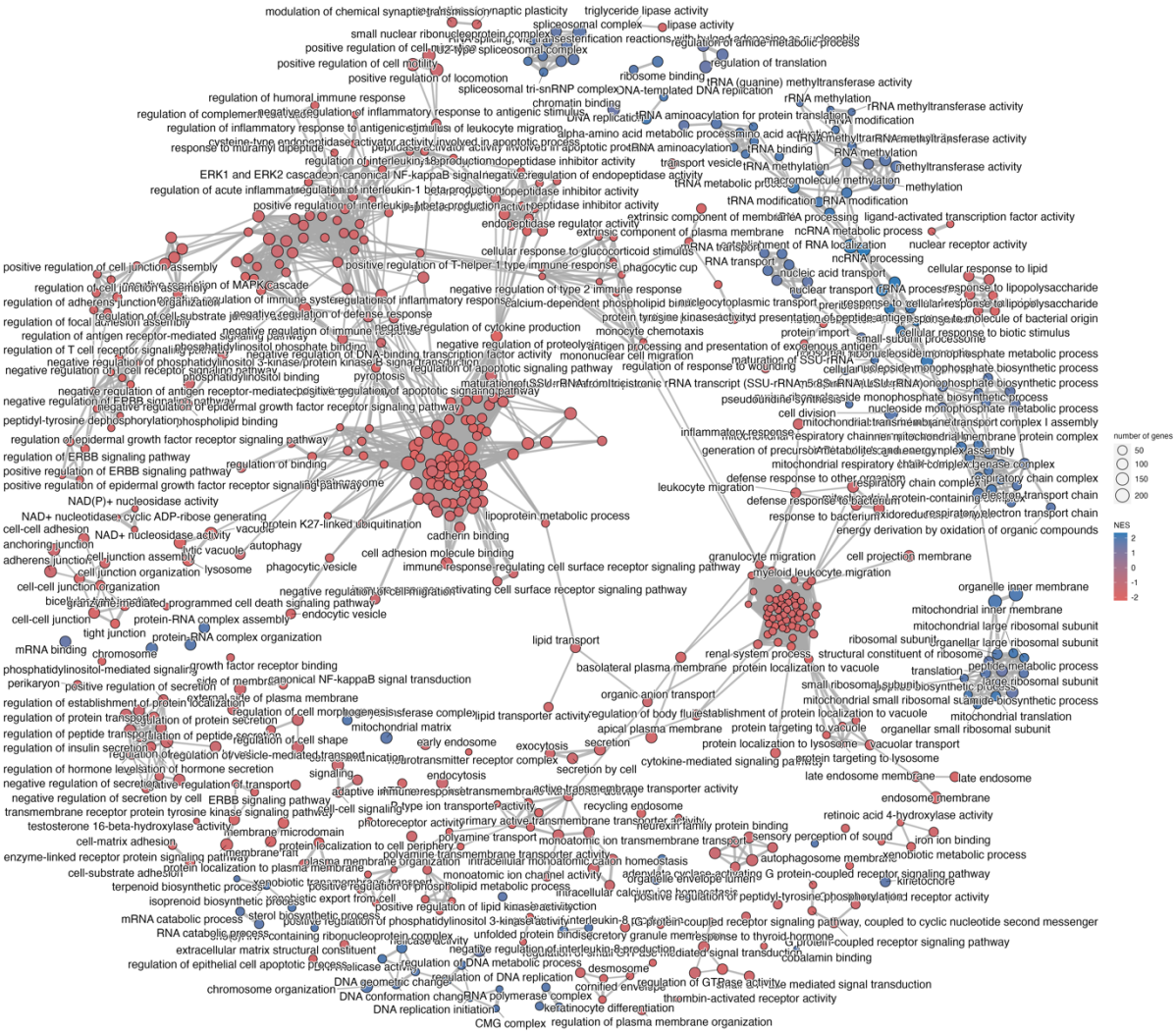


Figure 2.23. Enrichment map of GO terms enriched in the dorsal skin of Gosner stage ~34 wood frog larvae following exposure to a 1× microplastics mixture.

Gene set enrichment analysis was performed with clusterProfiler using shrunken $\log_2$ fold change values from DESeq2 comparisons of the dorsal skin of wood frogs at Gosner stage ~34 exposed to the 1× microplastics treatment versus the dorsal skin of wood frogs in the 0× control group. GO terms were assigned by homology transfer from BLASTP and BLASTX searches of the Swiss-Prot database. Similarity between enriched GO terms was calculated with the Jaccard similarity coefficient, then plotted with edges between any node with similarity score > 0.2. Nodes are coloured by the normalized enrichment score (NES).

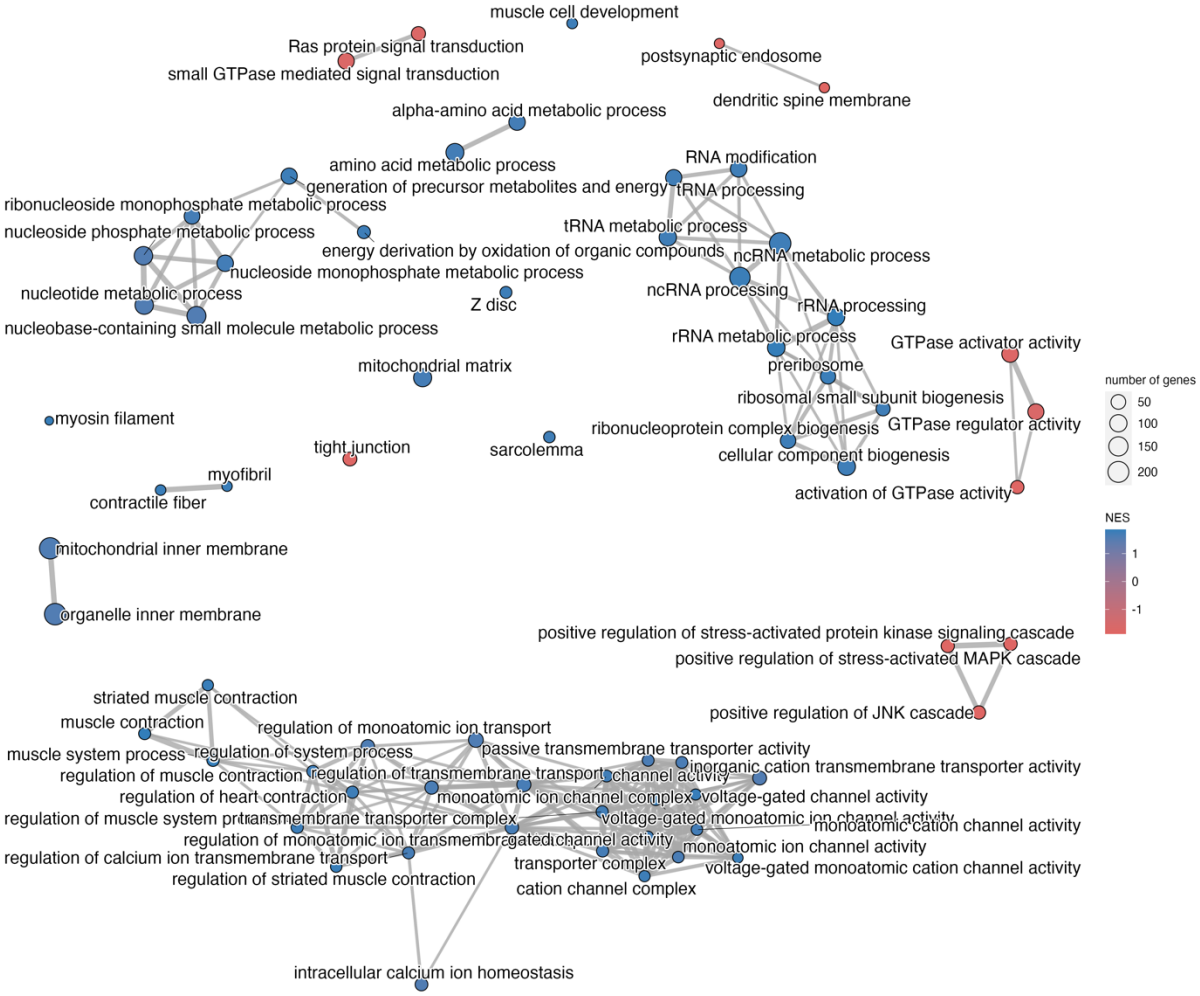


Figure 2.24. Enrichment map of GO terms enriched in the dorsal skin of Gosner stage ~34 wood frog larvae following exposure to a 10× microplastics mixture.
Gene set enrichment analysis was performed with clusterProfiler using shrunken $\log_2$ fold change values from DESeq2 comparisons of the dorsal skin of wood frogs at Gosner stage ~34 exposed to the 10× microplastics treatment versus the dorsal skin of wood frogs in the 0× control group. GO terms were assigned by homology transfer from BLASTP and BLASTX searches of the Swiss-Prot database. Similarity between enriched GO terms was calculated with the Jaccard similarity coefficient, then plotted with edges between any node with similarity score > 0.2. Nodes are coloured by the normalized enrichment score (NES).

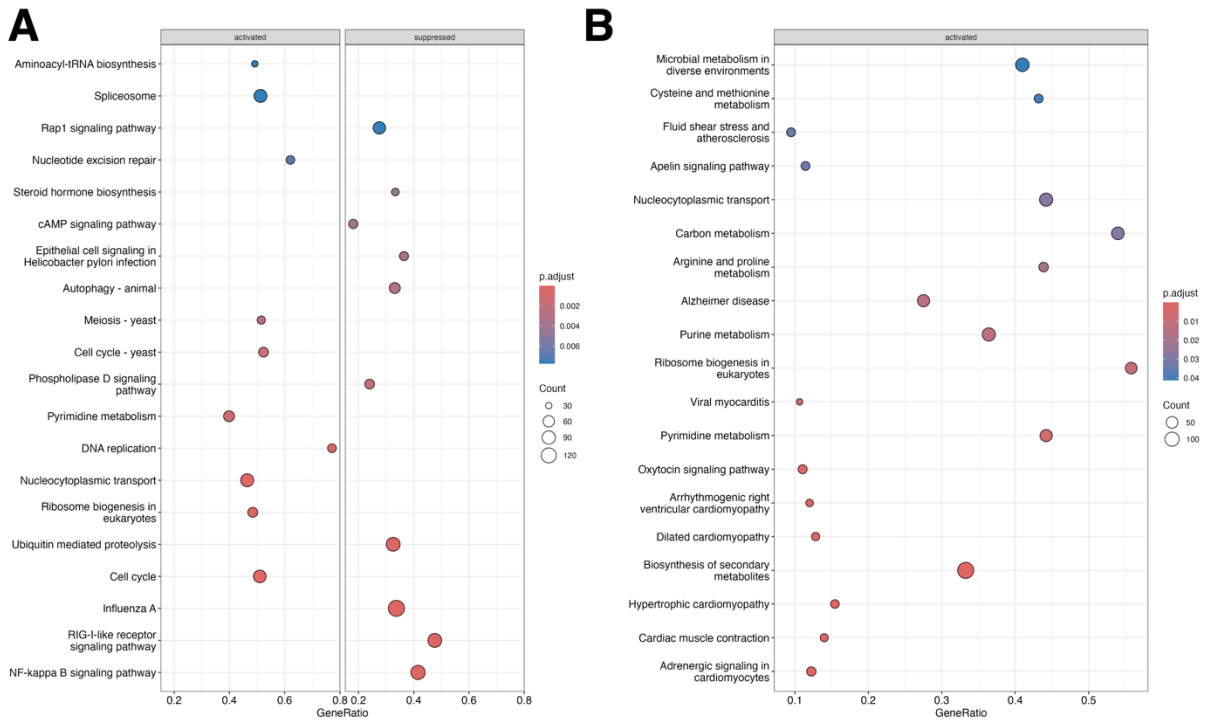


Figure 2.25. Top enriched KEGG pathways in the dorsal skin of Gosner stage ~34 wood frog larvae exposed to a 1× or 10× microplastics mixture.

Gene set enrichment analysis was performed with clusterProfiler using shrunken $\log_2$ fold change values from DESeq2 comparisons of the dorsal skin obtained from Gosner stage ~34 wood frog larvae following exposure to **A)** 1× microplastics treatment and **B)** 10× microplastics treatment versus the developmental stage-matched 0× control group. KEGG pathways were assigned by EggNOG-mapper. The top twenty most significantly enriched KEGG pathways by adjusted p-value are plotted for **A)**, while all enriched pathways are plotted for **B)**. "Activated" pathways indicate those with a positive normalized enrichment score (NES) and "suppressed" pathways are those with a negative NES. Count is the number of genes in the supplied gene list contained in the KEGG pathway. GeneRatio represents the ratio of Count over the total number of genes in the KEGG pathway.

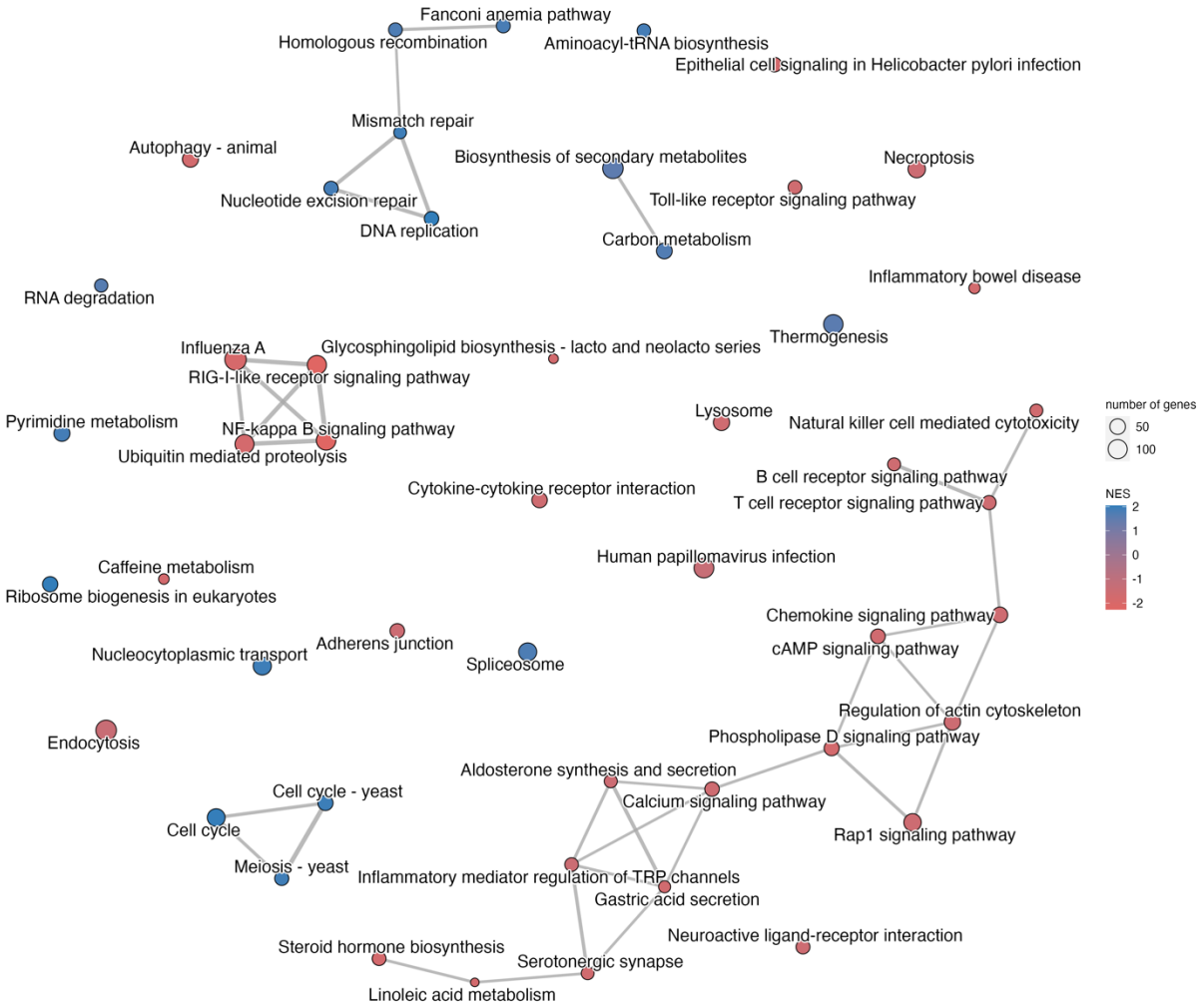


Figure 2.26. Enrichment map of KEGG pathways enriched in the dorsal skin of Gosner stage ~34 wood frog larvae folloing exposure to a 1× microplastics mixture.
Gene set enrichment analysis was performed with clusterProfiler using shrunken $\log_2$ fold change values from DESeq2 comparisons of the dorsal skin of wood frogs at Gosner stage ~34 exposed to the 1× microplastics treatment versus the dorsal skin of wood frogs in the 0× control group. KEGG pathways were assigned by EggNOG-mapper. Similarity between enriched KEGG pathways was calculated with the Jaccard similarity coefficient, then plotted with edges between any node with similarity score > 0.2. Nodes are coloured by the normalized enrichment score (NES).

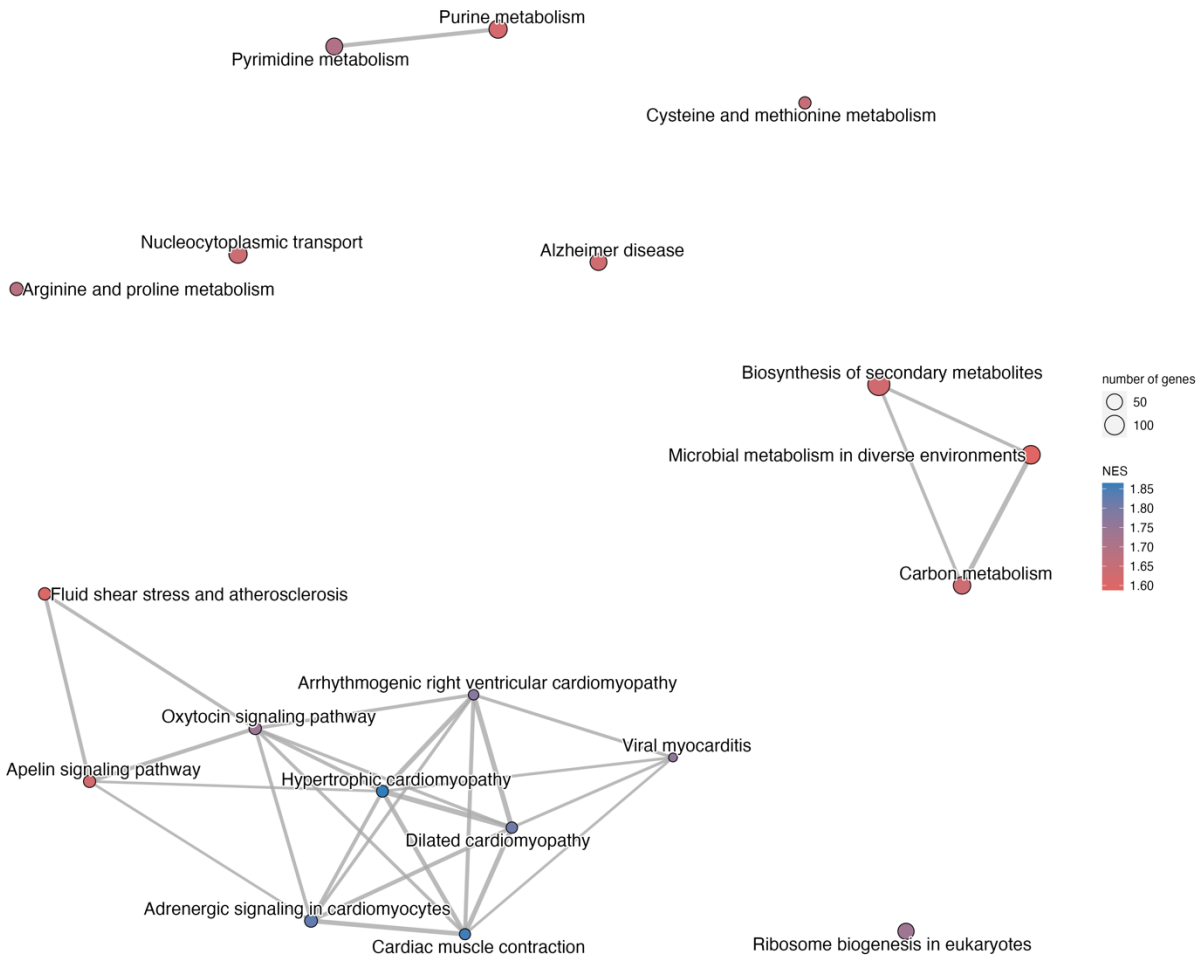


Figure 2.27. Enrichment map of KEGG pathways enriched in the dorsal skin of Gosner stage ~34 wood frog larvae following exposure to a 10× microplastics mixture.
Gene set enrichment analysis was performed with clusterProfiler using shrunken $\log_2$ fold change values from DESeq2 comparisons of the dorsal skin of wood frogs exposed to the 10× microplastics treatment versus the dorsal skin of wood frogs in the 0× control group. KEGG pathways were assigned by EggNOG-mapper. Similarity between enriched KEGG pathways was calculated with the Jaccard similarity coefficient, then plotted with edges between any node with similarity score > 0.2. Nodes are coloured by the normalized enrichment score (NES).

At GS ~42, enriched GO terms and KEGG pathways were only found in the 10× treatment. Enriched GO terms include suppression of terms related to mitochondria, translation, and RNA processes (Figure 2.28). Activated GO terms include peptidase activity, RNA nuclease activity, DNA polymerase activity, and virion-related terms (Figure 2.28). Clustering of all enriched GO terms shows three main clusters of suppressed terms involving translation, RNA processing and other RNA terms, and a large cluster of terms related to mitochondrial function (Figure 2.29). There is also a cluster of activated terms involving viral terms and nuclease activity (Figure 2.29). Suppressed KEGG pathways in the dorsal skin of GS ~42 wood frogs exposed to the 10× microplastics treatment include citrate cycle, oxidative phosphorylation, ribosome, proteasome, thermogenesis, and three human disease terms (Figure 2.30 & Figure 2.31).

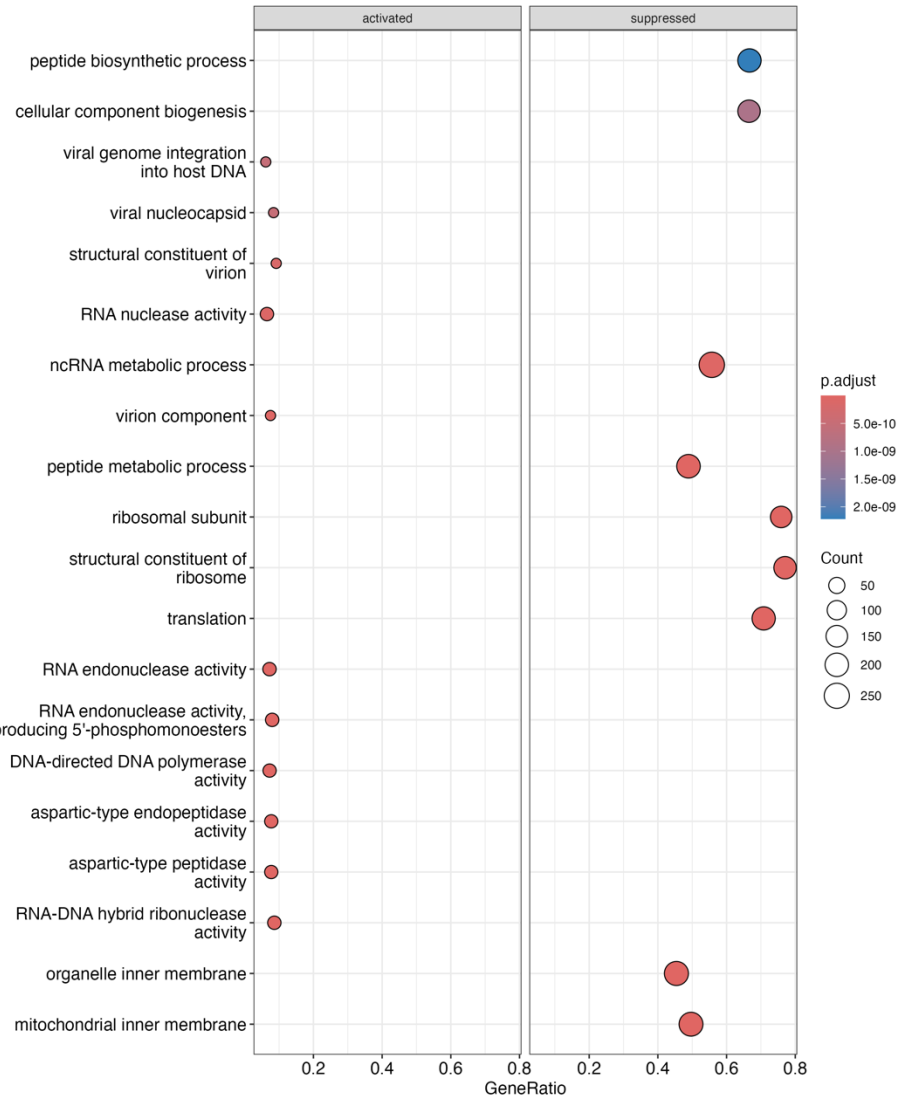


Figure 2.28. Top enriched GO terms in the dorsal skin of Gosner stage ~42 wood frogs exposed to a 10× microplastics mixture.

Gene set enrichment analysis was performed with clusterProfiler using shrunken $\log_2$ fold change values from DESeq2 comparison of the dorsal skin obtained from Gosner stage ~42 wood frogs following exposure to a 10× microplastics treatment versus the developmental stage-matched 0× control group. No enriched terms were found for the 1× treatment at GS ~42. GO terms were assigned by homology transfer from BLASTP and BLASTX searches of the Swiss-Prot database. The top twenty most statistically significantly enriched GO terms by adjusted p-value are plotted. "Activated" terms indicate those with a positive normalized enrichment score (NES) and "suppressed" terms are those with a negative NES. Count is the number of genes in the supplied gene list contained in the GO term. GeneRatio represents the ratio of Count over the total number of genes in the GO term.

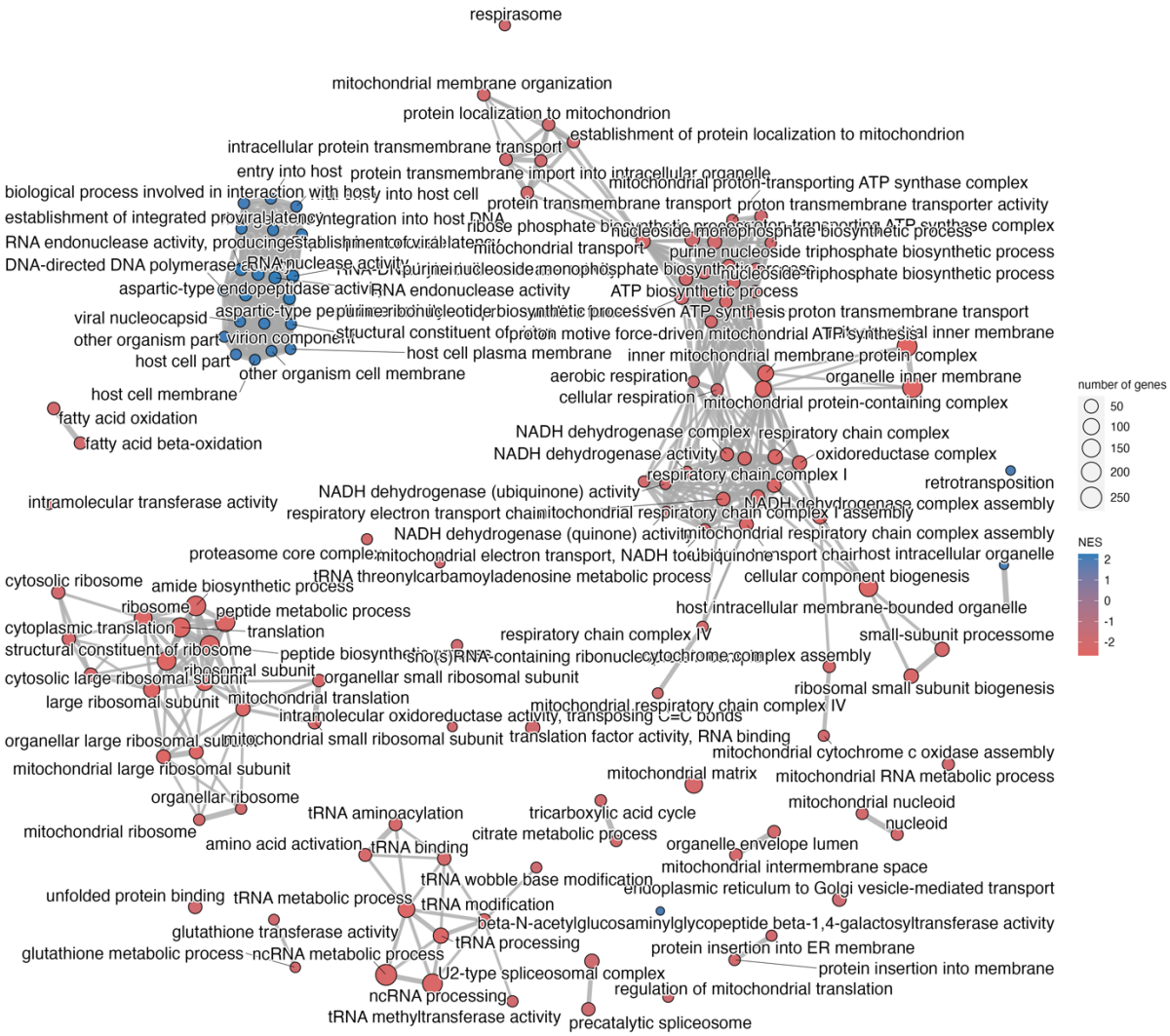


Figure 2.29. Enrichment map of GO terms enriched in the dorsal skin of Gosner stage ~42 wood frogs exposed to a 10× microplastics mixture.

Gene set enrichment analysis was performed with clusterProfiler using shrunken $\log_2$ fold change values from DESeq2 comparisons of the dorsal skin of wood frogs at Gosner stage ~42 exposed to the 10× microplastics treatment versus the dorsal skin of wood frogs exposed to the 0× control group. GO terms were assigned by homology transfer from BLASTP and BLASTX searches of the Swiss-Prot database. Similarity between enriched GO terms was calculated with the Jaccard similarity coefficient, then plotted with edges between any node with similarity score > 0.2. Nodes are coloured by the normalized enrichment score (NES).

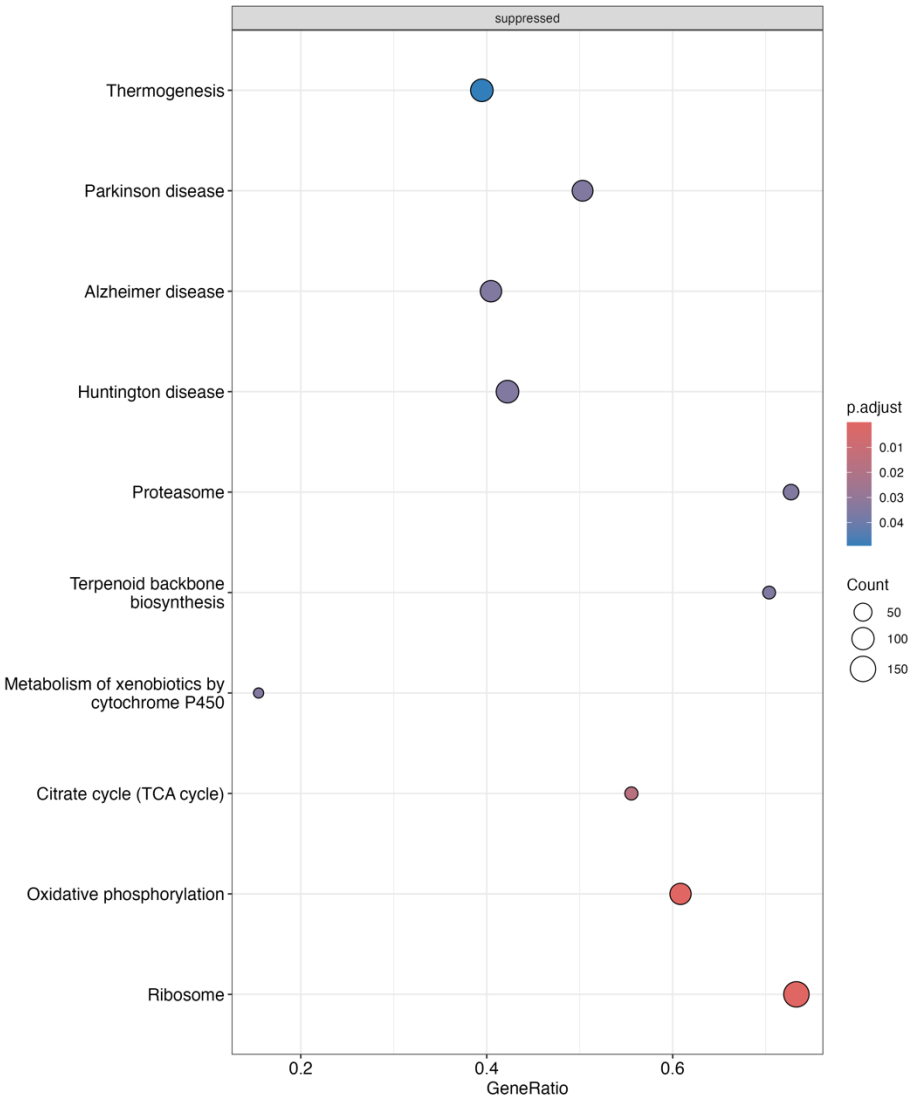


Figure 2.30. Enriched KEGG pathways in the dorsal skin of Gosner stage ~42 wood frogs exposed to a 10× microplastics mixture.

Gene set enrichment analysis was performed with clusterProfiler using shrunken $\log_2$ fold change values from DESeq2 comparisons of the dorsal skin obtained from Gosner stage ~42 wood frogs following exposure to a 10× microplastics treatment versus the developmental stage-matched 0× control group. KEGG pathways were assigned by EggNOG-mapper. "Suppressed" pathways are those with a negative normalized enrichment score (NES). Count is the number of genes in the supplied gene list contained in the KEGG pathway. GeneRatio represents the ratio of Count over the total number of genes in the KEGG pathway. No enriched pathways were found for the 1× treatment at Gosner stage ~42.

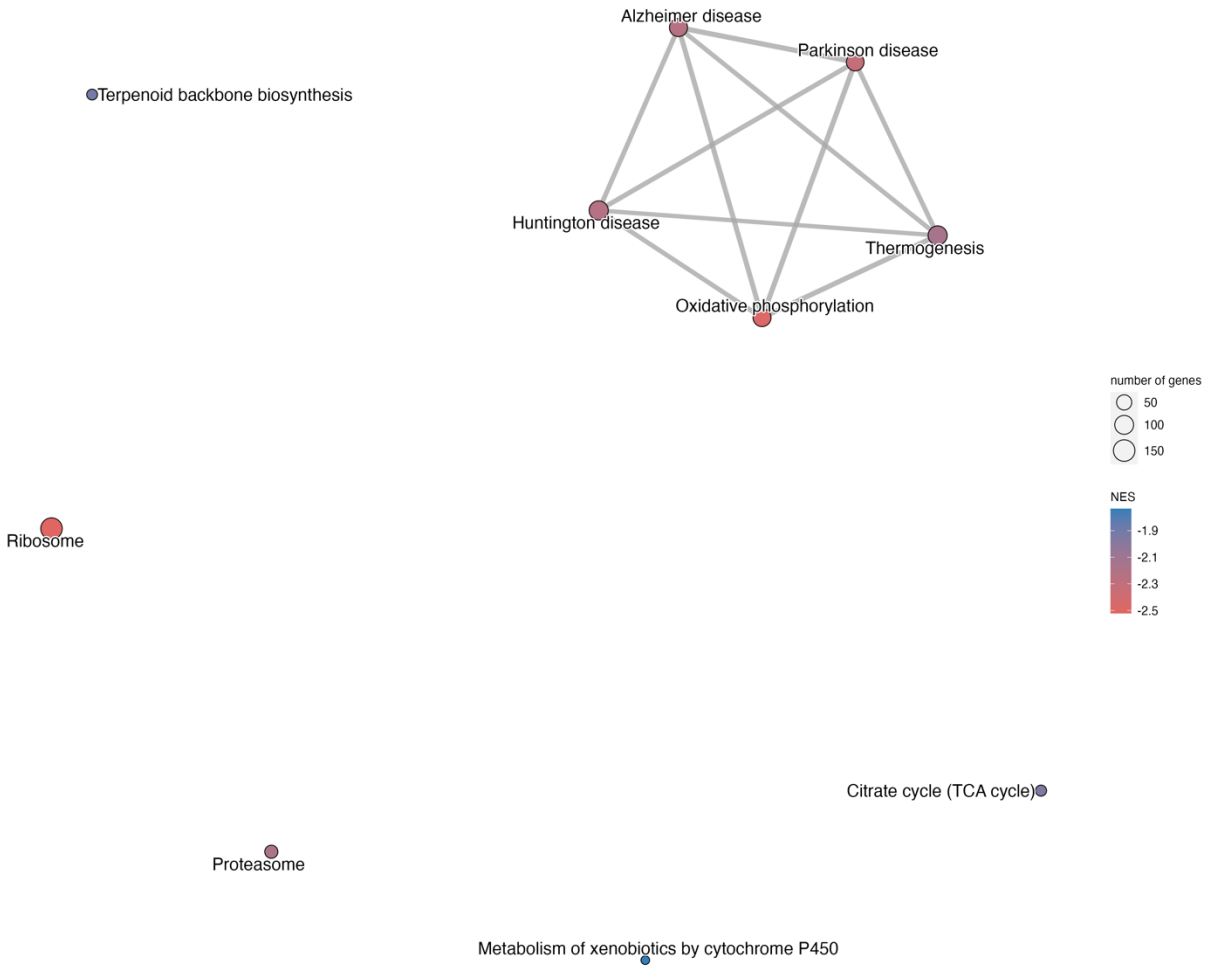


Figure 2.31. Enrichment map of KEGG pathways enriched in the dorsal skin of Gosner stage ~42 wood frogs exposed to a 10× microplastics mixture.
Gene set enrichment analysis was performed with clusterProfiler using shrunken $\log_2$ fold change values from DESeq2 comparisons of the dorsal skin of wood frogs at Gosner stage ~42 exposed to the 10× microplastics treatment versus the dorsal skin of wood frogs from the 0× control group. KEGG pathways were assigned by EggNOG-mapper. Similarity between enriched KEGG pathways was calculated with the Jaccard similarity coefficient, then plotted with edges between any node with similarity score > 0.2. Nodes are coloured by the normalized enrichment score (NES).

At GS 45, the top twenty enriched GO terms in the 1× treatment included suppression of terms related to phospholipids and phospholipase activity, while activated terms included a variety of terms related to development, muscle and movement, and other cellular processes (Figure 2.32A). Two large clusters were formed: a cluster of suppressed terms related to phospholipids and a cluster of activated terms including a wide variety of terms involving growth and development, muscle, coagulation, senescence, and others (Figure 2.33). No KEGG pathways were enriched in the 1× treatment. In the 10× treatment, 13 GO terms were enriched (Figure 2.32B). These included proteasome accessory complex (suppressed), and a cluster of activated terms related to polymerase, nuclease, and peptidase activity, as well as viral and cell membrane terms (Figure 2.34). A single KEGG pathway was enriched in the 10× treatment: proteasome, which was suppressed with a NES of -2.18 and adjusted p value of 0.022. Thirty-three detected genes were contained in the pathway, which was 75% of all genes in the pathway.

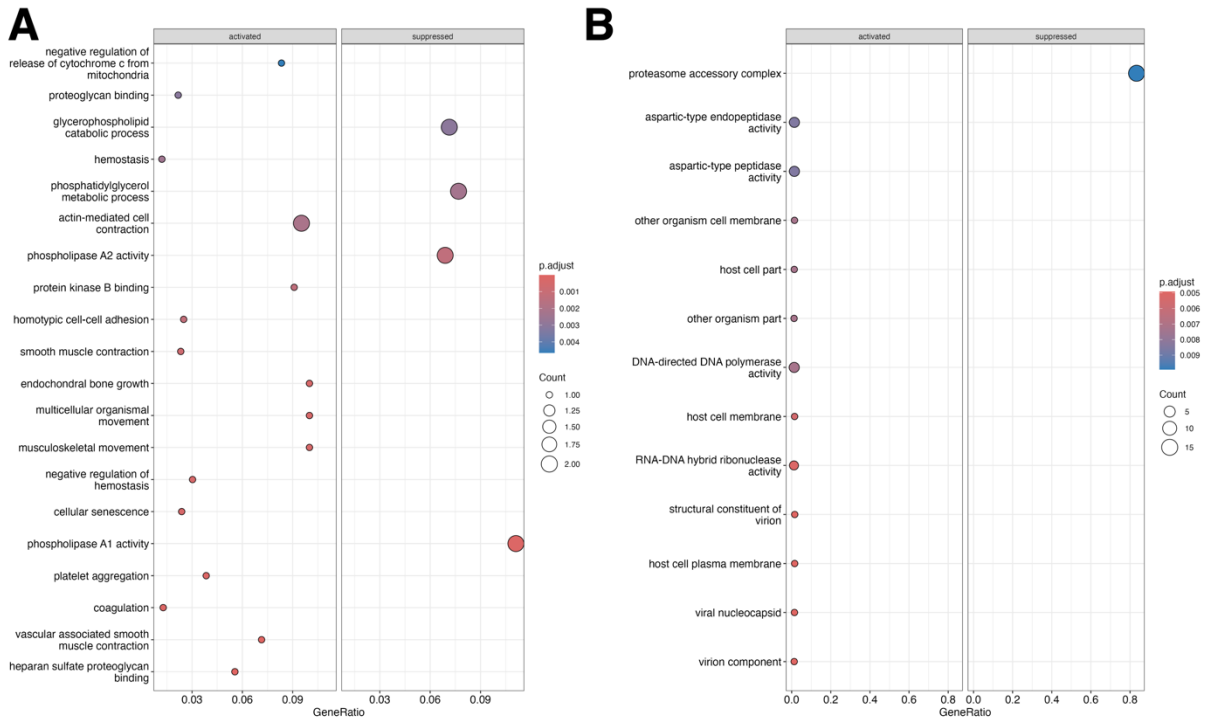


Figure 2.32. Top enriched GO terms in the dorsal skin of Gosner stage 45 wood frogs exposed to a microplastics mixture.

Gene set enrichment analysis was performed with clusterProfiler using shrunken $\log_2$ fold change values from DESeq2 comparisons of the dorsal skin obtained from Gosner stage 45 wood frogs following exposure to a **A)** 1× microplastics treatment or **B)** 10× microplastics treatment versus the developmental stage-matched 0× control group. GO terms were assigned by homology transfer from BLASTP and BLASTX searches of the Swiss-Prot database. The top twenty most statistically significantly enriched GO terms by adjusted p-value are plotted for **A)**, while all enriched terms are plotted for **B)**. "Activated" terms indicate those with a positive normalized enrichment score (NES) and "suppressed" terms are those with a negative NES. Count is the number of genes in the supplied gene list contained in the GO term. GeneRatio represents the ratio of Count over the total number of genes in the GO term.

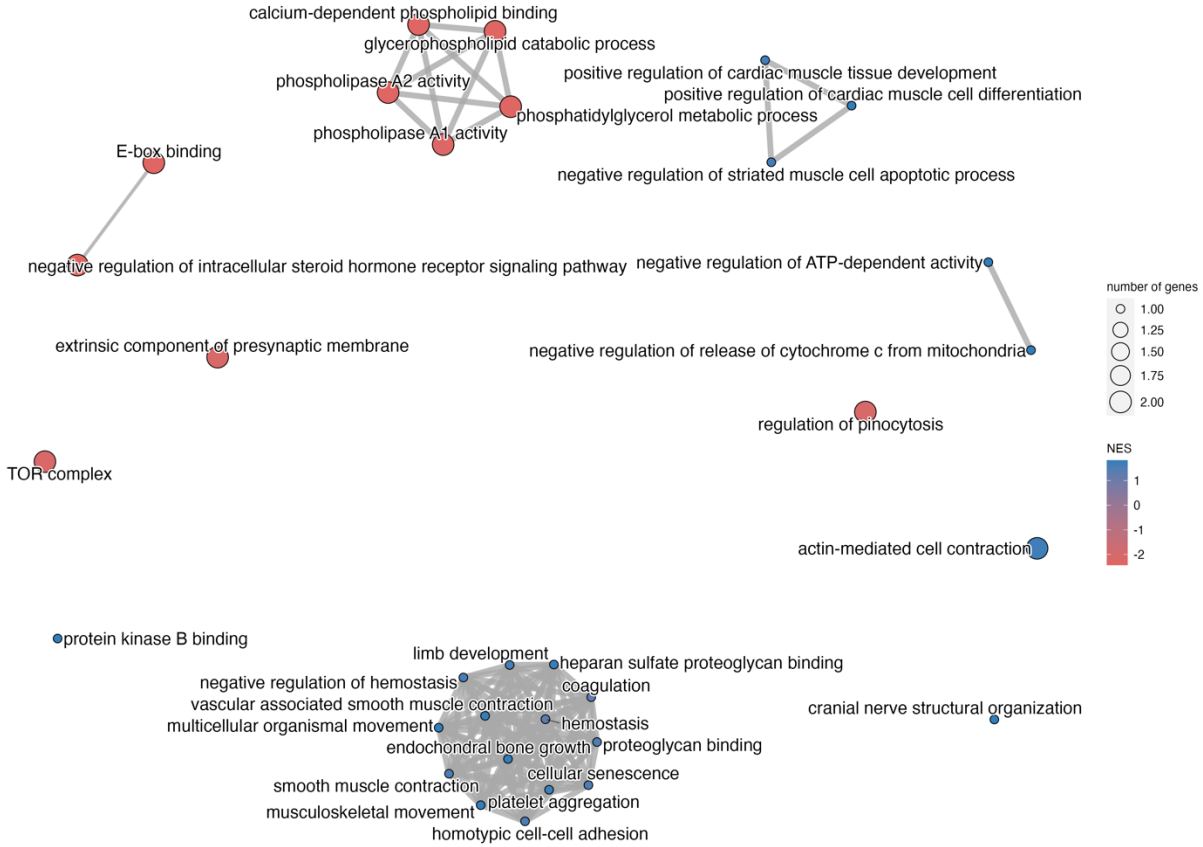


Figure 2.33. Enrichment map of GO terms enriched in the dorsal skin of Gosner stage 45 wood frogs following exposure to a 1× microplastics mixture.

Gene set enrichment analysis was performed with clusterProfiler using shrunken $\log_2$ fold change values from DESeq2 comparisons of the dorsal skin of wood frogs at Gosner stage 45 exposed to the 1× microplastics treatment versus the dorsal skin of wood frogs from the 0× control group. GO terms were assigned by homology transfer from BLASTP and BLASTX searches of the Swiss-Prot database. Similarity between enriched GO terms was calculated with the Jaccard similarity coefficient, then plotted with edges between any node with similarity score > 0.2. Nodes are coloured by the normalized enrichment score (NES).

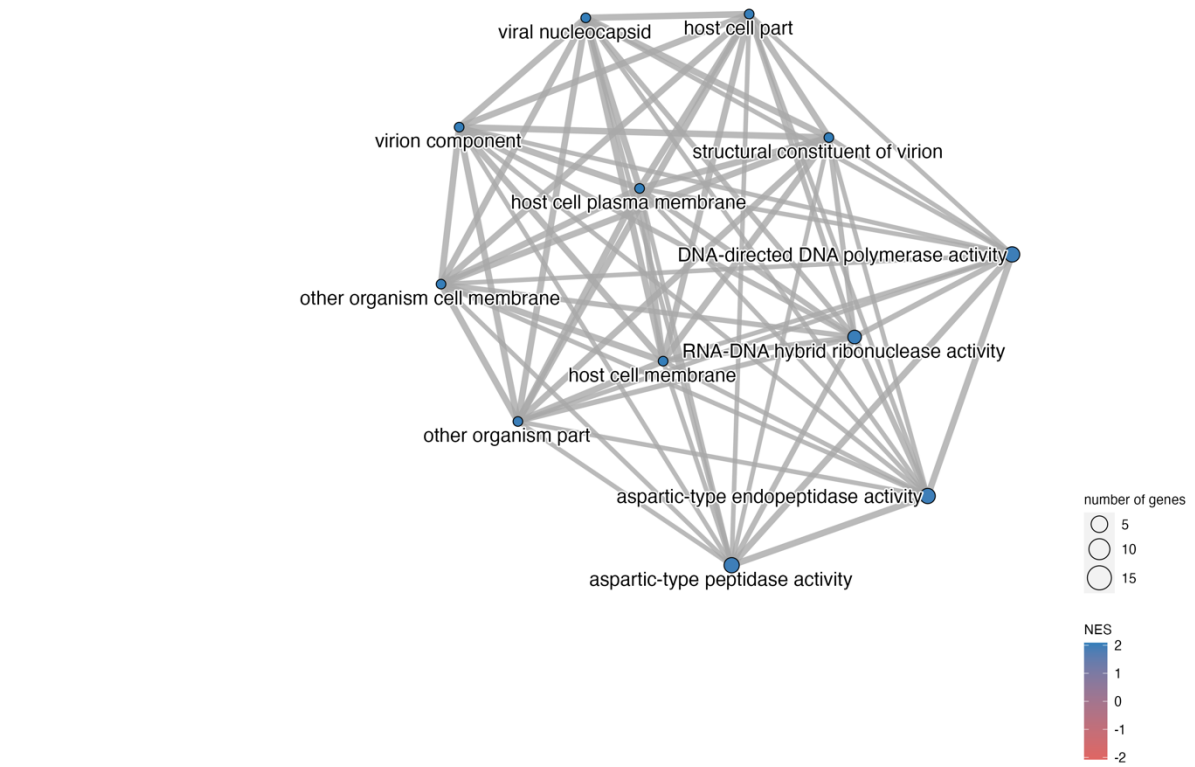


Figure 2.34. Enrichment map of GO terms enriched in the dorsal skin of Gosner stage 45 wood frogs following exposure to a 10× microplastics mixture.

Gene set enrichment analysis was performed with clusterProfiler using shrunken $\log_2$ fold change values from DESeq2 comparisons of the dorsal skin of wood frogs at Gosner stage 45 exposed to the 10× microplastics treatment versus the dorsal skin of wood frogs from the 0× control group. GO terms were assigned by homology transfer from BLASTP and BLASTX searches of the Swiss-Prot database. Similarity between enriched GO terms was calculated with the Jaccard similarity coefficient, then plotted with edges between any node with similarity score > 0.2. Nodes are coloured by the normalized enrichment score (NES).

Chapter 3
Discussion, Conclusions, and Future Directions

3.1 Discussion

Microplastics are a ubiquitous, persistent contaminant of concern with varied effects on organisms. Despite their semiaquatic lifestyle, the body of literature on the effects of microplastics on amphibians is lagging behind fishes and aquatic invertebrates. Of the studies that have been performed, few have evaluated the sub-organismal responses of amphibians to microplastic exposure. To my knowledge, this study is the first to evaluate sub-organismal responses of amphibians at multiple developmental stages to chronic exposure to an environmentally relevant microplastic mixture throughout development in realistic outdoor conditions. Additionally, little is known about how the transcriptional profile of North American wood frog skin changes during metamorphosis. To address these gaps, wood frogs were raised from eggs until the completion of metamorphosis in outdoor mesocosms containing a 0× (0 g/L), 1× (0.069 g/L), or 10× (0.691 g/L) dose of a microplastic mixture consisting of equal parts polypropylene, polystyrene, and polyethylene terephthalate microplastics. RNA sequencing was performed on RNA from the dorsal skin of wood frog larvae collected at three different developmental stages: after 50 days of exposure (corresponding to an average Gosner stage of 34; GS ~34), after 74 days of exposure (corresponding to an average Gosner stage of 42; GS ~42), and Gosner stage 45 (collected after 74 to 82 days of exposure; GS 45) (Figure 2.4). This data was leveraged to address two questions posed in this thesis: (1) what is the transcriptomic profile of juvenile wood frog dorsal skin under normal conditions and how does the transcriptional profile change with frog development? And (2) does chronic exposure to microplastics affect the dorsal skin transcriptome of wood frogs during development? Concordance was observed in the functions of genes expressed in the dorsal skin of wood frogs compared to other published amphibian skin transcriptomes. Differential gene expression and gene set enrichment analysis between developmental timepoints revealed enriched GO terms and KEGG

pathways which correspond to known phenomena in developing frogs, such as immunosuppression as tadpoles approach metamorphic climax. Evaluating the effects of microplastics on dorsal skin gene expression, the greatest effect was seen in GS ~34 tadpoles exposed to the 1× microplastics treatment, versus the tadpoles in the 0× control group, where immunosuppression and changes to mitochondrial function and protein synthesis were seen. This was followed by GS ~34 tadpoles exposed to the 10× treatment, where changes to transmembrane ion transport and various metabolic processes were seen, as compared to the 0× control. The effect at GS ~42 and GS 45 was less extreme than at GS ~34, demonstrating that tadpoles at different developmental stages respond differently to microplastic exposure.

3.1.1 Transcriptome Characteristics

When performing transcriptome assembly, metrics to consider include the number of assembled transcripts and genes, the N50 value of the transcriptome, and if applicable, the alignment rate of RNA-seq reads to the genome. When sequencing was performed on samples obtained from this study, a reference genome was not available for the North American wood frog and samples were sequenced deeply in anticipation of performing *de novo* transcriptome assembly. However, the release of the North American wood frog reference genome (GCA_028564925.1) enabled transcriptome assembly using reference-guided approaches, which is much less time and computationally intensive than a full *de novo* assembly. I therefore opted for high stringency quality control criteria of the RNA-seq reads. The infancy of the wood frog reference genome means that there is an absence of sufficient annotation information for a transcriptomics study. As a result, *de novo* approaches for the annotation of assembled transcripts were used. However, few amphibian studies have used this combined approach, presumably because a reference genome was not newly published in the middle of their analysis, making direct comparisons of transcriptome characteristics challenging. For example, *de novo* techniques tend to assemble many more sequences than expected based on the number of genes in the genome. A *de novo* assembly of the axolotl transcriptome resulted in over 1.5 million transcripts clustered into over 1.3 million gene groupings (Bryant et al., 2017), when the axolotl genome contains just over

23,000 genes (Nowoshilow et al., 2018). *Xenopus laevis*, one of the best-studied amphibian model species, has 45,099 annotated protein-coding genes (Session et al., 2016). The reference-guided assembly generated in this study contained 96,645 transcripts from 45,926 genes (Table 2.4). The assembly had an N50 of 4,622 (Table 2.4), meaning that 50% of the total length of the transcriptome sequences are covered by transcripts with a length of 4,622 or more base pairs. N50 values from reported *de novo* amphibian transcriptome assemblies range from 335 – 3,432 (Arenas Gómez et al., 2020; Bai et al., 2021; Campbell et al., 2018; Clay et al., 2019; Ellison et al., 2020, 2015; Fan et al., 2017, 2021; Firneno et al., 2022; Huang et al., 2016; Ke et al., 2018; Komaki et al., 2021; Lan et al., 2022; Pownall et al., 2018; Qi et al., 2016; Richardson et al., 2018; Row et al., 2016; Shibao et al., 2018; Smirnov et al., 2022; Torres-Sánchez et al., 2019; Viricel et al., 2018; Yang et al., 2016; Zhao et al., 2014). The larger N50 value observed in this study may be explained by the higher average transcript length and larger maximum transcript length in this transcriptome compared to previous *de novo* transcriptomes, where reported. This is likely due to *de novo* techniques assembling many small transcripts (Zhao et al., 2011), and possibly being unable to assemble very large transcripts accurately. The largest detected transcript in this study was 91,419 base pairs long (Table 2.4) and was annotated as coding for the full sequence of titin, the largest known protein, which functions in muscle (Wang et al., 1979). The distribution of predicted candidate coding sequence lengths in this study's transcriptome (Figure 2.6) was similar to previously reported coding region length distributions in the Chinese giant salamander (Bai et al., 2021).

Low RNA-seq read alignment rates to reference genomes could indicate sample contamination, quality control issues, or misassembled or missing reference sequences. Of the amphibian species with reference genomes available, few studies report the alignment rate of RNA-seq reads to the genome. One study reported an alignment rate of around 94% (Nakajima et al., 2020) in a study on RNA from *Xenopus tropicalis* whole tails, roughly 10% higher than the average alignment rate achieved in this study of 83.24%. This could be due to the infancy of the wood frog reference genome (GCA_028564925.1), being the first

published version, there could potentially be sequences missing. An additional reason for the lower alignment rate in this study could be a higher proportion of microbial reads present from commensal skin microbes in samples from the outdoor-raised wood frogs used in this study compared to the lab-raised *X. tropicalis*. However, an alignment rate of 83% is well within the acceptable range, with 70% or above generally being considered acceptable (Conesa et al., 2016; Musich et al., 2021).

Given the high-quality RNA reads and reference-guided transcriptome assembly methodology, and comparisons to transcriptomes in the literature, I believe this wood frog dorsal skin transcriptome is of high quality and reliable. However, the annotation rates, while typical for this type of study, does mean that many sequences do not have sufficient annotation information to be included in downstream gene set enrichment analysis. This may limit the sensitivity of these analyses and mean that some biological pathways which are being dysregulated in these organisms do not appear as statistically significant in this analysis. Although limited by the data available at the time of analysis, as additional annotation information becomes available, this data could be reanalyzed to detect additional dysregulated biological systems.

3.1.2 Wood Frog Dorsal Skin Transcriptome Profile

Amphibian skin has roles in respiration, osmotic regulation, and immune defence, employing physical, chemical, immunological, and microbiological defences to prevent infection (reviewed in Varga et al., 2019). To understand the functions of genes expressed in normal wood frog larvae skin, GO terms and KEGG pathway annotations of genes expressed in 0× control dorsal skin samples at all sequenced developmental timepoints were profiled. The GO database is organized as a directed acyclic graph, with three main ontologies (level 1): biological process, cellular component, and molecular function. Within the biological process ontology, the most common level 2 GO terms assigned to genes expressed in control dorsal skin were cellular process, biological regulation, metabolic process, and regulation of biological process (Figure 2.8), which were common terms seen in other amphibian

transcriptomes created from skin or a combination of skin and other tissues (Arenas Gómez et al., 2020; Bai et al., 2021; Fan et al., 2017, 2021; Huang et al., 2016). Genes expressed in the wood frog 0× control dorsal skin were annotated with only three level 2 GO terms in the cellular component ontology: protein-containing complex, virion component, and cellular anatomical entity (Figure 2.8). While other amphibian skin transcriptomes also contained annotations for virion-related cellular component terms (Bai et al., 2021; Fan et al., 2017; Huang et al., 2016), they also included additional cellular-component terms which the transcriptome generated in this study did not, such as organelle and macromolecular complex. Based on this observation, it is possible that structural genes were less well annotated in this study's transcriptome, resulting in this discrepancy, though this is just speculation. Finally, in the molecular function ontology, binding and catalytic activity had by far the greatest frequency in this study's transcriptome, followed by molecular function regulator activity, structural molecule activity, transporter activity, and molecular transducer activity (Figure 2.8). This was again in line with previous amphibian skin transcriptomes (Arenas Gómez et al., 2020; Bai et al., 2021; Fan et al., 2017; Huang et al., 2016), particularly binding and catalytic activity. KEGG pathways are categorized into six high-level categories: cellular processes, environmental information processing, genetic information processing, human diseases, metabolism, and organismal systems. They are further sub-categorized into classes within these six categories. The number of genes expressed in 0× control dorsal skin samples annotated with KEGG pathways were profiled, summarized by KEGG class (Figure 2.9). The most common KEGG class in this study's transcriptome was signal transduction (environmental information processing), followed by immune system (organismal systems), infectious disease: viral (human diseases), and endocrine system (organismal systems) (Figure 2.9). Within the cellular processes class, cell growth and death, followed by transport and catabolism were the most common classes (Figure 2.9); within the metabolism class, lipid metabolism and carbohydrate metabolism were the most common classes (Figure 2.9); and within the genetic information processing class, folding, sorting, and degradation, followed by translation were the most common classes (Figure 2.9). Many of these classes again appear in the annotations of other

amphibian skin transcriptomes (Bai et al., 2021; Fan et al., 2017). Notably, the annotation of these previously studied amphibian transcriptomes did not include annotation of pathways under the human diseases category. Reasons for this could be that these pathways were not reported in other studies due to their human-centric nature, that more genes with immune function were able to be detected in this study due to the availability of a reference genome, that these pathways were simply not annotated in other amphibian transcriptomes, or that despite the daily monitoring for disease in our mesocosm study, it was an outdoor study and an infection could have occurred. Databases such as GO and KEGG are often human- or model organism-centric, yet they can still be useful when interpreting information from non-model organisms, but care must be taken when interpreting them. For example, many immune genes tend to have low sequence conservation because immune systems need to evolve to deal with the specific threats different organisms face, therefore, many of the genes that were annotated with the immune system KEGG class are likely highly conserved core immune genes, or less-conserved genes that have been characterized in other amphibian species such as *Xenopus laevis*. Because the data in Figure 2.9 is not displaying differentially expressed or enriched genes or pathways, but simply profiling the functions of all transcripts detected in these tissues, genes expressed at a low level will be represented in the data. As deep sequencing was performed, it is expected that genes expressed at low levels would be detected. Therefore, it cannot be definitively concluded whether these animals were experiencing an infection, or if immune genes being expressed at a basal level are simply being detected. Despite this, many of the annotated GO terms and KEGG pathways align well with the functions of amphibian skin. Many of the genes annotated with the cellular process, biological regulation, binding, and catalytic activity GO terms (Figure 2.8) are likely involved in the basic functions and maintenance of skin cells. The immune functions of the skin are supported by the response to stimulus and immune system process GO terms (Figure 2.8) and immune system KEGG classes (Figure 2.9). Transporter activity (Figure 2.8) and membrane transport (Figure 2.9) support the skin's role in osmotic regulation.

3.1.3 Transcriptional Changes in Wood Frog Dorsal Skin During Development

The skin of amphibians undergoes drastic morphological changes during metamorphosis from larval to adult form (Yoshizato, 1992), which must be accompanied by changes in gene expression. To understand how transcription in the dorsal skin is changing during wood frog development, differential expression analysis and gene set enrichment analysis of GO terms and KEGG pathways was performed with 0× control samples between the three sequenced developmental stages. One of the morphological changes to amphibian skin during metamorphosis is the keratinization of the outer skin layer, the stratum corneum (Brunelli et al., 2015). The data presented in this thesis demonstrated this, with activated GO terms related to keratinization seen at GS ~42 versus GS ~34 and GS 45 versus GS ~34 (Figure 2.13 & Figure 2.15). Furthermore, amphibian skin is known to not begin active transport of sodium until metamorphic climax (Cox & Alvarado, 1979; Takada, 1985; Taylor & Barker, 1965), which may explain the enrichment of ion transport terms at later Gosner stages (Figure 2.13 & Figure 2.15). This is one of the first studies to evaluate how gene expression in the skin of a developing amphibian changes over time. Overall, the enriched GO terms and KEGG pathways found in the skin over development align well with known developmental changes of amphibian skin, giving us confidence in the utilized methodology.

Developing amphibians undergo a period of immunosuppression as they approach metamorphic climax (Rollins-Smith, 1998). This is supported in this thesis by the enrichment of clusters of suppressed immune GO terms and KEGG pathways in the dorsal skin of wood frogs at GS ~42 versus GS ~34 and GS 45 versus GS ~34 (Figure 2.13, Figure 2.15, Figure 2.17, & Figure 2.19). Between GS ~42 and 45 there is activation of immune pathways in the dorsal skin tissue such as TNF signalling pathway, an important pathway for the activation and regulation of immune cells (Owen et al., 2013), IL-17 signalling pathway, essential in neutrophil regulation (Zenobia & Hajishengallis, 2015), and T cell receptor signalling pathway, involved in the response of cytotoxic T cells to infected cells and the activation and differentiation of helper T cells (Shah et al., 2021), a potential sign of the turnover of the

immune system as metamorphosis and the period of immunosuppression completes (Figure 2.18). Though the occurrence of systemic immunosuppression during metamorphosis is well-known, it is interesting to see suppression of immune genes in skin tissues as well. As skin contains blood vessels, the sequencing results could contain RNA-seq reads from immune cells in circulation. However, this would account for a small proportion of reads, so it is likely that true downregulation of immune genes in the resident cells (epithelial cells, fibroblasts, macrophages, dendritic cells) that comprise the skin tissue is being detected. This is important as it means that in addition to systemic immunosuppression, the skin barrier itself may be immunologically compromised during metamorphosis. Consequently, pathogens of amphibian concern may more easily be able to cross the skin barrier during this period. Opportunistic pathogens could take advantage of this period of immunosuppression to establish an infection. Therefore, it is essential to determine how microplastics could affect the skin during this period of natural immunosuppression to ensure developing amphibians do not become even more susceptible to infection.

3.1.4 Effects of Microplastics on Gene Expression in the Dorsal Skin of Developing Wood Frogs

To evaluate how exposure to microplastics influences the wood frog dorsal skin transcriptome, dorsal skin from wood frogs exposed to a 0×, 1×, or 10× microplastics treatment was collected at three developmental stages: GS ~34, GS ~42, and GS 45. RNA sequencing, differential gene expression analysis, and gene set enrichment analysis of GO terms and KEGG pathways was performed. Each timepoint was analyzed independently, with the comparator group being the 0× treatment at the corresponding developmental stage (the 1× treatment versus the 0× treatment and the 10× treatment versus the 0× treatment). The greatest number of differentially expressed genes and enriched GO terms and KEGG pathways were observed at the earliest timepoint, GS ~34. Several proposed factors may account for this. The first potential explanation is that of developmental plasticity, which can mitigate effects seen early in development by the completion of metamorphosis (Zhang et al., 2023). A similar phenomenon may have occurred here, where a greater effect was observed

at the first timepoint (GS ~34) but is mitigated at latter timepoints, resulting in fewer differentially expressed genes. Second, metamorphosing amphibians tend to stop feeding as they approach metamorphic climax and the gastrointestinal tract rearranges to support the carnivorous diet of adults (reviewed in Hourdry et al., 1996). This could have resulted in reduced consumption of microplastics at the latter two sequenced timepoints, potentially reducing observed effects. Third, due to the increased thickness and keratinization of adult amphibian skin compared to larval skin, it is possible that microplastics could affect greater changes to the larval form than the adult form.

Furthermore, at GS ~34, a greater number of differentially expressed genes and enriched GO terms and KEGG pathways were seen in the 1× treatment than the 10× treatment, as compared to the 0× control. Since only two concentrations were tested in this study, whether the dose response is monotonic with negative slope or nonmonotonic cannot be determined. These types of responses are best studied in the context of hormones and endocrine-disrupting chemicals, where a number of mechanisms have been proposed including cytotoxicity at high doses, cell-specific responses, receptor selectivity, receptor down-regulation and desensitization, receptor competition, and endocrine negative feedback loops (Vandenberg et al., 2012). It is possible that one or more of these mechanisms are at play in this study, though it is not possible to demonstrate which. Interestingly, this trend did not continue at GS ~42 or GS 45, perhaps in part due to the considerations about developmental plasticity and changes in skin morphology mentioned above.

Two previous studies have profiled the expression of select genes in amphibians in the context of microplastic or nanoplastic exposure (Pekmezekmek et al., 2022; Tussellino et al., 2015), and one study which performed tadpole whole-body RNA-seq (Zhang et al., 2023) after exposure to microplastics. To my knowledge, the research reported in this thesis is the first RNA-seq transcriptomics study to evaluate the response of the skin transcriptome to microplastic exposure in amphibians. To my knowledge it is also the first transcriptomics study performed on organisms exposed to real-life conditions (exposed to an environmentally relevant microplastics mixture chronically from eggs in outdoor mesocosms), and the first

study evaluating transcriptional changes due to microplastics exposure in a North American amphibian species. Previous targeted studies found differential expression of the *pax6*, *bmp4, tbxt,* (also known as *bra*), *myod1*, and *sox9* genes in amphibian larvae in the context of microplastic or nanoplastic exposure (Pekmezekmek et al., 2022; Tussellino et al., 2015). These genes were not differentially expressed in response to either treatment at any timepoint in this study. However, parallels were observed with the whole-body transcriptomics study by Zhang et al. (2023) on tadpoles of the Aziatic toad (*Bufo garganzia*), which saw upregulation of genes related to protein synthesis and mitochondrial function, and downregulation of genes involved in neural function and cellular responses. Enrichment of terms and pathways related to mitochondrial function was also seen in this study at GS ~34 in the 1× and 10× treatments (Figure 2.23 & Figure 2.24) and at GS ~42 in the 10× treatment (Figure 2.28 – Figure 2.31). Interestingly, at GS ~34 these terms were activated by microplastic exposure, while they were suppressed at GS ~42. Activation of terms related to protein synthesis was also seen at GS ~34 in the 1× and 10 × treatments (Figure 2.23, Figure 2.26, & Figure 2.27) and suppression at GS ~45 in the 10× treatment (Figure 2.28 – Figure 2.31). These results suggest that different amphibian species may experience a similar transcriptional response to microplastics, however, additional transcriptomics studies must be performed on a greater diversity of amphibians to support this.

Evidence of immunosuppression was seen in the dorsal skin of 1× microplastic-exposed tadpoles at GS ~34, with the suppression of various immune-related GO terms as well as KEGG pathways such as NF-κB signalling pathway, RIG-I-like receptor signalling pathway, natural killer cell mediated cytotoxicity, cytokine-cytokine receptor interaction, and others (Figure 2.22, Figure 2.23, Figure 2.25, & Figure 2.26). The NF-κB signalling pathway is active in nearly all cell types and transduces signals from a variety of stimuli (reviewed in Oeckinghaus & Ghosh, 2009). NF-κB is essential in a wide variety of immune processes, including responding to the recognition of PAMPs by PRRs, responses to cytokine signals, binding of T and B cell receptors to antigens, and also the response to stressors like UV radiation and oxidation (Oeckinghaus & Ghosh, 2009). Downregulation of this pathway

could compromise the ability of skin to respond to the presence of a pathogen. RIG-I-like receptors (RLRs) are a family of cytosolic PRRs which recognize viral double stranded RNA or single stranded RNA containing viral motifs such as a 5' triphosphate (Saito & Gale, 2008), and initiate an immune response by signal transduction through a variety of pathways, including NF-κB (Loo & Gale, 2011). Suppression of the RIG-I-like receptor signalling pathway could compromise developing amphibian's ability to respond to viral infections. A previous study has reported immunosuppression in tadpoles exposed to microplastics, with microplastic exposure leading to increased loads of *B. dendrobatidis* (Bosch et al., 2021). As multiple immune-related processes are being down-regulated in response to microplastics in this study, this could be leading to general immunosuppression of the skin barrier. This could result in increased susceptibility to infections of the skin, such as chytridiomycosis, a hypothesis which the Bosch et al. (2021) study supports. Exposure to the 10× microplastics treatment did not appear to cause immunosuppression in GS ~34 larvae. Evidence of immunosuppression in GS ~42 wood frogs was not observed, however, the downregulation of genes related to the proteasome in the dorsal skin of GS 45 wood frogs exposed to the 10× treatment was seen, which could lead to deficits in antigen presentation. The greater level of suppressed immune terms and pathways in the dorsal skin at GS ~34 compared to ~42 and 45 could be due to the immunosuppression that occurs naturally leading up to metamorphic climax. Alternatively, immunosuppression caused by microplastics could lead to even further immunosuppression as tadpoles approach metamorphic climax, resulting in an already vulnerable life stage becoming even more vulnerable to infection.

Enrichment of terms related to transmembrane transport were also seen at GS ~34. Interestingly, in the 1× treatment, these terms were activated, while they were suppressed in the 10× treatment (Figure 2.23 & Figure 2.24). Though the mechanism behind this is uncertain, previous studies have demonstrated that microplastics increase lipid membrane tension, leading to mechanical stretching stress and a reduction in the lifetime of membranes (Choi et al., 2020; Fleury & Baulin, 2021). Nanoplastics can also influence the activity of ion channels (McCarthy et al., 2011; Roshanzadeh et al., 2021). These factors, in addition to

other unknown mechanisms, could potentially be contributing to the dysregulation of genes related to transmembrane transport. These terms were not enriched past GS ~34, perhaps due to the morphological rearrangements larval skin undergoes approaching and during metamorphic climax (Yoshizato, 1992).

3.1.5 Limitations

In this study, the objectives were to evaluate how the transcriptome of the dorsal skin changes during wood frog development, and to examine the potential effects of microplastics on developing wood frogs. The study of amphibians during development poses challenges because individuals develop at different rates due to genetic variation. This means that performing sampling by exposure duration results in the sampling of animals at varying developmental stages. However, the alternative of sampling animals at a particular developmental stage presents other challenges since the sampled animals would be exposed for different durations. Further complicating this is the potential for experimental treatments to alter developmental rates. As a result, a sample size of three to five individuals was obtained, depending on the treatment and developmental stage. Since individuals within a group may be at different developmental stages, this could introduce variation in transcriptome profiles, leading to decreased analytical power. This may not have been a limitation for some comparisons performed in this study, such as the 0× control comparison over time (Figure 2.10C) and the 1× and 10× comparisons at GS ~34 (Figure 2.20), where clear expression patterns emerged. However, this may have limited the ability to detect differentially expressed genes in the 1× and 10× treatments at GS ~42 and 45, where there appeared to be more variation between samples (Figure 2.20). This can also result in the overlap of developmental stages between sampling timepoints, which occurred in this study. The collections for the second sequencing timepoint occurred when the metamorphs in the mesocosms were at approximately Gosner stage 42 (timepoint GS ~42) and all organisms in the third timepoint were at Gosner stage 45. However, sample GS ~42 0× mesocosm 4 was collected from a metamorph at Gosner stage 45. Although this sample was preserved in whole-body form, and dissected later in the lab, while GS 45 samples were dissected in the

field, after observing that this sample clustered with the four GS 45 0× samples in a PCA (Figure 2.7A), it was decided to group the sample in question with the other GS 45 samples for gene expression analysis.

Two potential limitations lie in the sample collection and preservation methods used in this study. The animals used in this study were euthanized in a MS-222 bath prior to tissue collection and were then preserved in RNAlater due to the unavailability of liquid nitrogen at the field site. Both exposure to MS-222 (Félix et al., 2020) and storage in RNAlater (Kruse et al., 2017; Passow et al., 2019) can induce transcriptional changes in genes related to oxidative stress, apoptosis, osmotic stress, and RNA processing. Since this study was evaluating gene expression, these methods could influence the results of this study. Though this does pose a potential limitation, studies must still be performed in an ethical manner, using the best tools available in the study location, and are therefore difficult or impossible to mitigate. As all samples were handled in the same manner, any transcriptome alterations due to sample handling should be uniform across all samples and therefore not contribute to the differential gene expression analysis. However, there could be interactions between the cellular state brought on by microplastics exposure and MS-222 or RNAlater which cannot be detected with the experimental design of this study.

Two GS ~34 RNA samples (GS ~34 samples from 0× treatment mesocosm 5 and 1× treatment mesocosm 4) were included in the analysis that had underwent ethanol precipitation prior to sequencing to improve A260/280 and A260/230 ratios. However, during the final wash steps, the pelleted RNA was mistakenly washed with a 75% ethanol solution which was previously used to sterilize dissection tools instead of fresh 75% molecular-grade ethanol. To evaluate the potential for sample contamination with RNases or exogenous RNA, samples were evaluated during processing and during analysis. Both samples had sufficient RNA quantity, purity, and quality (RIN and DV200 values were within acceptable ranges; Table 2.3 & Figure A.1), indicating that samples were not degraded. Furthermore, these samples were monitored throughout the RNA-seq read quality control process via their FastQC reports to ensure no metrics differed from the remaining

sample set (Figure A.2 – Figure A.7). To evaluate the possibility that expression values were altered by the usage of the incorrect ethanol solution, hierarchical clustering and heatmap visualization of the expression values of sequenced samples was performed. In both heatmaps of all samples (Figure 2.7B), and heatmaps of differentially expressed genes at GS ~34 in both the 1× and 10× treatments (Figure 2.20), these samples always clustered with at least one other sample from the same timepoint/treatment combination, and when clustering based on differentially expressed genes (Figure 2.20), these samples showed clear concordance with the expression patterns of their treatment/timepoint sample set, indicating that the use of the non-molecular-grade ethanol likely did not alter the expression levels of these differentially expressed genes in these samples, providing confidence that the inclusion of these samples in the analysis is acceptable.

Additional limitations lie in the bioinformatics methodology utilized, though the best-available tools and data were used. The North American wood frog genome was published in early 2023, and being the first version of the genome, it is possible that sequences are missing or misassembled. Any genes present in these regions would therefore not be detected in this experiment. Additionally, as annotation information is not yet available for this genome, *de novo* annotation techniques were used in this study. Only a portion of the detected transcripts could be annotated (Table 2.5), meaning that transcripts without functional annotations could not contribute to functional analysis of differential expression. Fortunately, as additional annotation information becomes available, the RNA-seq data collected in this study could be reanalyzed to gain new insights into the changes to the wood frog dorsal skin transcriptome during development, and the effects of microplastics on developing wood frog dorsal skin.

3.2 Conclusions

With amphibian populations experiencing declines due to multiple stressors and diseases, it is important to learn more about the developmental biology of amphibians and to evaluate how emerging contaminants might affect disease susceptibility throughout the

amphibian lifecycle. To address the question of how microplastics affect developing amphibian skin, developing North American wood frogs were raised in microplastic-contaminated outdoor mesocosms. Transcriptomic analysis revealed gene expression changes during development that align with known changes to amphibian skin during metamorphosis such as keratinization and changes in ion transport. It also revealed that the systemic immunosuppression of amphibians during metamorphosis also occurs in the skin, with the downregulation of various immune pathways in the skin during metamorphosis. Transcriptomic analysis revealed that exposure to microplastics caused a greater number of differentially expressed genes in the dorsal skin wood frogs around Gosner stage 34 than those around Gosner stage 42 or at Gosner stage 45. Gene set enrichment analysis revealed processes involved in the immune system, protein synthesis, mitochondrial function, and transmembrane transport to be altered. Although immunosuppression was only seen in the dorsal skin of wood frogs at Gosner stage ~34 in the 1× treatment, infection and mortalities could be increased in young larvae by exposure to microplastics. In summary, this study provides evidence that microplastics could cause immunosuppression in developing amphibians. This study provides a foundation for future studies to investigate whole organism immunocompetency of amphibians exposed to microplastics. This study also provides a large transcriptomics dataset that could be mined for future hypothesis generation on microplastic exposure effects. In conclusion, because microplastic pollution is expected to continue to increase for the foreseeable future, it is essential to continue to assess the organismal and sub-organismal effects of a range of microplastics on various species. These studies will be important for informing future policy decisions.

3.3 Future Directions

The line of inquiry begun in this thesis could be continued in numerous ways. An investigation into the effects of microplastic exposure on the commensal skin bacterial microbiomes of developing wood frogs is underway, using the skin swab samples collected during the mesocosm experiment (Section 2.1.2.7, Figure 2.2). This investigation will provide information on whether microplastic exposure alters the composition of the wood

frog commensal skin microbiome, as well as a comparative analysis between the effects on the skin microbiome and effects on the skin transcriptome. This is important to evaluate because the commensal skin bacterial microbiome can assist the amphibian immune system in protecting against pathogens (Harris et al., 2009; Woodhams et al., 2007).

Although multiple tissues were collected from the mesocosm study, only the dorsal skin was analyzed in this thesis. Additional studies could be performed on other tissues collected from this mesocosm study. The gastrointestinal tract is another tissue that comes into direct contact with microplastics, with microplastics found in the gastrointestinal tracts of the developing wood frogs in this study (Gene et al., n.d.), and therefore likely has a transcriptional response to microplastics. Because the liver filters blood, any microplastics that cross the gastrointestinal barrier into the blood are likely to pass through or accumulate in the liver. Furthermore, the spleen hosts a diversity of immune cells that are essential for responding to pathogens (Owen et al., 2013). Evaluating the transcriptomic response of the spleen to microplastic exposure would shed additional light on how microplastics affect the function of immune cells.

Samples were collected at a total of nine timepoints, yet only three were selected for sequencing in the study described in this thesis. Future studies could utilize these samples to determine how gene expression changes in response to the chronic microplastic exposure performed in the mesocosm study in different tissues and at different timepoints than the ones profiled in this study. Considering the difference in response to microplastics seen between the three timepoints sequenced in this study, it is important to evaluate additional timepoints to gain a more comprehensive understanding of how microplastics affect amphibians throughout development.

Further lines of inquiry could involve assessing effects of additional polymers, sizes, and shapes of microplastics on wood frogs. Although this study included a mixture of three common microplastics with a range of sizes, other types of microplastics are extremely prevalent. One example is microplastic fibres. Fibres are one of the most common types of microplastics, and often can elicit effects on exposed organisms (Anbumani & Kakkar, 2018;

Koelmans et al., 2019), yet few studies have evaluated their effects on amphibians (Table 1.1).

Although the body of literature on the effects of microplastics on amphibians is growing, only a handful of studies have assessed the types and amount of microplastics present in wild amphibians or amphibian habitats (Iannella et al., 2020; Karaoğlu & Gül, 2020; Kolenda et al., 2020; Mackenzie & Vladimirova, 2021; Pastorino et al., 2022; Schessl et al., 2019). I am not aware of any studies which have assessed microplastic content in North American vernal pools, essential habitat for the reproduction of many amphibian species, including the wood frog. It is important for future studies to assess the types of microplastics North American amphibians would be exposed to in their natural habitats, so that further studies on the effects of microplastics can use microplastic types and concentrations that the species in question would be exposed to in the environment. Many research groups conduct spring field work to record data on or capture amphibians. Water samples and additional tissues could be collected during this type of field work to assess microplastic content.

Previous studies have shown that microplastics can have synergistic effects on amphibians when exposed in conjunction with other pollutants, such as pesticides (Lajmanovich et al., 2022). As developing amphibians in the wild are likely to be exposed to additional stressors such as elevated temperatures, high salinity, anthropogenic noise and light, and chemical pollutants in addition to microplastics, it is important that future research evaluates how combined exposure to microplastics and these additional stressors may affect amphibians. This could be conducted in a similar manner to the mesocosm study described in this thesis, adding additional treatment groups containing microplastics plus an additional contaminant, and the contaminant alone.

Though global changes in transcription in the dorsal skin of microplastic exposed wood frogs was assessed here, of particular interest were changes to immune gene expression to assess the sublethal effects on this important immune organ of frogs. It was hypothesized that microplastic exposure could be a stressor which predisposes developing amphibians to

infection. Though downregulation of immune genes in response to exposure to microplastics was observed in dorsal skin tissue, it cannot be determined from this study alone if this translates to real-life changes to susceptibility to infection and mortality. Ultimately, to demonstrate this, a similar experiment could be performed where wood frogs are raised in water in the absence or presence of microplastics. Tadpoles of various developmental stages, as well as adults, would then be exposed to a pathogen such as FV3 or *B. dendrobatidis*. The prevalence and intensity of infection and host mortality could then be assessed and compared between the control and microplastic-exposed groups to determine if exposure to microplastics altered host disease susceptibility.

References

Albecker, M. A., & McCoy, M. W. (2017). Adaptive responses to salinity stress across multiple life stages in anuran amphibians. *Frontiers in Zoology*, *14*(1), 40. https://doi.org/10.1186/s12983-017-0222-0

Álvarez-Ruiz, R., Picó, Y., & Campo, J. (2021). Bioaccumulation of emerging contaminants in mussel (*Mytilus galloprovincialis*): Influence of microplastics. *Science of The Total Environment*, *796*, 149006. https://doi.org/10.1016/j.scitotenv.2021.149006

Amoatey, P., & Baawain, M. S. (2019). Effects of pollution on freshwater aquatic organisms. *Water Environment Research*, *91*(10), 1272–1287. https://doi.org/10.1002/wer.1221

AmphibiaWeb. (n.d.). https://amphibiaweb.org

Anbumani, S., & Kakkar, P. (2018). Ecotoxicological effects of microplastics on biota: a review. *Environmental Science and Pollution Research*, *25*(15), 14373–14396. https://doi.org/10.1007/s11356-018-1999-x

Anderson, J. C., Park, B. J., & Palace, V. P. (2016). Microplastics in aquatic environments: Implications for Canadian ecosystems. *Environmental Pollution*, *218*, 269–280. https://doi.org/10.1016/j.envpol.2016.06.074

Andrady, A. L. (2011). Microplastics in the marine environment. *Marine Pollution Bulletin*, *62*(8), 1596–1605. https://doi.org/10.1016/j.marpolbul.2011.05.030

Andrews, S. (2010). *FastQC: A quality control tool for high throughput sequence data* [Computer software]. https://www.bioinformatics.babraham.ac.uk/projects/fastqc/

Arenas Gómez, C. M., Woodcock, M. R., Smith, J. J., Voss, S. R., & Delgado, J. P. (2020). A *de novo* reference transcriptome for *Bolitoglossa vallecula*, an Andean mountain

salamander in Colombia. *Data in Brief*, *29*, 105256. https://doi.org/10.1016/j.dib.2020.105256

Attademo, A. M., Cuzziol Boccioni, A. P., Peltzer, P. M., Franco, V. G., Simoniello, M. F., Passeggi, M. C. G., & Lajmanovich, R. C. (2022). Effect of microplastics on the activity of carboxylesterase and phosphatase enzymes in *Scinax squalirostris* tadpoles. *Environmental Monitoring and Assessment*, *194*(10), 718. https://doi.org/10.1007/s10661-022-10322-2

Audo, M. C., Mann, T. M., Polk, T. L., Loudenslager, C. M., Diehl, W. J., & Altig, R. (1995). Food deprivation during different periods of tadpole (*Hyla chrysoscelis*) ontogeny affects metamorphic performance differently. *Oecologia*, *103*(4), 518–522. https://doi.org/10.1007/BF00328691

Bacchetta, R., Winkler, A., Santo, N., & Tremolada, P. (2021). The toxicity of polyester fibers in *Xenopus laevis*. *Water*, *13*(23), 3446. https://doi.org/10.3390/w13233446

Bai, Y., Meng, Y., Luo, J., Wang, H., Li, G., & Li, C. (2021). Full-length transcriptome assembly of *Andrias davidianus* (amphibia: caudata) skin via hybrid sequencing. *Bioscience Reports*, *41*(8), BSR20210511. https://doi.org/10.1042/BSR20210511

Baitchman, E. J., & Pessier, A. P. (2013). Pathogenesis, diagnosis, and treatment of amphibian chytridiomycosis. *Veterinary Clinics of North America: Exotic Animal Practice*, *16*(3), 669–685. https://doi.org/10.1016/j.cvex.2013.05.009

Balestrieri, A., Winkler, A., Scribano, G., Gazzola, A., Lastrico, G., Grioni, A., Pellitteri-Rosa, D., & Tremolada, P. (2022). Differential effects of microplastic exposure on

anuran tadpoles: A still underrated threat to amphibian conservation? *Environmental Pollution*, *303*, 119137. https://doi.org/10.1016/j.envpol.2022.119137

Barnes, D. K. A., Galgani, F., Thompson, R. C., & Barlaz, M. (2009). Accumulation and fragmentation of plastic debris in global environments. *Philosophical Transactions of the Royal Society B: Biological Sciences*, *364*(1526), 1985–1998. https://doi.org/10.1098/rstb.2008.0205

Bates, K. A., Sommer, U., Hopkins, K. P., Shelton, J. M. G., Wierzbicki, C., Sergeant, C., Tapley, B., Michaels, C. J., Schmeller, D. S., Loyau, A., Bosch, J., Viant, M. R., Harrison, X. A., Garner, T. W. J., & Fisher, M. C. (2022). Microbiome function predicts amphibian chytridiomycosis disease dynamics. *Microbiome*, *10*(1), 44. https://doi.org/10.1186/s40168-021-01215-6

Berven, K. A., & Gill, D. E. (1983). Interpreting geographic variation in life-history traits. *American Zoologist*, *23*(1), 85–97. https://doi.org/10.1093/icb/23.1.85

Blighe, K., Rana, S., & Lewis, M. (2023). *EnhancedVolcano: Publication-ready volcano plots with enhanced colouring and labeling* (R package version 1.20.0) [Computer software]. https://doi.org/10.18129/B9.BIOC.ENHANCEDVOLCANO

Bliley, J. M., & Woodley, S. K. (2012). The effects of repeated handling and corticosterone treatment on behavior in an amphibian (Ocoee salamander: *Desmognathus ocoee*). *Physiology & Behavior*, *105*(5), 1132–1139. https://doi.org/10.1016/j.physbeh.2011.12.009

Bonfanti, P., Colombo, A., Saibene, M., Motta, G., Saliu, F., Catelani, T., Mehn, D., La Spina, R., Ponti, J., Cella, C., Floris, P., & Mantecca, P. (2021). Microplastics from

miscellaneous plastic wastes: Physico-chemical characterization and impact on fish and amphibian development. *Ecotoxicology and Environmental Safety*, *225*, 112775. https://doi.org/10.1016/j.ecoenv.2021.112775

Borrelle, S. B., Ringma, J., Law, K. L., Monnahan, C. C., Lebreton, L., McGivern, A., Murphy, E., Jambeck, J., Leonard, G. H., Hilleary, M. A., Eriksen, M., Possingham, H. P., De Frond, H., Gerber, L. R., Polidoro, B., Tahir, A., Bernard, M., Mallos, N., Barnes, M., & Rochman, C. M. (2020). Predicted growth in plastic waste exceeds efforts to mitigate plastic pollution. *Science*, *369*(6510), 1515–1518. https://doi.org/10.1126/science.aba3656

Bosch, J., Thumsová, B., López-Rojo, N., Pérez, J., Alonso, A., Fisher, M. C., & Boyero, L. (2021). Microplastics increase susceptibility of amphibian larvae to the chytrid fungus *Batrachochytrium dendrobatidis*. *Scientific Reports*, *11*(1), 22438. https://doi.org/10.1038/s41598-021-01973-1

Boyero, L., López-Rojo, N., Bosch, J., Alonso, A., Correa-Araneda, F., & Pérez, J. (2020). Microplastics impair amphibian survival, body condition and function. *Chemosphere*, *244*, 125500. https://doi.org/10.1016/j.chemosphere.2019.125500

Brannelly, L. A., Ohmer, M. E. B., Saenz, V., & Richards-Zawacki, C. L. (2019). Effects of hydroperiod on growth, development, survival and immune defences in a temperate amphibian. *Functional Ecology*, *33*(10), 1952–1961. https://doi.org/10.1111/1365-2435.13419

Brown, S. R., Flynn, R. W., & Hoverman, J. T. (2021). Perfluoroalkyl substances increase susceptibility of northern leopard frog tadpoles to trematode infection. *Environmental Toxicology and Chemistry*, *40*(3), 689–694. https://doi.org/10.1002/etc.4678

Brunelli, E., Bernabò, I., Coscarelli, F., La Russa, D., & Tripepi, S. (2015). Remodelling of the skin during metamorphosis in the Italian newt (*Lissotriton italicus*) (Amphibia, Urodela): localization pattern of keratins, stromelysin-3 (MMP-11), and pan-cadherin. *Zoomorphology*, *134*(1), 135–147. https://doi.org/10.1007/s00435-014-0239-2

Bryant, D. M., Johnson, K., DiTommaso, T., Tickle, T., Couger, M. B., Payzin-Dogru, D., Lee, T. J., Leigh, N. D., Kuo, T.-H., Davis, F. G., Bateman, J., Bryant, S., Guzikowski, A. R., Tsai, S. L., Coyne, S., Ye, W. W., Freeman, R. M., Peshkin, L., Tabin, C. J., … Whited, J. L. (2017). A tissue-mapped axolotl *de novo* transcriptome enables identification of limb regeneration factors. *Cell Reports*, *18*(3), 762–776. https://doi.org/10.1016/j.celrep.2016.12.063

Bui-Marinos, M. P., Todd, L. A., Wasson, M.-C. D., Morningstar, B. E. E., & Katzenback, B. A. (2021). Prior induction of cellular antiviral pathways limits frog virus 3 replication in two permissive *Xenopus laevis* skin epithelial-like cell lines. *Developmental & Comparative Immunology*, *124*, 104200. https://doi.org/10.1016/j.dci.2021.104200

Bui-Marinos, M. P., Varga, J. F. A., Vo, N. T. K., Bols, N. C., & Katzenback, B. A. (2020). Xela DS2 and Xela VS2: Two novel skin epithelial-like cell lines from adult African clawed frog (*Xenopus laevis*) and their response to an extracellular viral dsRNA

analogue. *Developmental & Comparative Immunology*, *112*, 103759. https://doi.org/10.1016/j.dci.2020.103759

Burns, E. E., & Boxall, A. B. A. (2018). Microplastics in the aquatic environment: Evidence for or against adverse impacts and major knowledge gaps. *Environmental Toxicology and Chemistry*, *37*(11), 2776–2796. https://doi.org/10.1002/etc.4268

Burraco, P., & Gomez-Mestre, I. (2016). Physiological stress responses in amphibian larvae to multiple stressors reveal marked anthropogenic effects even below lethal levels. *Physiological and Biochemical Zoology*, *89*(6), 462–472. https://doi.org/10.1086/688737

Buss, N., Sander, B., & Hua, J. (2022). Effects of polyester microplastic fiber contamination on amphibian–trematode interactions. *Environmental Toxicology and Chemistry*, *41*(4), 869–879. https://doi.org/10.1002/etc.5035

Camacho, C., Coulouris, G., Avagyan, V., Ma, N., Papadopoulos, J., Bealer, K., & Madden, T. L. (2009). BLAST+: architecture and applications. *BMC Bioinformatics*, *10*(1), 421. https://doi.org/10.1186/1471-2105-10-421

Campbell, L. J., Hammond, S. A., Price, S. J., Sharma, M. D., Garner, T. W. J., Birol, I., Helbing, C. C., Wilfert, L., & Griffiths, A. G. F. (2018). A novel approach to wildlife transcriptomics provides evidence of disease-mediated differential expression and changes to the microbiome of amphibian populations. *Molecular Ecology*, *27*(6), 1413–1427. https://doi.org/10.1111/mec.14528

Cantalapiedra, C. P., Hernández-Plaza, A., Letunic, I., Bork, P., & Huerta-Cepas, J. (2021). eggNOG-mapper v2: Functional annotation, orthology assignments, and domain

prediction at the metagenomic scale. *Molecular Biology and Evolution*, *38*(12), 5825–5829. https://doi.org/10.1093/molbev/msab293

Carlson, M. (2023). *GO.db: A set of annotation maps describing the entire Gene Ontology* (R package version 3.18.0) [Computer software].

Chamas, A., Moon, H., Zheng, J., Qiu, Y., Tabassum, T., Jang, J. H., Abu-Omar, M., Scott, S. L., & Suh, S. (2020). Degradation rates of plastics in the environment. *ACS Sustainable Chemistry & Engineering*, *8*(9), 3494–3511. https://doi.org/10.1021/acssuschemeng.9b06635

Chen, H. (2022). *VennDiagram: Generate high-resolution Venn and Euler plots* (1.7.3) [Computer software]. https://CRAN.R-project.org/package=VennDiagram

Chen, S. (2023). Ultrafast one-pass FASTQ data preprocessing, quality control, and deduplication using fastp. *iMeta*, *2*(2), e107. https://doi.org/10.1002/imt2.107

Choi, D., Bang, J., Kim, T., Oh, Y., Hwang, Y., & Hong, J. (2020). In vitro chemical and physical toxicities of polystyrene microfragments in human-derived cells. *Journal of Hazardous Materials*, *400*, 123308. https://doi.org/10.1016/j.jhazmat.2020.123308

Choi, J. S., Jung, Y.-J., Hong, N.-H., Hong, S. H., & Park, J.-W. (2018). Toxicological effects of irregularly shaped and spherical microplastics in a marine teleost, the sheepshead minnow (*Cyprinodon variegatus*). *Marine Pollution Bulletin*, *129*(1), 231–240. https://doi.org/10.1016/j.marpolbul.2018.02.039

Clay, T. A., Steffen, M. A., Treglia, M. L., Torres, C. D., Trujano-Alvarez, A. L., & Bonett, R. M. (2019). Multiple stressors produce differential transcriptomic patterns in a

stream-dwelling salamander. *BMC Genomics*, *20*(1), 482. https://doi.org/10.1186/s12864-019-5814-y

Cole, M., Lindeque, P., Fileman, E., Halsband, C., & Galloway, T. S. (2015). The impact of polystyrene microplastics on feeding, function and fecundity in the marine copepod *Calanus helgolandicus*. *Environmental Science & Technology*, *49*(2), 1130–1137. https://doi.org/10.1021/es504525u

Cole, M., Lindeque, P., Halsband, C., & Galloway, T. S. (2011). Microplastics as contaminants in the marine environment: A review. *Marine Pollution Bulletin*, *62*(12), 2588–2597. https://doi.org/10.1016/j.marpolbul.2011.09.025

Compton, B. W., McGARIGAL, K., Cushman, S. A., & Gamble, L. R. (2007). A resistant-kernel model of connectivity for amphibians that breed in vernal pools. *Conservation Biology*, *21*(3), 788–799. https://doi.org/10.1111/j.1523-1739.2007.00674.x

Conesa, A., Madrigal, P., Tarazona, S., Gomez-Cabrero, D., Cervera, A., McPherson, A., Szcześniak, M. W., Gaffney, D. J., Elo, L. L., Zhang, X., & Mortazavi, A. (2016). A survey of best practices for RNA-seq data analysis. *Genome Biology*, *17*(1), 13. https://doi.org/10.1186/s13059-016-0881-8

Constant, D. A., Nice, T. J., & Rauch, I. (2021). Innate immune sensing by epithelial barriers. *Current Opinion in Immunology*, *73*, 1–8. https://doi.org/10.1016/j.coi.2021.07.014

Corben, C. J., Ingram, G. J., & Tyler, M. J. (1974). Gastric brooding: Unique form of parental care in an Australian frog. *Science*, *186*(4167), 946–947. https://doi.org/10.1126/science.186.4167.946

Cox, T. C., & Alvarado, R. H. (1979). Electrical and transport characteristics of skin of larval *Rana catesbeiana*. *American Journal of Physiology-Regulatory, Integrative and Comparative Physiology*, *237*(1), R74–R79. https://doi.org/10.1152/ajpregu.1979.237.1.R74

Crespi, E. J., & Denver, R. J. (2005). Roles of stress hormones in food intake regulation in anuran amphibians throughout the life cycle. *Comparative Biochemistry and Physiology Part A: Molecular & Integrative Physiology*, *141*(4), 381–390. https://doi.org/10.1016/j.cbpb.2004.12.007

da Costa Araújo, A. P., De Melo, N. F. S., De Oliveira Junior, A. G., Rodrigues, F. P., Fernandes, T., De Andrade Vieira, J. E., Rocha, T. L., & Malafaia, G. (2020). How much are microplastics harmful to the health of amphibians? A study with pristine polyethylene microplastics and *Physalaemus cuvieri*. *Journal of Hazardous Materials*, *382*, 121066. https://doi.org/10.1016/j.jhazmat.2019.121066

da Costa Araújo, A. P., Gomes, A. R., & Malafaia, G. (2020). Hepatotoxicity of pristine polyethylene microplastics in neotropical *Physalaemus cuvieri* tadpoles (Fitzinger, 1826). *Journal of Hazardous Materials*, *386*, 121992. https://doi.org/10.1016/j.jhazmat.2019.121992

da Costa Araújo, A. P., Luz, T. M. da, Ahmed, M. A. I., Ali, M. M., Rahman, Md. M., Nataraj, B., de Melo e Silva, D., Barceló, D., & Malafaia, G. (2023). Toxicity assessment of polyethylene microplastics in combination with a mix of emerging pollutants on *Physalaemus cuvieri* tadpoles. *Journal of Environmental Sciences*, *127*, 465–482. https://doi.org/10.1016/j.jes.2022.05.013

da Costa Araújo, A. P., Luz, T. M. da, Gonçalves, S. de O., Rajagopal, R., Rahman, Md. M., Silva, D. de M. e, & Malafaia, G. (2022). How can “my shoes” affect the amphibian health? A study of the toxicity of microplastics from shoe sole (Polyvinyl chloride acetate) on *Physalaemus cuvieri* tadpoles (Anura, Leptodactylidae). *Journal of Hazardous Materials*, *440*, 129847. https://doi.org/10.1016/j.jhazmat.2022.129847

da Costa Araújo, A. P., & Malafaia, G. (2020). Can short exposure to polyethylene microplastics change tadpoles’ behavior? A study conducted with neotropical tadpole species belonging to order anura (*Physalaemus cuvieri*). *Journal of Hazardous Materials*, *391*, 122214. https://doi.org/10.1016/j.jhazmat.2020.122214

Danecek, P., Bonfield, J. K., Liddle, J., Marshall, J., Ohan, V., Pollard, M. O., Whitwham, A., Keane, T., McCarthy, S. A., Davies, R. M., & Li, H. (2021). Twelve years of SAMtools and BCFtools. *GigaScience*, *10*(2), giab008. https://doi.org/10.1093/gigascience/giab008

Davis, D. R., Ferguson, K. J., Schwarz, M. S., & Kerby, J. L. (2020). Effects of agricultural pollutants on stress hormones and viral infection in larval salamanders. *Wetlands*, *40*(3), 577–586. https://doi.org/10.1007/s13157-019-01207-1

De Felice, B., Bacchetta, R., Santo, N., Tremolada, P., & Parolini, M. (2018). Polystyrene microplastics did not affect body growth and swimming activity in *Xenopus laevis* tadpoles. *Environmental Science and Pollution Research*, *25*(34), 34644–34651. https://doi.org/10.1007/s11356-018-3408-x

de Sá, L. C., Luís, L. G., & Guilhermino, L. (2015). Effects of microplastics on juveniles of the common goby (*Pomatoschistus microps*): Confusion with prey, reduction of the

predatory performance and efficiency, and possible influence of developmental conditions. *Environmental Pollution*, *196*, 359–362. https://doi.org/10.1016/j.envpol.2014.10.026

de Sá, L. C., Oliveira, M., Ribeiro, F., Rocha, T. L., & Futter, M. N. (2018). Studies of the effects of microplastics on aquatic organisms: What do we know and where should we focus our efforts in the future? *Science of The Total Environment*, *645*, 1029–1039. https://doi.org/10.1016/j.scitotenv.2018.07.207

de Souza Machado, A. A., Kloas, W., Zarfl, C., Hempel, S., & Rillig, M. C. (2018). Microplastics as an emerging threat to terrestrial ecosystems. *Global Change Biology*, *24*(4), 1405–1416. https://doi.org/10.1111/gcb.14020

Deng, Z.-L., Münch, P. C., Mreches, R., & McHardy, A. C. (2022). Rapid and accurate identification of ribosomal RNA sequences via deep learning. *Nucleic Acids Research*, *50*(10), e60–e60. https://doi.org/10.1093/nar/gkac112

Ding, J., Zhang, S., Razanajatovo, R. M., Zou, H., & Zhu, W. (2018). Accumulation, tissue distribution, and biochemical effects of polystyrene microplastics in the freshwater fish red tilapia (*Oreochromis niloticus*). *Environmental Pollution*, *238*, 1–9. https://doi.org/10.1016/j.envpol.2018.03.001

Duellman, W. E., & Trueb, L. (1994). *Biology of amphibians*. Johns Hopkins University Press.

Eddy, S. R. (2020). *HMMER* (3.3.2) [Computer software]. http://hmmer.org

Ellison, A. R., Tunstall, T., DiRenzo, G. V., Hughey, M. C., Rebollar, E. A., Belden, L. K., Harris, R. N., Ibáñez, R., Lips, K. R., & Zamudio, K. R. (2015). More than skin deep:

Functional genomic basis for resistance to amphibian chytridiomycosis. *Genome Biology and Evolution*, *7*(1), 286–298. https://doi.org/10.1093/gbe/evu285

Ellison, A., Zamudio, K., Lips, K., & Muletz-Wolz, C. (2020). Temperature-mediated shifts in salamander transcriptomic responses to the amphibian-killing fungus. *Molecular Ecology*, *29*(2), 325–343. https://doi.org/10.1111/mec.15327

Espinosa, C., Esteban, M. Á., & Cuesta, A. (2019). Dietary administration of PVC and PE microplastics produces histological damage, oxidative stress and immunoregulation in European sea bass (*Dicentrarchus labrax* L.). *Fish & Shellfish Immunology*, *95*, 574–583. https://doi.org/10.1016/j.fsi.2019.10.072

Etkin, W. (1932). Growth and resorption phenomena in anuran metamorphosis. I. *Physiological Zoology*, *5*(2), 275–300. https://doi.org/10.1086/physzool.5.2.30152791

Ewels, P., Magnusson, M., Lundin, S., & Käller, M. (2016). MultiQC: summarize analysis results for multiple tools and samples in a single report. *Bioinformatics*, *32*(19), 3047–3048. https://doi.org/10.1093/bioinformatics/btw354

Fan, W., Huang, M., Xu, J., Zhang, M., Jiang, Y., Cai, M., Sun, H., & Li, X. (2021). Transcriptome analysis reveals the effects of temperature on growth in tadpoles of spiny-bellied frog (*Quasipaa boulengeri*). *Aquaculture International*, *29*(3), 925–939. https://doi.org/10.1007/s10499-021-00664-y

Fan, W., Jiang, Y., Zhang, M., Yang, D., Chen, Z., Sun, H., Lan, X., Yan, F., Xu, J., & Yuan, W. (2017). Comparative transcriptome analyses reveal the genetic basis underlying the immune function of three amphibians' skin. *PLOS ONE*, *12*(12), e0190023. https://doi.org/10.1371/journal.pone.0190023

Félix, L. M., Luzio, A., Santos, A., Antunes, L. M., Coimbra, A. M., & Valentim, A. M. (2020). MS-222 induces biochemical and transcriptional changes related to oxidative stress, cell proliferation and apoptosis in zebrafish embryos. *Comparative Biochemistry and Physiology Part C: Toxicology & Pharmacology*, *237*, 108834. https://doi.org/10.1016/j.cbpc.2020.108834

Firneno, T. J., Ramesh, B., Maldonado, J. A., Hernandez-Briones, A. I., Emery, A. H., Roelke, C. E., & Fujita, M. K. (2022). Transcriptomic analysis reveals potential candidate pathways and genes involved in toxin biosynthesis in true toads. *Journal of Heredity*, *113*(3), 311–324. https://doi.org/10.1093/jhered/esac015

Fleury, J.-B., & Baulin, V. A. (2021). Microplastics destabilize lipid membranes by mechanical stretching. *Proceedings of the National Academy of Sciences*, *118*(31), e2104610118. https://doi.org/10.1073/pnas.2104610118

Forzán, M. J., Jones, K. M., Ariel, E., Whittington, R. J., Wood, J., Markham, R. J. F., & Daoust, P.-Y. (2017). Pathogenesis of *Frog Virus 3* (*Ranavirus*, *Iridoviridae*) infection in wood frogs (*Rana sylvatica*). *Veterinary Pathology*, *54*(3), 531–548. https://doi.org/10.1177/0300985816684929

Fraker, M. E., Ludsin, S. A., Luttbeg, B., & Denver, R. J. (2021). Stress hormone-mediated antipredator morphology improves escape performance in amphibian tadpoles. *Scientific Reports*, *11*(1), 4427. https://doi.org/10.1038/s41598-021-84052-9

Gahl, M. K., Longcore, J. E., & Houlahan, J. E. (2012). Varying responses of northeastern North American amphibians to the chytrid pathogen *Batrachochytrium dendrobatidis*.

Conservation Biology, *26*(1), 135–141. https://doi.org/10.1111/j.1523-1739.2011.01801.x

Gehlenborg, N. (2019). *UpSetR: A more scalable alternative to Venn and Euler diagrams for visualizing intersecting sets* (R package version 1.4.0) [Computer software]. https://CRAN.R-project.org/package=UpSetR

Gene, S. M., Katzenback, B. A., Provencher, J. F., Rochman, C. M., & Orihel, D. M. (n.d.). *The effects of a microplastic mixture on Wood frogs (*Rana sylvatica*) throughout multiple life stages in an outdoor mesocosm experiment* [Manuscript in preparation].

Gosner, K. L. (1960). A simplified table for staging anuran embryos and larvae with notes on identification. *Herpetologica*, *16*(3), 183–190.

Haas, B. J. (2023). *TransDecoder* (5.7.1) [Computer software]. https://github.com/TransDecoder/TransDecoder

Hahladakis, J. N., Velis, C. A., Weber, R., Iacovidou, E., & Purnell, P. (2018). An overview of chemical additives present in plastics: Migration, release, fate and environmental impact during their use, disposal and recycling. *Journal of Hazardous Materials*, *344*, 179–199. https://doi.org/10.1016/j.jhazmat.2017.10.014

Hale, R. C., Seeley, M. E., La Guardia, M. J., Mai, L., & Zeng, E. Y. (2020). A global perspective on microplastics. *Journal of Geophysical Research: Oceans*, *125*(1), e2018JC014719. https://doi.org/10.1029/2018JC014719

Hall, E. M., Brunner, J. L., Hutzenbiler, B., & Crespi, E. J. (2020). Salinity stress increases the severity of ranavirus epidemics in amphibian populations. *Proceedings of the*

Royal Society B: Biological Sciences, *287*(1926), 20200062. https://doi.org/10.1098/rspb.2020.0062

Harris, R. N., Brucker, R. M., Walke, J. B., Becker, M. H., Schwantes, C. R., Flaherty, D. C., Lam, B. A., Woodhams, D. C., Briggs, C. J., Vredenburg, V. T., & Minbiole, K. P. C. (2009). Skin microbes on frogs prevent morbidity and mortality caused by a lethal skin fungus. *The ISME Journal*, *3*(7), 818–824. https://doi.org/10.1038/ismej.2009.27

Hartmann, N. B., Hüffer, T., Thompson, R. C., Hassellöv, M., Verschoor, A., Daugaard, A. E., Rist, S., Karlsson, T., Brennholt, N., Cole, M., Herrling, M. P., Hess, M. C., Ivleva, N. P., Lusher, A. L., & Wagner, M. (2019). Are we speaking the same language? Recommendations for a definition and categorization framework for plastic debris. *Environmental Science & Technology*, *53*(3), 1039–1047. https://doi.org/10.1021/acs.est.8b05297

Hirt, N., & Body-Malapel, M. (2020). Immunotoxicity and intestinal effects of nano- and microplastics: a review of the literature. *Particle and Fibre Toxicology*, *17*(1), 57. https://doi.org/10.1186/s12989-020-00387-7

Hocking, D. J., & Babbitt, K. J. (2014). Amphibian contributions to ecosystem services. *Herpetological Conservation and Biology*, *9*(1), 1–17.

Hourdry, J., L'Hermite, A., & Ferrand, R. (1996). Changes in the digestive tract and feeding behavior of anuran amphibians during metamorphosis. *Physiological Zoology*, *69*(2), 219–251. https://doi.org/10.1086/physzool.69.2.30164181

Hu, L., Chernick, M., Hinton, D. E., & Shi, H. (2018). Microplastics in small waterbodies and tadpoles from Yangtze River Delta, China. *Environmental Science & Technology*, *52*(15), 8885–8893. https://doi.org/10.1021/acs.est.8b02279

Hu, L., Fu, J., Zheng, P., Dai, M., Zeng, G., & Pan, X. (2022). Accumulation of microplastics in tadpoles from different functional zones in Hangzhou Great Bay Area, China: Relation to growth stage and feeding habits. *Journal of Hazardous Materials*, *424*, 127665. https://doi.org/10.1016/j.jhazmat.2021.127665

Huang, L., Li, J., Anboukaria, H., Luo, Z., Zhao, M., & Wu, H. (2016). Comparative transcriptome analyses of seven anurans reveal functions and adaptations of amphibian skin. *Scientific Reports*, *6*(1), 24069. https://doi.org/10.1038/srep24069

Iannella, M., Console, G., D'Alessandro, P., Cerasoli, F., Mantoni, C., Ruggieri, F., Di Donato, F., & Biondi, M. (2020). Preliminary analysis of the diet of *Triturus carnifex* and pollution in mountain karst ponds in Central Apennines. *Water*, *12*(1), 44. https://doi.org/10.3390/w12010044

Ishii, A., Kawasaki, M., Matsumoto, M., Tochinai, S., & Seya, T. (2007). Phylogenetic and expression analysis of amphibian *Xenopus* Toll-like receptors. *Immunogenetics*, *59*(4), 281–293. https://doi.org/10.1007/s00251-007-0193-y

Isidoro-Ayza, M., Lorch, J. M., Grear, D. A., Winzeler, M., Calhoun, D. L., & Barichivich, W. J. (2017). Pathogenic lineage of Perkinsea associated with mass mortality of frogs across the United States. *Scientific Reports*, *7*(1), 10288. https://doi.org/10.1038/s41598-017-10456-1

Issac, M. N., & Kandasubramanian, B. (2021). Effect of microplastics in water and aquatic systems. *Environmental Science and Pollution Research*, *28*(16), 19544–19562. https://doi.org/10.1007/s11356-021-13184-2

Jabeen, K., Li, B., Chen, Q., Su, L., Wu, C., Hollert, H., & Shi, H. (2018). Effects of virgin microplastics on goldfish (*Carassius auratus*). *Chemosphere*, *213*, 323–332. https://doi.org/10.1016/j.chemosphere.2018.09.031

Jang, M., Shim, W. J., Han, G. M., Cho, Y., Moon, Y., & Hong, S. H. (2021). Relative importance of aqueous leachate versus particle ingestion as uptake routes for microplastic additives (hexabromocyclododecane) to mussels. *Environmental Pollution*, *270*, 116272. https://doi.org/10.1016/j.envpol.2020.116272

Kaiser, K., Devito, J., Jones, C. G., Marentes, A., Perez, R., Umeh, L., Weickum, R. M., McGovern, K. E., Wilson, E. H., & Saltzman, W. (2015). Reproductive and immune effects of chronic corticosterone treatment in male White's treefrogs, *Litoria caerulea*. *Conservation Physiology*, *3*(1), cov022. https://doi.org/10.1093/conphys/cov022

Kalvari, I., Nawrocki, E. P., Ontiveros-Palacios, N., Argasinska, J., Lamkiewicz, K., Marz, M., Griffiths-Jones, S., Toffano-Nioche, C., Gautheret, D., Weinberg, Z., Rivas, E., Eddy, S. R., Finn, R. D., Bateman, A., & Petrov, A. I. (2021). Rfam 14: expanded coverage of metagenomic, viral and microRNA families. *Nucleic Acids Research*, *49*(D1), D192–D200. https://doi.org/10.1093/nar/gkaa1047

Karaoğlu, K., & Gül, S. (2020). Characterization of microplastic pollution in tadpoles living in small water-bodies from Rize, the northeast of Turkey. *Chemosphere*, *255*, 126915. https://doi.org/10.1016/j.chemosphere.2020.126915

Katz, U. (1986). The role of amphibian epidermis in osmoregulation and its adaptive response to changing environment. In J. Bereiter-Hahn, A. G. Matoltsy, & K. S. Richards (Eds.), *Biology of the Integument* (pp. 472–498). Springer Berlin Heidelberg. https://doi.org/10.1007/978-3-662-00989-5_24

Ke, F., Gui, J.-F., Chen, Z.-Y., Li, T., Lei, C.-K., Wang, Z.-H., & Zhang, Q.-Y. (2018). Divergent transcriptomic responses underlying the ranaviruses-amphibian interaction processes on interspecies infection of Chinese giant salamander. *BMC Genomics*, *19*(1), 211. https://doi.org/10.1186/s12864-018-4596-y

Kelly, D. E. (1966). The Leydig cell in larval amphibian epidermis. Fine structure and function. *The Anatomical Record*, *154*(3), 685–699. https://doi.org/10.1002/ar.1091540314

Kim, D., Paggi, J. M., Park, C., Bennett, C., & Salzberg, S. L. (2019). Graph-based genome alignment and genotyping with HISAT2 and HISAT-genotype. *Nature Biotechnology*, *37*(8), 907–915. https://doi.org/10.1038/s41587-019-0201-4

Koelmans, A. A., Mohamed Nor, N. H., Hermsen, E., Kooi, M., Mintenig, S. M., & De France, J. (2019). Microplastics in freshwaters and drinking water: Critical review and assessment of data quality. *Water Research*, *155*, 410–422. https://doi.org/10.1016/j.watres.2019.02.054

Kolde, R. (2019). *pheatmap: Pretty heatmaps* (R package version 1.0.12) [Computer software]. https://CRAN.R-project.org/package=pheatmap

Kolenda, K., Kuśmierek, N., & Pstrowska, K. (2020). Microplastic ingestion by tadpoles of pond-breeding amphibians—first results from Central Europe (SW Poland). *Environmental Science and Pollution Research*, *27*, 33380–33384. https://doi.org/10.1007/s11356-020-09648-6

Komaki, S., Matsunami, M., Lin, J.-W., Lee, K.-H., Lin, Y.-P., Lee, Y., Lin, S.-M., & Igawa, T. (2021). Transcriptomic changes in hot spring frog tadpoles (*Buergeria otai*) in response to heat stress. *Frontiers in Ecology and Evolution*, *9*, 706887. https://doi.org/10.3389/fevo.2021.706887

Kovaka, S., Zimin, A. V., Pertea, G. M., Razaghi, R., Salzberg, S. L., & Pertea, M. (2019). Transcriptome assembly from long-read RNA-seq alignments with StringTie2. *Genome Biology*, *20*(1), 278. https://doi.org/10.1186/s13059-019-1910-1

Krogh, A., Larsson, B., Von Heijne, G., & Sonnhammer, E. L. L. (2001). Predicting transmembrane protein topology with a hidden Markov model: application to complete genomes. *Journal of Molecular Biology*, *305*(3), 567–580. https://doi.org/10.1006/jmbi.2000.4315

Kruse, C. P. S., Basu, P., Luesse, D. R., & Wyatt, S. E. (2017). Transcriptome and proteome responses in RNAlater preserved tissue of *Arabidopsis thaliana*. *PLOS ONE*, *12*(4), e0175943. https://doi.org/10.1371/journal.pone.0175943

Lajmanovich, R. C., Attademo, A. M., Lener, G., Cuzziol Boccioni, A. P., Peltzer, P. M., Martinuzzi, C. S., Demonte, L. D., & Repetti, M. R. (2022). Glyphosate and

glufosinate ammonium, herbicides commonly used on genetically modified crops, and their interaction with microplastics: Ecotoxicity in anuran tadpoles. *Science of The Total Environment*, *804*, 150177. https://doi.org/10.1016/j.scitotenv.2021.150177

Lan, Y., He, L., Dong, X., Tang, R., Li, W., Wang, J., Wang, L., Yue, B., Price, M., Guo, T., & Fan, Z. (2022). Comparative transcriptomes of three different skin sites for the Asiatic toad (*Bufo gargarizans*). *PeerJ*, *10*, e12993. https://doi.org/10.7717/peerj.12993

Lei, L., Wu, S., Lu, S., Liu, M., Song, Y., Fu, Z., Shi, H., Raley-Susman, K. M., & He, D. (2018). Microplastic particles cause intestinal damage and other adverse effects in zebrafish *Danio rerio* and nematode *Caenorhabditis elegans*. *Science of The Total Environment*, *619–620*, 1–8. https://doi.org/10.1016/j.scitotenv.2017.11.103

Li, W., Chen, X., Li, M., Cai, Z., Gong, H., & Yan, M. (2022). Microplastics as an aquatic pollutant affect gut microbiota within aquatic animals. *Journal of Hazardous Materials*, *423*, 127094. https://doi.org/10.1016/j.jhazmat.2021.127094

Liedtke, H. C., Wiens, J. J., & Gomez-Mestre, I. (2022). The evolution of reproductive modes and life cycles in amphibians. *Nature Communications*, *13*(1), 7039. https://doi.org/10.1038/s41467-022-34474-4

Limonta, G., Mancia, A., Benkhalqui, A., Bertolucci, C., Abelli, L., Fossi, M. C., & Panti, C. (2019). Microplastics induce transcriptional changes, immune response and behavioral alterations in adult zebrafish. *Scientific Reports*, *9*(1), 15775. https://doi.org/10.1038/s41598-019-52292-5

Liu, F., Olesen, K. B., Borregaard, A. R., & Vollertsen, J. (2019). Microplastics in urban and highway stormwater retention ponds. *Science of The Total Environment*, *671*, 992–1000. https://doi.org/10.1016/j.scitotenv.2019.03.416

Liu, F., Vianello, A., & Vollertsen, J. (2019). Retention of microplastics in sediments of urban and highway stormwater retention ponds. *Environmental Pollution*, *255*, 113335. https://doi.org/10.1016/j.envpol.2019.113335

Loo, Y.-M., & Gale, M. (2011). Immune signaling by RIG-I-like receptors. *Immunity*, *34*(5), 680–692. https://doi.org/10.1016/j.immuni.2011.05.003

Lorenz, C., Opitz, R., Lutz, I., & Kloas, W. (2009). Teratogenic effects of chronic treatment with corticosterone on tadpoles of *Xenopus laevis*. *Annals of the New York Academy of Sciences*, *1163*(1), 454–456. https://doi.org/10.1111/j.1749-6632.2009.04429.x

Love, M. I., Huber, W., & Anders, S. (2014). Moderated estimation of fold change and dispersion for RNA-seq data with DESeq2. *Genome Biology*, *15*(12), 550. https://doi.org/10.1186/s13059-014-0550-8

Luedtke, J. A., Chanson, J., Neam, K., Hobin, L., Maciel, A. O., Catenazzi, A., Borzée, A., Hamidy, A., Aowphol, A., Jean, A., Sosa-Bartuano, Á., Fong G., A., De Silva, A., Fouquet, A., Angulo, A., Kidov, A. A., Muñoz Saravia, A., Diesmos, A. C., Tominaga, A., … Stuart, S. N. (2023). Ongoing declines for the world's amphibians in the face of emerging threats. *Nature*, *622*(7982), 308–314. https://doi.org/10.1038/s41586-023-06578-4

Lusher, A. L., Tirelli, V., O'Connor, I., & Officer, R. (2015). Microplastics in Arctic polar waters: the first reported values of particles in surface and sub-surface samples. *Scientific Reports*, *5*(1), 14947. https://doi.org/10.1038/srep14947

Mackenzie, C. M., & Vladimirova, V. (2021). Preliminary study and first evidence of presence of microplastics in terrestrial herpetofauna from Southwestern Paraguay. *Studies on Neotropical Fauna and Environment*, 1–9. https://doi.org/10.1080/01650521.2021.1895466

Malafaia, G., Luz, T. M. D., Ahmed, M. A. I., Karthi, S., & Araújo, A. P. D. C. (2022). When toxicity of plastic particles comes from their fluorescent dye: a preliminary study involving neotropical *Physalaemus cuvieri* tadpoles and polyethylene microplastics. *Journal of Hazardous Materials Advances*, *6*, 100054. https://doi.org/10.1016/j.hazadv.2022.100054

Malafaia, G., Nascimento, Í. F., Estrela, F. N., Guimarães, A. T. B., Ribeiro, F., da Luz, T. M., & de Lima Rodrigues, A. S. (2021). Green toxicology approach involving polylactic acid biomicroplastics and neotropical tadpoles: (Eco)toxicological safety or environmental hazard? *Science of The Total Environment*, *783*, 146994. https://doi.org/10.1016/j.scitotenv.2021.146994

May, D., Shidemantle, G., Melnick-Kelley, Q., Crane, K., & Hua, J. (2019). The effect of intensified illuminance and artificial light at night on fitness and susceptibility to abiotic and biotic stressors. *Environmental Pollution*, *251*, 600–608. https://doi.org/10.1016/j.envpol.2019.05.016

McCarthy, J., Gong, Nahirney, Duszyk, & Radomski. (2011). Polystyrene nanoparticles activate ion transport in human airway epithelial cells. *International Journal of Nanomedicine*, 1343. https://doi.org/10.2147/IJN.S21145

Middlemis Maher, J., Werner, E. E., & Denver, R. J. (2013). Stress hormones mediate predator-induced phenotypic plasticity in amphibian tadpoles. *Proceedings of the Royal Society B: Biological Sciences*, *280*(1758), 20123075. https://doi.org/10.1098/rspb.2012.3075

Mistry, J., Chuguransky, S., Williams, L., Qureshi, M., Salazar, G. A., Sonnhammer, E. L. L., Tosatto, S. C. E., Paladin, L., Raj, S., Richardson, L. J., Finn, R. D., & Bateman, A. (2021). Pfam: The protein families database in 2021. *Nucleic Acids Research*, *49*(D1), D412–D419. https://doi.org/10.1093/nar/gkaa913

Mouchet, F., Rowenczyk, L., Minet, A., Clergeaud, F., Silvestre, J., Pinelli, E., Ferriol, J., Leflaive, J., Ten-Hage, L., Gigault, J., Ter Halle, A., & Gauthier, L. (2022). Ecotoxicity of heteroaggregates of polystyrene nanospheres in Chironomidae and amphibian. *Nanomaterials*, *12*(15), 2730. https://doi.org/10.3390/nano12152730

Murray, C. J. L., Ikuta, K. S., Sharara, F., Swetschinski, L., Robles Aguilar, G., Gray, A., Han, C., Bisignano, C., Rao, P., Wool, E., Johnson, S. C., Browne, A. J., Chipeta, M. G., Fell, F., Hackett, S., Haines-Woodhouse, G., Kashef Hamadani, B. H., Kumaran, E. A. P., McManigal, B., … Naghavi, M. (2022). Global burden of bacterial antimicrobial resistance in 2019: a systematic analysis. *The Lancet*, *399*(10325), 629–655. https://doi.org/10.1016/S0140-6736(21)02724-0

Musich, R., Cadle-Davidson, L., & Osier, M. V. (2021). Comparison of short-read sequence aligners indicates strengths and weaknesses for biologists to consider. *Frontiers in Plant Science*, *12*, 657240. https://doi.org/10.3389/fpls.2021.657240

Nakajima, K., Tanizaki, Y., Luu, N., Zhang, H., & Shi, Y. B. (2020). Comprehensive RNA-Seq analysis of notochord-enriched genes induced during *Xenopus tropicalis* tail resorption. *General and Comparative Endocrinology*, *287*, 113349. https://doi.org/10.1016/j.ygcen.2019.113349

Narayan, E. J., Cockrem, J. F., & Hero, J.-M. (2013a). Are baseline and short-term corticosterone stress responses in free-living amphibians repeatable? *Comparative Biochemistry and Physiology Part A: Molecular & Integrative Physiology*, *164*(1), 21–28. https://doi.org/10.1016/j.cbpa.2012.10.001

Narayan, E. J., Cockrem, J. F., & Hero, J.-M. (2013b). Sight of a predator induces a corticosterone stress response and generates fear in an amphibian. *PLoS ONE*, *8*(8), e73564. https://doi.org/10.1371/journal.pone.0073564

Narayan, E. J., Forsburg, Z. R., Davis, D. R., & Gabor, C. R. (2019). Non-invasive methods for measuring and monitoring stress physiology in imperiled amphibians. *Frontiers in Ecology and Evolution*, *7*, 431. https://doi.org/10.3389/fevo.2019.00431

Narayan, E. J., & Hero, J.-M. (2014). Repeated thermal stressor causes chronic elevation of baseline corticosterone and suppresses the physiological endocrine sensitivity to acute stressor in the cane toad (*Rhinella marina*). *Journal of Thermal Biology*, *41*, 72–76. https://doi.org/10.1016/j.jtherbio.2014.02.011

Nawrocki, E. P., & Eddy, S. R. (2013). Infernal 1.1: 100-fold faster RNA homology searches. *Bioinformatics*, *29*(22), 2933–2935. https://doi.org/10.1093/bioinformatics/btt509

Nguyen, A. V., & Soulika, A. M. (2019). The dynamics of the skin's immune system. *International Journal of Molecular Sciences*, *20*(8), 1811. https://doi.org/10.3390/ijms20081811

Nieuwkoop, P. D., & Faber, J. (Eds.). (1994). *Normal table of* Xenopus laevis *(Daudin): a systematical and chronological survey of the development from the fertilized egg till the end of metamorphosis*. Garland Publ.

Nishikawa, S., Hirata, J., & Sasaki, F. (1992). Fate of ciliated epidermal cells during early development of *Xenopus laevis* using whole-mount immunostaining with an antibody against chondroitin 6-sulfate proteoglycan and anti-tubulin: transdifferentiation or metaplasia of amphibian epidermis. *Histochemistry*, *98*(6), 355–358. https://doi.org/10.1007/BF00271070

Nokhbatolfoghahai, M., Downie, J. R., Clelland, A. K., & Rennison, K. (2005). The surface ciliation of anuran amphibian embryos and early larvae: Patterns, timing differences and functions. *Journal of Natural History*, *39*(12), 887–929. https://doi.org/10.1080/00222930400002937

Nokhbatolfoghahai, M., Downie, J. R., & Ogilvy, V. (2006). Surface ciliation of anuran amphibian larvae: Persistence to late stages in some species but not others. *Journal of Morphology*, *267*(10), 1248–1256. https://doi.org/10.1002/jmor.10469

Nowoshilow, S., Schloissnig, S., Fei, J.-F., Dahl, A., Pang, A. W. C., Pippel, M., Winkler, S., Hastie, A. R., Young, G., Roscito, J. G., Falcon, F., Knapp, D., Powell, S., Cruz, A., Cao, H., Habermann, B., Hiller, M., Tanaka, E. M., & Myers, E. W. (2018). The axolotl genome and the evolution of key tissue formation regulators. *Nature*, *554*(7690), 50–55. https://doi.org/10.1038/nature25458

Ockenden, A., Northcott, G. L., Tremblay, L. A., & Simon, K. S. (2022). Disentangling the influence of microplastics and their chemical additives on a model detritivore system. *Environmental Pollution*, *307*, 119558. https://doi.org/10.1016/j.envpol.2022.119558

Oeckinghaus, A., & Ghosh, S. (2009). The NF-κB family of transcription factors and its regulation. *Cold Spring Harbor Perspectives in Biology*, *1*(4), a000034–a000034. https://doi.org/10.1101/cshperspect.a000034

Olesen, Stephansen, Alst, & Vollertsen. (2019). Microplastics in a stormwater pond. *Water*, *11*(7), 1466. https://doi.org/10.3390/w11071466

Oliveira, M., Ribeiro, A., Hylland, K., & Guilhermino, L. (2013). Single and combined effects of microplastics and pyrene on juveniles (0+ group) of the common goby *Pomatoschistus microps* (Teleostei, Gobiidae). *Ecological Indicators*, *34*, 641–647. https://doi.org/10.1016/j.ecolind.2013.06.019

Owen, J. A., Punt, J., Stranford, S. A., Jones, P. P., & Kuby, J. (2013). *Kuby immunology* (7th ed). W.H. Freeman.

Passow, C. N., Kono, T. J. Y., Stahl, B. A., Jaggard, J. B., Keene, A. C., & McGaugh, S. E. (2019). Nonrandom RNAseq gene expression associated with RNAlater and flash

freezing storage methods. *Molecular Ecology Resources*, *19*(2), 456–464. https://doi.org/10.1111/1755-0998.12965

Pastorino, P., Prearo, M., Di Blasio, A., Barcelò, D., Anselmi, S., Colussi, S., Alberti, S., Tedde, G., Dondo, A., Ottino, M., Pizzul, E., & Renzi, M. (2022). Microplastics occurrence in the European common frog (*Rana temporaria*) from Cottian Alps (Northwest Italy). *Diversity*, *14*(2), 66. https://doi.org/10.3390/d14020066

Patocka, J., Nepovimova, E., Klimova, B., Wu, Q., & Kuca, K. (2019). Antimicrobial peptides: Amphibian host defense peptides. *Current Medicinal Chemistry*, *26*(32), 5924–5946. https://doi.org/10.2174/0929867325666180713125314

Paysan-Lafosse, T., Blum, M., Chuguransky, S., Grego, T., Pinto, B. L., Salazar, G. A., Bileschi, M. L., Bork, P., Bridge, A., Colwell, L., Gough, J., Haft, D. H., Letunić, I., Marchler-Bauer, A., Mi, H., Natale, D. A., Orengo, C. A., Pandurangan, A. P., Rivoire, C., … Bateman, A. (2023). InterPro in 2022. *Nucleic Acids Research*, *51*(D1), D418–D427. https://doi.org/10.1093/nar/gkac993

Pekmezekmek, A. B., Emre, M., Erdogan, S., Yilmaz, B., Tunc, E., Sertdemir, Y., & Emre, Y. (2022). Effects of high-molecular-weight polyvinyl chloride on *Xenopus laevis* adults and embryos: the mRNA expression profiles of Myf5, Esr1, Bmp4, Pax6, and Hsp70 genes during early embryonic development. *Environmental Science and Pollution Research*, *29*(10), 14767–14779. https://doi.org/10.1007/s11356-021-16527-1

Pertea, G., & Pertea, M. (2020). GFF Utilities: GffRead and GffCompare. *F1000Research*, *9*, 304. https://doi.org/10.12688/f1000research.23297.1

Pownall, M. E., Cutler, R. R., & Saha, M. S. (2018). Transcriptome of *Xenopus andrei*, an octoploid frog, during embryonic development. *Data in Brief*, *19*, 501–505. https://doi.org/10.1016/j.dib.2018.05.017

Puskic, P. S., Lavers, J. L., & Bond, A. L. (2020). A critical review of harm associated with plastic ingestion on vertebrates. *Science of The Total Environment*, *743*, 140666. https://doi.org/10.1016/j.scitotenv.2020.140666

Qi, Z., Zhang, Q., Wang, Z., Ma, T., Zhou, J., Holland, J. W., & Gao, Q. (2016). Transcriptome analysis of the endangered Chinese giant salamander (*Andrias davidianus*): Immune modulation in response to *Aeromonas hydrophila* infection. *Veterinary Immunology and Immunopathology*, *169*, 85–95. https://doi.org/10.1016/j.vetimm.2015.11.004

Quaranta, A., Bellantuono, V., Cassano, G., & Lippe, C. (2009). Why amphibians are more sensitive than mammals to xenobiotics. *PLoS ONE*, *4*(11), e7699. https://doi.org/10.1371/journal.pone.0007699

Quinzio, S., & Fabrezi, M. (2014). The lateral line system in anuran tadpoles: Neuromast morphology, arrangement, and innervation. *The Anatomical Record*, *297*(8), 1508–1522. https://doi.org/10.1002/ar.22952

Quinzio, S. I., & Goldberg, J. (2019). Transient integumentary structures in *Boana riojana* (Anura, Hylidae) tadpoles. *Amphibia-Reptilia*, *40*(4), 543–549. https://doi.org/10.1163/15685381-20191226

R Core Team. (2023). *R: A language and environment for statistical computing* (4.3.2) [Computer software]. R Foundation for Statistical Computing. https://www.R-project.org/

Ramos, J., Barletta, M., & Costa, M. (2012). Ingestion of nylon threads by Gerreidae while using a tropical estuary as foraging grounds. *Aquatic Biology*, *17*(1), 29–34. https://doi.org/10.3354/ab00461

Reeve, B. C., Crespi, E. J., Whipps, C. M., & Brunner, J. L. (2013). Natural stressors and ranavirus susceptibility in larval wood frogs (*Rana sylvatica*). *EcoHealth*, *10*(2), 190–200. https://doi.org/10.1007/s10393-013-0834-6

Regueira, E., Dávila, C., & Hermida, G. N. (2016). Morphological changes in skin glands during development in *Rhinella arenarum* (Anura: Bufonidae). *The Anatomical Record*, *299*(1), 141–156. https://doi.org/10.1002/ar.23284

Resnick, B. (2016, December 16). What we lose when we lose the world's frogs. *Vox*. https://www.vox.com/science-and-health/2016/10/14/13147056/amphibian-extinction-frog-bd

Richardson, M. F., Sequeira, F., Selechnik, D., Carneiro, M., Vallinoto, M., Reid, J. G., West, A. J., Crossland, M. R., Shine, R., & Rollins, L. A. (2018). Improving amphibian genomic resources: a multitissue reference transcriptome of an iconic invader. *GigaScience*, *7*(1). https://doi.org/10.1093/gigascience/gix114

Robert, J. (2010). Emerging ranaviral infectious diseases and amphibian decline. *Diversity*, *2*(3), 314–330. https://doi.org/10.3390/d2030314

Robert, J., McGuire, C. C., Kim, F., Nagel, S. C., Price, S. J., Lawrence, B. P., & De Jesús Andino, F. (2018). Water contaminants associated with unconventional oil and gas extraction cause immunotoxicity to amphibian tadpoles. *Toxicological Sciences*, *166*(1), 39–50. https://doi.org/10.1093/toxsci/kfy179

Rochman, C. M., Brookson, C., Bikker, J., Djuric, N., Earn, A., Bucci, K., Athey, S., Huntington, A., McIlwraith, H., Munno, K., De Frond, H., Kolomijeca, A., Erdle, L., Grbic, J., Bayoumi, M., Borrelle, S. B., Wu, T., Santoro, S., Werbowski, L. M., … Hung, C. (2019). Rethinking microplastics as a diverse contaminant suite. *Environmental Toxicology and Chemistry*, *38*(4), 703–711. https://doi.org/10.1002/etc.4371

Rollins-Smith, L. A. (1998). Metamorphosis and the amphibian immune system. *Immunological Reviews*, *166*(1), Article 1. https://doi.org/10.1111/j.1600-065X.1998.tb01265.x

Romano, N., Ashikin, M., Teh, J. C., Syukri, F., & Karami, A. (2018). Effects of pristine polyvinyl chloride fragments on whole body histology and protease activity in silver barb *Barbodes gonionotus* fry. *Environmental Pollution*, *237*, 1106–1111. https://doi.org/10.1016/j.envpol.2017.11.040

Romero, L. M., Dickens, M. J., & Cyr, N. E. (2009). The reactive scope model — A new model integrating homeostasis, allostasis, and stress. *Hormones and Behavior*, *55*(3), 375–389. https://doi.org/10.1016/j.yhbeh.2008.12.009

Roshanzadeh, A., Oyunbaatar, N.-E., Ganjbakhsh, S. E., Park, S., Kim, D.-S., Kanade, P. P., Lee, S., Lee, D.-W., & Kim, E.-S. (2021). Exposure to nanoplastics impairs collective

contractility of neonatal cardiomyocytes under electrical synchronization. *Biomaterials*, *278*, 121175. https://doi.org/10.1016/j.biomaterials.2021.121175

Row, J. R., Donaldson, M. E., Longhi, J. N., Saville, B. J., & Murray, D. L. (2016). Tissue-specific transcriptome characterization for developing tadpoles of the northern leopard frog (*Lithobates pipiens*). *Genomics*, *108*(5–6), 232–240. https://doi.org/10.1016/j.ygeno.2016.10.002

Ruthsatz, K., Domscheit, M., Engelkes, K., & Vences, M. (2022). Microplastics ingestion induces plasticity in digestive morphology in larvae of *Xenopus laevis*. *Comparative Biochemistry and Physiology Part A: Molecular & Integrative Physiology*, *269*, 111210. https://doi.org/10.1016/j.cbpa.2022.111210

Ruthsatz, K., Schwarz, A., Gomez-Mestre, I., Meyer, R., Domscheit, M., Bartels, F., Schaeffer, S.-M., & Engelkes, K. (2023). Life in plastic, it's not fantastic: Sublethal effects of polyethylene microplastics ingestion throughout amphibian metamorphosis. *Science of The Total Environment*, *885*, 163779. https://doi.org/10.1016/j.scitotenv.2023.163779

Saito, T., & Gale, M. (2008). Differential recognition of double-stranded RNA by RIG-I–like receptors in antiviral immunity. *The Journal of Experimental Medicine*, *205*(7), 1523–1527. https://doi.org/10.1084/jem.20081210

Salzman, N. H., Hung, K., Haribhai, D., Chu, H., Karlsson-Sjöberg, J., Amir, E., Teggatz, P., Barman, M., Hayward, M., Eastwood, D., Stoel, M., Zhou, Y., Sodergren, E., Weinstock, G. M., Bevins, C. L., Williams, C. B., & Bos, N. A. (2010). Enteric

defensins are essential regulators of intestinal microbial ecology. *Nature Immunology*, *11*(1), 76–82. https://doi.org/10.1038/ni.1825

Schessl, M., Johns, C., & Ashpole, S. L. (2019). Microbeads in dediment, *Dreissenid* mussels, and anurans in the littoral zone of the Upper St. Lawrence River, New York. *Pollution*, *5*(1), 41–52. https://doi.org/10.22059/poll.2018.257596.468

Scribano, G., Gazzola, A., Winkler, A., Balestrieri, A., Grioni, A., Lastrico, G., Tremolada, P., & Pellitteri-Rosa, D. (2022). Anti-predator behavioral responses of Italian agile frog tadpoles (*Rana latastei*) exposed to microplastics. *Environmental Science and Pollution Research*. https://doi.org/10.1007/s11356-022-23131-4

Session, A. M., Uno, Y., Kwon, T., Chapman, J. A., Toyoda, A., Takahashi, S., Fukui, A., Hikosaka, A., Suzuki, A., Kondo, M., Van Heeringen, S. J., Quigley, I., Heinz, S., Ogino, H., Ochi, H., Hellsten, U., Lyons, J. B., Simakov, O., Putnam, N., … Rokhsar, D. S. (2016). Genome evolution in the allotetraploid frog *Xenopus laevis*. *Nature*, *538*(7625), 336–343. https://doi.org/10.1038/nature19840

Shah, K., Al-Haidari, A., Sun, J., & Kazi, J. U. (2021). T cell receptor (TCR) signaling in health and disease. *Signal Transduction and Targeted Therapy*, *6*(1), 412. https://doi.org/10.1038/s41392-021-00823-w

Shibao, P. Y. T., Cologna, C. T., Morandi-Filho, R., Wiezel, G. A., Fujimura, P. T., Ueira-Vieira, C., & Arantes, E. C. (2018). Deep sequencing analysis of toad *Rhinella schneideri* skin glands and partial biochemical characterization of its cutaneous secretion. *Journal of Venomous Animals and Toxins Including Tropical Diseases*, *24*(1), 36. https://doi.org/10.1186/s40409-018-0173-8

Smirnov, D. N., Shekhovtsov, S. V., Shipova, A. A., Gazizova, G. R., Shagimardanova, E. I., Bulakhova, N. A., Meshcheryakova, E. N., Poluboyarova, T. V., Khrameeva, E. E., Peltek, S. E., & Berman, D. I. (2022). *De novo* assembly and analysis of the transcriptome of the Siberian wood frog *Rana amurensis*. *Vavilov Journal of Genetics and Breeding*, *26*(1), 109–116. https://doi.org/10.18699/VJGB-22-07

Smith-Unna, R., Boursnell, C., Patro, R., Hibberd, J. M., & Kelly, S. (2016). TransRate: reference-free quality assessment of de novo transcriptome assemblies. *Genome Research*, *26*(8), 1134–1144. https://doi.org/10.1101/gr.196469.115

Song, L., & Florea, L. (2015). Rcorrector: efficient and accurate error correction for Illumina RNA-seq reads. *GigaScience*, *4*(1), 48. https://doi.org/10.1186/s13742-015-0089-y

Springborn, M. R., Weill, J. A., Lips, K. R., Ibáñez, R., & Ghosh, A. (2022). Amphibian collapses increased malaria incidence in Central America. *Environmental Research Letters*, *17*(10), 104012. https://doi.org/10.1088/1748-9326/ac8e1d

Stuart, S. N., Chanson, J. S., Cox, N. A., Young, B. E., Rodrigues, A. S. L., Fischman, D. L., & Waller, R. W. (2004). Status and trends of amphibian declines and extinctions worldwide. *Science*, *306*(5702), 1783–1786. https://doi.org/10.1126/science.1103538

Susanti, N. K. Y., Mardiastuti, A., & Wardiatno, Y. (2020). Microplastics and the impact of plastic on wildlife: A literature review. *IOP Conference Series: Earth and Environmental Science*, *528*(1), 012013. https://doi.org/10.1088/1755-1315/528/1/012013

Székely, D., Denoël, M., Székely, P., & Cogălniceanu, D. (2017). Pond drying cues and their effects on growth and metamorphosis in a fast developing amphibian. *Journal of Zoology*, *303*(2), 129–135. https://doi.org/10.1111/jzo.12468

Takada, M. (1985). Differentiation of the active sodium transport system during metamorphosis in *Rana catesbeiana* skin in relation to cadmium- and amiloride-induced responses. *The Japanese Journal of Physiology*, *35*(3), 525–534. https://doi.org/10.2170/jjphysiol.35.525

Tattersall, G. J. (2007). Skin breathing in amphibians. In W. C. Aird (Ed.), *Endothelial Biomedicine* (1st ed., pp. 85–91). Cambridge University Press. https://doi.org/10.1017/CBO9780511546198.010

Taylor, R. E., & Barker, S. B. (1965). Transepidermal potential difference: Development in anuran larvae. *Science*, *148*(3677), 1612–1613. https://doi.org/10.1126/science.148.3677.1612

Tenenbaum, D. (2023). *KEGGREST: Client-side REST access to the Kyoto Encyclopedia of Genes and Genomes (KEGG)* (R package version 1.42.0) [Computer software]. https://doi.org/10.18129/B9.BIOC.KEGGREST

Tennessen, J. B., Parks, S. E., & Langkilde, T. (2014). Traffic noise causes physiological stress and impairs breeding migration behaviour in frogs. *Conservation Physiology*, *2*(1), cou032–cou032. https://doi.org/10.1093/conphys/cou032

Teufel, F., Almagro Armenteros, J. J., Johansen, A. R., Gíslason, M. H., Pihl, S. I., Tsirigos, K. D., Winther, O., Brunak, S., Von Heijne, G., & Nielsen, H. (2022). SignalP 6.0

predicts all five types of signal peptides using protein language models. *Nature Biotechnology*, *40*(7), 1023–1025. https://doi.org/10.1038/s41587-021-01156-3

The UniProt Consortium, Bateman, A., Martin, M.-J., Orchard, S., Magrane, M., Ahmad, S., Alpi, E., Bowler-Barnett, E. H., Britto, R., Bye-A-Jee, H., Cukura, A., Denny, P., Dogan, T., Ebenezer, T., Fan, J., Garmiri, P., Da Costa Gonzales, L. J., Hatton-Ellis, E., Hussein, A., … Zhang, J. (2023). UniProt: the Universal Protein Knowledgebase in 2023. *Nucleic Acids Research*, *51*(D1), D523–D531. https://doi.org/10.1093/nar/gkac1052

Torres-Sánchez, M., Creevey, C. J., Kornobis, E., Gower, D. J., Wilkinson, M., & San Mauro, D. (2019). Multi-tissue transcriptomes of caecilian amphibians highlight incomplete knowledge of vertebrate gene families. *DNA Research*, *26*(1), 13–20. https://doi.org/10.1093/dnares/dsy034

Trizio, D., Basketter, D. A., Botham, P. A., Graepel, P. H., Lambré, Cl., Magda, S. J., Pal, T. M., Riley, A. J., Ronneberger, H., Van Sittert, N. J., & Bontinck, W. J. (1988). Identification of immunotoxic effects of chemicals and assessment of their relevance to man. *Food and Chemical Toxicology*, *26*(6), 527–539. https://doi.org/10.1016/0278-6915(88)90006-3

Tursi, A., Baratta, M., Easton, T., Chatzisymeon, E., Chidichimo, F., De Biase, M., & De Filpo, G. (2022). Microplastics in aquatic systems, a comprehensive review: origination, accumulation, impact, and removal technologies. *RSC Advances*, *12*(44), 28318–28340. https://doi.org/10.1039/D2RA04713F

Tussellino, M., Ronca, R., Formiggini, F., Marco, N. D., Fusco, S., Netti, P. A., & Carotenuto, R. (2015). Polystyrene nanoparticles affect *Xenopus laevis* development. *Journal of Nanoparticle Research*, *17*(2), 70. https://doi.org/10.1007/s11051-015-2876-x

van Sebille, E., Wilcox, C., Lebreton, L., Maximenko, N., Hardesty, B. D., van Franeker, J. A., Eriksen, M., Siegel, D., Galgani, F., & Law, K. L. (2015). A global inventory of small floating plastic debris. *Environmental Research Letters*, *10*(12), 124006. https://doi.org/10.1088/1748-9326/10/12/124006

Vandenberg, L. N., Colborn, T., Hayes, T. B., Heindel, J. J., Jacobs, D. R., Lee, D.-H., Shioda, T., Soto, A. M., Vom Saal, F. S., Welshons, W. V., Zoeller, R. T., & Myers, J. P. (2012). Hormones and endocrine-disrupting chemicals: Low-dose effects and nonmonotonic dose responses. *Endocrine Reviews*, *33*(3), 378–455. https://doi.org/10.1210/er.2011-1050

Varga, J. F. A., Bui-Marinos, M. P., & Katzenback, B. A. (2019). Frog skin innate immune defences: Sensing and surviving pathogens. *Frontiers in Immunology*, *9*, 3128. https://doi.org/10.3389/fimmu.2018.03128

Venâncio, C., Melnic, I., Tamayo-Belda, M., Oliveira, M., Martins, M. A., & Lopes, I. (2022). Polymethylmethacrylate nanoplastics can cause developmental malformations in early life stages of *Xenopus laevis*. *Science of The Total Environment*, *806*, 150491. https://doi.org/10.1016/j.scitotenv.2021.150491

Veneman, W. J., Spaink, H. P., Brun, N. R., Bosker, T., & Vijver, M. G. (2017). Pathway analysis of systemic transcriptome responses to injected polystyrene particles in

zebrafish larvae. *Aquatic Toxicology*, *190*, 112–120. https://doi.org/10.1016/j.aquatox.2017.06.014

Viricel, A., Becquet, V., Dubillot, E., & Pante, E. (2018). *De novo* assembly and functional annotation of the transcriptome of *Mimachlamys varia*, a bioindicator marine bivalve. *Marine Genomics*, *41*, 42–45. https://doi.org/10.1016/j.margen.2018.04.002

Wang, K., McClure, J., & Tu, A. (1979). Titin: major myofibrillar components of striated muscle. *Proceedings of the National Academy of Sciences*, *76*(8), 3698–3702. https://doi.org/10.1073/pnas.76.8.3698

Whiles, M. R., Lips, K. R., Pringle, C. M., Kilham, S. S., Bixby, R. J., Brenes, R., Connelly, S., Colon-Gaud, J. C., Hunte-Brown, M., Huryn, A. D., Montgomery, C., & Peterson, S. (2006). The effects of amphibian population declines on the structure and function of Neotropical stream ecosystems. *Frontiers in Ecology and the Environment*, *4*(1), 27–34. https://doi.org/10.1890/1540-9295(2006)004[0027:TEOAPD]2.0.CO;2

Wickham, H. (2016). *ggplot2: Elegant graphics for data analysis*. Springer-Verlag New York. https://ggplot2.tidyverse.org

Wong, J. K. H., Lee, K. K., Tang, K. H. D., & Yap, P.-S. (2020). Microplastics in the freshwater and terrestrial environments: Prevalence, fates, impacts and sustainable solutions. *Science of The Total Environment*, *719*, 137512. https://doi.org/10.1016/j.scitotenv.2020.137512

Woodhams, D. C., Vredenburg, V. T., Simon, M.-A., Billheimer, D., Shakhtour, B., Shyr, Y., Briggs, C. J., Rollins-Smith, L. A., & Harris, R. N. (2007). Symbiotic bacteria contribute to innate immune defenses of the threatened mountain yellow-legged frog,

Rana muscosa. *Biological Conservation*, *138*(3–4), 390–398. https://doi.org/10.1016/j.biocon.2007.05.004

Wu, T., Hu, E., Xu, S., Chen, M., Guo, P., Dai, Z., Feng, T., Zhou, L., Tang, W., Zhan, L., Fu, X., Liu, S., Bo, X., & Yu, G. (2021). clusterProfiler 4.0: A universal enrichment tool for interpreting omics data. *The Innovation*, *2*(3), 100141. https://doi.org/10.1016/j.xinn.2021.100141

Xu, X., & Lai, R. (2015). The chemistry and biological activities of peptides from amphibian skin secretions. *Chemical Reviews*, *115*(4), 1760–1846. https://doi.org/10.1021/cr4006704

Xuan, J., Feng, W., Wang, J., Wang, R., Zhang, B., Bo, L., Chen, Z.-S., Yang, H., & Sun, L. (2023). Antimicrobial peptides for combating drug-resistant bacterial infections. *Drug Resistance Updates*, *68*, 100954. https://doi.org/10.1016/j.drup.2023.100954

Yang, W., Qi, Y., & Fu, J. (2016). Genetic signals of high-altitude adaptation in amphibians: a comparative transcriptome analysis. *BMC Genetics*, *17*(1), 134. https://doi.org/10.1186/s12863-016-0440-z

Yoshizato, K. (1992). Death and transformation of larval cells during metamorphosis of anura. *Development, Growth & Differentiation*, *34*(6), 607–612. https://doi.org/10.1111/j.1440-169X.1992.tb00028.x

Yu, G. (2023). *enrichplot: Visualization of functional enrichment result* (R package version 1.22.0) [Computer software]. https://doi.org/10.18129/B9.BIOC.ENRICHPLOT

Zenobia, C., & Hajishengallis, G. (2015). Basic biology and role of interleukin-17 in immunity and inflammation. *Periodontology 2000*, *69*(1), 142–159. https://doi.org/10.1111/prd.12083

Zhang, Q., Lv, Y., Liu, J., Chang, L., Chen, Q., Zhu, L., Wang, B., Jiang, J., & Zhu, W. (2023). Size matters either way: Differently-sized microplastics affect amphibian host and symbiotic microbiota discriminately. *Environmental Pollution*, *328*, 121634. https://doi.org/10.1016/j.envpol.2023.121634

Zhao, F., Yan, C., Wang, X., Yang, Y., Wang, G., Lee, W., Xiang, Y., & Zhang, Y. (2014). Comprehensive transcriptome profiling and functional analysis of the frog (*Bombina maxima*) immune system. *DNA Research*, *21*(1), 1–13. https://doi.org/10.1093/dnares/dst035

Zhao, Q.-Y., Wang, Y., Kong, Y.-M., Luo, D., Li, X., & Hao, P. (2011). Optimizing *de novo* transcriptome assembly from short-read RNA-Seq data: a comparative study. *BMC Bioinformatics*, *12*(S14), S2. https://doi.org/10.1186/1471-2105-12-S14-S2

Zhu, A., Ibrahim, J. G., & Love, M. I. (2019). Heavy-tailed prior distributions for sequence count data: removing the noise and preserving large differences. *Bioinformatics*, *35*(12), 2084–2092. https://doi.org/10.1093/bioinformatics/bty895

Zipkin, E. F., & DiRenzo, G. V. (2022). Biodiversity is decimated by the cascading effects of the amphibian-killing chytrid fungus. *PLOS Pathogens*, *18*(7), e1010624. https://doi.org/10.1371/journal.ppat.1010624

Appendix A

RNA-seq Quality Control

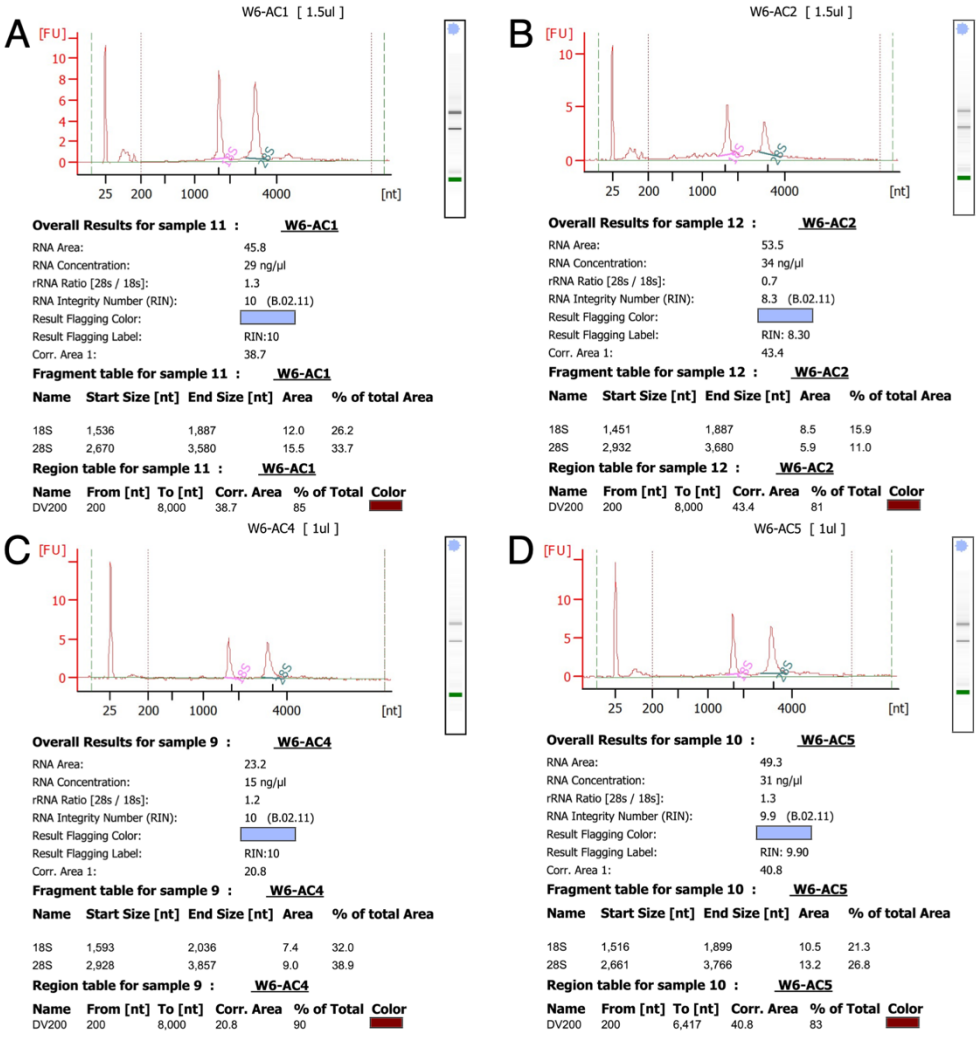


Figure A.1. Bioanalyzer reports of sequenced RNA samples from the dorsal skin of developing wood frogs exposed to varying concentrations of a microplastics mixture. RNA samples were assessed for integrity with a Bioanalyzer (Aligent) by The Centre for Applied Genomics (TCAG; Toronto, Ontario, Canada). Bioanalyzer reports were provided by TCAG for the following samples: **A)** Gosner stage (GS) ~34 0× mesocosm 1, **B)** GS ~34 0× mesocosm 2, **C)** GS ~34 0× mesocosm 4, **D)** GS ~34 0× mesocosm 5, **E)** GS ~34 1× mesocosm 1, **F)** GS ~34 1× mesocosm 3, **G)** GS ~34 1× mesocosm 4, **H)** GS ~34 10× mesocosm 3, **I)** GS ~34 10× mesocosm 4, **J)** GS ~34 10× mesocosm 5, **K)** GS ~42 0× mesocosm 1, **L)** GS ~42 0× mesocosm 2, **M)** GS ~42 0× mesocosm 4, **N)** GS ~42 0× mesocosm 5, **O)** GS ~42 1× mesocosm 1, **P)** GS ~42 1× mesocosm 3, **Q)** GS ~42 1× mesocosm 4, **R)** GS ~42 1× mesocosm 5, **S)** GS ~42 10× mesocosm 1, **T)** GS ~42 10× mesocosm 3, **U)** GS ~42 10× mesocosm 4, **V)**

GS ~42 10× mesocosm 5, **W)** GS 45 0× mesocosm 1 replicate b, **X)** GS 45 0× mesocosm 2 replicate c, **Y)** GS 45 0× mesocosm 4 replicate b, **Z)** GS 45 0× mesocosm 5 replicate b, **α)** GS 45 1× mesocosm 1 replicate b, **β)** GS 45 1× mesocosm 3 replicate a, **γ)** GS 45 1× mesocosm 4 replicate b, **δ)** GS 45 1× mesocosm 5 replicate a, **ε)** GS 45 10× mesocosm 1c, **ζ)** GS 45 10× mesocosm 3 replicate b, **η)** GS 45 10× mesocosm 4 replicate a, and **θ)** GS 45 10× mesocosm 5 replicate b. W6 corresponds to GS ~34 samples, W8 corresponds to GS ~42 samples, and GS45 or G345 (typo at TCAG) corresponds to GS 45 samples. AC = Set A, 0× treatment mesocosm, AL = Set A, 1× treatment mesocosm, AH = Set A, 10× treatment mesocosm. This figure is continued on the following five pages.

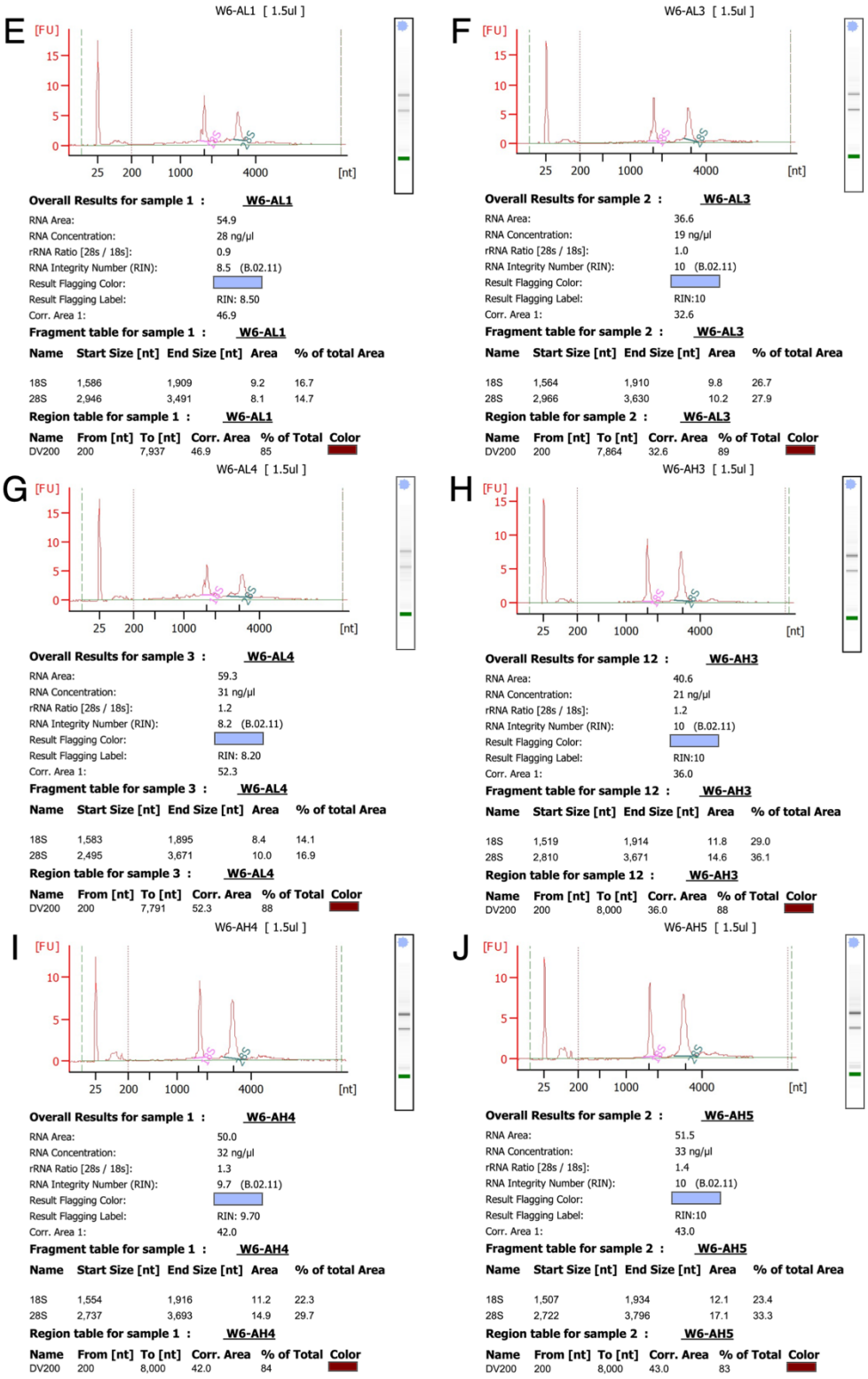
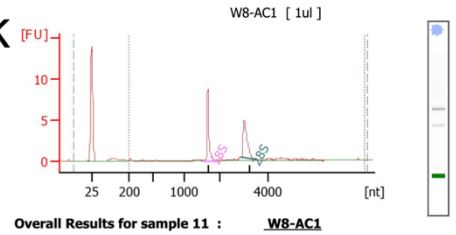


Figure A.1. continued.

K



Overall Results for sample 11 : **W8-AC1**

RNA Area:	21.9
RNA Concentration:	14 ng/µl
rRNA Ratio [28s / 18s]:	1.0
RNA Integrity Number (RIN):	10 (B.02.11, Anomaly Threshold(s) manually adapted)
Result Flagging Color:	
Result Flagging Label:	RIN:10
Corr. Area 1:	19.8

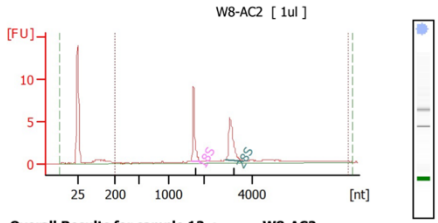
Fragment table for sample 11 : **W8-AC1**

Name	Start Size [nt]	End Size [nt]	Area	% of total Area
18S	1,548	1,890	7.5	34.4
28S	2,871	3,572	7.7	35.2

Region table for sample 11 : **W8-AC1**

Name	From [nt]	To [nt]	Corr. Area	% of Total	Color
DV200	200	8,000	19.8	90	

L



Overall Results for sample 12 : **W8-AC2**

RNA Area:	34.8
RNA Concentration:	22 ng/µl
rRNA Ratio [28s / 18s]:	1.1
RNA Integrity Number (RIN):	10 (B.02.11)
Result Flagging Color:	
Result Flagging Label:	RIN:10
Corr. Area 1:	29.7

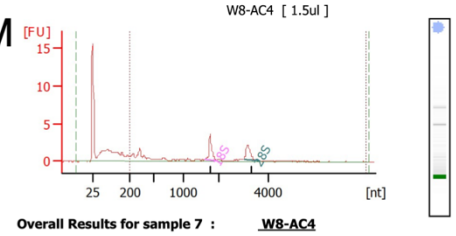
Fragment table for sample 12 : **W8-AC2**

Name	Start Size [nt]	End Size [nt]	Area	% of total Area
18S	1,605	1,881	8.2	23.6
28S	2,847	3,637	9.2	26.4

Region table for sample 12 : **W8-AC2**

Name	From [nt]	To [nt]	Corr. Area	% of Total	Color
DV200	200	8,000	29.7	85	

M



Overall Results for sample 7 : **W8-AC4**

RNA Area:	53.3
RNA Concentration:	31 ng/µl
rRNA Ratio [28s / 18s]:	0.8
RNA Integrity Number (RIN):	7.7 (B.02.11, Anomaly Threshold(s) manually adapted)
Result Flagging Color:	
Result Flagging Label:	RIN: 7.70
Corr. Area 1:	28.9

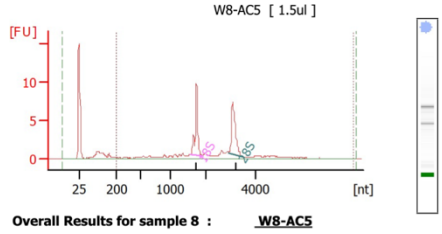
Fragment table for sample 7 : **W8-AC4**

Name	Start Size [nt]	End Size [nt]	Area	% of total Area
18S	1,588	1,934	4.3	8.1
28S	2,995	3,649	3.6	6.8

Region table for sample 7 : **W8-AC4**

Name	From [nt]	To [nt]	Corr. Area	% of Total	Color
DV200	200	8,000	28.9	54	

N



Overall Results for sample 8 : **W8-AC5**

RNA Area:	50.4
RNA Concentration:	29 ng/µl
rRNA Ratio [28s / 18s]:	1.0
RNA Integrity Number (RIN):	9.1 (B.02.11, Anomaly Threshold(s) manually adapted)
Result Flagging Color:	
Result Flagging Label:	RIN: 9.10
Corr. Area 1:	43.3

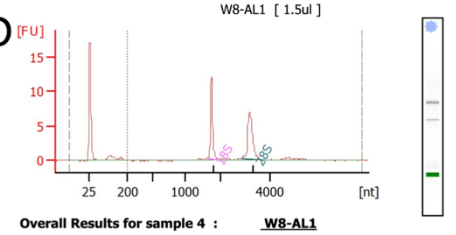
Fragment table for sample 8 : **W8-AC5**

Name	Start Size [nt]	End Size [nt]	Area	% of total Area
18S	1,563	1,892	10.6	21.1
28S	2,910	3,516	10.9	21.6

Region table for sample 8 : **W8-AC5**

Name	From [nt]	To [nt]	Corr. Area	% of Total	Color
DV200	200	8,000	43.3	86	

O



Overall Results for sample 4 : **W8-AL1**

RNA Area:	33.5
RNA Concentration:	17 ng/µl
rRNA Ratio [28s / 18s]:	1.2
RNA Integrity Number (RIN):	10 (B.02.11, Anomaly Threshold(s) manually adapted)
Result Flagging Color:	
Result Flagging Label:	RIN:10
Corr. Area 1:	28.7

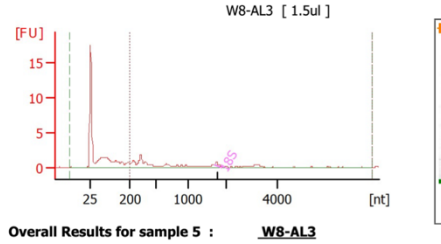
Fragment table for sample 4 : **W8-AL1**

Name	Start Size [nt]	End Size [nt]	Area	% of total Area
18S	1,619	1,961	10.7	31.9
28S	2,815	3,757	13.2	39.2

Region table for sample 4 : **W8-AL1**

Name	From [nt]	To [nt]	Corr. Area	% of Total	Color
DV200	200	7,682	28.7	86	

P



Overall Results for sample 5 : **W8-AL3**

RNA Area:	38.7
RNA Concentration:	20 ng/µl
rRNA Ratio [28s / 18s]:	0.0
RNA Integrity Number (RIN):	2.4 (B.02.11)
Result Flagging Color:	
Result Flagging Label:	RIN: 2.40 ; DV200 30-50%
Corr. Area 1:	18.0

Fragment table for sample 5 : **W8-AL3**

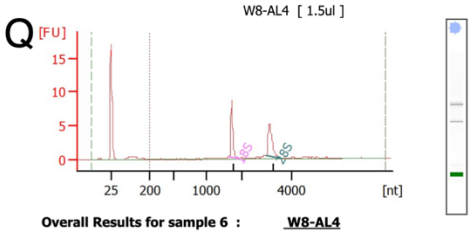
Name	Start Size [nt]	End Size [nt]	Area	% of total Area
18S	1,683	1,896	0.7	1.8

Region table for sample 5 : **W8-AL3**

Name	From [nt]	To [nt]	Corr. Area	% of Total	Color
DV200	200	7,718	18.0	46	

Figure A.1. continued.

Q



Overall Results for sample 6 : W8-AL4

RNA Area:	23.7
RNA Concentration:	12 ng/µl
rRNA Ratio [28s / 18s]:	1.1
RNA Integrity Number (RIN):	10 (B.02.11)
Result Flagging Color:	
Result Flagging Label:	RIN:10
Corr. Area 1:	21.0

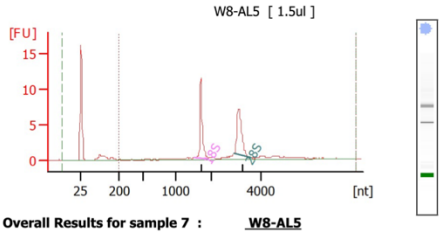
Fragment table for sample 6 : W8-AL4

Name	Start Size [nt]	End Size [nt]	Area	% of total Area
18S	1,657	1,903	6.9	29.3
28S	2,963	3,611	7.7	32.5

Region table for sample 6 : W8-AL4

Name	From [nt]	To [nt]	Corr. Area	% of Total	Color
DV200	200	7,791	21.0	89	

R



Overall Results for sample 7 : W8-AL5

RNA Area:	42.2
RNA Concentration:	22 ng/µl
rRNA Ratio [28s / 18s]:	1.1
RNA Integrity Number (RIN):	10 (B.02.11, Anomaly Threshold(s) manually adapted)
Result Flagging Color:	
Result Flagging Label:	RIN:10
Corr. Area 1:	38.1

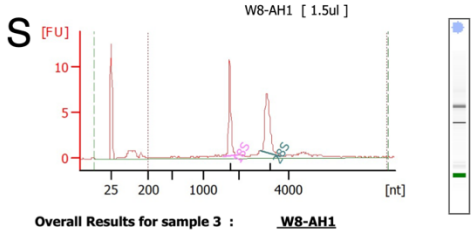
Fragment table for sample 7 : W8-AL5

Name	Start Size [nt]	End Size [nt]	Area	% of total Area
18S	1,546	1,926	11.8	28.1
28S	2,944	3,633	12.6	29.8

Region table for sample 7 : W8-AL5

Name	From [nt]	To [nt]	Corr. Area	% of Total	Color
DV200	200	7,900	38.1	90	

S



Overall Results for sample 3 : W8-AH1

RNA Area:	47.1
RNA Concentration:	30 ng/µl
rRNA Ratio [28s / 18s]:	1.2
RNA Integrity Number (RIN):	9.6 (B.02.11)
Result Flagging Color:	
Result Flagging Label:	RIN: 9.60
Corr. Area 1:	40.1

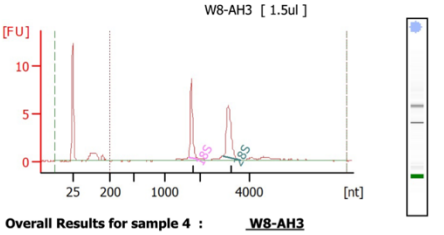
Fragment table for sample 3 : W8-AH1

Name	Start Size [nt]	End Size [nt]	Area	% of total Area
18S	1,560	1,935	10.6	22.4
28S	2,878	3,704	13.0	27.6

Region table for sample 3 : W8-AH1

Name	From [nt]	To [nt]	Corr. Area	% of Total	Color
DV200	200	8,000	40.1	85	

T



Overall Results for sample 4 : W8-AH3

RNA Area:	31.3
RNA Concentration:	20 ng/µl
rRNA Ratio [28s / 18s]:	1.2
RNA Integrity Number (RIN):	9.9 (B.02.11, Anomaly Threshold(s) manually adapted)
Result Flagging Color:	
Result Flagging Label:	RIN: 9.90
Corr. Area 1:	25.9

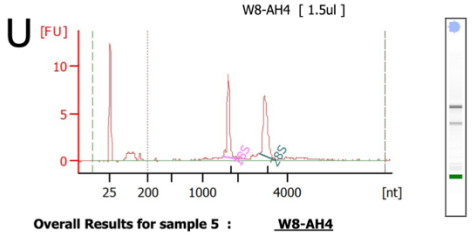
Fragment table for sample 4 : W8-AH3

Name	Start Size [nt]	End Size [nt]	Area	% of total Area
18S	1,663	1,920	8.4	26.8
28S	2,909	3,670	9.9	31.5

Region table for sample 4 : W8-AH3

Name	From [nt]	To [nt]	Corr. Area	% of Total	Color
DV200	200	7,980	25.9	82	

U



Overall Results for sample 5 : W8-AH4

RNA Area:	40.1
RNA Concentration:	25 ng/µl
rRNA Ratio [28s / 18s]:	1.1
RNA Integrity Number (RIN):	9.6 (B.02.11)
Result Flagging Color:	
Result Flagging Label:	RIN: 9.60
Corr. Area 1:	33.9

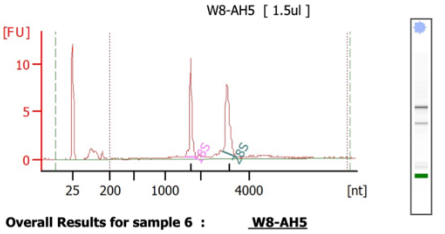
Fragment table for sample 5 : W8-AH4

Name	Start Size [nt]	End Size [nt]	Area	% of total Area
18S	1,579	2,052	9.8	24.5
28S	2,875	3,576	11.2	28.0

Region table for sample 5 : W8-AH4

Name	From [nt]	To [nt]	Corr. Area	% of Total	Color
DV200	200	8,000	33.9	85	

V



Overall Results for sample 6 : W8-AH5

RNA Area:	40.9
RNA Concentration:	26 ng/µl
rRNA Ratio [28s / 18s]:	1.2
RNA Integrity Number (RIN):	9.9 (B.02.11)
Result Flagging Color:	
Result Flagging Label:	RIN: 9.90
Corr. Area 1:	34.5

Fragment table for sample 6 : W8-AH5

Name	Start Size [nt]	End Size [nt]	Area	% of total Area
18S	1,558	1,893	10.5	25.6
28S	2,891	3,476	12.2	29.8

Region table for sample 6 : W8-AH5

Name	From [nt]	To [nt]	Corr. Area	% of Total	Color
DV200	200	8,000	34.5	84	

Figure A.1. continued.

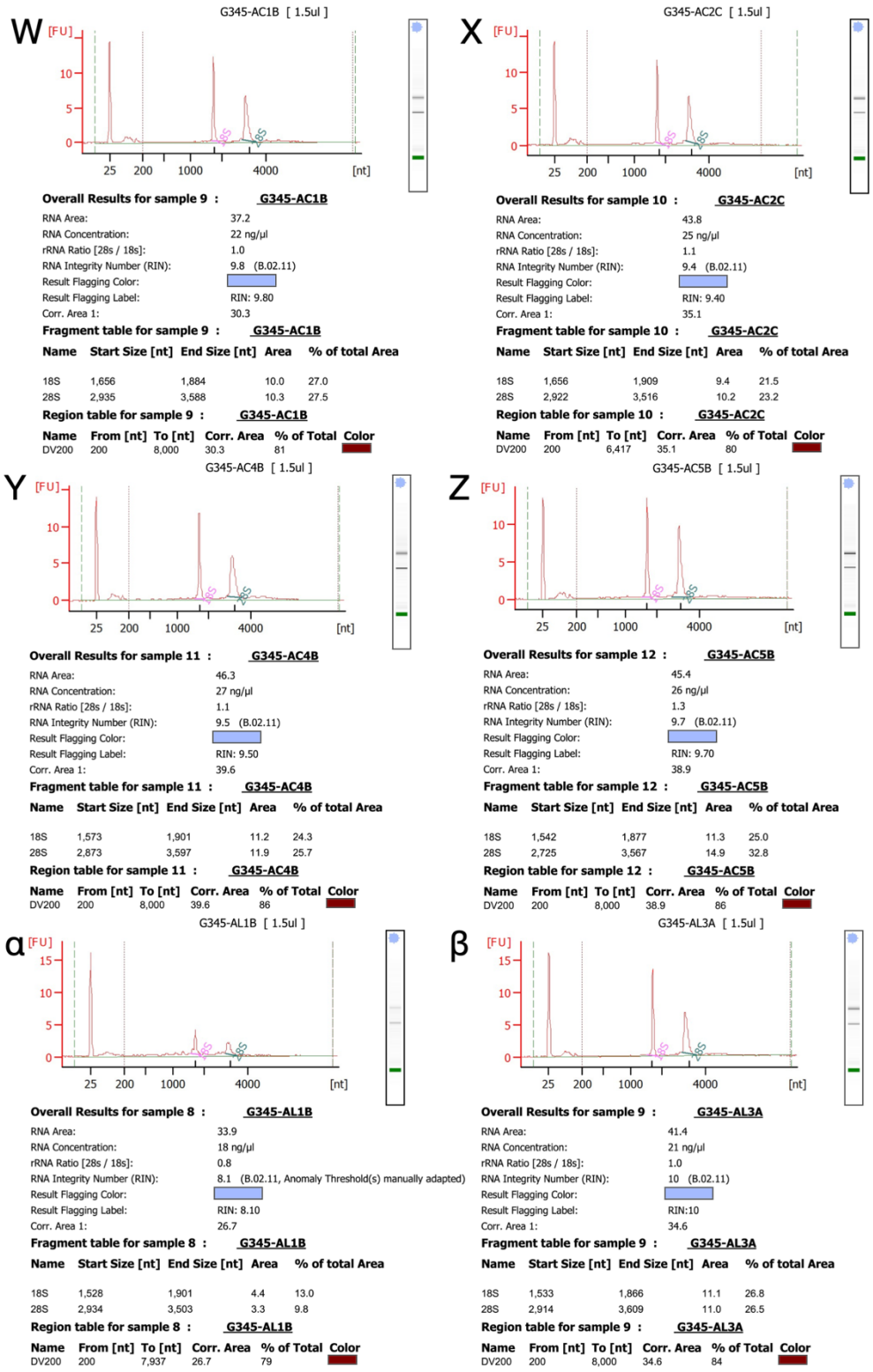
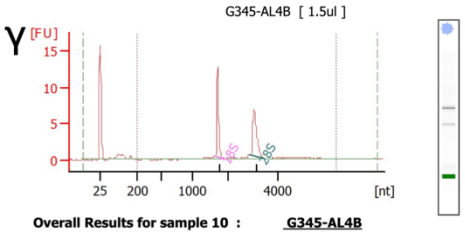


Figure A.1. continued.

γ



Overall Results for sample 10 : G345-AL4B

RNA Area:	34.9
RNA Concentration:	18 ng/µl
rRNA Ratio [28s / 18s]:	1.0
RNA Integrity Number (RIN):	10 (B.02.11)
Result Flagging Color:	
Result Flagging Label:	RIN:10
Corr. Area 1:	29.4

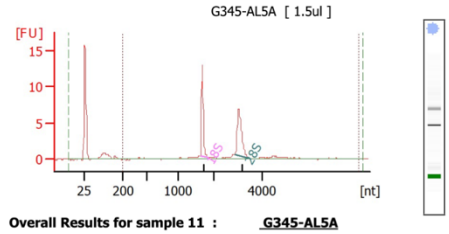
Fragment table for sample 10 : G345-AL4B

Name	Start Size [nt]	End Size [nt]	Area	% of total Area
18S	1,631	1,873	10.3	29.7
28S	2,868	3,469	10.5	30.2

Region table for sample 10 : G345-AL4B

Name	From [nt]	To [nt]	Corr. Area	% of Total	Color
DV200	200	6,417	29.4	84	

δ



Overall Results for sample 11 : G345-AL5A

RNA Area:	40.1
RNA Concentration:	21 ng/µl
rRNA Ratio [28s / 18s]:	1.1
RNA Integrity Number (RIN):	9.8 (B.02.11)
Result Flagging Color:	
Result Flagging Label:	RIN: 9.80
Corr. Area 1:	33.7

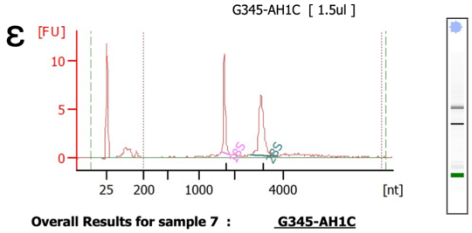
Fragment table for sample 11 : G345-AL5A

Name	Start Size [nt]	End Size [nt]	Area	% of total Area
18S	1,637	1,864	10.9	27.2
28S	2,884	3,561	11.5	28.8

Region table for sample 11 : G345-AL5A

Name	From [nt]	To [nt]	Corr. Area	% of Total	Color
DV200	200	8,000	33.7	84	

ε



Overall Results for sample 7 : G345-AH1C

RNA Area:	41.1
RNA Concentration:	26 ng/µl
rRNA Ratio [28s / 18s]:	1.3
RNA Integrity Number (RIN):	9.8 (B.02.11, Anomaly Threshold(s) manually adapted)
Result Flagging Color:	
Result Flagging Label:	RIN: 9.80
Corr. Area 1:	33.7

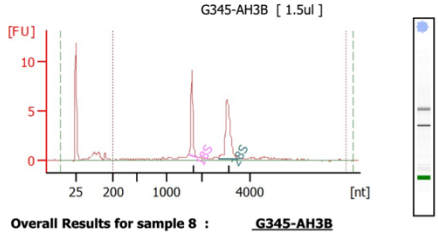
Fragment table for sample 7 : G345-AH1C

Name	Start Size [nt]	End Size [nt]	Area	% of total Area
18S	1,640	1,892	9.5	23.2
28S	2,662	3,751	12.8	31.1

Region table for sample 7 : G345-AH1C

Name	From [nt]	To [nt]	Corr. Area	% of Total	Color
DV200	200	8,000	33.7	82	

ζ



Overall Results for sample 8 : G345-AH3B

RNA Area:	36.1
RNA Concentration:	23 ng/µl
rRNA Ratio [28s / 18s]:	1.5
RNA Integrity Number (RIN):	9.2 (B.02.11, Anomaly Threshold(s) manually adapted)
Result Flagging Color:	
Result Flagging Label:	RIN: 9.20
Corr. Area 1:	30.3

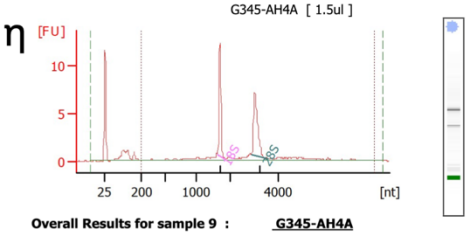
Fragment table for sample 8 : G345-AH3B

Name	Start Size [nt]	End Size [nt]	Area	% of total Area
18S	1,637	1,874	8.0	22.0
28S	2,676	3,524	11.8	32.7

Region table for sample 8 : G345-AH3B

Name	From [nt]	To [nt]	Corr. Area	% of Total	Color
DV200	200	8,000	30.3	84	

η



Overall Results for sample 9 : G345-AH4A

RNA Area:	48.4
RNA Concentration:	31 ng/µl
rRNA Ratio [28s / 18s]:	1.1
RNA Integrity Number (RIN):	9 (B.02.11)
Result Flagging Color:	
Result Flagging Label:	RIN:9
Corr. Area 1:	39.8

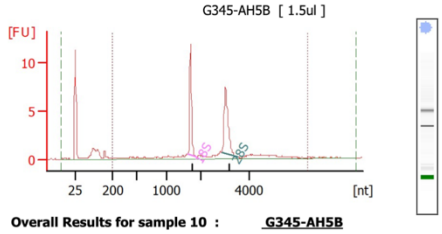
Fragment table for sample 9 : G345-AH4A

Name	Start Size [nt]	End Size [nt]	Area	% of total Area
18S	1,635	1,822	10.0	20.6
28S	2,851	3,555	11.1	22.9

Region table for sample 9 : G345-AH4A

Name	From [nt]	To [nt]	Corr. Area	% of Total	Color
DV200	200	8,000	39.8	82	

θ



Overall Results for sample 10 : G345-AH5B

RNA Area:	46.5
RNA Concentration:	29 ng/µl
rRNA Ratio [28s / 18s]:	1.1
RNA Integrity Number (RIN):	9.4 (B.02.11)
Result Flagging Color:	
Result Flagging Label:	RIN: 9.40
Corr. Area 1:	37.4

Fragment table for sample 10 : G345-AH5B

Name	Start Size [nt]	End Size [nt]	Area	% of total Area
18S	1,624	1,846	10.0	21.5
28S	2,854	3,524	11.3	24.4

Region table for sample 10 : G345-AH5B

Name	From [nt]	To [nt]	Corr. Area	% of Total	Color
DV200	200	6,417	37.4	80	

Figure A.1. continued.

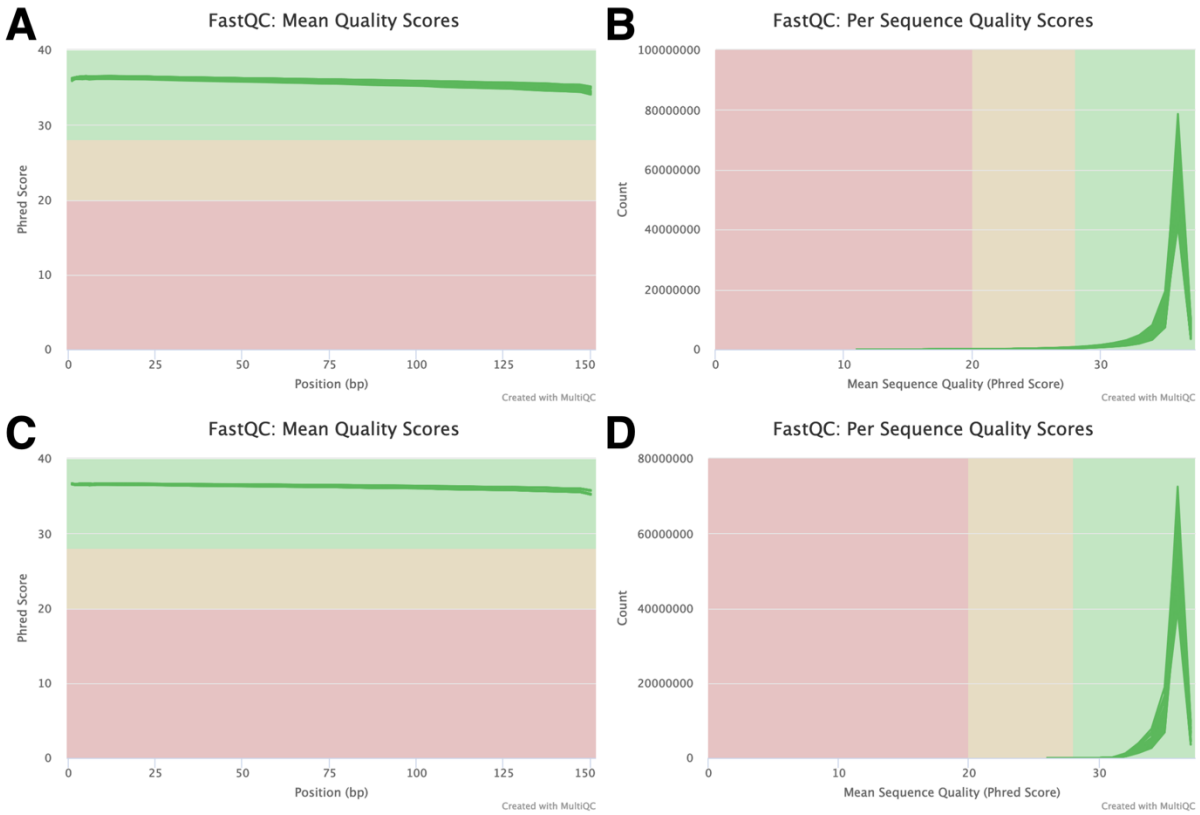


Figure A.2. Sequence quality of RNA-seq reads from the dorsal skin of developing wood frogs exposed to a microplastics mixture.

RNA-seq reads from the dorsal skin of developing wood frogs exposed to a 0×, 1×, or 10× microplastics mixture underwent quality control with Rcorrector (Song & Florea, 2015), fastp (Chen, 2023), and RiboDetector (Deng et al., 2022). Plots of **A, C)** per base sequence quality and **B, D)** per sequence quality were produced with MultiQC (Ewels et al., 2016) from FastQC (Andrews, 2010) reports for **A, B)** raw and **C, D)** cleaned reads.

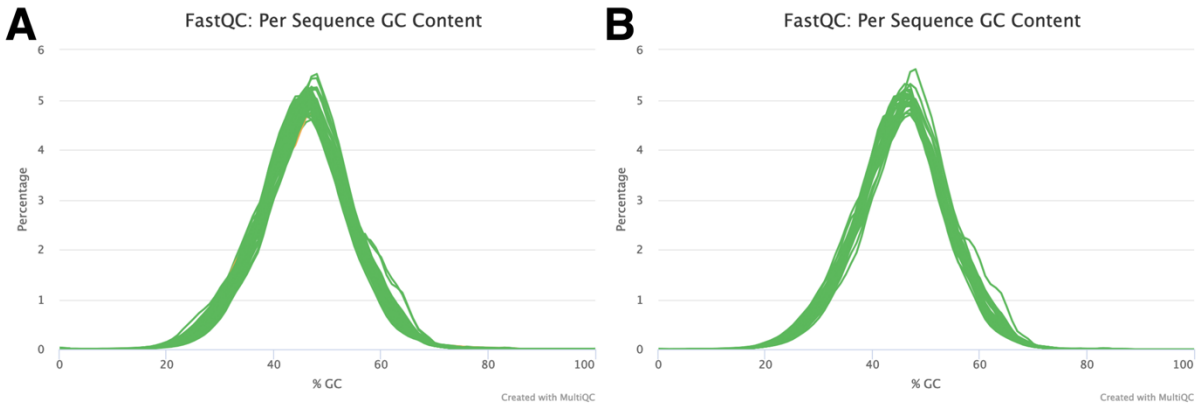


Figure A.3. GC content of RNA-seq reads from the dorsal skin of developing wood frogs exposed to a microplastics mixture.
RNA-seq reads from the dorsal skin of developing wood frogs exposed to a 0×, 1×, or 10× microplastics mixture underwent quality control with Rcorrector (Song & Florea, 2015), fastp (Chen, 2023), and RiboDetector (Deng et al., 2022). Plots of per sequence GC content were produced with MultiQC (Ewels et al., 2016) from FastQC (Andrews, 2010) reports for **A)** raw and **B)** cleaned reads.

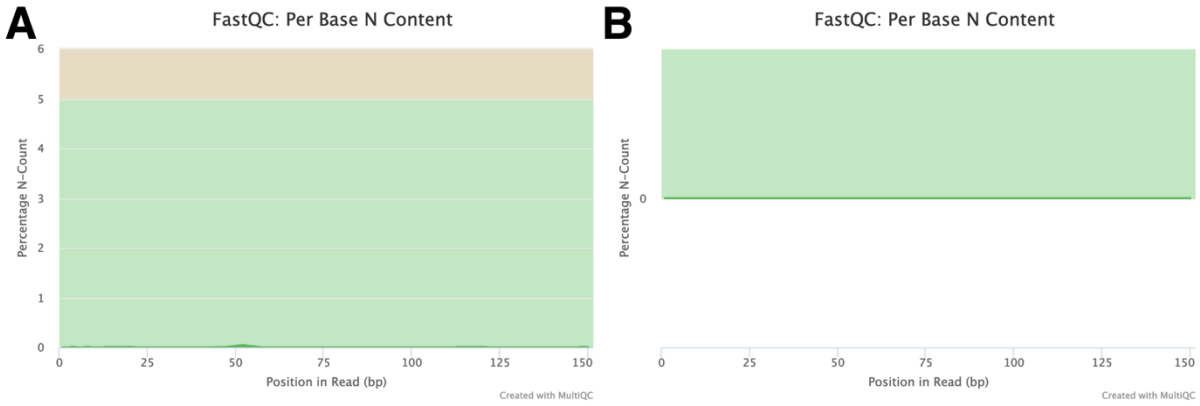


Figure A.4. N content of RNA-seq reads from the dorsal skin of developing wood frogs exposed to a microplastics mixture.
RNA-seq reads from the dorsal skin of developing wood frogs exposed to a 0×, 1×, or 10× microplastics mixture underwent quality control with Rcorrector (Song & Florea, 2015), fastp (Chen, 2023), and RiboDetector (Deng et al., 2022). Plots of per base N content were produced with MultiQC (Ewels et al., 2016) from FastQC (Andrews, 2010) reports for **A)** raw and **B)** cleaned reads.

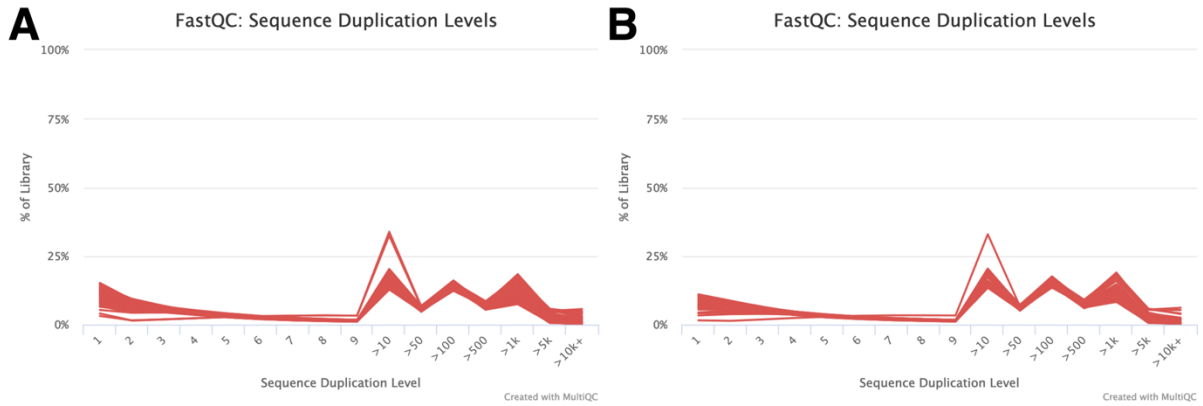


Figure A.5. Sequence duplication levels of RNA-seq reads from the dorsal skin of developing wood frogs exposed to a microplastics mixture.

RNA-seq reads from the dorsal skin of developing wood frogs exposed to a 0×, 1×, or 10× microplastics mixture underwent quality control with Rcorrector (Song & Florea, 2015), fastp (Chen, 2023), and RiboDetector (Deng et al., 2022). Plots of sequence duplication levels were produced with MultiQC (Ewels et al., 2016) from FastQC (Andrews, 2010) reports for **A)** raw and **B)** cleaned reads.

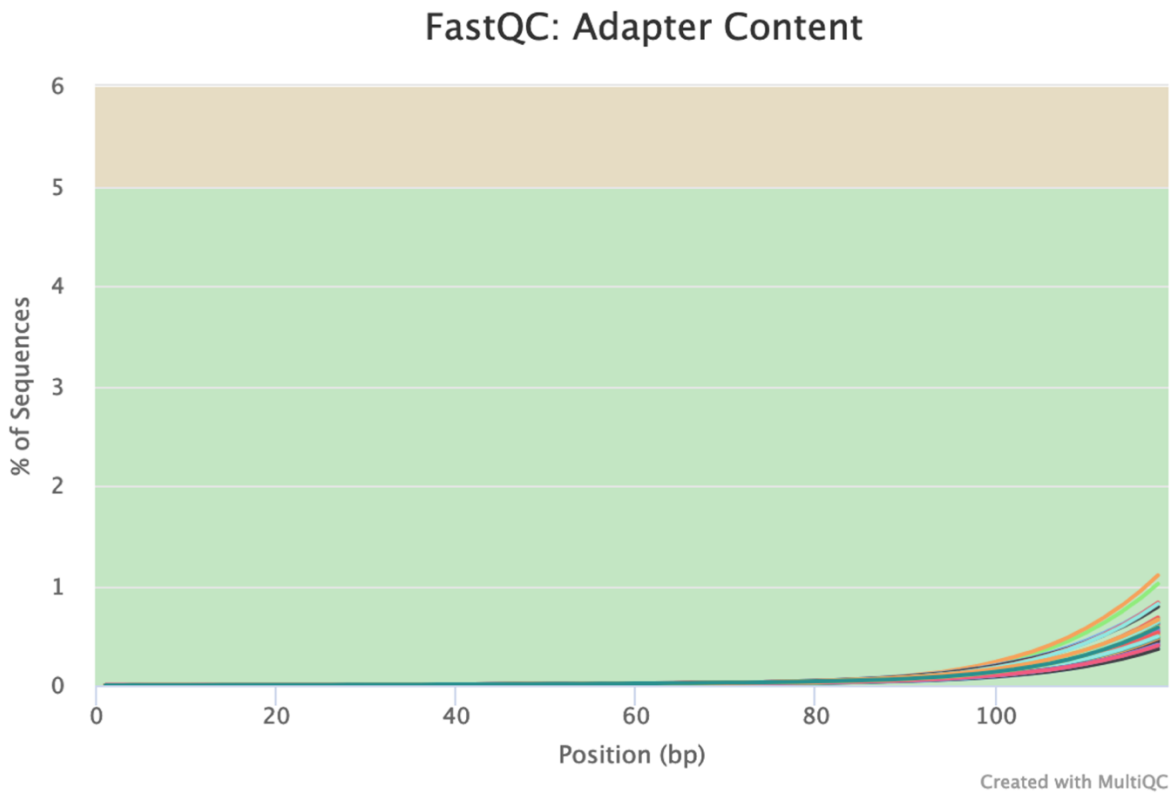


Figure A.6. Adaptor content in raw RNA-seq reads from the dorsal skin of developing wood frogs exposed to a microplastics mixture.
RNA-seq reads from the dorsal skin of developing wood frogs exposed to a 0×, 1×, or 10× microplastics mixture underwent quality control with Rcorrector (Song & Florea, 2015), fastp (Chen, 2023), and RiboDetector (Deng et al., 2022). Adapter content in raw reads is depicted in the plot, produced with MultiQC (Ewels et al., 2016) from FastQC (Andrews, 2010) reports. In cleaned reads, no samples were found with adaptor contamination > 0.1% and no plot was generated.

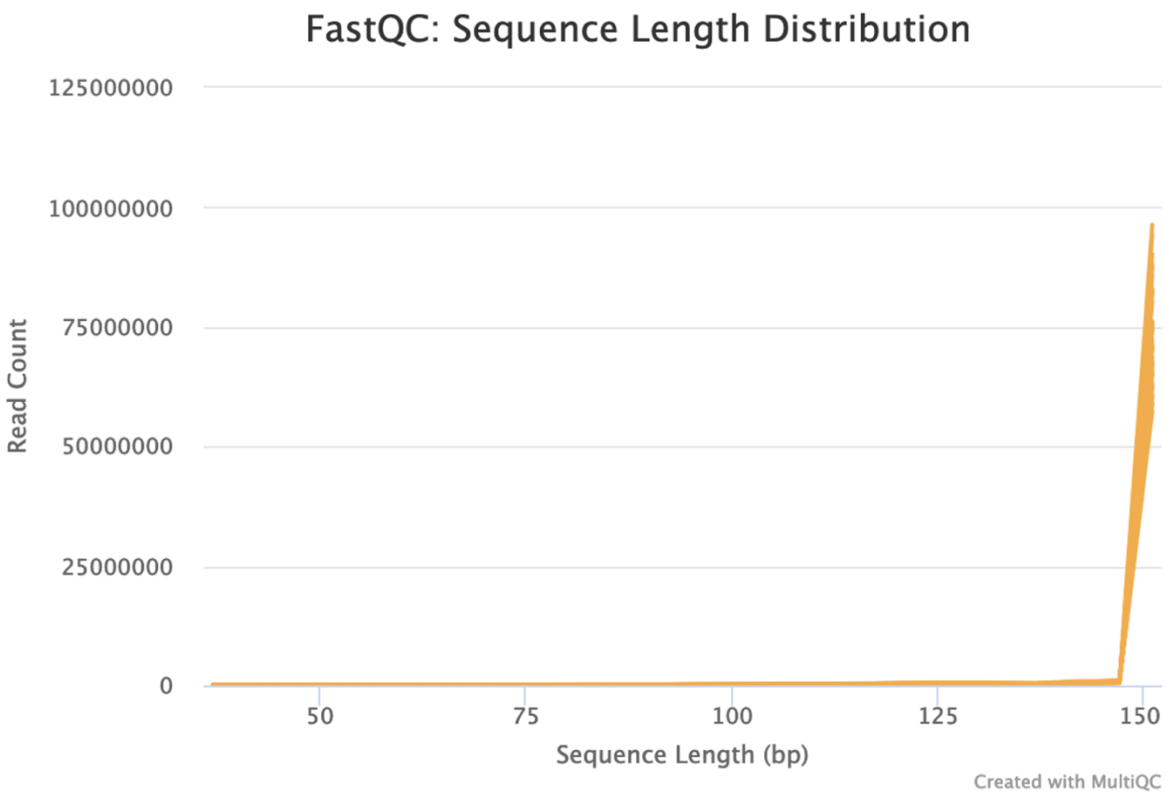


Figure A.7. Length of cleaned RNA-seq reads from the dorsal skin of developing wood frogs exposed to a microplastics mixture.
RNA-seq reads from the dorsal skin of developing wood frogs exposed to a 0×, 1×, or 10× microplastics mixture underwent quality control with Rcorrector (Song & Florea, 2015), fastp (Chen, 2023), and RiboDetector (Deng et al., 2022). The sequence lengths of cleaned reads are depicted in the plot, produced with MultiQC (Ewels et al., 2016) from FastQC (Andrews, 2010) reports. Raw reads had a uniform length of 151 bp.

Appendix B

Supplemental Figures



Figure B.1. Overview of Gene Ontology (GO) terms assigned to transcribed genes in the dorsal skin of Gosner stage ~42 wood frog tadpoles from the control (0× microplastics exposure) group.

Quality-controlled RNA-seq reads obtained from the dorsal skin of developing wood frogs were aligned to the *Rana sylvatica* reference genome (GCA_028564925.1) with HISAT2 and

assembled into transcripts with StringTie. TransDecoder was used to predict candidate coding sequences in the assembled transcripts and Trinotate was used to assign GO terms by homology transfer from BLASTP and BLASTX searches of the Swiss-Prot database. GO term assignments were filtered to retain level 2 GO terms, and the number of genes expressed in the 0× (control) dorsal skin samples from Gosner stage ~42 wood frogs for each level 2 GO term were plotted.



Figure B.2. Overview of Gene Ontology (GO) terms assigned to transcribed genes in the dorsal skin of Gosner stage 45 wood frog tadpoles from the control (0× microplastics exposure) group.

Quality-controlled RNA-seq reads obtained from the dorsal skin of developing wood frogs were aligned to the *Rana sylvatica* reference genome (GCA_028564925.1) with HISAT2 and

assembled into transcripts with StringTie. TransDecoder was used to predict candidate coding sequences in the assembled transcripts and Trinotate was used to assign GO terms by homology transfer from BLASTP and BLASTX searches of the Swiss-Prot database. GO term assignments were filtered to retain level 2 GO terms, and the number of genes expressed in the 0× (control) dorsal skin samples from Gosner stage 45 wood frogs for each level 2 GO term were plotted.



Figure B.3. Overview of KEGG pathways assigned to transcribed genes in the dorsal skin of Gosner stage ~42 wood frog tadpoles from the control (0× microplastics exposure) group.

Quality-controlled RNA-seq reads obtained from the dorsal skin of developing wood frogs were aligned to the *Rana sylvatica* reference genome (GCA_028564925.1) with HISAT2 and

assembled into transcripts with StringTie. TransDecoder was used to predict candidate coding sequences in the assembled transcripts. Trinotate and EggNOG-mapper were used to assign KEGG pathways to assembled transcripts. The number of genes expressed in the 0× (control) dorsal skin samples from Gosner stage ~42 wood frogs for each level 2 KEGG pathway classification were plotted.

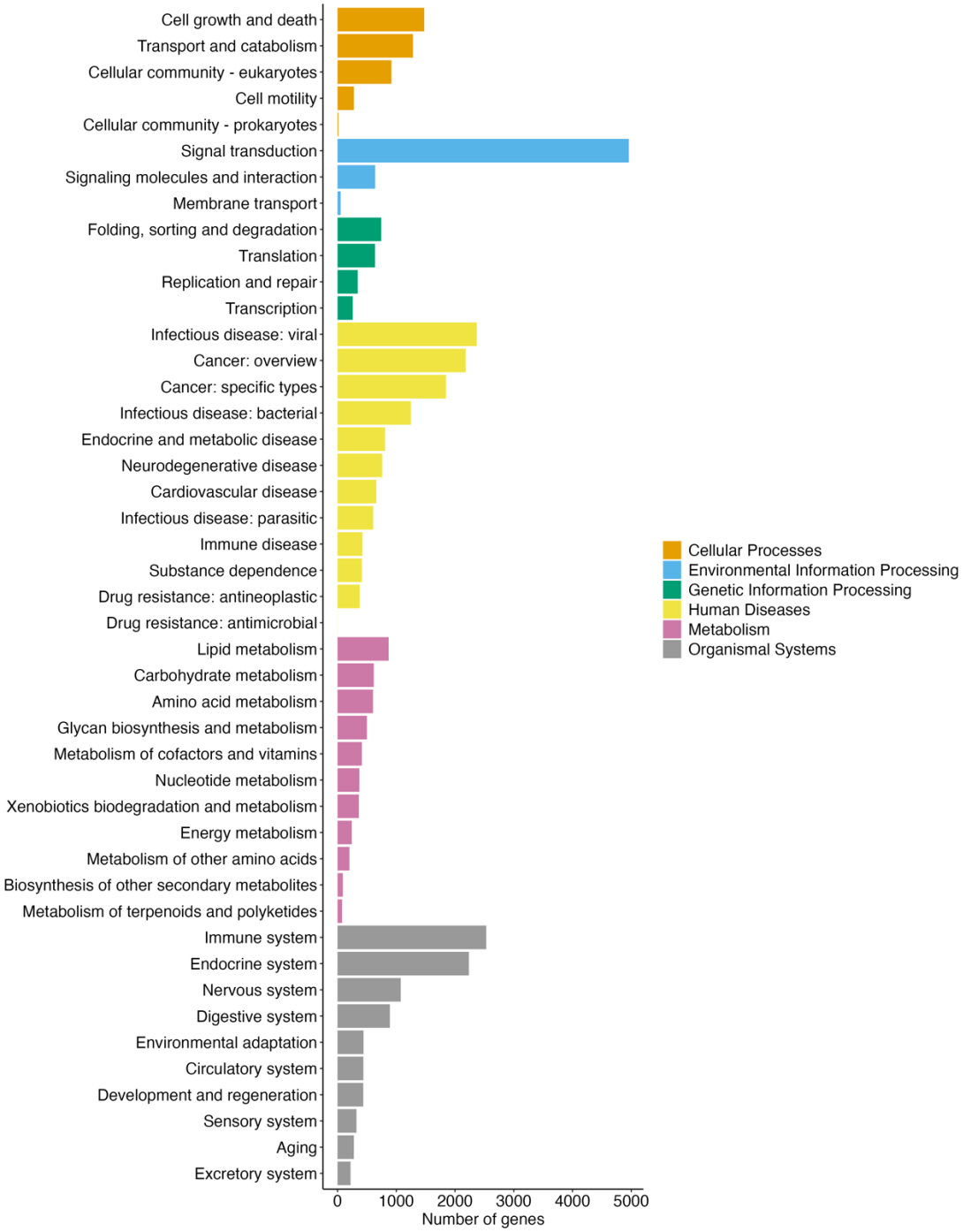


Figure B.4. Overview of KEGG pathways assigned to transcribed genes in the dorsal skin of Gosner stage 45 wood frog tadpoles from the control (0× microplastics exposure) group.

Quality-controlled RNA-seq reads obtained from the dorsal skin of developing wood frogs were aligned to the *Rana sylvatica* reference genome (GCA_028564925.1) with HISAT2 and

assembled into transcripts with StringTie. TransDecoder was used to predict candidate coding sequences in the assembled transcripts. Trinotate and EggNOG-mapper were used to assign KEGG pathways to assembled transcripts. The number of genes expressed in the 0× (control) dorsal skin samples from Gosner stage 45 wood frogs for each level 2 KEGG pathway classification were plotted.

Appendix C

R sessionInfo()

```
R version 4.3.2 (2023-10-31)
Platform: x86_64-apple-darwin20 (64-bit)
Running under: macOS Sonoma 14.2.1

Matrix products: default
BLAS:
/System/Library/Frameworks/Accelerate.framework/Versions/A/Frameworks/vecLib.framework/Versions/A/libBLAS.dylib
LAPACK: /Library/Frameworks/R.framework/Versions/4.3-x86_64/Resources/lib/libRlapack.dylib;  LAPACK version 3.11.0

locale:
[1] en_US.UTF-8/en_US.UTF-8/en_US.UTF-8/C/en_US.UTF-8/en_US.UTF-8

time zone: America/Toronto
tzcode source: internal

attached base packages:
 [1] tools     grid      stats4    stats     graphics  grDevices utils     datasets  methods   base

other attached packages:
 [1] EnhancedVolcano_1.20.0      ggrepel_0.9.5               VennDiagram_1.7.3           futile.logger_1.4.3
 [5] pheatmap_1.0.12             seqinr_4.2-36               UpSetR_1.4.0                GO.db_3.18.0
 [9] AnnotationDbi_1.64.1        KEGGREST_1.42.0             clusterProfiler_4.10.0      DESeq2_1.42.0
[13] SummarizedExperiment_1.32.0 Biobase_2.62.0              MatrixGenerics_1.14.0       matrixStats_1.2.0
[17] GenomicRanges_1.54.1        GenomeInfoDb_1.38.5         IRanges_2.36.0              S4Vectors_0.40.2
[21] BiocGenerics_0.48.1         lubridate_1.9.3             forcats_1.0.0               stringr_1.5.1
[25] dplyr_1.1.4                 purrr_1.0.2                 readr_2.1.5                 tidyr_1.3.0
[29] tibble_3.2.1                ggplot2_3.4.4               tidyverse_2.0.0

loaded via a namespace (and not attached):
 [1] RColorBrewer_1.1-3      rstudioapi_0.15.0       jsonlite_1.8.8          magrittr_2.0.3
 [5] farver_2.1.1            fs_1.6.3                zlibbioc_1.48.0         vctrs_0.6.5
 [9] memoise_2.0.1           RCurl_1.98-1.14         ggtree_3.10.0           S4Arrays_1.2.0
[13] lambda.r_1.2.4          SparseArray_1.2.3       gridGraphics_0.5-1      plyr_1.8.9
[17] futile.options_1.0.1    cachem_1.0.8            igraph_1.6.0            lifecycle_1.0.4
[21] pkgconfig_2.0.3         Matrix_1.6-5            R6_2.5.1                fastmap_1.1.1
[25] gson_0.1.0              GenomeInfoDbData_1.2.11 digest_0.6.34           aplot_0.2.2
[29] enrichplot_1.22.0       colorspace_2.1-0        patchwork_1.2.0         RSQLite_2.3.5
[33] fansi_1.0.6             timechange_0.3.0        httr_1.4.7              polyclip_1.10-6
[37] abind_1.4-5             compiler_4.3.2          bit64_4.0.5             withr_3.0.0
[41] BiocParallel_1.36.0     viridis_0.6.4           DBI_1.2.1               ggforce_0.4.1
```

```
[45] MASS_7.3-60.0.1        DelayedArray_0.28.0    HDO.db_0.99.1          ape_5.7-1
[49] scatterpie_0.2.1       glue_1.7.0             nlme_3.1-164           GOSemSim_2.28.1
[53] shadowtext_0.1.3       reshape2_1.4.4         ade4_1.7-22            fgsea_1.28.0
[57] generics_0.1.3         gtable_0.3.4           tzdb_0.4.0             data.table_1.14.10
[61] hms_1.1.3              tidygraph_1.3.0        utf8_1.2.4             XVector_0.42.0
[65] pillar_1.9.0           yulab.utils_0.1.3      splines_4.3.2          tweenr_2.0.2
[69] treeio_1.26.0          lattice_0.22-5         bit_4.0.5              tidyselect_1.2.0
[73] locfit_1.5-9.8         Biostrings_2.70.1      gridExtra_2.3          graphlayouts_1.1.0
[77] stringi_1.8.3          lazyeval_0.2.2         ggfun_0.1.4            codetools_0.2-19
[81] ggraph_2.1.0           qvalue_2.34.0          ggplotify_0.1.2        cli_3.6.2
[85] munsell_0.5.0          Rcpp_1.0.12            png_0.1-8              parallel_4.3.2
[89] blob_1.2.4             DOSE_3.28.2            bitops_1.0-7           viridisLite_0.4.2
[93] tidytree_0.4.6         scales_1.3.0           crayon_1.5.2           rlang_1.1.3
[97] formatR_1.14           cowplot_1.1.3          fastmatch_1.1-4
```